# Macro-scale performance of a mega-feeder nourishment

## Describing and predicting the long-term feeding performance

P. C. Drenth



TU Delft

Deltares

# Macro-scale performance of a mega-feeder nourishment

## Describing and predicting the long-term feeding performance

by

P. C. Drenth

to obtain the degree of Master of Science
at the Delft University of Technology,
to be defended publicly on Tuesday 8, 2018 at 11:00 AM.


| | | |
|---|---|---|
| Student number: | 4438671 | |
| Project duration: | May 20, 2017 – May 8, 2018 | |
| Thesis committee: | Prof. dr. ir. S.G.J. Aarninkhof, | TU Delft |
| | Dr. Ir. M. A. Schipper, | TU Delft |
| | Ir. A. P. Luijendijk, | Deltares |
| | Dr. Ir. J. E. A. Storms | TU Delft |

An electronic version of this thesis is available at `http://repository.tudelft.nl/`.


TU Delft

Deltares

# Abstract

A mega-feeder nourishment is a concentrated nourishment that disperses over time due to wind, waves, and tide, and as a result 'feeds' its adjacent coasts. Engineers and policy makers are interested in (predictions of) the performance of mega-feeder nourishments. During the design phase of a nourishment, performance indicators can enable an objective comparison of a mega-feeder nourishment to alternative nourishment strategies, In the case of an existing mega-feeder nourishment, predictions of the performance enable an objective assessment of the need for additional nourishments in the proximity of a mega-feeder nourishment.

Today, engineers and policy makers rely on expert judgement when assessing alternative nourishment strategies, or the need for additional nourishments. Currently no tool exists that enables quantification of the performance of a mega-feeder nourishment. Existing models that describe and predict developments of nearshore coastal areas have been applied before to assess the developments of a mega-feeder nourishment, but have not been validated specifically to describe the performance in terms of alongshore feeding. The research question is therefore: *"How to describe and predict macro-scale mega-feeder nourishment performance with behaviour-based coastal indicators?"*

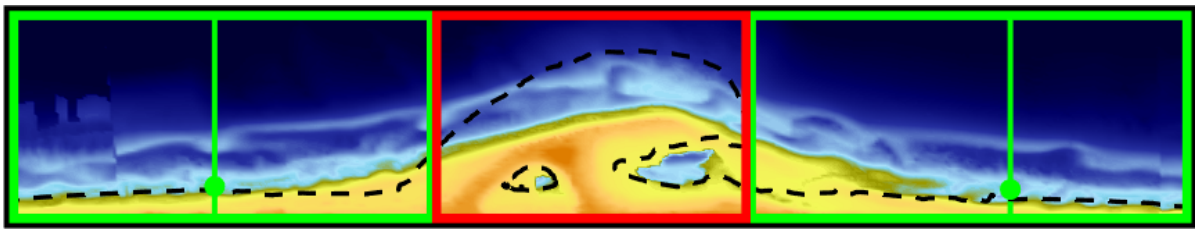

Figure 1: The proposed performance tool. The black box on the edges denotes the Region of Influence, the green boxes depict the Regions of Contributions, and the red box shows the Region of the Feeder. The green circles indicate the Accretion Points.

A tool is proposed that enables the quantification of the performance of a mega-feeder nourishment, as well as the validation of models that describe and predict the performance of a mega-feeder nourishment, The tool is specifically aimed at quantifying the performance in terms of the alongshore feeding (figure 1).

The tool first of all comprises of a data reduction into volume densities of the active depth (-10/+3m + NAP). Second, the nourishment is split up into three types of alongshore segments. The first is the Region of Influence, the alongshore section where a mega-feeder nourishment influences the coast. The second is the Region of the Feeder, the section where the sediment that is fed to the adjacent coasts, originates from. The Regions of Contribution define the sections where an accretion of sediment can be observed as a result of the feeding of sediment by the mega-feeder nourishment.

The performance of a mega-feeder nourishment is based upon indicators that represent the objective of a mega-feeder nourishment: to contribute sediment (volume) along adjacent coasts (sections) for a specified duration (lifetime). The feeding of sediment to adjacent coasts is quantified in terms of a volumetric growth in the Regions of Contribution. Secondly, the Accretion Points quantitatively indicate the location up until where accretion can be observed as a result of feeding by a mega-feeder nourishment, denoted with the green circles in (figure 1). The volume reduction in the Region of the Feeder is proposed as an indicator to quantitatively assess the age or predicted lifetime.

The tool is applied to the Sand Engine, used as a case study to examine the applicability of the indicators of the tool. This Sand Engine, constructed during the spring of 2011, has a nourishment volume of 21.5Mm3, initially spanned a width of 2.4km and extended 1km into the sea. If shown to be successfully applicable to the monitoring data, the examination of the indicators consists first off of an assessment on the presence of clear trends, indicating a long-term, predictable development. Second, it is verified whether the indicators reflect the behaviour. Behaviour is here defined as the change of the planform shape of the mega-feeder nourishment as a result of forcing conditions, e.g. wind, waves, and tide. From previous research it was proposed that the behaviour is dominated by alongshore diffusivity, or spreading. Results of this thesis showed that the diffusivity, expressed in the second order central moment (M2), developed following a clear long-term trend (curve fits performed well with $R^2 = 0.99$), that decelerates in growth over time. The three performance

indicators, i.e. the volumetric growth, the Accretion Points, and the volume reduction of the Regions of the Feeder, showed a similar decelerating developments. The performance indicators were found to be linearly correlated to M2 ($R^2 \approx 0.9$). The Accretion Points develop at a rate of circa 3 times the rate of the spreading.

Both a range of analytical model approaches, as well as a number of 2D numerical model (Delft3D) approaches were validated based on the quantified performance of the Sand Engine. First the results of the application of the analytical model approaches are discussed, followed by the results of the application to the numerical model approaches. The first analytical model approach consists of a non-calibrated prediction. The diffusivity imposed on the model is derived from the bulk longshore sediment transport equation by Kamphuis (1991). Following this approach, the performance is reasonably well described, with mild under-predictions (Average under-predictions of performance by 40% - 50%). A second approach comprises of calibration of the diffusivity (Spreading approach). This results in a good description of the performance. Additional calibration of the advection (a northward alongshore migration) improved the description of the performance by the analytical model mildly (Centroid approach). It is therefore concluded the diffusivity and advection make up the dominant behaviour of a mega-feeder nourishment.

Three calibrated 2D numerical model (Delft3D) approaches are validated: 1) bruteforce, 2) mormerge, using a curved nearshore grid, and 3) a mormerge approach with a rectangular nearshore grid (Stive). With the bruteforce approach, the model is able to describe the performance of a mega-feeder nourishment. Application of the mormerge approach over-predicts the performance. The rectangular nearshore grid applied in the Stive approach, prevents the numerical model from reshaping into a Gaussian curve entirely. Consequently, the model approach reflects the performance poorly.

From the validation of the model approaches, it is concluded that the analytical model can be used to predict the initial (i.e. first 25% of the lifetime) performance of a mega-feeder nourishment, if the spreading is derived from the bulk longshore sediment transport equation by Kamphuis (1991). Second, if the bathymetry is regularly monitored (e.g. semi-annually), the input of the analytical model can be calibrated, enabling long-term predictions of the performance. If more detailed descriptions of the developments of a mega-feeder nourishment are needed, the bruteforce approach can serve as a method to describe and predict the volumetric feeding performance of a mega-feeder nourishment.

The performance of the Sand Engine is predicted with the analytical model (calibrated for spreading, centroid, and net volume loss in RoI) and the numerical bruteforce approach up until 2030. The volumetric growth will stagnate on the south, while on the north it is expected to grow up to 4Mm3. The Region of Influence will increase to approximately 7km. From this, it is concluded that it is unlikely the Sand Engine will meet its original objective of contributing to coastal safety along the Westland coast (17.2km) between 2011- 2031. Further, the half-life of the Sand Engine will be reached near 2030, indicating the actual lifetime is significantly longer than the design lifetime (20 years).

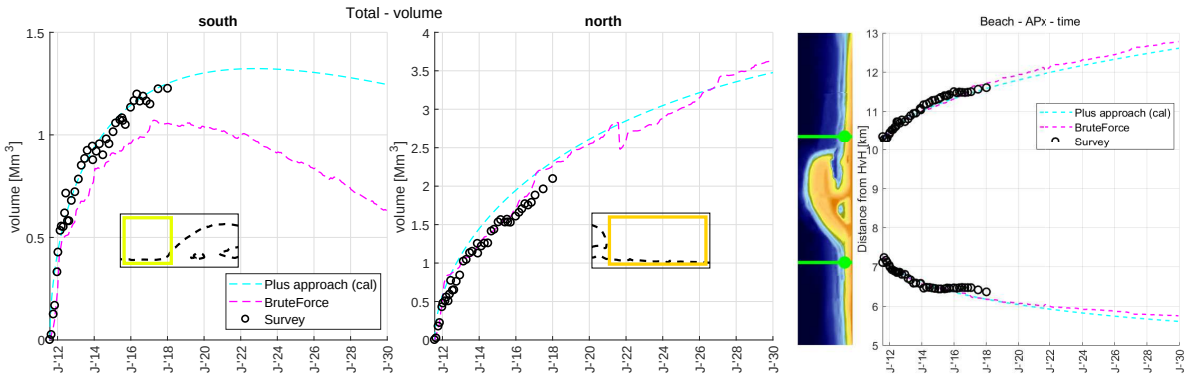


Figure 2: Prediction of volumetric and geometric performance of Sand Engine. a) Volumetric growth on the south, b) volumetric growth on the north, c) alongshore expansion on south and north. Note the different axes on the vertical.

The results of this thesis show that potentially mega-feeder nourishment performance can be included in the annual assessment for coastal safety. Currently, the Dutch coastline is maintained by extrapolating the shoreline position five years into the future, not taking nearby feeder nourishments into account. To account for alongshore feeding the outcomes of the models may be added to the equation. Applications are exemplified using Kijkduin as a case study. The model predictions indicate a clear feeding in the next decade. More in general, the results show the model approaches can serve reasonably (mean error of 25%) as a means to assess the need for extra nourishments in the proximity of a mega-feeder nourishments.

# Preface

This master thesis is the product of a research executed in collaboration with Deltares and the Delft University of Technology. With it, I conclude my degree of Master of Science in Civil Engineering.

Although mildly unconventional, pride was part of my reason to go study hydraulic engineering. Globally known as experts on flood protection, the Sand Engine exemplifies this pride and expertise and combined it in an incredible result of Dutch engineering. Through the entire year the topic kept my interest and I was honoured to dedicating my last year of studying to one of the most oldest Dutch practices a student can graduate in; an alternative method of flood protection. I feel proud to have contributed to increasing our understanding of the Sand Engine as a means to protect ourselves from one of the greatest challenges of human kind in the next century: sea-level rise. I hope the thesis encourages other students and researchers to continue working on this topic, as there is much still to learn.

My motivation and enthusiasm to my research is partially a result of the aforementioned reasons, but primarily a result of the incredible passion that each of my committee members shared during countless meetings. Where many co-students share their experience of the thesis as being a work of solitude, I enjoyed the supervision rather as a collaboration, for which I thank the entire committee. Their passion and enthusiasm for their own work will remain an inspiration to me in my future career.

I got to see Matthieu's passion for his work initially during lectures of the Coastal Dynamics II coarse. I admired his capacity to share highly complicated hydrodynamics in simplistic language, without losing the essence. Ever since, he has guided me as a supervisor during my internship in Dubai and now my thesis. Thank you for your creativity and inspiration during the countless meetings. Arjen shares the same passion and enthusiasm. During meetings I got to know Arjen as a hard worker, in which I recognised myself. I appreciate greatly his advise to sometimes take a break in order to reflect on the results, and to remember there is more in life than a thesis itself. I wish you well during your final stages of your dissertation. Albeit more of the same, I wish to give my thanks to Joep as well for his likewise enthusiasm. His interest in the topic from the perspective of a geologist inspired and motivated me to view the Sand Engine from a different perspective. As the chair of the committee, I thank Stefan for supporting me in keeping track of the higher goal as to ensure the thesis will find the light of day in other ways than purely its educational contribution. It is admirable how Stefan is committed to each of the theses he is a part of. Finally, although not a part of the committee, I want to thank Bart Roest for his time to share his thoughts. His thesis has been the pillar on which this work was built. The results from this thesis could not have been established without it.

Some people think and then talk. I talk and then think. Throughout the year, I have harassed pretty much everybody with detailed and abstract talks on problems I experienced during the research of my thesis. Thanks to all members of my hockey team, who had to experience this on a weekly basis. Thank you Nitant, for supporting me throughout the entire year. Specific thanks to the last four weeks before my greenlight. Without your guidance and keeping my eyes on the target during these final weeks, I would not have finished it in time. Miriam, thank you for your unconditional faith in the quality of my work, whenever I was (over)critical. Being there with my during the ups and downs that was my path of the research and writing of the thesis. Your never ending positive look on the world makes the world, and my life, a better place. Finally, many thanks go out to my parents. My mother in supporting me, giving me courage to continue, but mostly that I should perhaps take a little break. And my dad. For his enthusiasm to, as a banker, guide his son into the right path of a thesis with a highly technical topic.

*P. C. Drenth*
*Delft, May 2018*

# Contents

# List of Figures

# List of Tables

# 1 Introduction

## 1.1. The challenge of climate change on the Dutch policy for coastal safety

Protection of hinterlands from floods is an increasing problem in world wide due to sea-level rise (Dasgupta et al., 2009, Hurst et al., 2016, Leatherman et al., 2000, Pilkey and Cooper, 2014, Silva et al., 2014). One interesting case study is the delta that covers the Dutch coast, which has been challenged by nature since the moment people started to inhabit the region.

To ensure protection of the hinterlands, the government of The Netherlands enacted a law in the 1990s that dictates the position of the coastline is maintained by means of nourishments. An ambitious law, given that the coastline had been structurally eroding for centuries. With 488 people per $km^2$, The Netherlands is the most densely populated country in the European Union. Around nine million people live in the coastal area, of which vast regions lie below mean sea level Approximately 65% of the gross national product is generated here. The Dutch coastal zone is put under pressure more and more because of sea-level rise, a continuous increase of the population in the hinterland, and because they arguably host the world's most productive urban, industrial and agricultural metropolises (Parry et al., 2007).

The Dutch law enacted in 1990 proved to be effective, reducing the the percentage of coastal sections where the desired position was transgressed from fifteen percent to five percent (Stive et al., 2013). Though the required nourishment volumes to sustain the coastline are increasing. Between 1990 and 2002, the average volume of annual nourishment was 6 $Mm^3$. By 2004, this value had increased to 12 $Mm^3$, which again had increased to 20 $Mm^3$/year in 2008 (De Ronde, 2008)).

The law that induced these high volumes of nourishments is based on a standardised policy rule that anticipates on any transgressions of the coastline. The so called Dynamic Preservation Act defines a desired state of the coastline, the Basal Coastline (BCL), which is compared to a Test Coastline (TCL). The BCL and TCL are representatives of the coastline position, based on the the beach and the upper part of the foreshore, computed from a cross-shore section (figure 1.1). The actual position (the momentary coastline, or MCL) of the coastline in the past ten years is extrapolated five years into the future to derive the TCL. If the TCL transgresses the BCL, a nourishment is planned.

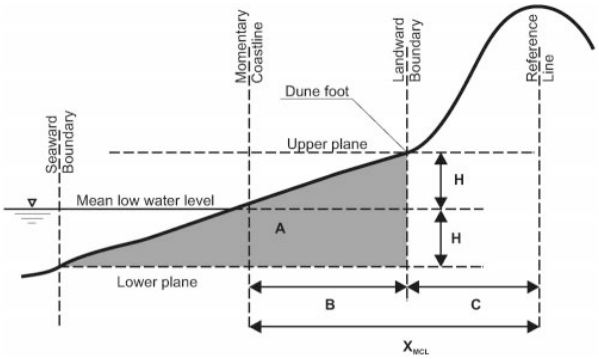


Figure 1.1: Method for computing the Momentary Coastline (Hillen et al., 1991)

It is expected that the demand for sediment will continue to grow and even accelerate in the near future, due to global warming inducing sea-level rise, thermal expansion and regional effects such as ice discharge and coastal subsidence. In the past century, the relative sea-level has risen by 20 cm along the Dutch coast. The Intergovernmental Panel on Climate Change (IPCC), estimates a global sea-level rise

between 18 and 59 cm by 2100 (Parry et al., 2007). To ensure safety of flooding at the Dutch coast a study was undertaken to make a prediction of climate change. By 2100 the relative sea-level rise in The Netherlands is expected to be between 65 and 130 cm by 2100, nearly twice as high as the global average. High-end estimates for 2200 are even expecting a 2.0 to 4.0 m relative sea-level rise (Kabat et al., 2009). In response to these expectations, the New Delta committee concluded that the yearly sand nourishment volume for the Dutch coast may need to increase to circa 80Mm$^3$ by the end of the century (or ~ 250m$^3$/m/year), given the high scenario of climate change (Kabat et al., 2009). Recent research from The Royal Netherlands Meteorological Institute (Bars et al., 2017) even suggests a sea-level rise of up to 2.5 - 3.0 m in 2100. Protecting the low lands from flooding seems ever more challenging, while at the same time also more important than ever.

If the applied strategy of beach and foreshore nourishments would be maintained, nourishments of this scale would need to be executed yearly along the entire Dutch coastline. This increases the beach width by a significant amount, which is considered unattractive for beach users as the water becomes less accessible. Next to a larger sand deficit, a second question arises with regard to the ecology. It is questionable whether frequent re-nourishing is not detrimental for the fauna e.g. (Janssen et al., 2008, Peterson et al., 2006, Speybroeck et al., 2006). Because of these reasons, alternative methods need to be considered.

## 1.2. A response to climate change: The Sand Engine

An alternative that might adhere to the increasing demand of sediment and reduction of the impact on the ecology, is proposed by Stive et al. (2013). The concept of the 'mega-nourishment' as it was called initially, consists of a large volume of dredged sand placed locally in front of the beach in a relatively small area. Contrary to the traditional beach and dune nourishment, the highly concentrated nourishment (locally up to 10.000m$^3$/m) 'feeds' the adjacent coasts and dunes via as waves, wind, and tide (figure 1.2). Because of this mechanism, it is sometimes also referred to as a mega-feeder nourishment. The redistribution of the sediment, results in an effectively nourished coastal zone that is much larger than where the nourishment was placed initially. An additional feature of the nourishment is its size, a magnitude larger than regular nourishments, chosen to lower the required frequency of nourishments, to reduce the ecological impact. It was argued that by only disturbing a small section of the coastline would reduce the detrimental effect on the ecology.

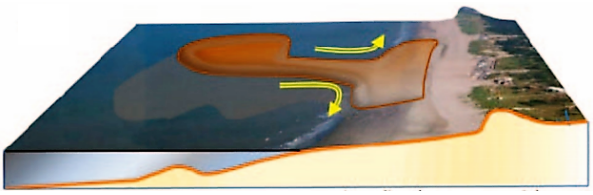

Figure 1.2: Schematisation of conceptual mechanism of feeder nourishment

To test the concept of a mega-feeder nourishment, an unprecedented pilot called the Sand Engine (SE) was implemented at the Dutch coast, as a new alternative to beach and foreshore nourishments. First and foremost, its goal is to contribute to coastal safety in the long term (10 -20 yrs), over a O (10 km) stretch of the coastline. Next to this goal, it is also meant as a temporary addition for attractive recreational and a natural reserve. Thirdly, the generation of knowledge on the applicability of this new concept was ascribed as a goal.

### 1.2.1. Observations of the Sand Engine

To increase the understanding of the bathymetric developments of the Sand Engine, an extensive monitoring program was set up. Analyses of the surveys has lead to the confirmation that the concept of feeding the alongshore coasts is indeed working.

In extension of this observed feeding, it was proposed that the SE reshaped into a Gaussian bell shaped curve, that diffuses over time((Arriaga et al., 2017, De Schipper et al., 2016, Roest, 2017). Curve-fits of Gaussian bell shaped curves with the shorelines showed to fit well ($R^2 \approx 0.95$).

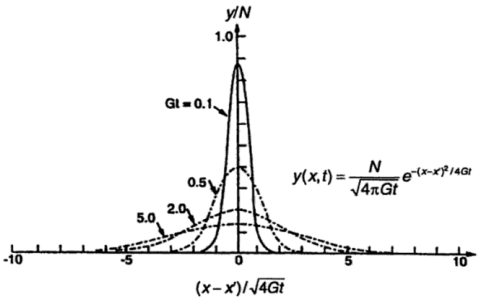


Figure 1.3: Evolution of the shoreline with time, following a Gaussian bell shaped curve. (Dean, 2002)

The Gaussian shape matches the diffusion concept introduced by Pelnard-Considere (1956) (figure 1.3)). It was stated that a nourishment spread over time following a diffusion equation $\frac{\delta y}{\delta t} = G\frac{\delta^2 y}{\delta x^2}$: (Dean, 2002):

$$y(x,t) = \frac{N}{\sqrt{4\pi G t}} e^{-\frac{(x-x')^2}{4Gt}} \tag{1.1}$$

Where G denotes the alongshore diffusivity coefficient N the planform area, $x'$ the centroid, x and y the coordinates of the shoreline position, and t the time after construction.

### 1.2.2. Model predictions of the Sand Engine

Numerous numerical models have been developed to describe and predict the bathymetric developments of the Sand Engine, ranging from faster 1D one-line models to the more computationally extensive 2D process-based models (Luijendijk et al., 2017, Stive et al., 2013) (figure 1.4).

So far, the outcomes of the numerical models have been validated based on classic validation methods. The methods included (Arriaga et al., 2017, Luijendijk et al., 2017, Tonnon et al., 2018):

- A visual comparison of the distinct features
- The Brier Skill score (BSS)
- Performance of the observed and computed volumetric changes of alongshore segments
- Performance of the observed and computed changes of the shoreline position.

Another classic validation instrument, is the assessment of the volume remaining at the site (Dean, 2002). Visual comparison of the model outcomes in the middle section, shows that the approaches simulate the developments of the middle sections rather well (figure 1.4, depicted with the red dashed box). Though, since the concept of a mega-feeder nourishment is not to place sediment locally, but to feed adjacent coasts, it is more relevant to validate the capacity to which the model approaches reflect the performance of the adjacent coasts. Contrary to the middle section, quite large differences are observed when comparing the simulation of the right (northern) adjacent coast.

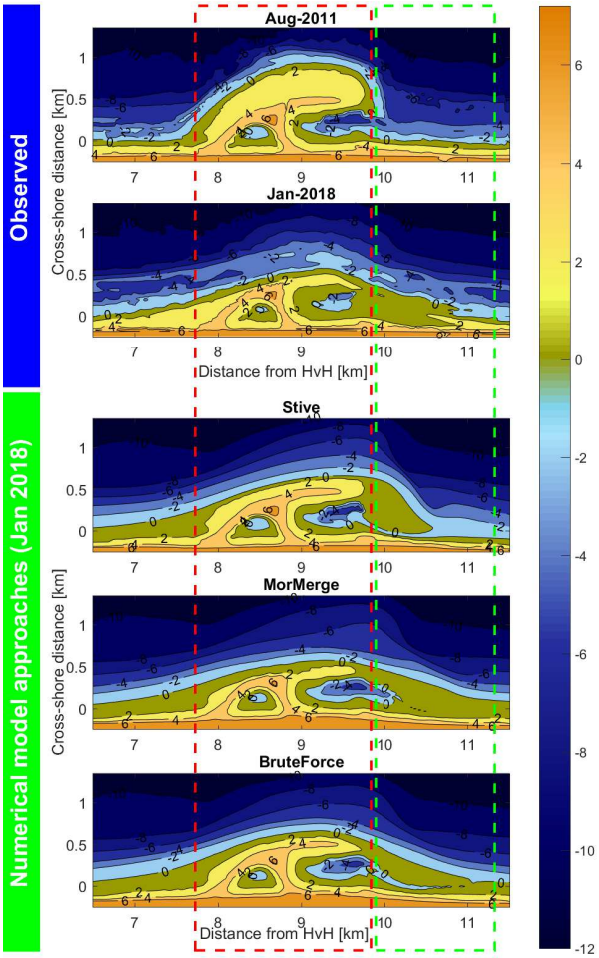


Figure 1.4: Bathymetries of Sand Engine as observed and modelled. Colours represent the height of the bathymetry, further indicated with the contours with respect to NAP (≈Mean Sea Level). Top two panels: observed bathymetry as measured in August 2011 and January 2018. Bottom three panels: simulated bathymetry by 2D numerical model approaches using Delft3D. The red box marks the middle section from which the sediment of the mega-feeder originates. The green box marks the section where the sediment is fed to.

In order to validate to what extent the performance of a mega-feeder nourishment can be described and predicted by models, the classic validation methods do not suffice. The validation must be aimed more at the feeding performance of a mega-feeder nourishment. This requires a shift in thinking from a focus on the developments at the original site of the nourishment, to the adjacent coasts along the shore and how to quanfity developments in thosre regions.

One good example of is recently proposed by Arriaga et al. (2017), who introduced a number of indicators aimed at the feeding performance of teh Sand Engine. A Q2D-morfo model was validated based indicators more related to the feeding performance. One distinct example was the validation of the observed versus the simulated diffusivity (figure 1.5).

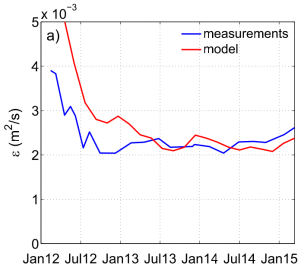


Figure 1.5: Measured vs modelled diffusivity (Q2D morfo model. From Arriaga et al. (2017)).

Though, the proposed indicator does not pose a direct link to the performance of a mega-feeder nourishment. A policymaker or a designer cannot use

the diffusivity as an indicator to assess the effectiveness of a mega-feeder nourishments. A set of indicators is required that measures the performance of the mega-feeder nourishment, and can be used to validate the capacity of models to reflect that performance. If validation shows to be successful, they can be used to predict the performance of a mega-feeder nourishment with greater reliability.

## 1.3. Knowledge gaps

The expected acceleration of world-wide sea-level rise has necessitated the search for new alternatives to protect sandy coasts from flooding hinterlands with high populations and economic value. For this reason, the concept of a mega-feeder nourishments was introduced.

Engineers and policy makers are interested in (predictions of) the performance of mega-feeder nourishments, that may serve as an alternative to the widely applied beach and shoreface nourishments. Today, engineers and policy makers rely on expert judgement when assessing alternative nourishment strategies, or the need of additional nourishments in the proximity of a mega-feeder nourishment. The first identified knowledge gap is that currently, no tool exists that enables quantification of the performance of a mega-feeder nourishment.

The second knowledge gap is related to prediction methods. Existing models that describe and predict developments of nearshore coastal areas have been applied before to assess the developments of a mega-feeder nourishment, but have not been validated specifically to describe the performance in terms of alongshore feeding.

More specifically towards the application of numerical models, different approaches can be opted for, such as the bruteforce approach or the mormerge approach. The latter is an example of an acceleration technique that significantly reduces the computation time. The identified knowledge gap, is that the influence of different modelling approaches on the capacity to describe the performance of a mega-feeder nourishment has not yet been quantified.

## 1.4. Research questions

This research adheres to describing and predicting the macro-scale performance of a mega-feeder nourishment with behaviour-based coastal indicators. The main research question is therefore:

> **How to describe and predict mega-feeder nourishment performance with behaviour-based coastal indicators?**

Where a mega-feeder nourishment is defined as a concentrated nourishment, that feeds sediment to adjacent coasts in alongshore direction, through physical forcing conditions such as waves, tide, and wind. An indicator is a measurable value that represents the performance. All analyses of developments are based on macro-scale developments, i.e. on a length scale O (100 - 1000m), and time scale of O (years).

The research question is answered via three supportive research questions:

1. How to represent the macro-scale performance of a mega-feeder nourishment with coastal indicators?
2. How do the macro-scale performance indicators develop and relate to the macro-scale behaviour of a mega-feeder nourishment?
3. How to describe the performance of a mega-feeder nourishment with analytical and numerical models?

Additionally, a set of secondary objectives is aimed at throughout the thesis as well:

1. To describe the performance of the Sand Engine up until January 2018
2. To assess the presence of differences in the feeding performance of over depth.
3. To assess the dominant behavioural elements of a mega-feeder nourishment
4. To assess the influence of acceleration techniques and gridtype in the nearshore in numerical models, on the capacity to reflect the performance of a mega-feeder nourishment.
5. To predict of the performance of the Sand Engine up until 2030.

With respect to the second item, two motivations are distinguished for this objective: first, the presence of different feeding velocity is intrinsically related to quantifying the performance of a mega-feeder nourishment, and second, it is of interest to review whether depth contours or regions can be used as representatives for the performance and macro-scale behaviour of a mega-feeder nourishment.

This research is limited by the availability of survey data. Since the survey used in this thesis, limitedly monitored the the dunes (>+3m + NAP), this depth region is not a part of the scope of this research.

## 1.5. Approach and outline

The research questions are answered first all, by the development of a performance and validation tool. This is developed from an analysis of the objectives of the Sand Engine, the one unique case study of a mega-feeder nourishment, and indicators that quantify the development, previously applied in literature (see figure 1.6 for a schematic overview). Second, the performance tool is applied to the Sand Engine, in order to verify the performance and validation tool. The presence of long-term trends is checked, to assess whether the performance develops continuously and thus predictably over time. Additionally, it is verified whether the performance indicators represent the diffusive behaviour of a mega-feeder nourishment.

The third research question, related to the validation of models, is executed by means of first the application of a number of approaches of the analytical model. Output of the data of the simulations from the numerical model approaches are pre-processed. The performance and validation tool is then applied to the models, after which the capacity to which the model approaches describe the performance is quantitatively validated. Models that are shown to reflect the performance well, are used to predict the performance of the case study, the final step of this research.

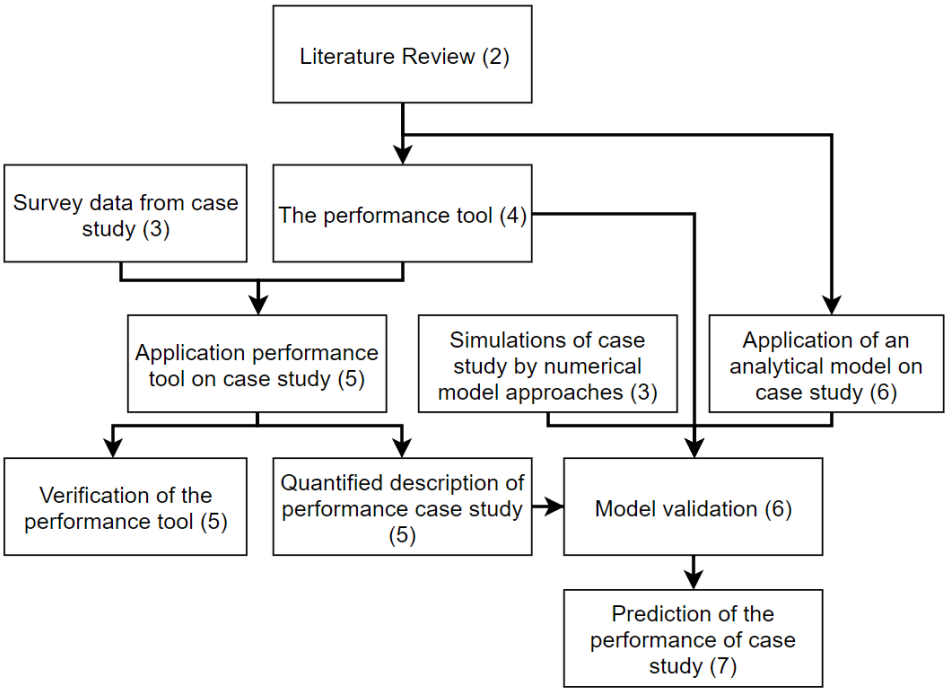


Figure 1.6: Schematic view of approach. Arrows show the relation between the different components. Numbers indicate the chapters in which the component is discussed.

The outline of the report is as follows. First the relevant literature is discussed in chapter two. In chapter three, the case study of the Sand Engine is introduced, including a review of relevant literature on previously observed developments and existing numerical models. In chapter four, the performance and validation tool is presented. The performance and validation tool is then applied to the case study for the verification of the performance tool in chapter five. In chapter six, the models are validated with the performance and validation tool. In chapter seven, models that showed to describe well the observed feeding performance, are used to predict the future performance up until 2030. In the final chapters of the report, the conclusion are given, as well as recommendations for design and further research.

# 2

# Literature Review

In this chapter, the literature relevant for this research is discussed. In the first paragraph, some definitions of the nearshore coastal area are defined. Subsequently, the modern coastal maintenance strategy is discussed, consisting of the nourishment strategies and applied performance indicators. A specific review of the Dutch policy is included as well, followed by a brief summary of numerical model approaches with specific attention to the acceleration techniques that reduce the computation time.

## 2.1. Coastal terminology

The transitional area between land and sea is the coastal zone (figure 2.1). It is separated into four regions: the coast, the beach, the shoreface, and the continental self. The beach region extents from the Mean Low Water (MLW) up until the the dune foot The shoreface extents from the MLW up until the point where the bathymetry is no longer influenced by yearly wave conditions. The region seaward of this point is referred to as the continental shelf. Landward of the Coastline, the coast is defined as the region where dunes dominate the topography.

The beach is further split up into the backshore and the foreshore, the former above and the latter below the Mean High Water (MHW). The breaker zone reaches from the first offshore breaking point (here dominated by a bar) up until the shoreline, located at Mean High Water (MHW). The shoreline is located at Mean Sea Level (MSL). The Dutch unit for the height is the 'Normaal Amsterdams Peil' (NAP), more or less equal to the MSL. It is used interchangeably with the MSL in this thesis.

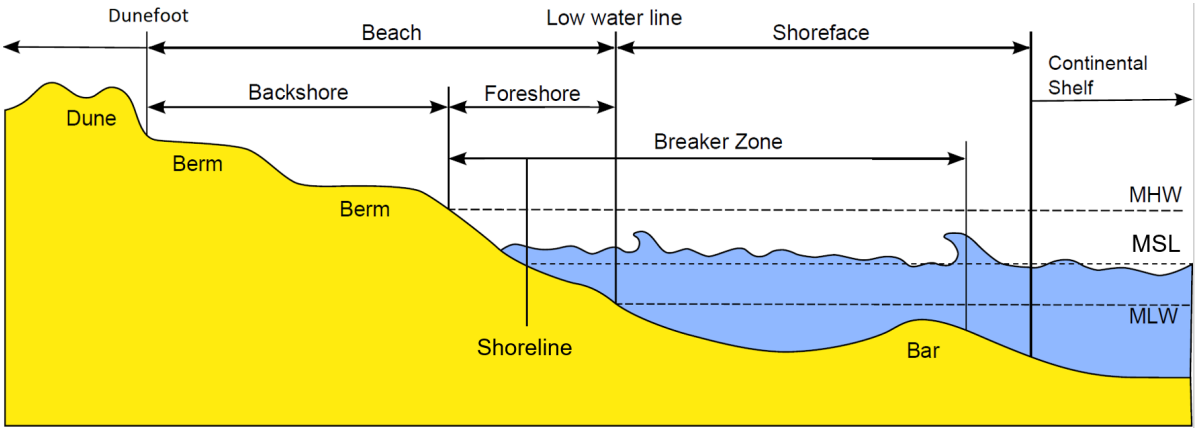


Figure 2.1: Definitions of the coastal zone referred to in this thesis. From U. S. Army Corps Of Engineers (2002)

## 2.2. Coastal maintenance

Coastal maintenance is defined as the process of preserving a sufficient level of safety and to maintain the various functions of beach and dune areas (Dean and Yoo, 1993). Maintenance of the coast, rather than countering the erosion was introduced world wide by application of beach fills developed in the 20th century, when a shift took place from the hard, stone groins, to the soft beach fill nourishments (Hanson et al., 2002). In The Netherlands, this shift took place in the 1970s. Mainly two types of nourishments are distinguished, the beach and dune nourishments, and the shoreface nourishments (figure 2.2). Average sizes of these interventions or nourishments are in the order of 2 $Mm^3$, requiring frequent re-nourishments (every 3 to 10 years) (Cooke et al., 2012, Hamm et al., 2002).

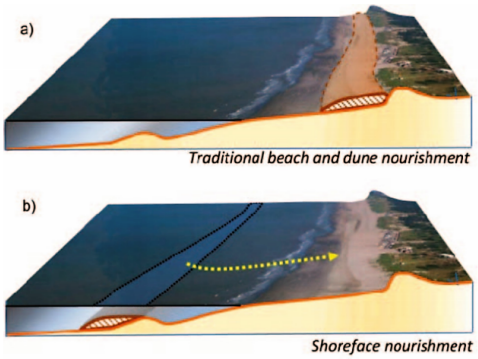


Figure 2.2: Schematisation of most applied used nourishments. a) Beach nourishments, b) Shoreface nourishments (from Stive et al. (2013)

### 2.2.1. Beach nourishments

Initially, beach and dune nourishments were executed to prevent breaching of dunes (figure 2.2a). The first projects aimed at strengthening locally weak spots. Nourishments were placed using pipes and shovels on the backshore. Their cross-shore size is typically in the order of 100 $m^3$ per m beach width, although initially, these were smaller. Modern beach nourishment are defined as large near-shore perturbations that eventually equilibrate with the surrounding system via longshore and cross-shore sediment transport (Komar and J., 1983).

Although there are numerous reasons for (beach) nourishments, in general the goal of a beach nourishment is to counter structural erosion by the addition of sediment. It is considered a local solution, since its aim is repairing the coastal system at the location where it is needed. Dean (1992) argues there are three main advantages to beach nourishments:

- Increase in desirability of residing along shorelines and values of structures and infrastructure behind the shorelines make additional costs of these nourishment justifiable to provide protection against storms and recreational amenities.
- As a second argument it is stated "This approach has only beneficial effects on adjacent shorelines." Whereas groins or detached breakwaters trap any sand to the disadvantage of littoral drift, a beach nourishment merely adds sand to the adjacent beaches.
- As a third argument, he mentions that beach nourishments can restore habitat in areas where it has been degraded through erosion.

### 2.2.2. Shoreface nourishments

In the 1990s, the Dutch introduced a policy which stated that the coastline was to be maintained at its position of that year under the name of the Dynamic Preservation Act (Rijkswaterstaat, 1990). During this same period, the shoreface nourishments were introduced (figure 2.2b). The cross-shore size is roughly four times as large as the beach nourishments. These nourishments were placed in front of the shore at depths of around 5 m below Mean Sea Level (MSL). This feeding in the shoreface results in a cross-shore feeder function, by a stimulation of gradual movement of sand in landward direction leading to a seaward movement of the shoreline, or a trapping of sediment behind the shoreface nourishment (Van Duin et al., 2004). Also, these shoreface nourishments may serve as the building of sand buffers, reducing the incoming wave energy and long-shore wave driven currents higher up the profile, thus erosion of the coastline (De Schipper et al., 2016). The advantages of the shoreface nourishments over the beach nourishments are:

- First off, based on findings over the years it has been concluded that the placement of sand on the shoreface near the breaker zone is equally effective as the more traditional beach nourishments, since shoreface nourishments are placed by marine equipment rather than land-based equipment (Bruun et al., 1996, Stive et al., 2013). As a result, the shoreface nourishments are the more economical alternative per cubic meter.
- A second benefit is the lower degree of disruption to recreational activities on beaches. These nourishments were less intrusive on beach amenity, and thus more acceptable to the public (Cooke et al., 2012).

- Thirdly, this methodology is regarded as more appropriate to import sediment and to let nature do its job, instead of counteracting the natural forcing factors (Hamm et al., 2002). It allows sediment to be re-deposited onto the beach via natural forces such as wave and wind, such that the degree of sorting and patterns that are formed of accumulation may more closely match the native beach sediments.

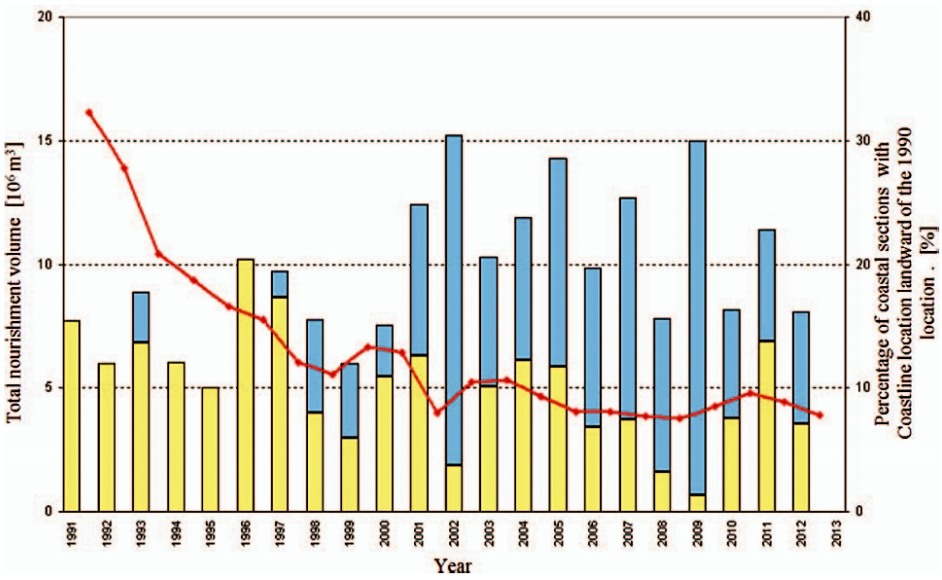


Figure 2.3: Yearly nourishment volumes along the Dutch coast since 1990. The yellow bars indicate the beach nourishment volumes, and the blue bars the shoreface nourishments. The red line depicts the percentage of coastal sections where the position transgressed the desired state of 1990. The Sand Engine project, a mega-feeder nourishment of 21.5Mm$^3$ is not included (Stive et al., 2013).

Because of these reasons, shoreface nourishments quickly gained popularity over the beach nourishments and the majority of nourishments along the Dutch coast today are executed at the shoreface, rather than on at the beaches or dunes (figure 2.3).

### 2.2.3. Performance and behaviour indicators for evaluation of nourishments

Since the initiation of the soft solutions, different evaluations have been executed to assess the effectiveness. More specifically, these methods quantify the performance based upon the three main goals of a nourishment: flood protection, recreation, and nature. Related to the effectiveness of flood protection, the following indicators have been used (Roelse (1996), (Hillen and Roelse, 1995), (Roelse, 2002), (Hanson et al., 2002), (Margheritini et al., 2007)):

- The erosion rate before and after the placement of a nourishment. This can be expressed volumetrically, in a surface area, or a (representative) coastline position.
- The ratio between the volume of sediment that was 'lost' to a nearby area *with* the nourishment over the sediment 'lost' *without* the nourishment.
- The actual lifetime versus the design lifetime in maintaining the dune profile.

Additionally, Dean (2002) expressed the performance of nourishments in terms of the macro-scale behaviour of nourishments. First of all, he represented the behaviour by a diffusivity coefficient. By analysing the observations and computing the remaining volume in the area, an approximation of this indicator can be made. Secondly, he assessed the movement of centre of mass of the added sediment volume, a result of a difference between size of the native and the artificially placed sediment. In the case of a difference, the centroid will move alongshore. When the sediment size is of the nourished sediment is smaller, this will lead to a higher sediment transport, and thus a downdrift migration. In case of larger nourished sediment, the opposite is true, causing an updrift of sediment (further elaborated on in section 2.3.1).

### 2.2.4. The Dutch policy for coastal safety

The Dutch government enacted a law in the 1990s that dictates it is responsible for maintaining the coastline position of that year. In line with this law, a decision tool was developed to enable an objective assessment of the need for nourishments at a location along the coast.

To clarify the objectives of maintenance of the Dutch coast, the Dutch policy was analysed (Mulder et al., 2011, Van Koningsveld and Mulder, 2004). They concluded maintenance of the Dutch coast occurs by assessment of the coast at three scales (figure 2.4). Each scale comprises a coastal cell with its own temporal and spatial size. A coastal sediment cell is defined by: *"A length of coastline and associated near-shore areas where movement of sediments is largely self-contained*". It specifies an area for which the sediment budget can be determined and thus provides input for a quantitative analysis of coastal erosion and accretion. The larger scales provide boundary conditions to the smaller scales.

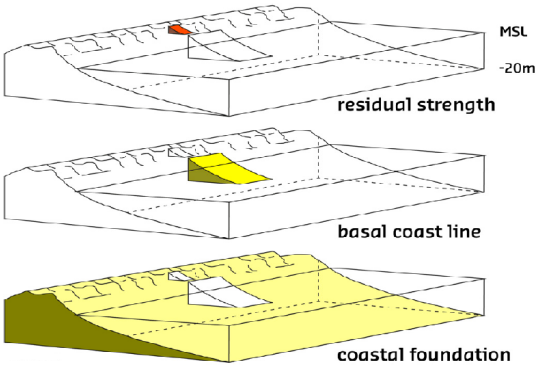


Figure 2.4: The three scales in coastal management of the Dutch policy for coastal safety. 1) Residual Strength O (days,meters), 2) Basal Coast Line (years, kilometres), 3) Coastal foundation O (decades,10s-100s kilometres). After Mulder et al. (2011)

A Frame-of-Reference approach was developed that can be applied to evaluate the health of the beach at each of the scales (figure 2.5). At the highest scale, the strategic objective is defined by law: *"To guarantee a sustainable safety level and sustainable preservation of values and functions in the dune area"* (Mulder et al., 2011, From Delta Committee, 1958). With the most important tactical objective being: *"The coastline will be maintained at its position in the year 1990"* (Rijkswaterstaat, 1990).

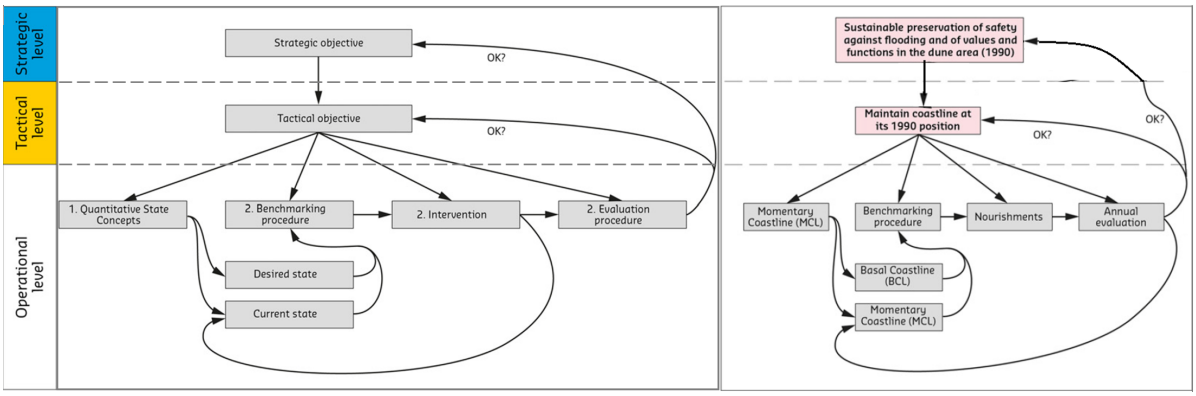


Figure 2.5: a) The Frame-of-Reference for implementing coastal erosion management policy in the Netherlands b) Application of the approach on Basal Coast line. Adjusted from De Weerdt (2015))

The residual strength is quantified in either terms of the dune foot position, or the dune volume. On the second scale, a representative shoreline is quantified. On the third scale, the coastal foundation, no quantitative state concept has yet been developed. In practice however, the momentary coast line has been used predominantly for deciding on the need for nourishments. For the quantification of the Dune foot and dune volume, reference is made to e.g. Hillen et al. (1991); Tonnon and Nederhoff (2016).

To ensure the coastline is maintained, the quantitative state concept of the Momentary Coastline (MCL) was introduced. It defines the coastline position as a function of the volume of sand in the near shore zone (Van Koningsveld and Mulder, 2004). This indicator is compared to the Basal Coastline (BCL), the reference coastline from 1990. A trend line is extrapolated five years into the future from the previous ten years to derive a Test Coastline (TCL). A nourishment is executed if: $TCL < BCL$. The nourishment policy has been effective, reducing the percentage of sections where the location of the MCL is landwards of the 1990 baseline (figure 2.3).

Roelse (2002) quantified the effects of the nourishment policy on the dunes as well. He concluded the applied nourishment strategy had resulted in an overall seaward migration of the dune foot and increase of the dune volume over the period 1980 and 1998.

## 2.3. Predicting nourishment evolution; an analytical model

The application of analytical models to understand and predict shoreline change has proven a useful and elegant technique for engineering applications (Horikawa, 1988, Komar, 1998, Larson et al., 1997, Pelnard-Considere, 1956). The advantage of mathematical models is that they provide a concise and quantitative means to describe long term trends of shoreline perturbations. Also they enable a qualitative and quantitative understanding of the morphological response to the physical forcing conditions. Analytical models originate from closed form solutions that relate the basic physics to the essential features of a beach response. With it, the behaviour is more clearly derived from analytical models, than more complex and computationally intensive numerical models. A second advantage is that they provide a starting point with which to rapidly estimate the developments of a proposed shoreline perturbations. The disadvantage of these models is that its results are based upon a number of simplifications and assumptions. Awareness is stressed when deriving conclusions from the results without a consideration of simplifications and assumptions.

### 2.3.1. Theory

The aim of one-line models is to describe the medium to long term variation of the coast. The one-line model was first proposed by Pelnard-Considere (1956). The cross-shore profile is assumed to be in an equilibrium profile. An approximation of the equilibrium profile was first proposed by Bruun (1954). He examined profiles from Denmark and Monterey Bay, CA and proposed the following relation:

$$h(y) = \psi y^{2/3} \tag{2.1}$$

Where $h$ is the water depth at a distance y from the shoreline and $\psi$ is a 'profile scale parameter' with dimensions of length to the 1/3 power. Later it was shown that parameter $\psi$ is to be related approximately linearly to the fall velocity $w$ (Dean, 2002);

$$\psi = 0.067 w^{0.44} \tag{2.2}$$

Where the settling velocity $\omega$ can be derived from Hallermeier (1981):

$$\omega = 14 D_{50}^{1.1} \tag{2.3}$$

With $D_{50}$ the median grain diameter. Under the assumption of an equilibrium beach profile, all depth contours are parallel. Based on this assumption, the shoreline change represents the changes observed in the active region, defined here as the depth region between which waves induce a sediment transport, i.e. the depth of closure and minimum of either the wave run-up and the berm height (B) of the coast:

$$D = h_c + B \tag{2.4}$$

The depth of closure describes the seaward limit of effective seasonal profile fluctuations and can be approximated by Hallermeier (1978):

$$h_c = 2.28 H_e - 68.5 \frac{H_e^2}{g T_e^2} \tag{2.5}$$

Where $h_c$ is the depth of closure and $H_e$ and $T_e$ are the effective significant wave height and period which is exceeded only 12 hours per year or 0.137% of the year. It is noted that because of the construct of the exceedance variable, the closure depth may differ per year. Furthermore, since in general the construction slope of a nourishment may be rather steep, sediment transport at depths greater than the closure depth may occur initially due to gravity accentuating the development of the profile.

In the one-line model, it is assumed no alongshore sediment transport occurs seaward of this depth. In the assumption of a fixed equilibrium cross-shore profile, a change in the shoreline position $\Delta y$ represents the change in the overall beach profile in the active region:

$$\Delta A = \Delta y D \tag{2.6}$$

Where $\Delta A$ denotes the change of the cross-sectional area of the cross-shore profile in the active region and D the height of the active region. This is only valid in cases where the gains to or losses of volume from a beach profile are associated with a sand size compatible with the native material, or after the equilibrium

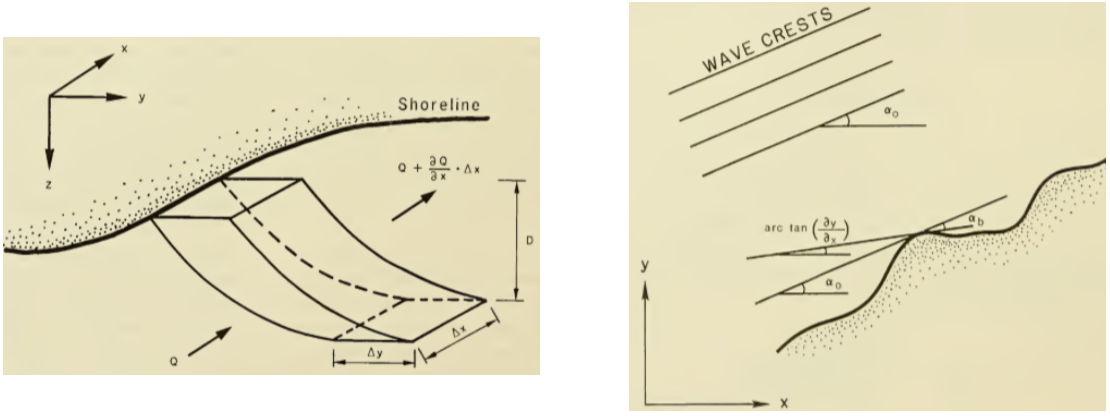


Figure 2.6: a) Visualisation of conservation of mass in a schematised equilibrium cross-shore profile b) Definition sketch for geometric properties, from: (Hanson and Kraus, 1987).

profile of the new sediment has been reached. Though for either of these conditions, it does hold for any arbitrary shaped profile, including sub-tidal bars.

The flux in sediment transport parallel to the coastline and the change of cross-sectional area of the beach make up for the conservation of mass (see figure 2.6a):

$$\frac{\delta Q}{\delta x} + \frac{\delta A}{\delta t} = 0 \tag{2.7}$$

With Q the longshore sediment transport rate, x the space coordinate parallel to the trend of the shore line, and t the time. The equation balances the shoreline change to the sediment transport rate. A general expression of the longshore sediment transport is:

$$Q = Q_0 \sin 2\alpha_b \tag{2.8}$$

With $Q_0$ the amplitude of the longshore sediment transport, and $\alpha_b$ the incidence wave angle with respect to the local coastlines (see figure 2.6b):

$$\alpha_b = \alpha_0 - \tan^{-1}\left(\frac{\delta y}{\delta x}\right) \tag{2.9}$$

Where $\alpha_0$ denotes the angle of breaking wave crests relative to an axis set parallel to the trend of the shoreline (figure 2.6). Linearisation of equation 2.8 and application of Taylor series expansion to the first order leads to:

$$Q = Q_0\left(2\alpha_b - 2\frac{\delta y}{\delta x}\right) \tag{2.10}$$

Assuming $Q_0$ and $\alpha_b$ are independent of space and time, the diffusion equation is derived from equation 2.6, equation 2.7, and equation 2.10:

$$\frac{\delta y}{\delta t} = G\frac{\delta^2 y}{\delta x^2} \tag{2.11}$$

with

$$G = \frac{2Q}{D} \tag{2.12}$$

### Solutions for the Longshore-sediment transport

Sediment transport is the integral of the product of the concentration of sediment in the water column and the displaced volume in a window of time.

The longshore transport $Q$ can be expressed in a function of the product of the energy flux $(Enc)_b$ per unit length of wave crest is at breaking wave height:

$$P_0 = \frac{\rho g}{16} H_b^2 c_g \tag{2.13}$$

With:

- $P$ the energy flux [J/ms]
- $\rho$ the density of water [kg/m$^3$]
- $g$ the gravitational acceleration [m/s$^2$]
- $H_b$ the breaking wave height [m]
- $c_g$ the group velocity of the waves [m/s]
- $\alpha_b$ the incidence wave angle with respect to the local coastlines [deg]

To account for an angle of the wave crests with the local shoreline $\cos\alpha_b$, and the longshore component $\sin\alpha_b$, leads to the 'longshore component of wave power'. AS $\cos\alpha_b \sin\alpha_b = 1/2 \sin 2\alpha_b$), this becomes:

$$P = P_0 \sin 2\alpha_b \tag{2.14}$$

If longshore transport is only driven by the waves, it can be imagined that both concentration of sediment and the longshore current velocity can be related to the incoming wave height, the two contributing factors to sediment transport (**?**). The Coastal Engineering Research Center (CERC) empirically relates the longshore component of wave energy flux to the immersed sediment moved by a transport coefficient K, i.e

$$I = KP \tag{2.15}$$

With

- $I$ the immersed weight of the sediment transport [J/ms]
- K the sediment transport coefficient [-]
- $P$ the energy flux [J/ms]

The sediment transport Q can be substituted by the relation

$$Q = \frac{I}{(\rho_s - \rho) g (1-p)} \tag{2.16}$$

Where:

- $\rho_s$ the density of the sediment [kg/m$^3$]
- $\rho$ the density of water [kg/m$^3$]
- p is the in-place sediment porosity [-]

leading to:

$$Q = \frac{\rho K}{16(\rho_s - \rho)(1-p)} H_b^2 c_g \sin 2\alpha_b \tag{2.17}$$

At shallow water, $c_g = c_b = \sqrt{g h_b}$, and given $H_b/h = \gamma$, and the $s = \frac{\rho_s - \rho}{\rho}$ the longshore sediment transport can be rewritten as:

$$Q = \frac{\rho K H_b^2 c_b}{16(\rho_s - \rho)(1-p)} \sin 2\alpha_b = \frac{K H_b^{5/2} \sqrt{g/\gamma}}{16(s-1)(1-p)} \sin 2\alpha_b \tag{2.18}$$

With:

- $c_b$ the wave celerity of waves at the point of breaking [m/s]
- $\gamma$ the ratio between the breaking wave height and the water depth at breaking[-]
- s is the sediment specific gravity [-]

The transport coefficient K has not been made explicit so far. Ideally, beach nourishment material matches with the native sediment. In some cases this is not feasible. With these projects the coarser or finer sediment will no longer experience the same transport rate along the shore parallel portion of the project as that is flowing toward and away from the project. In other words, the diffusivity coefficient G will no longer be uniform along the coast. If for example the nourished sediment is smaller than the native, transport rates updrift will be smaller, while sediment transport rates at the project will be higher. As a result, the centre of mass of the planform will migrate updrift and downdrift for $K_F < K_N$ and $K_F > K_N$ respectively (Dean, 2002), with F and N denoting Fill and Native sand respectively.

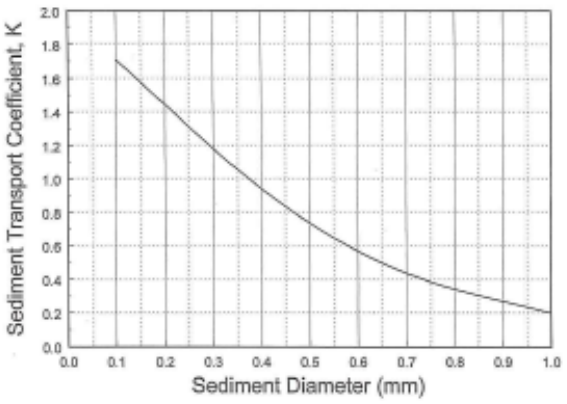


Figure 2.7: Transport coefficient K

Kamphuis (1991) proposed an alternative longshore sediment transport formulation, that includes the influence of the peak period, the bed slope, and the median grain size:

$$Q = K_2 H_b^2 T_p^{1.5} S^{0.75} D_{50}^{-.25} sin^{0.6}(2\alpha_b) \tag{2.19}$$

With:

- $K_2$ a dimensional transport coefficient [$m^{1.25}s^{-2.5}$]
- $\gamma$ the ratio between the breaking wave height and the water depth at breaking [-]
- $T_P$ the nearshore peak wave period [s]
- $S$ the mean slope in the breaker zone [-]
- $D_{50}$ the median grain size [m]

Field studies of Kamphuis (1991) showed the a value of the transport coefficient of $K_2 = 0.0023 m^{1.25}s^{-2.5}$. Here, the sediment transport is proportional to $H^2$ instead of $H^{2.5}$, which "...corrects [for] the criticism often levelled at the earlier expressions that they over-predict sediment transport rate in major storms." The equation has a higher sensitivity to the wave period, while some inverse variation exists with the sediment grain size.

### Formulae of the diffusivity equation

Following the longshore sediment equations, and the diffusivity equation (2.12), four versions of the diffusivity coefficient are distinguished.

First, the most elementary solution is found by application of the CERC formulation of the sediment transport (equation 2.18). Assuming $\alpha_b$ is small, the diffusivity becomes:

$$G = \frac{K H_b^{5/2} \sqrt{g/\gamma}}{8(s-1)(1-p)D} \tag{2.20}$$

To account for the incidence of the wave angles, results in:

$$G = \frac{K H_b^{5/2} \sqrt{g/\gamma}}{8(s-1)(1-p)D} \cos\alpha_b \tag{2.21}$$

An alternative is adopted from the equation for the longshore sediment transport by Kamphuis (1991). This alternative includes the influence of the peak wave period and the mean bottom slope in the breaker zone:

$$G = \frac{2K_2 H_b^2 T_p^{1.5} S^{0.75} D_{50}^{-.25}}{D} \frac{0.6}{\sin^{0.4} 2\alpha_b} \cos 2\alpha_b \tag{2.22}$$

### 2.3.2. A solution of the diffusivity equation

Many solutions to the diffusivity equation are available, and because of the linearity of this equation solutions can be superposed. Here, only one idealised solution and the application developed by Dean (2002) are considered. This solution considers an infinitely long beach and a uniform background erosion. It is based on the linear the diffusion or conduction equations. The solution is a Gaussian of form:

$$y(x,t) = \frac{Y}{\sqrt{2\pi\sigma^2}} e^{-\frac{(x-x')^2}{2\sigma^2}} \tag{2.23}$$

With Y the (cross-shore) seaward extension of the nourishment, x is the location along the shoreline, and x' is the x-coordinate at the peak of the beach nourishment. Applying $2Gt = \sigma^2(t)$, rewriting gives:

$$y(x,t) = \frac{Y}{\sqrt{4\pi Gt}} e^{-\frac{(x-x')^2}{4Gt}} \tag{2.24}$$

The above displays the influences of parameters on the duration related to the amplitude reduction of the initial nourishment. Most striking seems that the longevity of the project varies with square the project length and inversely with the 2.5 power of the wave height, while it is only mildly related to the sediment size (via the transport coefficient K). The depth of closure reduces the diffusivity linearly

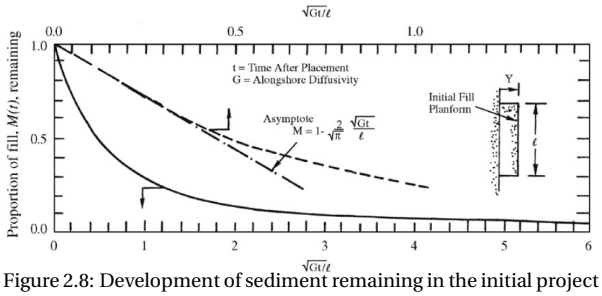


Figure 2.8: Development of sediment remaining in the initial project area, given an initially rectangular shape, from Dean (2002)

By integration of equation 2.24 over the length (l) of the initial nourishment, the development of the portion of sediment remaining in the initial project area can be derived. The erosion rate of the sediment remaining in the initial area is shown to decelerate over time. Figure 2.8 depicts the normalised solution of $M(t)$ over $\frac{\sqrt{Gt}}{l}$. The integration can be used to approximate the value to estimate the longevity of a project. For example in the half-life $t_50$ can be computed as (using figure 2.8) becomes:

$$t_{50} \approx 0.46^2 \frac{l^2}{G} \tag{2.25}$$

Another interesting relation that was found was relates the cross-shore extent inversely to the spreading:

$$\frac{y}{Y} \propto \frac{l}{\sqrt{Gt}} \propto \frac{l}{\sigma} \tag{2.26}$$

### 2.3.3. Assumptions and limitation of the derivation to the diffusivity coefficient

Before derivation of conclusions, the assumptions and limitations of the applicability must be reviewed critically. In the above derivation, the following assumptions/limitations have been made throughout the derivation (Pelnard-Considere, 1956), (**?**), (Hanson and Kraus, 1987):

1. The profile shape is constant in time and space: an equilibrium beach profile. The volume change can be simplified to the coastline change. multiplied by the height of the active region (the closure depth and the berm height, see equation 2.6).
2. In line with the previous assumption, longshore sediment transport occurs uniformly over depth in the active region of the profile.
3. The longshore sediment transport Q is proportional to the incident wave angle. As a result of this assumption, the centroid of a perturbation does thus not migrate over time, irrespective of the angle of incidence.
4. The angle between the coastline and the angle of breaking waves is small ( $cos2(\alpha_b) \approx 1$).
5. The shoreline change due ($\beta$) to a beach nourishment is assumed to be small $\beta \leq 25$ deg). The influence of a perturbation is mostly of influence on the sediment transport at the end transitions. The local wave transformation patterns are altered here, which results in higher losses near the edges of the perturbations (Elko and Wang, 2007).
6. It is assumed the gradients of wave set-up along the coast are negligible, i.e. gradients in the background erosion of a perturbation are neglected.

7. An infinitely long beach is considered.

With respect to the second assumption, the following remark is made. At the head of a nourishment erosion will create scarps with possibly (temporarily) steep slopes, that collapse after a while, erode, and scarps will develop again, in a vicious cycle. On the other hand, accretion only occurs up until the wave-run up. creating a difference in the cross-shore profile along the coast(Dean, 2002).

### 2.3.4. Influence of high angular waves on diffusivity of shoreline perturbations

The longshore sediment transport rate Q is a function of of the incidence wave angle $\alpha_b$. The transport rate increases up until a critical level where $\alpha_c < 42$ deg, after which it decreases again (Ashton et al., 2001). In case of a low angular waves (LAW), perturbations diffuse over time, as explained in the previous section. In case of these LAW a coast is considered stable. Ashton et al. (2001) extended the analytical solutions. They showed that in case of high angular waves (HAW) ($\alpha_c \geq 42$ deg), coasts may be unstable, or diffuse negatively. At these unstable coasts, macro-scale shoreline sand waves (SSW), that continue to grow over time are to be expected according to the study. Shoreline sand waves are for instance observed along the coast of West-Africa, (figure 2.9).

It was shown by Falqués and Calvete (2005) that the critical value $\alpha_c$, indicating high angular waves and an unstable coast, is in fact a minimum value. The analytical solution was extended further by accounting for the influence of the slope of the shoreface and the wave length, with milder slopes and longer wave lengths increasing the critical value.

The extended analytical solution was applied to the Dutch coast. The Dutch coast is characterised by HAW from the south west or the north. Small SSW may have been observed in the order 1km and 10m in the cross-shore (Ruessink and Jeuken, 2002). From the study it was concluded that the Dutch coast is stable. It was concluded that if all waves would originate from the SW, the coast would indeed have been unstable. The presence of swell waves prevent an unstable coast. In the study it was further concluded that spontaneous development of SSW requires at least 80% of waves to be HAW, a requirement supposedly not met in case of the Dutch coast (van Den Berg et al., 2012).

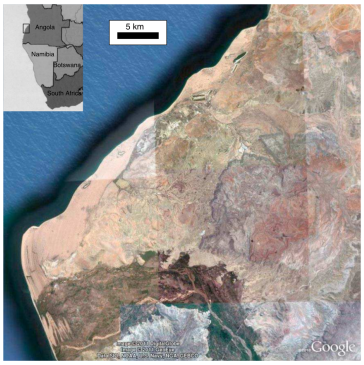

Figure 2.9: Shoreline sand waves with a wavelength of about 3 km along the coast of Angola, south of Baia Farta (van Den Berg et al., 2012, From Google Earth imagery)

## 2.4. A 2D model

The simple analytical model developed by Pelnard-Considere (1956), followed by one line models (Komar, 1998), (Horikawa, 1988), showed to have satisfactory results. As mentioned, the 1D (analytical or on-line model) approach is based upon a number of limitations and assumptions, described in section 2.3.3. If modelling of a nearshore sandy coastal area is required where the limitations of the 1D models are not met and/or the assumptions at not valid, a 2D model may be an attractive alternative.

From the 1980s and 1990s, 2D numerical models were added as an alternative, predominantly for river engineering. Early applications of 2D models were lesser successful in coastal areas. Results were highly sensitive to small disturbances. In 2004 the Delft 3D model was introduced Lesser et al. (2004). This model has shown to be capable of producing many of the relevant processes in coastal environments, e.g. wind shear, wave forces, tidal forces, and drying of intertidal flats. As a result, Delft3D can be applied to a wide range of nearshore coastal situations, with specific applicability to complex sedimentation and erosion problems in complicated hydrodynamic locations. Over the years, increasing computation power has made 3D modelling more common, enabling the inclusion of the return flow, bed-slope effects, and wave asymmetry Deltares (2014).

This paragraph briefly elaborates on the structure of the numerical model. Delft3D is used as an example, since the analysed simulations of 2DH numerical models in this thesis are made with Delft3D. Applied equations are mentioned, but not all included in this review. Reference is made to respective literature. In the second part, different acceleration techniques of Delft3D are discussed that significantly reduce the computation time.

### 2.4.1. Structure

In case of a 2D numerical model, the cross-shore profile is not in a cross-shore profile any more The starting point is often an initial arbitrary (design of a) bathymetry. Consequently, developments of the coastal environment are computed using the system of unsteady shallow water equations.

The structure of Delft3D is given in figure 2.10. A full description of the structure is given by Lesser et al. (2004) and summarised briefly here. The basic structure of Delft3D consists of an iterative feedback loop between the hydrodynamics and the morphology, referred to as online modelling (versus offline modelling, where the bathymetry is not updated). The tidal hydrodynamics are derived from unsteady shallow-water equations in two or three dimensions. The system of equation is composed of the horizontal momentum equation, the continuity equation, the transport equation and a turbulence closure model. Developments in the vertical are assumed to be hydrostatic in the water column, since it is assumed that the vertical accelerations are small compared to the gravitational acceleration. To discretise the equations in space, the considered coast is covered in a rectangular, curvilinear, or spherical grid.

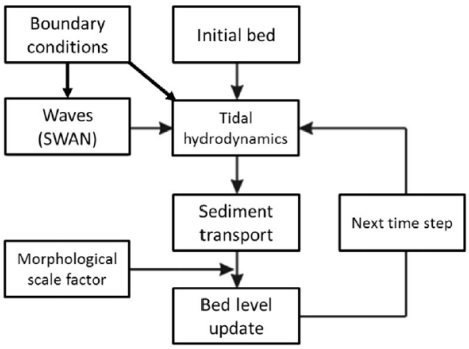

Figure 2.10: Morphodynamic cycle as applied in Delft3D

The waves that are impose=d onto the tidal hydrodynamics are computed with the SWAN module, which computes the properties of waves in the nearshore region (Booij et al., 1999). It accounts for refraction over an arbitrary bathymetry and current field. Further, the SWAN module computes the non-linear wave-wave interaction, wind generated waves, energy dissipation, and depth induced wave breaking.

Sediment transport can be computed using several sediment transport formulations. The Van Rijn et al. (2007)formulation is frequently used. Delft3D can be used for steady and oscillatory flows with particle sizes between 0.1 - 2mm.

The exchange of the sediment in suspension from the bottom computational layer to the bed and vice-versa is computed with the sediment deposition and erosion fluxes. At every hydrodynamic time step the bathymetry is updated, providing the required information to compute the hydrodynamics of the following time step.

### 2.4.2. Computational acceleration techniques

In general, morphodynamic changes occur at a larger time scale than hydrodynamic changes, e.g. the tidal flows change significantly on a scale of hours, whereas the morphology of a coastline occurs on a scale of weeks to even years. This provides the opportunity to reduce the computational effort significantly. Two reduction techniques based on this phenomenon are discussed that reduce the computational time. Additionally a widely applied method referred to the parallel method is reviewed.

#### Morphological acceleration factor

Latteux (1995) proposed the application of an elongated tide as a method to reduce the computation time considerably. In this approach, N successive tides are simulated by a small number of representative tides. This enables the use of longer time steps in morphological simulations, since application results in hydrodynamic changes more in the same order as the morphological changes. Deciding on the representative tides is done based upon field measurements, such that sediment transport rates of the representative tides are equal to that of the actual set of natural tides.

In line with the above, the morphological acceleration factor was proposed by Lesser et al. (2004). It multiplies the sediment fluxes from the bed at each computational time step, and the number of hydrodynamic time steps is reduced likewise. Use of this acceleration factor is allowed if the hydrodynamics is not significantly influenced. Applications of the acceleration factor have shown to remain stable in moderately morphological situations with a factor excessing 1000, although usually of O (10) Deltares (2014). Preferably results are calibrated. In case it is a predictive model, validation of the correct application of a morphological factor can be done by comparing model results of a simulation with a factor twice as low as initially applied. If no differences are observed, it can be stated the factor does not influence the model results.

Application of the morphological factor can be an effective measure to reduce the computational effort significantly. It is noted though, that when it is applied to a coastal area the number of events of the tidal

cycles is considerably reduced. As a result, possible conflicts may arise in combination with limited sediment availability and bed stratigraphy simulations.

#### Wave reduction technique

The numerical model imposes the nearshore wave climate to compute the bathymetric changes. The wave climate consists of a large number of wave conditions, that differs in wave height, period and direction. To reduce the computation time, a representative wave climate can be derived, similar to the derivation of the representative tide presented by Latteux (1995). One method to derive the representative wave conditions is by manually selecting a set of conditions that approximately results in the same net and gross sediment transport rates.

Alternatively, the Opti program has been developed (Mol, 2007). This program is incorporated in Delft3D and can be used to reduce the number of wave conditions. The program uses the results of short morphological simulations that have been run with all the wave conditions. This input is used as a target, on which reduced wave climates are calibrated. Additionally, the duration of all the separate wave conditions is included, which is used as a weighing factor of the conditions. The program then reduces the wave climate by removing the condition that has the smallest influence on the sediment transport. Iteratively, the representative wave climate is derived, with newly adjusted weights that result in the best representation of the sediment transport rates.

#### The parallel online method

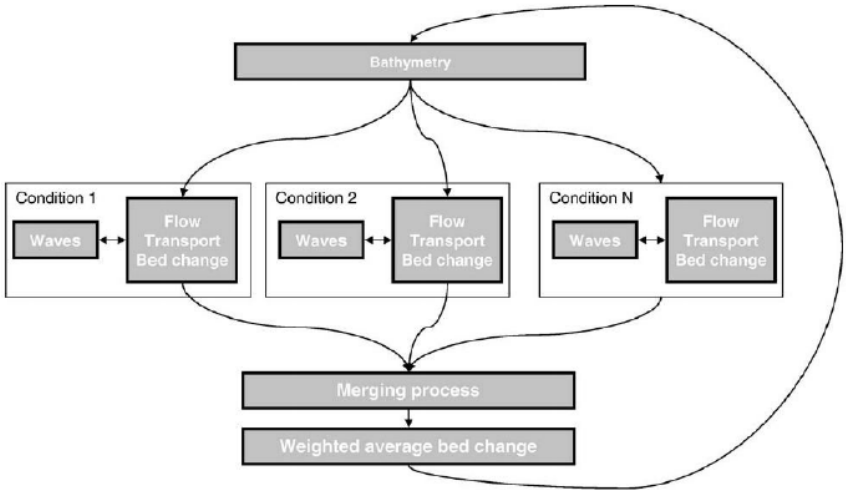


Figure 2.11: Parallel online scheme (Roelvink, 2006)

If the parallel online method is applied, or mormerge, the (representative) wave conditions are run simultaneously, using the same bathymetry (Roelvink, 2006) (figure 2.11). After each time step, the separate changes of the weighted average bed level changes are merged, considerably reducing the computational time.

### 2.4.3. Modelling assessment methodologies

Application of 2D numerical models demanded an objective measures to quantify the performance. Two commonly used model skill scores are discussed here; the skill scores proposed by Sutherland et al. (2004), and the shore line change skill score (Dean, 2002)).

#### Skill Scores

The most well known and frequently used skill score is referred to as the Brier Skill Score, or BSS (Sutherland et al., 2004). The skill score was derived by setting the following criteria to a validation tool of a numerical model:

- The statistic should be easy to understand

- Expert opinion should agree with the result
- It should be 'honest', or robust, i.e. not easily manipulated by changing boundaries
- Transferable between data-sets, i.e. non-dimensional.
- Take intuitive values
- Show skill rather than accuracy

Accuracy is here defined as a measure of the averaged difference between predictions and measurements, whereas skill is the accuracy of a prediction, relative to the accuracy of a baseline prediction (often defined as the initial bathymetry). The skill scores are derived by a number of statistical measures, including the Mean Absolute Error:

$$MAE = \sum_{i}^{N} \left| y_i - \hat{y}_i \right| \tag{2.27}$$

The Mean Squared Error:

$$MSE = \frac{1}{N} \sum_{i}^{N} (y_i - \hat{y}_i) \tag{2.28}$$

Which is commonly used in a rooted form, since this gives a value in the same units as the test variable:

$$RMSE = \sqrt{\frac{1}{N} \sum_{i}^{N} (y_i - \hat{y}_i)^2} \tag{2.29}$$

Using these statistical measures, three skill scores were developed, the Brier Skill Score, Root Mean-Square Skill Score, and the Mean Absolute Skill Score, denoted respectively as:

$$BSS = 1 - \frac{MSE(Y,X)}{MSE(B,X)} \tag{2.30}$$

$$RMSSS = 1 - \frac{RMSE(Y,X)}{RMSE(B,X)} \tag{2.31}$$

$$MASS = 1 - \frac{MAE(Y,X)}{MAE(B,X)} \tag{2.32}$$

Where B, X, and Y are sets of N of the baseline, measured, and modelled predictions respectively (e.g. for B $b_1$,$b_2$,$b_3$,...,$b_N$) occurring at the same place and time. Perfect agreement gives a score of 1, whereas the score is 0 if the model error is as large as the change that has been observed in the measurements compared to the initial bathymetry.

| Performance | BSS |
|---|---|
| Excellent | 0.5 - 1.0 |
| Good | 0.2 - 0.5 |
| Reasonable | 0.1 - 0.2 |
| Poor | 0.0 - 0.1 |
| Bad | <0.0 |

Table 2.1: Classification of the Brier Skill Score (from (Sutherland et al., 2004))

### The shoreline change

An alternative often used measure to quantify the performance of numerical models comprises of a comparison of the computed versus the observed shoreline change (Dean, 1992):

$$\epsilon \equiv \frac{\sum_i \left( \Delta y_{m_i} - \Delta y_{p_i} \right)^2}{\sum_i \Delta y_{m_i}^2} \tag{2.33}$$

Where i denotes the longshore position of the shoreline change, and m and p denote the measured and predicted change respectively. It is suggested to apply volume densities as well for a more reliable basis.

# 3

# The Sand Engine

In this chapter, the first Sand Engine is introduced. This first ever application of a mega-feeder nourishment is used as a case study throughout this thesis. First, the study site is briefly discussed. Subsequently, the goals of the Sand Engine and the monitoring program are mentioned. The main part of this chapter consists of an overview of findings related to the Sand Engine. The chapter ends with a review of the outcomes of simulation of 2D numerical models that have been developed for the Sand Engine.

## 3.1. The study site


Figure 3.1: a) Location of the Sand Engine along the Holland Coast. b) The Westland coast. c) aerial photograph of the Sand engine in July 2011 after construction (courtesy: Rijkswaterstaat/Joop van Houdt). After Luijendijk et al. (2017)

The Sand Engine is implemented in front of the Westland Coast of the Netherlands, just north of the Meuse estuary (figure 3.1). This coast has suffered from structural erosion, presumably since the 12th century. After a long period of narrowing of dunes as a result of the erosion, a storm caused a first breach occurred in 1564. Between 1564 and 1765, the coastline retreated approximately 1000m. In 1791, After many experiments to stop the structural erosion, stone groins were placed. These groins successfully reduced the retreat considerably to approximately 0.5 - 1 m/yr ((Van Rijn, 1995), (Hendriks, 2011), see appendix A for a more complete review of the historical developments.

The Westland coast is bound by the harbour moles of Scheveningen (The Hague) in the north. From the south, the nearshore alongshore sediment transport is completely blocked by the Noorderdam, built in the $19^{th}$ century, which makes the Westland coast a nearly closed coastal cell with a width of 17.2km. Estimates of the sediment transport show gross alongshore sediment transport in both directions are approximately 0.76 $Mm^3$ northward excluding pores, and 0.38 $Mm^3$ southward, resulting in a net yearly-averaged alongshore sediment transport of 0.38 $Mm^3$ (Van Rijn, 1995).

Before installation of the Sand Engine, the morphology was rather uniform alongshore. The beach has a mild slope (1:300), with a width of 150m. Before construction of the Sand Engine, the slope of the cross-shore profile of the surf zone (-4/+1m + NAP) was 1:55 (Van Rijn, 1995) The median grain size is roughly 250 $\mu m$.

Sub-tidal bars have been observed to migrate offshore in a cyclical manner, with return intervals of 4 - 16 years (Wijnberg and Terwindt, 1995). The coast is further characterised by occasionally narrow width of the dune area from the dune foot (in the order of 150 - 250 m) in the central Westland coast, up to greater widths just north of the constructed Sand Engine (500m). Dune heights on average are 10 - 15 m + NAP, but can reach heights locally of up to 20 m + NAP (Luijendijk et al., 2017).

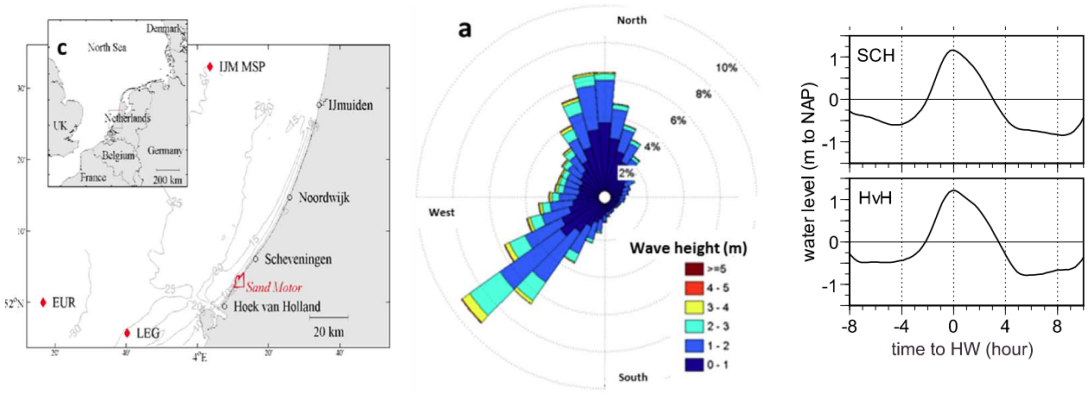


Figure 3.2: a) Location of measuring stations, b) Wave rose of 25 years of years of wave records at the Europlatform, c)Tidal curves at the Hoek van Holland (southern boundary of the Westland coastal cell). After Luijendijk et al. (2017) and Wijnberg (2002)

The tide is semi-diurnal, with a mean tidal range is 1.7m (1.98m and 1.48m for the spring and neap tide respectively). The asymmetry of the tide causes the rising period of the tide to be circa 4.5 hours, while the falling period is almost twice that period (figure 3.2). The amplitude of the flood tidal currents is roughly 0.7m/s (to the north east), while the ebb tidal currents tide are circa 0.5m/s (to the south west).

The wave dominated Westland coast is located on the shallow North sea. As a result, the wave climate is wind sea dominated. The annual mean significant wave height Hs = 1.3m, with wave periods of 5-6s (Wijnberg, 2002). The wave climate shows little spatial variation, but a clear seasoning in the wave heights results in Hs = 1.7m during the winter season and Hs = 1m in the summer. Waves are highly oblique, with dominant wave angles from the south west and north secondarily. The depth of closure is between 5 - 9m (Hinton and Nicholls, 1998).

Structural erosion of the Westland coast is caused by a reduction of the sediment supply from the rivers south of the Westland coast, ever since the 12th century. The recent construction of the Noorderdam resulted in a complete blockage of the sediment, accelerating the erosion (Luijendijk et al., 2017). To ensure a sufficient sufficient depth, the entrance channel of the Rotterdam Harbour is frequently dredged. All dredged sediment is placed on the below the shoreface (>-10m + NAP)of the Westland coast, which should compensate the losses of the Noorder dam for the bigger part (Tonnon and Nederhoff, 2016).

Nonetheless structural erosions have been observed, which required large nourishment volumes to ensure protection of the hinterland. Since the placement of the first nourishment in 1986, circa 55 $Mm^3$ of sand was added to the coast (including a nature compensation for the Port of Rotterdam and the Maasvlakte II and the Dixhoorn triangle, 18.4$Mm^3$). In more recent years, nourishment volumes have increased to approximately 1.7 $Mm^3$ per year, an equivalent of 100 $m^3$ per meter beach width per year (Luijendijk et al., 2017). An overview of all executed nourishments is given in figure 3.3, see also appendix A.

## 3.2. The Sand Engine nourishment design

In the original design, the cross-shore extent of the Sand Engine was 1.5km from the original shoreline, while its alongshore width was designed at 2000m. The design cross-shore profile was aimed at 1:50, to agree with the natural slope of 1:55. The planned nourishment was designed to be placed up until a depth of -8m + NAP, in line with the depth of closure.

The design included sharp coastline angles intended to stimulate a rapid distribution of the sediment. The distinctive design of the hook-shaped peninsula was inspired by the potential added values for recreation and natural purposes. The lagoon, protected from waves on the north side of the SE, was meant to offer habitats for fish, and recreation for kite surfers and swimmers. On the south side of the SE, a lake was included in the design for the habitat of birds and to prevent the freshwater lens in the dunes to migrate seaward, which

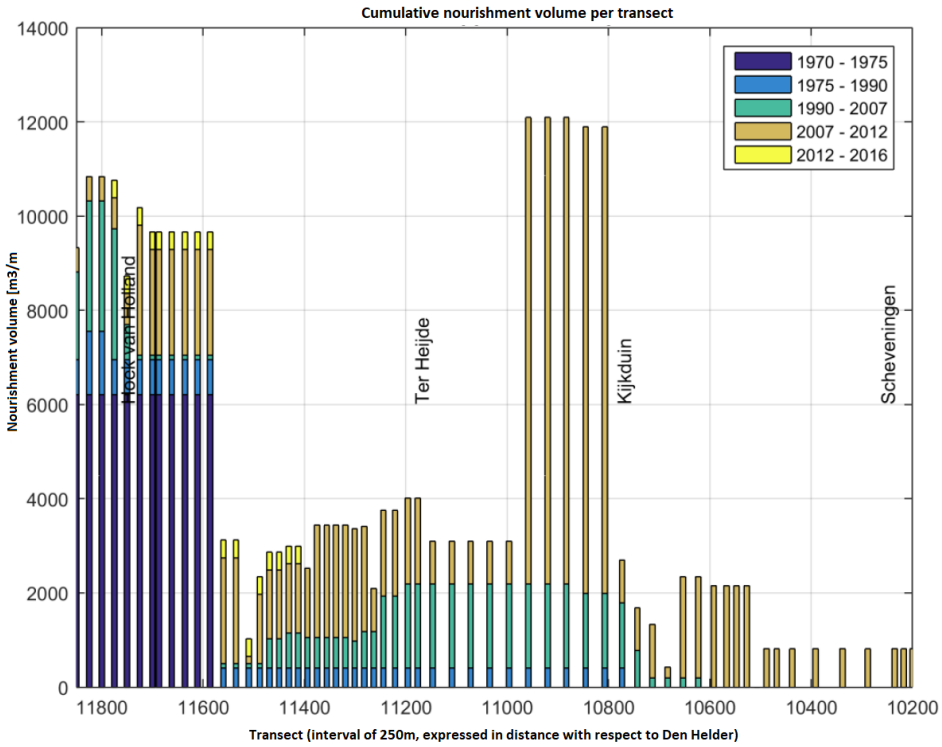


Figure 3.3: Overview of cumulative nourishment volumes per transect (cross-shore profile of the coast each 250m). Horizontal axis expresses the distance with respect to Den Helder, see figure 3.1, adjusted from (Tonnon and Nederhoff, 2016)

would otherwise unable the extraction of ground water from the landward dune area.

The design of the Sand Engine was implemented by the contractor with some alterations compared to the design. The actual constructed nourishment consisted of a peninsula and two flanking nourishments, with a total volume of 21.5Mm$^3$ of dredged sediment, originating from circa 10 km offshore. 19Mm$^3$ of the sediment was planned for the peninsula. Of the remainder of the nourishment, 2Mm$^3$ was intended for the northern, and 0.5Mm$^3$ for the southern flanks. The Sand Engine initially spanned a width slightly wider than originally planned with an alongshore extent of 2.4 km. On the other hand, the cross-shore extent was smaller than in the design, with a cross-shore extent of 1 km.

During construction of the Sand Engine, which took place between March and July 2011, grain size analysis revealed the mean D50 was circa 280$\mu m$ (De Schipper et al., 2016), a little larger than the mean sediment sizes measured in the natural coasts (250$\mu m$) (Wijnberg and Terwindt, 1995). The contractor implemented a steeper convex profile with on a slope of 1:32, rather than a concave profile as was planned, to stimulate the feeding mechanism. This reduced the initial cross-shore extent to 1km instead of 1.5km

## 3.3. Objectives with respect to coastal safety

De Weerdt (2015) extensively analysed the objectives of the Sand Engine as described in numerous reports in documents. The objectives can be divided into four themes: coastal safety, nature, recreation, and innovation and knowledge development. Elaborating on coastal safety, the following sub-objectives have been formulated in accordance with the Frame-of Reference approach (see section 2.2.4):

- Achieve sufficient volume of dunes between Hoek van Holland and Scheveningen for protection during dune erosion.
- Maintain the Basic Coast Line (BCL) between Hoek van Holland and Scheveningen.
- The coastal foundation in the coastal area between Hoek van Holland and Scheveningen grows with the sea level rise.

Further, De Weerdt (2015) concluded that it is unclear during what timespan the Sand Engine is to contribute to coastal safety, e.g. 20 years according to the Environmental Impact Assessment (Projectteam Zandmotor, 2010), and 50 years according to the monitoring program (Deltares and IMARES, 2011).

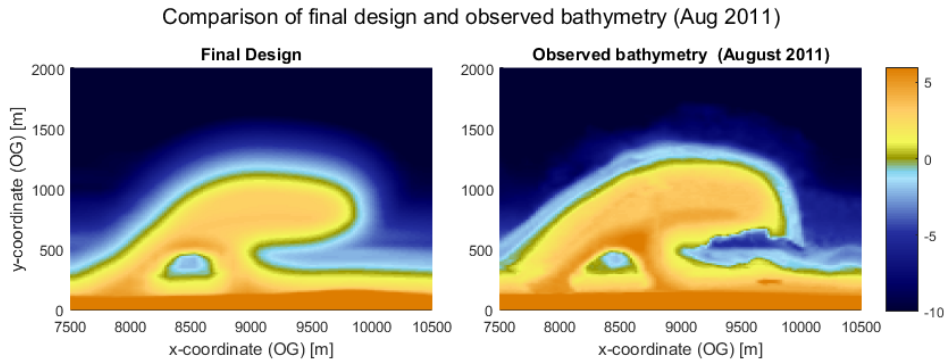


Figure 3.4: Final design of Sand Engine versus initial bathymetry. Colours represent the height of the bathymetry, further indicated with the contours with respect to NAP

## 3.4. Monitoring program

To assess the development of the SE and hereby assist in evaluation of the objectives, an unprecedented monitoring program was set up after the construction of the Sand Engine. The monitoring programs from which data is available are briefly discussed here. The survey areas are shown in figure 3.5. In appendix C a full overview of all available surveys is given.

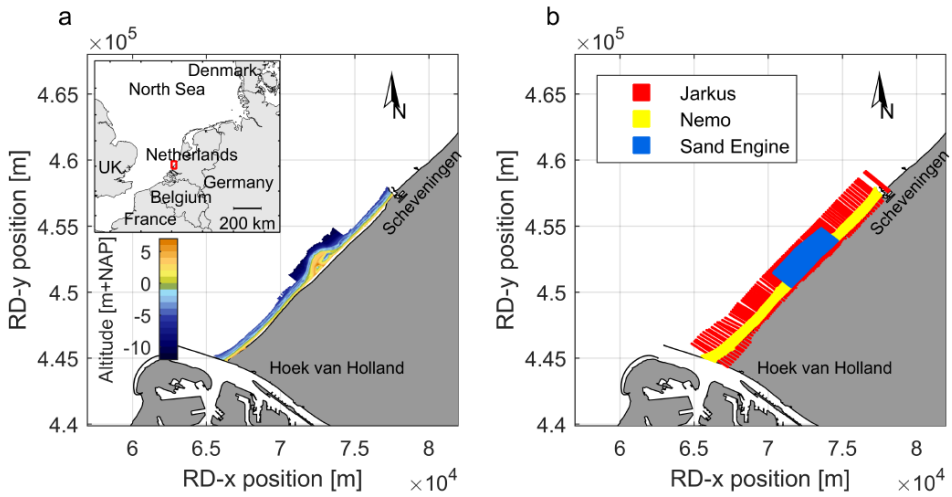


Figure 3.5: Survey areas of different programs.From Roest et al. (Submitted)

The Sand Engine surveys (blue, figure 3.5), reach from the shoreface (<-10m + NAP), up to the lower parts of the dunes (5m NAP), with a survey domain of 4.7km alongshore and 1.6km cross-shore. The survey grid consists of long 59 cross-shore transects, with a mean spacing of 80m. Additionally near the shore and on the northern side near the lagoon, 68 shorter transects were executed to reduce the alongshore spacing between transects to approximately 40m (De Schipper et al., 2016).

Parallel to the Sand Engine surveys, the Nearshore Monitoring and Modelling program (NeMo) also provides surveys that can be used for analysis of the Sand Engine (yellow, figure 3.5). As part of the goal of this program, to increase the understanding to predict the shape of the Dutch coast in future decades, the NeMo program monitors the remainder of the Westland on a bimonthly scale, between the lower part of the dunes (≈ 5m + NAP) and the lower part of the breaker zone ((≈-5m + NAP).

Thirdly, data is available from the "Jaarlijkse Kustmetingen" (JarKus), which are yearly coastal surveys (red, figure 3.5). Since 1965 the entire Dutch coast is monitored yearly to reaffirm the coastline position and to assess the coastal safety. It consists of circa 2500 transects, ranging from the dunes (>+10m + NAP) to the continental shelf (<-8m + NAP), with an alongshore spacing of circa 250m.

The data is retrieved using three different techniques (figure 3.6). All methods apply the real-time kinematic differential global position system (RTK-DGPS). First of all, sub-aerial sections of the beach were monitored with a four wheel drive quad bike. The sub-aqueous parts were surveyed via a jet ski mounted with

Figure 3.6: Survey techniques. a) 4WD quad, b) jetski, c) wheeled pole. From De Schipper et al. (2016).

a single beam echo sounder. Areas that were difficult to reach by either of these techniques were measured with a wheeled pole. Accuracy of the techniques are in the order of 5, 3, and 10 cm respectively (Huang et al., 2002). The data of both the Sand Engine and the NeMo surveys is retrieved by the same institution, during the same days with calm weather conditions.

## 3.5. Macro-scale developments

Figure 3.7 depicts the developments of the Sand Engine. The main developments of the Sand Engine are:

- In the middle section of the peninsula, a significant erosion is observed. As a result, the cross-shore extent of the coastline position has considerably been reduced. The shoreface has widened in the middle section.
- After the first six months, a pronounced spit northward had formed and elongated up to 300-400m, which nearly closed off the lagoon. Consequently, a channel developed that connected the lagoon to the open sea. This channel has been highly dynamic and has repositioned after storms multiple times, reaching lengths of up to 2700m. High current velocities had been observed up to 1m/s during rising and falling tide.
- In the southern area, an initially rapid accretion was observed, predominantly near the sharp angles of the southern edge of the Sand Engine (near x = 7500m of figure 3.4).
- The coastline developed into a Gaussian bell shaped curve. The curve widened over time, although after 2015 no further widening of the shoreline position could be observed. After 2013, the sub-tidal bars and coastline position seem to be linked to each other.

Figure 3.7: Aerial photos of the Sand Engine (looking southward). Photographs courtesy of Rijkswaterstaat/Joop van Houdt and Jurriaan Brobbel

In previous research, the macro-scale developments have been quantified by numerous indicators (e.g. (De Schipper et al., 2016, Roest, 2017, Tonnon and Nederhoff, 2016, **?**)). In the remainder of this section these are discussed, starting with the volumetric changes. Subsequently the developments of the cross-shore profile are reviewed, and the planform shape as well.

### 3.5.1. Volumetric changes

Quantification of the volumetric changes has been done extensively (e.g. (De Schipper et al., 2016, Roest, 2017, Roest et al., Tonnon and Nederhoff, 2016). The studies are split up into their respective goals, i.e. knowledge development and evaluation of the performance of the Sand Engine with respect to the coastal safety.

### Observations by De Schipper et al. (2016) and Roest (2017)

The studies executed by De Schipper et al. (2016) and Roest et al. (Submitted) were aimed at knowledge development. The objective of the study of **?** was to present the morphological evolution of the Sand Engine in the first 18 months after construction, with special attention to the feeding character. Roest (2017) who pursued the same objective over a timespan of five years, with the addition of reviewing the influence of the Sand Engine on the sediment budgets of the Westland as well.

*Alongshore Sectioning method*

To quantify the volumetric changes, a sectioning method was applied (figure 3.8). This included a section dedicated to the peninsula of the middle that underwent erosion, sections for the southern and northern flank, and a section that quantifies the sum of all sections. The sectioning is derived from the initial shape of the peninsula: the southern and middle section are split up at the location of the sharp angle, while the northern section and the middle section is defined based upon the most northern location of the nourished sediment (at the shoreline). Roest (2017) applied a similar approach, and additionally included two sections south and north of the sections proposed by De Schipper et al. (2016), to enable an assessment of the full Westland coast (figure 3.9a).

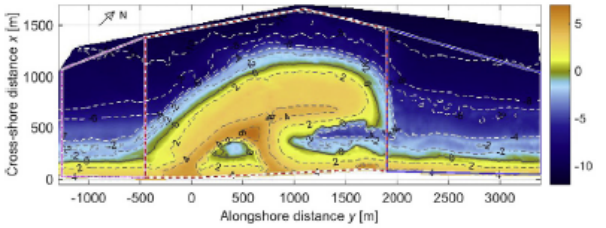


Figure 3.8: Example of sectioning in previous research by De Schipper et al. (2016)

*Observations*

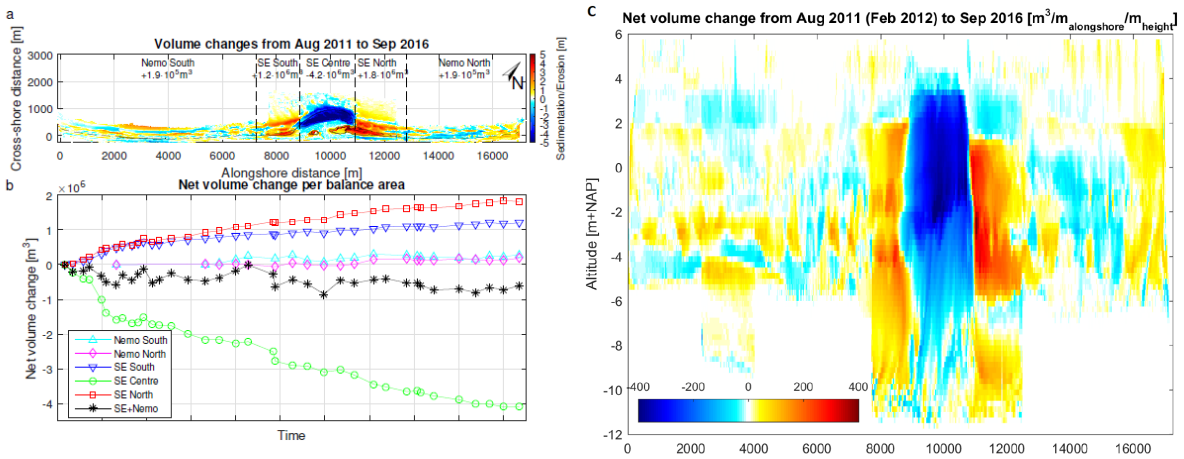


Figure 3.9: a)Volumetric Developments between August 2011 and September 2016, b) Cumulative net volume change in vertical plane ([$m^3/m_{alongshore}$]. Warm colours indicate accretion, cold colours erosion.]. After Roest (2017))

During the first six months 12% of the middle section of the SE had eroded (figure 3.9b). This erosion was dominated by a large winter storm in 2011. Compared to other periods, a relatively large net loss (out of the any of the sections considered) of sediment was observed during this initial period. After this rapid loss, lower erosion rates have been observed up until September 2016, cumulating to a loss of 4.2$Mm^3$. The erosive area is bounded between 8800 $\pm 80m$ and 10900 $\pm 80m$ with respect to Hoek van Holland (the southern boundary of the coastal cell). The majority of the eroded material in the middle section was compensated by accretions along adjacent coasts (3.4$Mm^3$, 1.8$Mm^3$ to the north, 1.2$Mm^3$ to the south).

Erosion of the middle section is concentrated near the region of the breaking waves (-3/+3m + NAP, figure 3.9c). Whereas a concentration of the eroded sediment is observed in the middle, visual assessment of volume changes show the compensated accretion is spread more evenly over depth (-10m/+2m + NAP). A net offshore migration of sediment is observed during the first 5 years, partially the result of the initially steepened profile of the nourishment design, deliberately placed there by the contractor to speed up the reshaping of the SE. This offshore migration seems to have resulted in a dominant bar behaviour (**?**), with largest accretive concentrations in the lower section of the shoreface (-6/-3m + NAP).

The dunes have shown an accretion of 100,000m$^3$ in the first 18 months (De Schipper et al., 2016). Between March 2012 and September 2016, the dunes have grown up to 450,000m$^3$, presumably stemming from the Sand Engine (Roest, 2017). The remainder of net observed erosion of 350,000m$^3$ has migrated out of the survey area (<-10 m + NAP), or up- or downdrift of the survey area (figure 3.5. Also a consolidation of the subsoil could attribute to the losses.

*Correlation of the volumetric changes to the wave power*

De Schipper et al. (2016) showed there is a clear correlation between the volumetric changes of the Sand Engine and the cumulative wave power. The strongest correlation was found between wave forcing and gross sediment transport rates. The alongshore net transport showed a strong significant correlation as well with both the cumulative wave power $r = 0.85$, as well as the averaged wave power $r = 0.79$. Since the bottom changes during the months with low incoming waves are limited, it was concluded that the motion of the horizontal tide ($\sim 0.5-1m$) was by itself insufficiently large to generate the feeding behaviour. This is in line with earlier findings by Grunnet et al. (2005), that the influence of wave power is by far the largest component resulting in alongshore sediment transport, whereas the effect of the horizontal tide was negligible (in the study case).

A ratio $R = \Delta V_{p,net}(x)/\Delta V_{p,gross}(x)$ was introduced used to indicate to what extent the bottom changes were related to the alongshore feeding. Results showed a positive correlation of R with the wave forcing (r = 0.68), supporting the observation that mostly cross-shore changes occurred during periods of mild wave action, including minor net volume loss on the tip and consequently no feeding of the adjacent coasts.

Roest (2017) additionally found a strong relation between the gross volume changes per transect, and the cumulative wave energy between consecutive surveys, with a mean of $R^2 = 0.72$. Remarkably, no correlation was found between the Wave power and the net volumetric changes, in contrast to the findings of De Schipper et al. (2016). It is remarked that the method for finding these correlations is different. Roest (2017) computed the correlation between the net sediment transport rate per m alongshore and the wave power, whereas De Schipper et al. (2016) compared the sum of the net sediment transport rates.

### Observations by Deltares, (Tonnon and Nederhoff, 2016)

In 2016, an evaluation of the morphological development was executed to assess to what extent the sub-objectives with respect to coastal safety were being met.

As in the case of the previous assessments, a similar sectioning was applied to quantify the assessment of the Sand Engine (see Appendix I). Additionally, this assessment included an analysis over a variety of depth regions. This is of importance to enable a quantification of contribution to coastal safety on the three levels in accordance with the Frame of Reference approach. An overview of the depth regions is given in table 3.1.

| Depth region | Boundaries |
|---|---|
| Dunes | >+3m NAP |
| Beach | +3/-1m NAP |
| Breaker Zone | -1/-8m NAP |
| Shoreface | -8/-12m NAP |
| Deep water | -12/-20m NAP |

Table 3.1: Depth Region assessed in research by Deltares (Tonnon and Nederhoff, 2016)

The developments of indicators of the coastal safety from different periods were compared to assess the contribution of the Sand engine. A comparison is made of the periods before (1993 - 2007) and after (2012 - 2016), along the Westland coast. The study revealed that:

- Since the construction of the Sand Engine, the dune foot has transgressed. This is primarily a result of erosion of artificial dunes that had been placed just before the construction of the SE. The growth of the dune volume per year has also decreased, which is mainly the result of the lagoon and the lake which act as a local sink. Deltares predicted a positive future development of the dune growth.
- The average position of the Momentary Coastline (the shoreline position averaged over a depth between -4.4/+3 m + NAP) has increased. Although based on estimates (trends of the coastline position indicating that the Basal Coastline is exceeded) nourishments are required near Kijkduin and Ter Heijde, Deltares predicts these nourishments will not be necessary, since the SE will feed these sections of the coastline. Deltares predicted a positive future development of the MCL along the Westland coastal cell.
- With respect to the overall sediment budget within the Coastal foundation, the study was less conclusive. Assuming a sea-levels rise (SLR) of 3mm per year, the required additional sediment budget is $\sim 20Mm^3$, meaning that the SE would fully compensate for the SLR. Though, the expected SLR is still a point of debate. Next to that, the government responsible for sustaining the coast, has started to dump

the dredged sediment of the nearby Euro Meuse Channel. With some caution it was concluded that the coastal foundation would be maintained for the next fifty years.

Interestingly, the majority of the eroded volume in the centre of the SE is found at the beach (+3/-1m NAP, figure 3.10). Accretions at adjacent coasts are primarily found near the surf zone (-1/-8 m + NAP), although it is difficult to assess whether this also holds after normalisation over depth. The strong erosions in the middle section agree with the earlier described findings by Roest (2017).

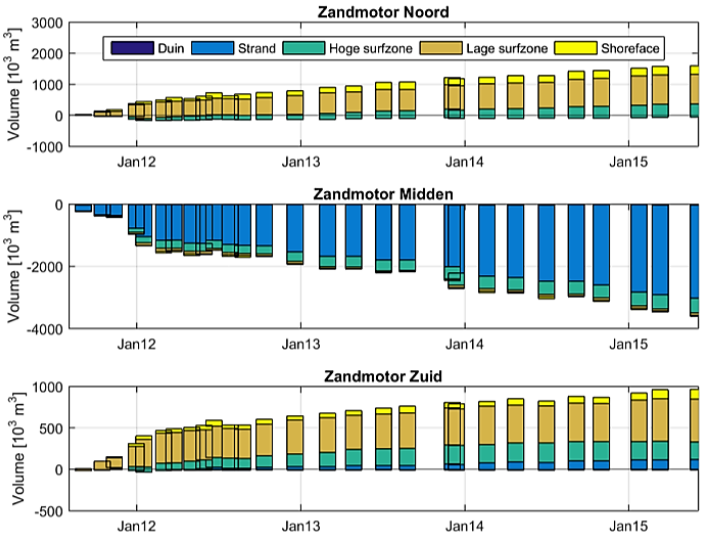


Figure 3.10: Volume changes for the different sections, per depth region (Tonnon and Nederhoff, 2016)

### 3.5.2. Cross-shore developments

The averaged slope of the peninsula had decreased significantly in the first six months after construction, on averaged from 1:32 to 1:45. After this rapid decrease in steepness, it returned back fully to its equilibrium after 18 months (1:53), although a steep slope remained near and above the mean sea-level of circa 1:20. The equilibration of the cross-shore profile occurred in an episodic manner rather than gradually (De Schipper et al., 2016).

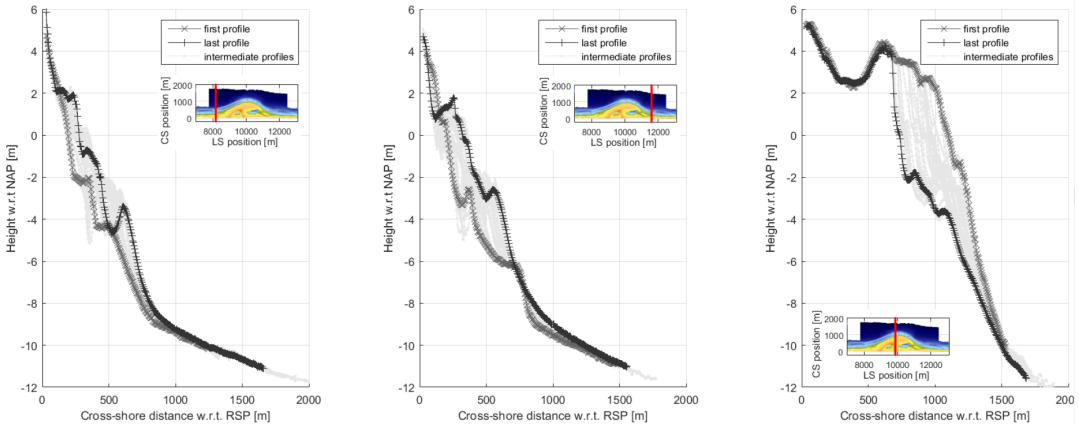


Figure 3.11: Developments of the cross-shore profile a) on the south, b, on the north, and c) in the middle, after Roest (2017)

The research of the cross-shore profiles was extended by Roest (2017), and it was found that a general flattening of the cross-shore profiles in the middle section is observed, whilst a steepening of the profiles in the flanks can be seen. From the results it was concluded the accretions are limited to the wave run up of circa 2m + NAP. In the middle section, erosion results in the formation of scarps that occasionally collapse, through which erosion of higher altitudes than the wave run-up, also occurs.

### 3.5.3. Planform developments

With respect to the planform developments, a large number of indicators have been used for quantification of the adaptation of the Sand Engine, briefly discussed here.

A widely used indicator of the planform shape is the maximum cross-shore extent $X_{max}$, i.e. the maximum cross-shore distance of the 0 m + NAP contour $x_{0m}(y)$ with respect to its position prior to construction $x_{0m,pre}(y)$ 3.12. The reduction of $X_{max}$ was largest in the first half year and most notably during January 2012, coinciding with the largest storm. The remainder of the data show a gradual decrease in $X_{max}$ without large variations (De Schipper et al., 2016). Regarding the geometry of the middle section, the cross-shore extent of

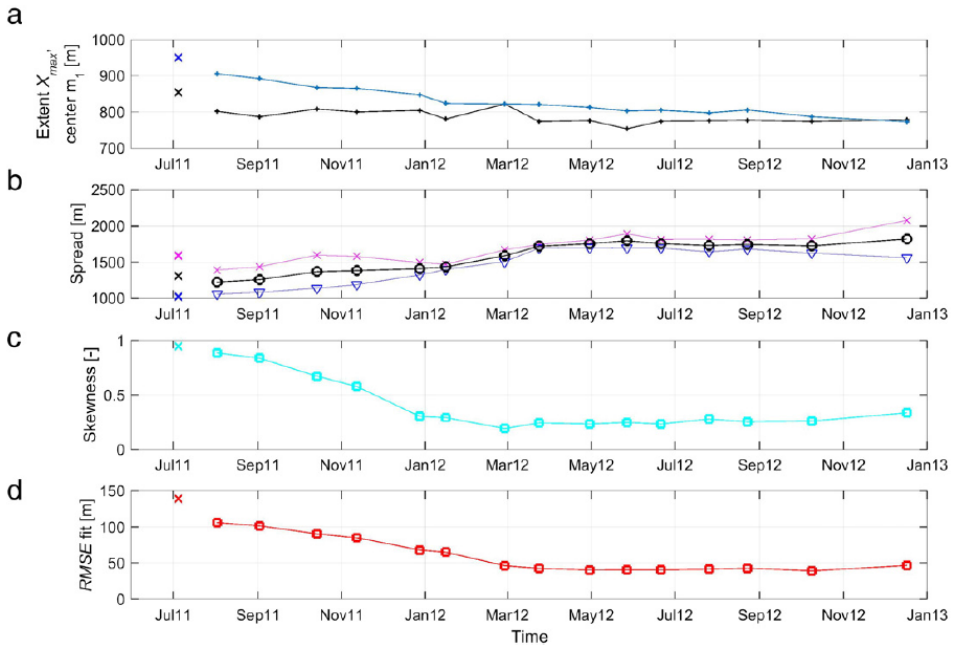


Figure 3.12: Development of suggested parameters by De Schipper et al. (2016) displayed over time. Panels show: a) he development of the maximum cross-shore extend $X_{max}$ (blue line) and the centre of mass of the planform shape $m_1$ (black line), b) the mean spread of the distribution (black line) and the spread to the southern (northern) side $s_{left}$, ($s_{right}$) of the centre of mass in magenta (blue) c) depicts the skewness of the planform shape. Negative values indicate a skew towards the north-east, d) the root-mean-squared error (RMSE) between the best-fitted Gaussian function and the measured contour. Cross symbols in July 2011 represent values as extracted from the post construction survey by the contractor.

the shoreline decreased from circa a 1000m to 660m in September 2016. Additionally, it was proposed the advection of the Sand Engine can be expressed in terms of the maximum cross-shore extent, which, depending on the depth contour, showed a migration of 50 - 300 m (Roest, 2017).

As an alternative to the cross-shore extent, the centre of the planform shape $m_1$ was proposed as well as an indicator to quantify the advective behaviour. It is calculated as the first order central moment of $x_{0m}(y)$. The $m_1$ centre-point of the nourishment position migrated southward mildly (20 m) during the first 18 months (De Schipper et al., 2016).

In line with the functionality of feeding the adjacent coasts, the width of the peninsula was quantified. This was done by the indicators $s_{left}$ and $s_{right}$, i.e. the spread to either side of the centre of mass, as calculated by the distance on both sides between the centre-point $m_1$ and the crossings of the current 0 m + NAP contour. During the first year the alongshore width increased by 90 m per month. No signature of energetic months can be observed. In contrast the monthly increase in $s_{left}$ and $s_{right}$ was largest during the mild energetic months in spring 2012 (De Schipper et al., 2016). In extension to this, Roest (2017) found that the accretive regions grew up to $1700 \pm 20m$ on the north, and $1000 \pm 20m$ on the south.

The velocities of the increasing alongshore and decreasing cross-shore extent both slow down with increasing depth, up until - 10m NAP, where no trends are observed over time. Because of these differences over depth, no single representative depth-contour could be pointed out (**?**).

The asymmetry of the shoreline was expressed by a statistical measure referred to as the skewness of the shoreline. During the first 8 months the ZM evolved from the strongly asymmetric shape to a near symmetrical shape (De Schipper et al., 2016).

In line with the observations of the shape migrating towards a Gaussian bell shaped curve, a function was fitted to test the performance. The Gaussian curve $a \exp\left(-\frac{1}{2}\frac{y-y_p}{\sigma}^2\right)$ was fitted onto the shoreline, where parameters a and $y_p$ define the cross-shore amplitude and alongshore location of the centre of the Gaussian and $\sigma$ defines the spreading. The root mean squared error (RMSE) between the fit and the contour was used to quantify how well the contour resembled a Gaussian function. In line with the developments of the skewness, the planform adjusted from the initially distinctive asymmetric hook-shape to a near symmetrical Gaussian bell shape function during the first eight months (figure 3.13). Roest (2017) added to this result that after this initial period of 1.5 years, the SE remained in this shape. Also, he concluded this was observed over

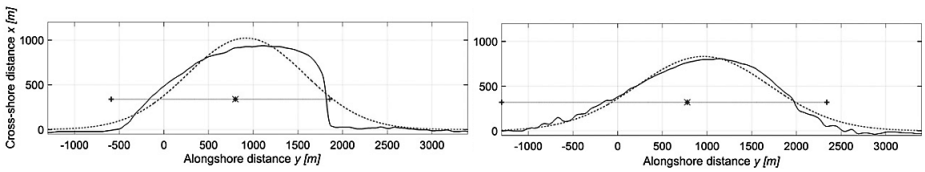


Figure 3.13: Example of best normal distribution Gaussian fit (dashed lines) of the 0m + NAP contours of the Sand Engine (solid lines) and the shape parameters for a) August 2011 and b) December 2012. The alongshore position of the centre of mass, $m_1$, of the planform shape is depicted with an asterisk (*). Both the plus (+) signs visualise the alongshore position of crossing of the pre-construction survey (De Schipper et al., 2016).

a the entire region of the active depth (between -10/+2m + NAP).

*The Diffusivity*

Arriaga et al. (2017) applied a quasi 2D numerical model to simulate the long-term behaviour of the Sand Engine and in order to calibrate and validate the model itself. Amongst others, validation of the model was done by means of assessing the observed and modelled diffusivity. The diffusivity was computed as a function of the cross-shore extent, based upon the existing relation between the cross-shore extent and the spreading coefficient ($\frac{y}{Y} \propto \frac{l}{\sigma}$) and the CERC equation for the bulk sediment transport rate 2.17, resulting in:

$$\epsilon = \left[\left(\frac{Y_0}{Y(t)}\right)^2 - 1\right]\frac{L^2}{4t} \tag{3.1}$$

Approximately 200 days after construction of the Sand Engine, the observed diffusion stabilised at $\epsilon$ = 0.0022m$^2$/s (0.069km$^2$/yr). This value is less than half of the value derived from the classical diffusivity ($G_{cla} = 0.16 km^2/yr$), see section 2.3.1. It was suggested the higher observed spreading is a result of the classic diffusivity and the redistribution of the initially steep cross-shore profile combined.

## 3.6. Aspects that influence the macro-scale developments

Next to developments on a macro-scale, two interesting aspects have been observed that influence the macro-scale developments, i.e. a coarsening of the sediment size and a dominant sub-tidal bar behaviour.

### 3.6.1. The sediment size

One parameter required for the derivation of the classical diffusivity using the CERC formulation, is the transport coefficient K, see section 2.3.1. In this the transport coefficient K which is dependent on the sediment size (Dean, 2002). An observed coarsening of the sediment is thus highly of interest, since it would result in a lowering of the diffusivity.

A coarsening of the sediment sizes at the middle section of the Sand Engine was observed with respect to the sediment at the depositional areas north and south (90 to +150$\mu m$). The heterogeneity was most clearly observed just outside the surf zone. This coarsening is a result of the hydrodynamic sorting process. Finer sediment transport is transported alongshore, which results in the coarsening. This is most dominantly observed during mild conditions. During a storm, both coarser and finer sediment is picked up, and causes a mixing of the sediment (**?**).

### 3.6.2. Sub-tidal bars

Sub-tidal bars influence the bathymetry significantly. One long stretched bar is observed in the south, while in the middle the sub-tidal bars are the largest. The sub-tidal area has flattened. Sand Waves have been observed at the middle section of the Sand Engine. In the north, the sub-tidal bars is more irregular in the alongshore direction and showed to change frequently over time.

Before a large storm in 2013, the alongshore variation of the sub-tidal bars in the south had increased, while the opposite was observed in the middle section. After the storm, the shape of the sub-tidal bars have a more uniform shape in the south and middle, and to a lesser extent in the north as well.

Interestingly, the situation reversed in 2015: sub-tidal bars have become of a more regular shape in the north with larger uniformity, while on the south, the sub-tidal bars show a larger degree of alongshore variation. In 2016, irregularity is observed on both sides of the Sand Engine again.

## 3.7. 2D numerical models

A wide rang of models have been developed to increase the understanding of the behaviour of the Sand Engine, and to predict the developments. Three simulations of 2D numerical model approaches are considered in this thesis. The outputs of the model results for January 2018 are given in figure 3.14, the main settings of the models are displayed in table 3.2. This section first discusses the model settings, followed by the model verification that was done for BruteForce model (none available for the other models).

### 3.7.1. Model Settings

The main model settings are shown in table 3.2. Regarding the grid, a slightly higher resolution is used for the Stive (2013) model, combined with a more traditional rectangular nearshore grid, as shown in figure 3.15a. In the more recent models from Luijendijk et al., 2017) (In preparation), a curved nearshore grid is applied, as shown in figure 3.15b. The advantage of this is presumably that the sediment travels 'easier' through the grid cells, which are now in the same direction as the direction of the sediment transport.

With respect to the forcing conditions, The Mormerge approaches of Stive et al. (2013) and Luijendijk et al. (In preparation) are more similar. Both apply a number of computational acceleration techniques, including a morphological acceleration factor, the parallel online method, and a wave and tide reduction technique, discussed previously in section 2.4.2. The representative wave conditions applied for both of the models are presented in appendix B. The acceleration techniques considerably reduce the computational effort (of a five year simulation) from the order of weeks in case of the Bruteforce approach, to the order of days in the case of the mormerge approach.

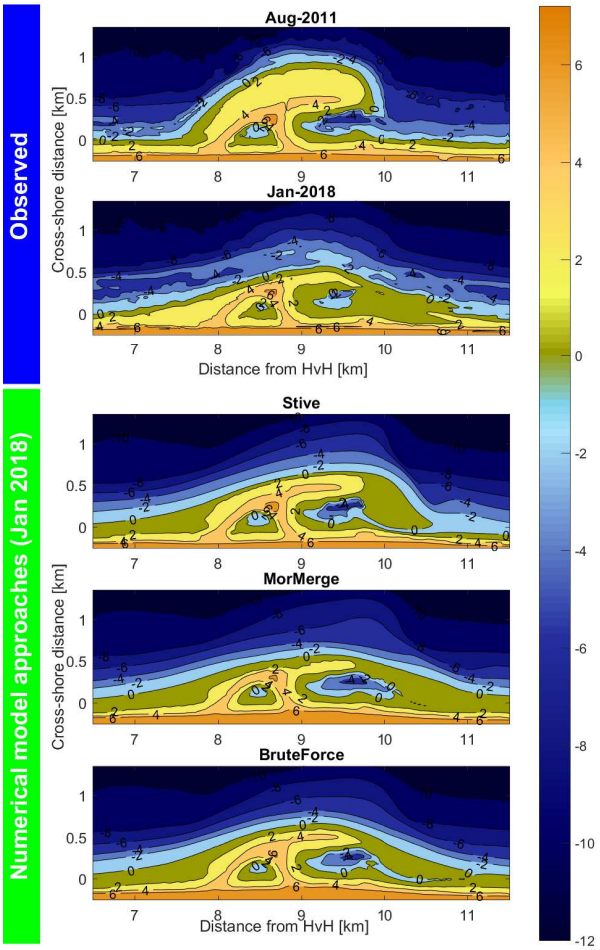


Figure 3.14: Bathymetries of Sand Engine as observed and modelled. Colours represent the height of the bathymetry, further indicated with the contours with respect to NAP (≈Mean Sea Level). Top two panels: observed bathymetry as measured in August 2011 and January 2018. Bottom three panels: simulated bathymetry by 2D numerical model approaches using Delft3D. The red box marks the middle section from which the sediment of the mega-feeder originates. The green box marks the section where the sediment is fed to.

Table 3.2: Model settings of considered 2D Numerical models

| Run reference | Mormerge | | Bruteforce |
|---|---|---|---|
| | Stive (2013) | Luijendijk (2018) | Luijendijk (2017) |
| Initial bathymetry | Survey 1-Aug-2011 | | |
| Calibration period | Until Aug 2012 | Until Aug 2016 | |
| Grid resolution | 18 x 35m | 32 x 65 m | |
| Grid alignment | 2010 coastline | Slightly curved along ZM contour | |
| Wave climate | 10 repr wave conditions | | As observed |
| Tide | Repr tidal cycle | | As observed |
| Surge & wind | Constant per wave condition | | As observed |
| Upscaling method | Parallel Online | | Serial online |
| MorFac | 66 | | 1 |

The Bruteforce approach, used in Luijendijk et al. (2017) does not apply any of the above men-

tioned reduction techniques. The physical forcing conditions are based on the observed wave conditions with hourly measurements [1]. During the calibration of the Luijendijk et al. (2017) model, results showed that significant bed level changes only occurred for significant wave heights higher than 1.5m. Therefore waves lower than 1.5m and waves with offshore oriented wave directions, were omitted in the simulation. This resulted in a reduction of the computational effort of 45%.

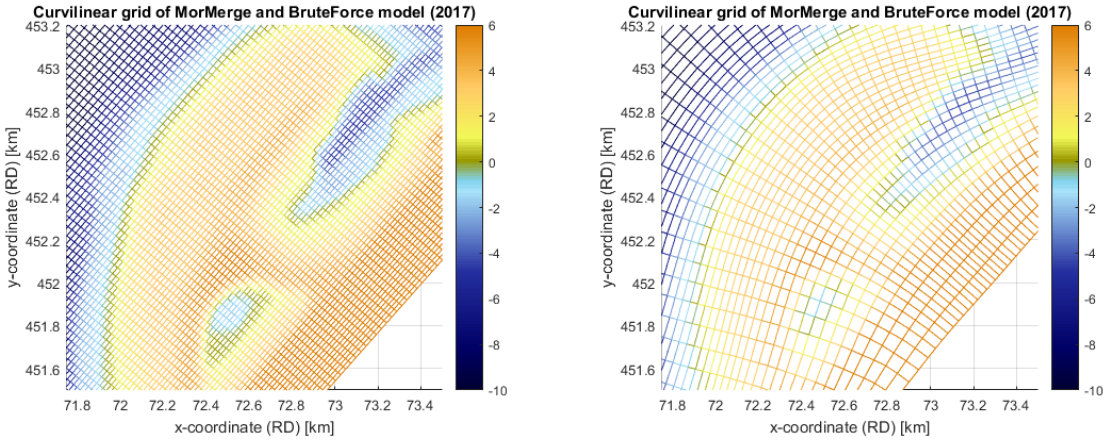


Figure 3.15: Visualisation of applied grids in Numerical models. a) Rectangular grid of Stive et al. (2013), b) Curved grid of Luijendijk et al. (2017) and Luijendijk et al. (In preparation).

### 3.7.2. Validation methods

The validation of the performance of the Bruteforce approach was done both qualitatively as well as quantitatively. Visual comparison of the model results is not discussed, reference is made to (Luijendijk et al., 2017). The Brier Skill Score was used as a measure to quantify the performance. Results of the validation are shown in figure 3.16, indicating the model performs excellently according to the classification of Sutherland et al. (2004).

Additionally Luijendijk et al. (2017) quantified the performance of the output of the model approach by comparing the volumetric changes in control areas, or sections. Figure 3.17 depicts the results. It shows the volumetric changes are well reflected by the model approach.

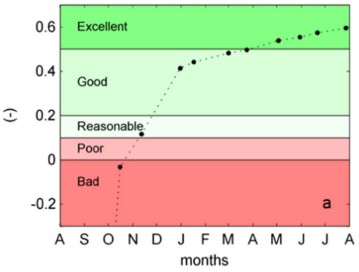


Figure 3.16: Brier Skill Score of Bruteforce approach of 2D numerical model of Delft 3D. The horizontal axis depicts the months in time, whereas the vertical axis shows the performance in terms of the BSS. The line visualises the performance of the Bruteforce approach at the time steps considered. From Luijendijk et al. (2017).

[1] As observed during the first five years. Results after august 2016 are based upon the observed forcing conditions during the first five years.

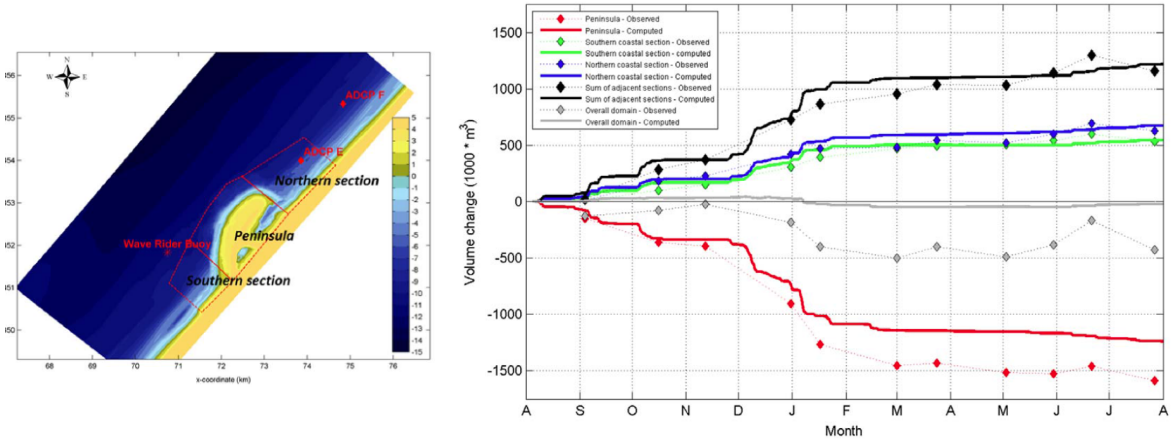


Figure 3.17: a) Applied sectioning method, b) Observed (diamonds) versus computed (lines) volumetric changes of the Bruteforce 2D numerical model approach (Luijendijk et al., 2017)

# 4

# Performance and validation tool

In this chapter, a performance and validation tool is proposed. The aim of the tool is to provide quantifiable measures that can be used to describe and predict the performance of a mega-feeder nourishment, as well as measures that enable validation of models. The (indicators of the) performance and validation tool must meet the following requirements:

1. The indicators must be measurable from a variety of datasets.
2. The indicators must represent the objectives of a mega-feeder nourishment.
3. The indicators must be easily comprehensible.
4. The indicators must be predictable.

o ensure the performance and validation tool can be used to a wide variety of data, volume densities, or depth regions, are used to quantify the performance indicators with, discussed in the first section. In the second, a method is proposed to define alongshore sections. The indicators, including their representation of the objectives, are discussed In the fourth section.

Whether the indicators are applicable to different types of datasets is tested by application to survey data and model data in chapter 5 and 6. In these chapters, focus will also lie on the predictability of the indicators.

## 4.1. The profile integrated volume

To simplify, but also to extent the applicability of the performance and validation tool, the input of the performance and validation tool is the profile integrated volume, which can easily be transformed to a shoreline representation, and vice versa. In case a dataset is considered that consists of the bathymetric developments, the data is simplified to a profile integrated volume; $V(x) = \int_L^U z(x,y)dy$, where V [$m^3/m$] is the integrated volume at location x along the coast, L and U [m] represent the lower and upper boundary of the volume densities, or depth region, of the cross-shore profile considered, and z [m + NAP] the elevation at a location (x,y), see figure 4.1) (Zanten, 2015). An example of the profile integrated volume is depicted in figure 4.2. In previous research depth contours were sometimes considered instead of depth regions for analysis of the developments of the Sand Engine. As remarked by Dean (2002), assessment of a depth region is the preferred alternative, since this gives more robust results.

Comparing volumetric changes of depth regions with lower and upper boundaries with different heights, obscures a homogeneous comparison of the developments. To enable this, the volumetric shape ($V_s$ [$m_3/m/m$]) is used, with which the profile integrated volume is normalised over depth: $V_s(x) = \frac{V(x)}{U-L}$. Defined in units, it represents the volumetric contribution of a mega-feeder nourishment per meter alongshore coast, averaged over depth.

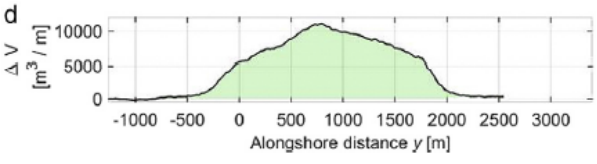


Figure 4.2: Profile integrated volume difference prior to and after just after the construction of the Sand Engine. It is remarked that no lower and upper boundary were imposed here. From (De Schipper et al., 2016)

With respect to the boundaries of the profile integrated volumes, the depth regions are derived from the characteristics of the coastal profile, such as the breaker zone, or sub-tidal bars.

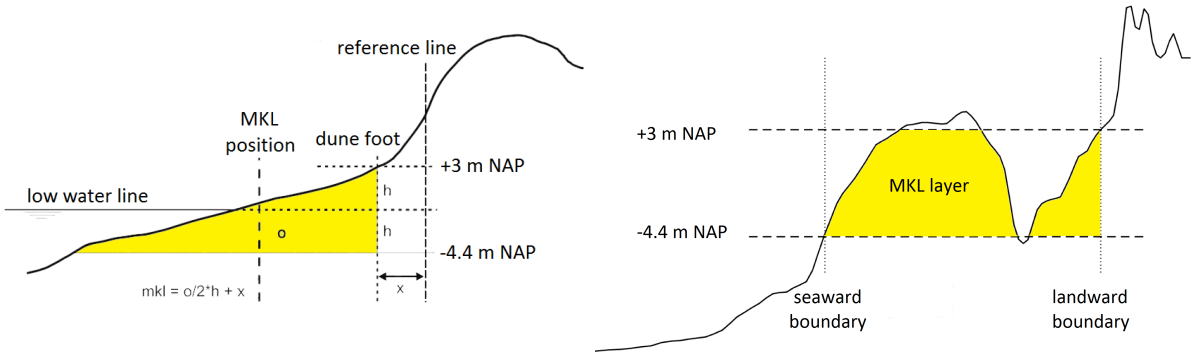


Figure 4.1: Visualisation of the computation method for deriving the profile integrated volume of the momentary coast line along a stretch of coast with Lower and Upper boundaries of -4.4 and 3 m + NAP respectively. On the left, a regular coast is exemplified, while on the right plot the derivation of the volume integrated profile at a mega-feeder nourishment is shown (Zanten, 2015)

## 4.2. The alongshore sectioning

Previous literature on the Sand Engine applied an alongshore sectioning, see appendix I, in order to quantify the erosive and accretive volumes of the Sand Engine in the alongshore direction. The alongshore sectioning was based upon the initial shape of the Sand Engine at the shoreline, and the availability of survey data. To improve the analysis, it is proposed to define the sections based upon observed cumulative differences in the volumetric shape. Following this approach, the middle section can be defined based upon the observed alongshore section where a net erosion has occurred *since* the implementation of the Sand Engine. The alongshore point along the coast where erosion turns to accretion are referred as Transition Points (TP).

Following the same reasoning, it is preferred to define the alongshore outer bounds of a mega-feeder nourishment based upon the observed location where no longer accretion is observed. These location are referred to as Accretion Points.

The regions between et Transition Point, the middle section, can be referred to as the Region of the Feeder (RoF). The south and north section are defined by the sections between the Transition and Accretion Points, referred to as the Regions of Contribution (RoC). The Region of Influence (RoI) represents all sections combined (figure 4.3).

## 4.3. The performance indicators

The tool comprises of a set of indicator that represent the performance. Using the overview of objectives and indicators given in chapters 2 and 3, it is ensured the indicators represent the desired objectives. The objective is first translated into quantifiable parameters. Existing indicators, applied in previous literature (see section 2.2.3 and section 3.5 for a literature review), can then be categorised into these quantifiable parameters. This lays bare potential gaps and/or required adaptations in existing indicators. The objectives of the Sand Engine were already discussed in section 3.3, repeated here for clarity (De Weerdt, 2015):

- Achieve sufficient volume of dunes between Hoek van Holland and Scheveningen for protection of dune erosion during storms.
- Maintain the Basic Coast Line (BCL) between Hoek van Holland and Scheveningen.
- The coastal foundation in the coastal area between Hoek van Holland and Scheveningen grows with the sea level rise.
- The Sand is to contribute to coastal safety for a period of 20 years.

This research is limited by the availability of survey data. Since the dunes are monitored in a lower frequency, this study is focussed on the developments induced by the marine processes. The objective of a mega-feeder nourishment is generalised from the listed objectives to: *"To contribute sediment (volumetric performance) along adjacent coasts (geometric performance) for a specified duration (lifetime)."* Here, the terms between brackets indicate the quantifiable parameters. The relevant indicators from previous literature are categorised here using the identified quantifiable parameters:

- The volumetric performance. This includes the accretions at the adjacent coasts, erosion of peninsula, and net erosions of the Sand Engine as a whole.
- The geometric performance. The alongshore expansion has been quantified as the width over which an accretion has been observed since its construction.
- The lifetime (or age). The cross-shore extent has been used as a measure to quantify this, or the volume reduction of the middle section.

To account for potential differences in volumetric contribution over depth, the volumetric performance can be quantified for multiple depth regions, e.g. the foreshore of the beach and a region with bars.

In previous research, the geometric performance was based upon the location up until where a net accretion of 200$m^3$/m could be observed (Roest, 2017). It is argued that the implications of the boundary on the results are difficult to estimate. As the nourishment diffuses over time, The ratio between the region where a net accretion of 200m is observed, and the region where any accretion (no boundary) is observed, will decrease with time. Therefore as an alternative to this definition, it is proposed to derive the location without imposing any boundary. This point is referred to as the Accretion Point (AP).

Another alternative is to represent the alongshore expansion with the development of the centroid of the accreted volumes (of the RoC). Since this indicator is the average alongshore location of the net volumetric growth, it is expected to be more robust than the more sensitive Accretion Point.. The disadvantage of this indicator is that it is rather abstract, and above that, has no direct link to the performance as specified by the objective ('between Scheveningen and Hoek van Holland'). Application of the indicators to a case study will reveal which of the indicators is the preferred alternative.

In terms of the lifetime, two indicators have previously been used for this quantifiable parameter. Dean (2002) related the volume remaining and the cross-shore extent directly to the half-life. Both can adhere to reflect the performance with respect to the lifetime.

An overview of the proposed performance indicators is given in table 4.1

Table 4.1: Overview of performance indicators

| **Sub-objectives** | **Quantifiable parameters** | **Indicators** |
|---|---|---|
| Contribute to coastal safety | Volumetric performance | Volumetric accretions of the RoC |
| Between Hoek van Holland and Scheveningen | Geometric performance | Accretion Points with and without a boundary, Centroids of the RoC |
| For 20/50 years | Lifetime | Cross-shore extent, Volume remaining in RoF |

In figure 4.3 visualisation of the indicators is shown. Volumetric indicators are computed from each of the four regions considered, not visualised here.

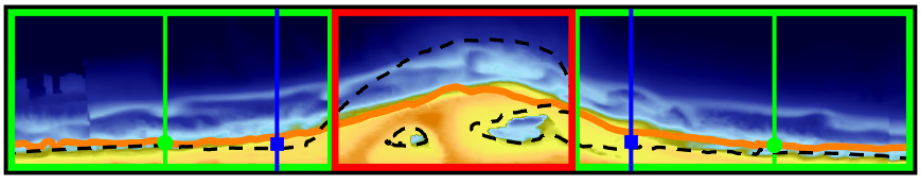

Figure 4.3: The proposed performance tool. The black box on the edges denotes the Region of Influence, the green boxes depict the Regions of Contributions, and the red box shows the Region of the Feeder. The green circles indicate the Accretion Points, blue squares the proposed centroids of the RoC. The Orange line visualises the volumetric shape (based on the volume integrated profile between -10 and +3 m = NAP))

# 5

# Verification of the performance and validation tool

In this chapter, the proposed performance and validation tool of chapter 4 is applied to survey data of the Sand Engine. The tool is applied to the unique case study, in order to first verify the performance and validation tool, and secondly to quantify the performance of the Sand Engine itself. As stated in the previous chapter, the indicators are to be predictable. Predictability of the indicators is verified in two manners: 1) by assessing whether long-term trends can be identified in the current developments of the performance indicators, and 2) by verifying the performance depends on the behaviour. **The performance** is defined as the degree to which a mega-feeder nourishment contributes sediment to adjacent coasts for a specific duration. **The behaviour** is the change of the shape of the mega-feeder nourishment as a result of forcing conditions, e.g. wind, waves, and tide. By earlier studies it was found the behaviour can be represented by a Gaussian curve diffusion over time. If the performance indicators develop proportionally to this behaviour, the predictability of the indicators is further confirmed.

This chapter is split up into four sections. In the first section, the data-processing is discussed, including the pre-processing of the survey data, and a description of how the Sand Engine is split up into sections both in the cross-shore and alongshore direction. In the second section, the performance indicators are applied and the presence of clear trends is verified. Third, the behaviour is quantitatively described. The quantification of the behaviour is used in the fourth section to verify whether the performance indicators develop similarly to the quantified behaviour.

## 5.1. Data processing

Before the analysis of this research is explained, first all data pre-processing is described. In this first section, the pre-processing is elaborated on, followed by application of the volumetric shape.

### 5.1.1. Data gridding

The data that is retrieved during the surveys of the Sand Engine, is pre-processed to enable a quantification of the developments of the Sand Engine. The main steps are included here briefly, and more extensively in appendix C. For a complete overview of the data processing and a review of the accuracy, reference is made to (Roest, 2017). The point cloud of a survey contains data along survey trajectories (5.1a). The coordinate system used for the surveys is the Rijksdriehoek coordinate system, the official system used by the Dutch government, altitude levels wrt

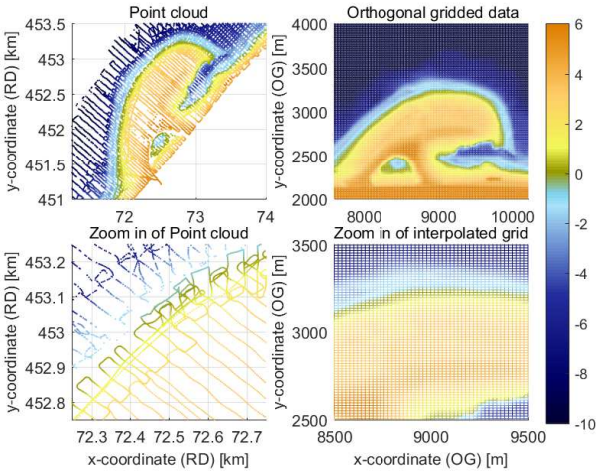


Figure 5.1: Data-preprocessing products (left plots): point cloud in Rijksdriehoek coordinate system and (right plots): interpolated data with orthogonal grid (20x20m). Survey data from August 2011. Colours indicate heights wrt NAP.

NAP[1].

As a first step, the point cloud data of the Sand Engine data was combined with the NeMo data, after which it is interpolated to transects. These transects were interpolated again over a standardised grid of 20x20m$^2$. Next, it is rotated and transformed to an orthogonal grid, which origin lies on the south edge of the Westland coast at the Hoek van Holland. A limitation of the NeMo data is the depth over which the surveys are executed (-5/+5m NAP). To fill up the missing data at the deeper sections, the JarKus data is used additionally. Since the spacing between the transects of the JarKus data is roughly 200 - 250m, interpolating to a grid of 20x20m leads to a highly averaged bathymetric profile. The data is used as a last resort; only if no other data is available, the bathymetric information is retrieved from the interpolated JarKus data. A last pre-processing step includes an updating technique. The JarKus survey is only executed on a yearly basis, while the Sand Engine and NeMo measurements were executed on a bimonthly scale. The most recent data at each grid point is used to increase the homogeneity of the comparison.

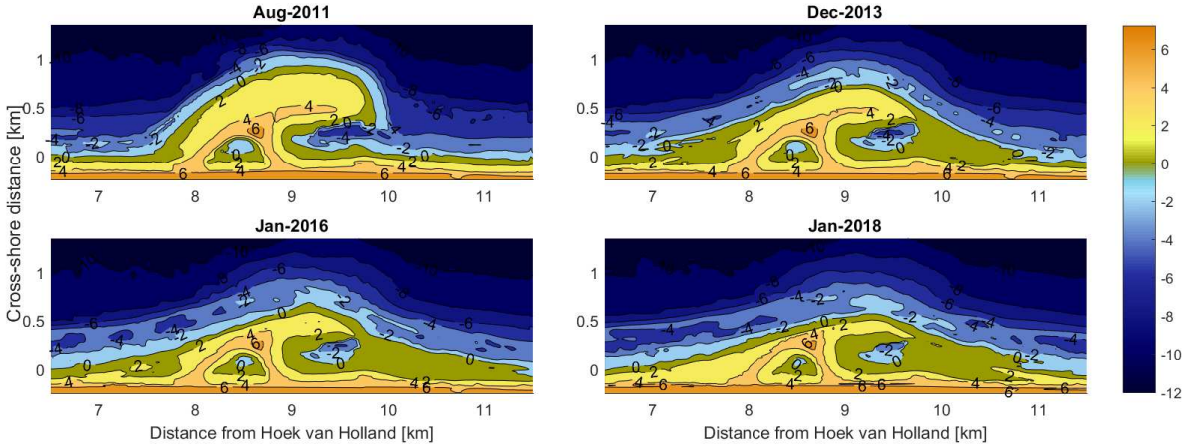


Figure 5.2: Observed bathymetry as monitored by surveys of the Sand Engine in first six and a half years. Colours represent the height of the bathymetry with respect to NAP, further indicated with the contours.

All assessments of the developments are derived from the volumetric shape: the volumetric contribution per m alongshore beach, compared to prior the construction of the Sand Engine. The volumetric shape is computed with cross-shore profiles from the interpolated bathymetry (figure 5.3). The influence of the assessment of a depth region rather than the shoreline is depicted in figure 5.3. Initially a clear difference is present between the shoreline (0m + NAP) and the active region, from here onwards referred to as the Total region (-10/+3m + NAP). Interestingly, the distinct hooked shape feature observed at the shoreline of the Sand Engine cannot be distinguished if the volumetric shape of the Total region is reviewed. What's more, both the shoreline position as well as the MCL seem to have migrated towards the volumetric shape of the Total region. From this, it is shown that deriving observations based on the shoreline will lead to biased conclusions: both those of the developments of the Sand Engine, and the migration of the shoreline towards the volumetric shape.

### 5.1.2. Cross-shore section boundaries

The performance of the Sand Engine is quantified for a number of depth regions, to answer one of the secondary objectives: to assess the presence of differences in performance over depth. This is done for two reasons. First, the velocities of feeding may differ over depth. The presence of a difference is of interest to increase the understanding of a mega-feeder nourishment further. Second, it is of interest to review whether specific depth regions can be used as representatives for the performance of a mega-feeder nourishment as a whole.

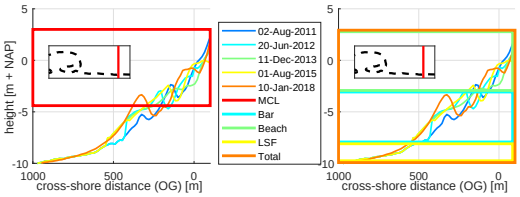


Figure 5.4: Considered depth regions based on cross-shore profiles of the Sand Engine in the north (11.5km from Hoek van Holland). On the left the boundaries of the Momentary Coastline. On the right the depth regions considered in this thesis.

[1] NAP is an abbreviation for the Normaal Amsterdams Peil, approximately equal to the mean sea-level of the North Sea
[2] Preferably the data is directly interpolated over the point cloud data, but this was not available during the research

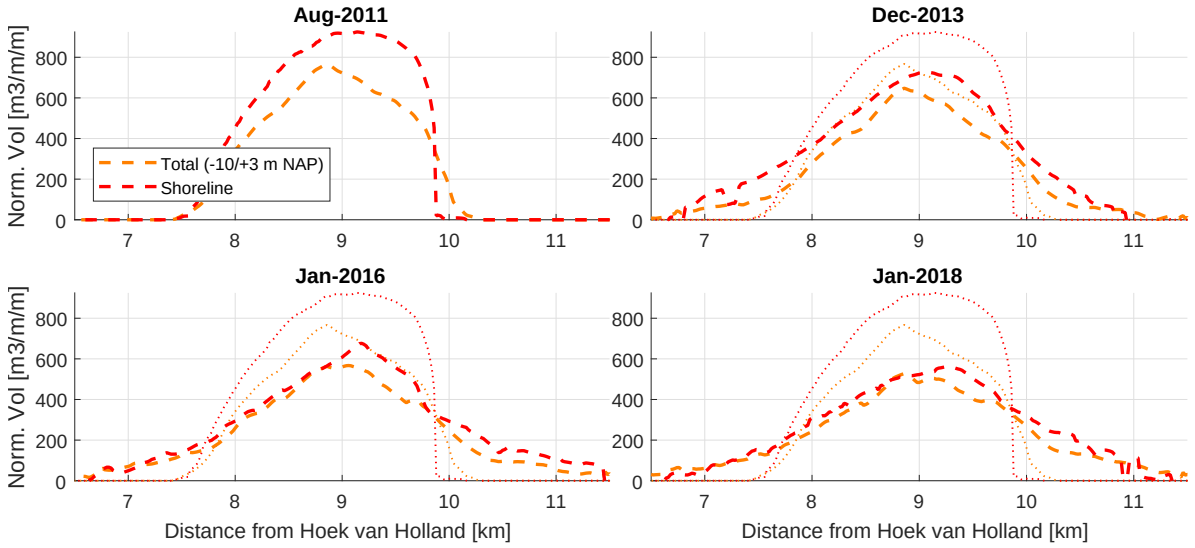


Figure 5.3: Volumetric shape of the Total region (-10/+3m + NAP) versus the shoreline (0 m + NAP) over time. On the horizontal axis the distance from Hoek van Holland, on the vertical the volumetric shape [m3/m/m]: the volume per m beach, averaged over depth. The thick dashed lines depict the volumetric shape over time, whereas the thin dotted line visualises the initial volumetric shapes of the shoreline and considered depth regions.

| Depth region | Lower limit | Upper limit |
|---|---|---|
| | [m + NAP] | [m + NAP] |
| Beach | -3 | +3 |
| Bar | -8 | -3 |
| LSF | -10 | -8 |
| Total | -10 | +3 |
| MCL | -4.4 | +3 |

Table 5.1: Boundaries of considered depth regions. Heights expressed in m + NAP.

In light of the large difference between the initial volumetric shape and the shoreline position, the cross-shore profiles of the south, middle, and north were analysed to derive depth profiles that behave homogeneously over time. In a first attempt the applicability of the momentary coastline was reviewed. However, the MCL did not appear a suitable depth region to consider (figure 5.4). This is a result by the presence of sub-tidal bars, located partially in, and partially out of the depth contours of the MCL. This is considered undesirable, since migration of the sub-tidal bars in and out of the MCL obscures a desired analysis of trends in the alongshore direction. The depth regions are therefore redefined based upon the presence of the sub-tidal bars resulting in three regions: 1) a region above the bars, referred to as the Beach region (-3/+3m + NAP), the Bar (-8/-3m + NAP), and the region below the bars, the Lower Shore Face (LSF, -10/-8m + NAP). The Total (-10/+3m) region is considered as well to compare the differences per region with the developments in the active region.

### 5.1.3. Alongshore section boundaries

The alongshore section boundaries are based upon on Transition Points and Accretion Points. The TP defines the location where erosion turns to accretion, and the AP defines the location up until where accretion is observed (from the centroid of the Sand Engine). How these develop over time is further discussed in section 5.2.3. The Transition Point has shown to be a robust indicator, with which the sectioning can be clearly defined. The alongshore section in between the Transition Points marks the Region of the Feeder (RoF), located between 7700m and 9800m (figure 5.8).

The Accretion Point is by definition less robust than the Transition Point. The location of the Accretion Point is further made unclear in the case of the Sand Engine due to the presence of two additional nourishments placed south and north of the peninsula to prevent initially expected losses (Projectteam Zandmotor, 2010) near the outer edges. The presence of the additional nourishment on the south is not observed for

before the 10th of January 2018, and shows a sudden growth of volume integrated profile (figure 5.6, middle panel). On the north, the additional nourishment can be clearly observed between 13km and 14 km from Hoek van Holland.

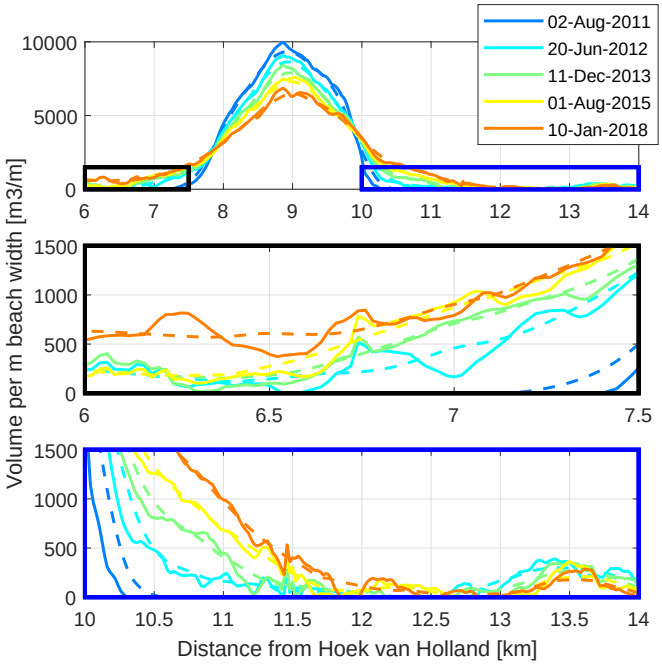


Figure 5.5: Analysis of alongshore sectioning. Volumetric developments along the coast, 5 moments in time since its construction, with detailed plots, marked in the top plot on the left and right with the black and blue boxes respectively. The continuous lines depict the calculated value alongshore, while the dashed line the moving average, in an attempt to decrease the fluctuations and enable a more robust computation of the Accretion Point.

Because of this complication, the Region of Influence (RoC), is defined as a fixed section, ranging from 6400m up to 12800m. These outer bounds simultaneously also mark the southern and northern edges of the Regions of Contribution on the south and north respectively. Observed accretions south and north of the RoC, are not a part of the assessment. In appendix D the influence of this decision is further discussed.

## 5.2. The performance of the Sand Engine

This section discusses the application of the performance indicators of the performance and validation tool to the Sand Engine. The performance of a mega-feeder nourishment is split up into three quantifiable parameters in the tool: 1) the volumetric performance, 2) the geometric performance, and 3) the lifetime. Prior to the quantification, first three frequently applied statistical measures are described, used to quantify the degree to which the curve-fits can describe the developments of an indicator.

### 5.2.1. Statistical measures

To assess the usability of an indicator, the presence of a trend is an important asset. Trends suggest continuation of a development of a system. Lack thereof on the other hand, prevents extrapolation of trends and thus the making of predictions.

The presence, velocity, and type of trends are analysed using the non-linear least squares method (Swann, 1969). Fits of linear functions ($y = at + b$) and square root functions ($y = a\sqrt{t} + b$)) are fitted onto the developments of the indicators. To quantify the performance of these trends, two frequently used statistical measures are applied, namely the coefficient of determination $R^2$, and the Root Mean Squared Error (Devore, 2011). The $R^2$ is defined by

$$R^2 = 1 - \frac{SSE}{SST} \tag{5.1}$$

Where SSE ($\sum(y_i - \hat{y})^2$) denotes the sum of squared error of the curve-fit, and SST ($\sum(y_i - \bar{y})^2$) the sum of squared error around the mean value of the analysed indicator.

The coefficient of determination if often explained as the proportion of observed variation in y that can be explained by the regression. The value ranges between 0 and 1, with higher values indicating the curve-fit has been more successful. The Root Mean Squared Error is another measure to quantify the accuracy of a curve-fit, which states the mean standard deviation of observations around the curve-fit.

The second measure is the Root Mean Square Error (RMSE) (Devore, 2011):

$$RMSE = \sqrt{\frac{1}{N}\sum_{i=1}^{N}(y_i - \hat{y}_i)^2} \tag{5.2}$$

with N the sample size, $y_i$ the value of the model of the i$^{th}$ output and $\hat{y}$ the i$^{th}$ observed value.

Throughout the remainder of this chapter, the performance of curve-fits is quantified using these statistical measures. For a full overview of the results of the performances of the curve-fits, reference is made to appendix D.

### 5.2.2. Quantification of the volumetric performance

Figure 5.6 shows the volumetric changes of the four different sections: the Region of the Feeder (middle), the Regions of Contribution by the south and the north, and the Region of Influence by the net volume of the Sand Engine of the Total region (-10m/+3m + NAP). Analysis reveals 4.3Mm$^3$of the initial volume in the middle section has eroded (28%) as of January 2018, 6.5 years after construction. This erosion is compensated for by accretions in the Regions of Contribution. In the south, a volume equal to 1.2Mm$^3$ (28% of the eroded volume) is observed, while 2.1Mm$^3$ of the eroded volume is compensated for in the north (49%). The volumetric change in the Region of influence, represented by the net volume change in the graph, has shown a continuous mild erosion in the middle of 0.8% per year of the initial volume(0.8Mm$^3$).

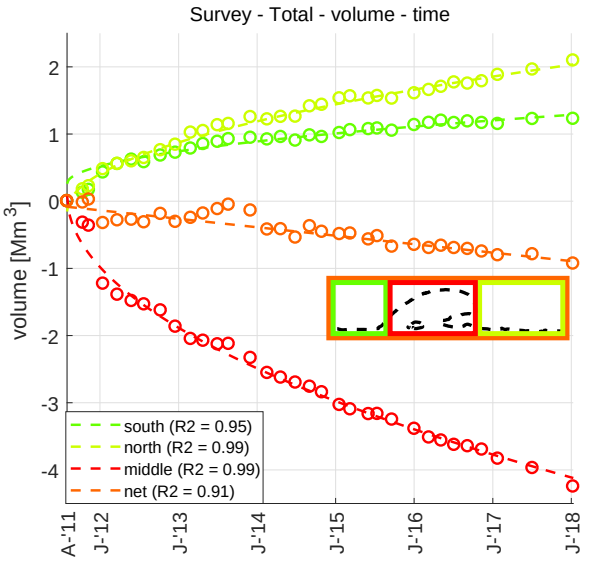


Figure 5.6: Volumetric performance of alongshore sections of the Sand Engine.

Curve-fits of square root functions describe well the volumetric performance indicators of the separate Regions of the Feeder and Contribution, with coefficients of determination of $R^2$ = 95% or higher. The volumetric performance is thus dominated by continuous long term trends that decays in velocity over time. A seasonality in the accretion can be observed in adjacent beaches, the RoC. More rapid accretions occur during winter when waves are higher, and stagnations is observed during the summer periods (e.g. between January 2015 and January 2016, barely any accretions were observed). This seasonality is not observed in the middle section, which shows a more continuous development over time.

The net volumetric change develops differently. During the first 2.5 years, the volume remained more or less constant, after which a nearly linear trend of continuous erosion can be observed. The increase observed between January 2013 and January 2014 is ascribed to the influx of sediment from the higher dry area of the peninsula (>+3m + NAP). The net erosion is a consequence of sediment moving out of the Survey area in the alongshore (out of the alongshore sections), see appendix D.

Figure 5.7 visualises the volumetric changes of the considered depth regions (Beach (-3/+3m + NAP), Bar (-8/-3m + NAP), LSF (-10/-8m + NAP), Total (-10/+3m + NAP)) in all of the four alongshore sections (RoF, RoC, and RoI), normalised over depth to enable a homogeneous comparison. Quantification of the volumetric changes of the middle section lays bare clear differences in erosion velocities over depth. Largest erosion velocities are observed in the Beach region (-3/+3m + NAP), whereas milder velocities are observed towards deeper regions (figure 5.7c). Contrary to the Region of the Feeder, accretions are uniform over depth in the Regions of Contributions (figure 5.7a and figure 5.7b). The north shows an approximately equal volumetric growth over depth, aside from a rapid sub-tidal bar development. In the south a similar development is observed, although the LSF (-10/-8m + NAP) arguably shows a more linear trend than the other depth regions.

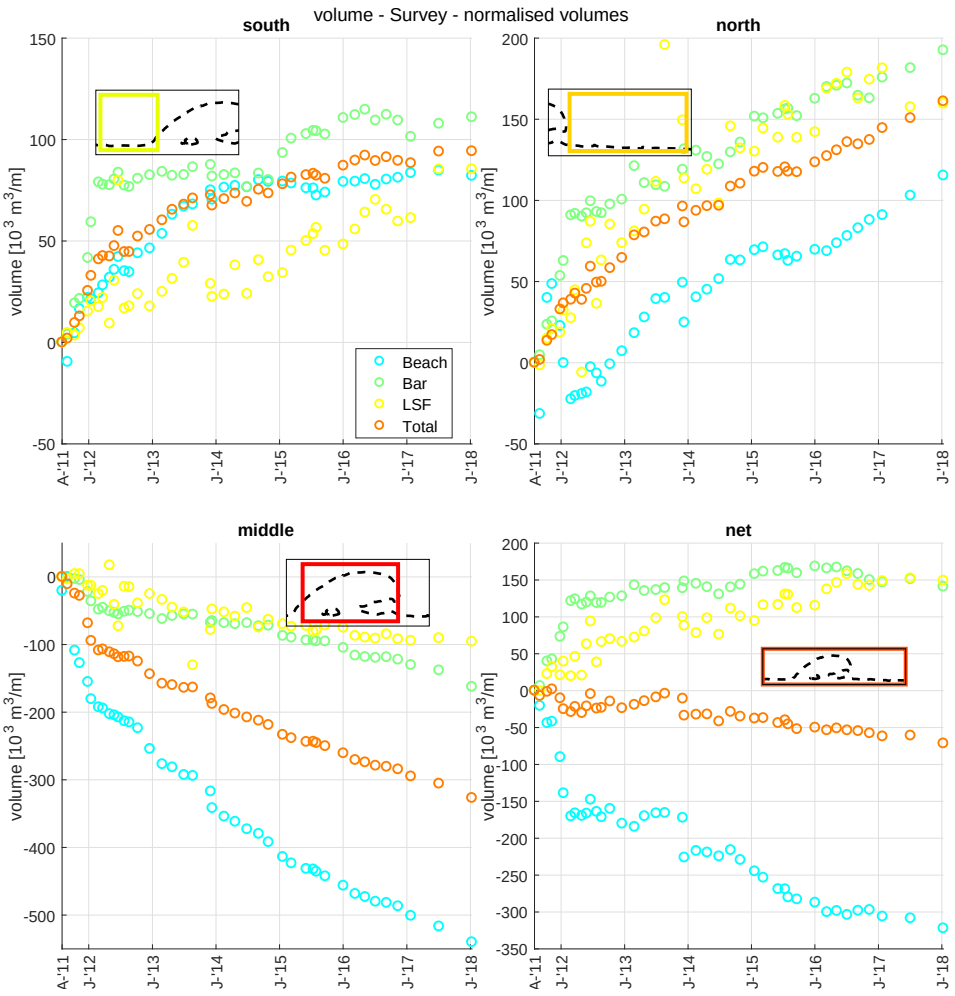


Figure 5.7: Normalised volumes of the section of the Sand Engine. Comparison of volumetric changes over depth, with the Beach region (-3/+3m + NAP), the Bar region (-8/-3m + NAP), the Lower Shore Face (LSF, -10/-8m + NAP), Total (-10/+3m + NAP)

This uniform feeding over depth implies there is a redistribution of the sediment over the depth regions in the Regions of Contribution. This is supported by the results of the net volumetric changes (figure 5.7d). An initially rapid volumetric growth is observed in the Bar region (-8/-3m + NAP) during the first eight months, whereas the LSF (-10/-8m + NAP) has grown more linearly over time. Contrary to the accretion of the lower regions, the Beach has (-3/+3m + NAP) initially eroded rapidly during the same period. The Beach region has continued to erode, with an observable decay in velocity over time.

### 5.2.3. The geometric performance

In chapter 4, three indicators were introduced to quantify the geometric performance: the Transition Points (TP), the Accretion Points (AP), and the Centre of Mass (CoM). The TPs mark the location where erosion turns to accretion, with respect to the initial volumetric shape. Although, the TPs are not a performance indicator; they enable an objective methodology for deriving the alongshore section boundaries. Since it is a measure of the alongshore geometric development of a mega-feeder nourishment, the results are included in this section. The two other indicators are geometric performance indicators. First, the APs quantify the location up until where accretion is observed prior to the construction of a mega-feeder nourishment. Second, the CoMs quantify the centroid of the accreted volumes in the Regions of Contributions.

Before discussing the results, first the considered depth regions are elaborated on. In the case of the Sand Engine, the Total region (-10/+3m + NAP) could not be used to assess the geometric performance. This is caused by two additional nourishments placed at the adjacent coasts on the south and north to prevent initial erosion near the outer edges of the Sand Engine. As a result of these additional nourishments, quantification of the geometric performance with either the APs or the CoMs, proved difficult. Contrary to the APs and the

CoMs, the TPs are not located near the additional nourishments, and could therefore be derived in all depth regions without difficulty. In the previous section, it was concluded that no single representative depth region could be found, although the Beach region (-3/+3m + NAP) could be used as a representative in the accretive regions. Based on this conclusion, the Beach region is used here to derive the geometric performance of the Sand Engine.

The results of the application of the performance and validation tool show that no movement of the TPs is observed over time (figure 5.8). In other words, the Region of the Feeder does not widen over time, but stays approximately constant (2100m). Interestingly, the non-movement is observed over all considered depth regions, after an initiation period of circa six months. The Accretion Point on the north has migrated 1250m to the north since the construction. Expressed in the distance between the centroid of the SE and the Accretion Point, the width has increased by 83%. Normalizing for the mild northward movement of the centroid of the entire Sand Engine over time (see figure 5.10b), the migration is 1130m (an extension of 75% expressed in the distance between the centroid and the AP). On the south, the Accretion Point migrated southward with 750m (+43%). Normalising over depth gives a migration of 870m (+50%) respectively. The Region of Influence developed from circa 3000m wide up to 5250m as of January 2018 (+60%). The migrations of the CoMs are smaller with values normalised for the centroid movement of the SE as a whole: 300m (+50%) northward and 193m (+37%) southward.

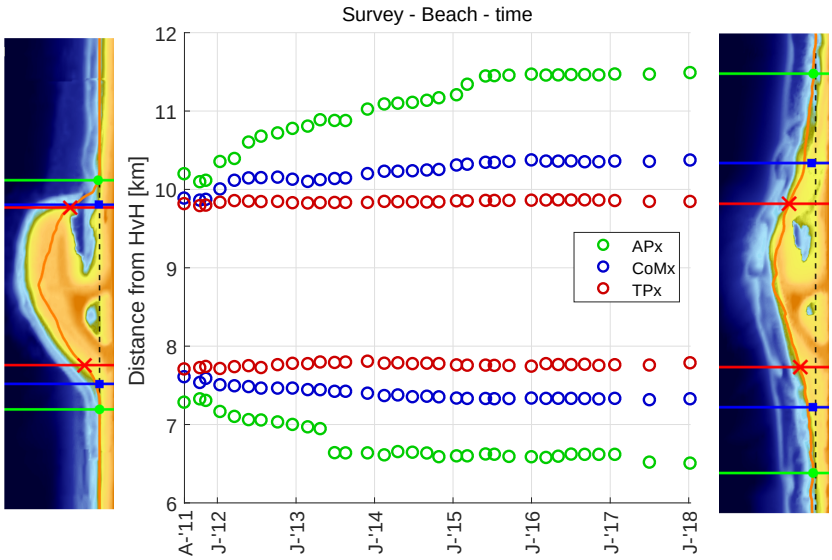


Figure 5.8: Development of the geometric performance expressed in the Accretion Points (APx), Transition Points (TPx), and Centre of Mass (CoM). The subscript x denotes the movement of the geometric indicators in the alongshore direction.

Curve-fitting of the indicators reveals trends describe well the continuous developments over time. A square root fit of the APs performs well in the north ($R^2$ = 0.95) (table 5.2), while a square root curve-fit of the southern AP performs poorer ($R^2$ = 0.78) as a result less continuous movement over time. The curve-fits are mildly improved if a moving average is applied onto the volumetric shape ($R^2$ = 0.97 and $R^2$ = 0.84 for the north and south respectively, see appendix D).

Curve-fits describe both the developments of the CoM in the north and south poorer ($R^2$ = 0.86 and $R^2$ = 0.74), though it is argued the definition of the $R^2$ prevents a homogeneous comparison of the performance of the curve-fits of the APs and CoMs[3]. The same goes for the TPs ($R^2$ = 0.03 and $R^2$ = 0.19 for the south and south respectively). In terms of the RMSE, the errors are equal for all indicators (RMSE ≈40 - 50m).

### 5.2.4. Lifetime

The lifetime is the third parameter used to quantify the performance of a mega-feeder nourishment. It is quantified here by means of two performance indicators: the eroded volume in the Region of the Feeder

[3]The $R^2$ quantifies the performance in terms of the proportion of observed variation in y that can be explained by the regression. The performance of a curve is quantified by comparing the error of the curve to the error of a curve with a constant value, the mean of the considered variable. Data that shows smaller changes in the y (in this case a development in the distance from HvH), will therefore in general perform poorer in terms of the $R^2$.

Table 5.2: Performance of curve-fitting quantified with statistical measures R2 and RMSE

| **Geometric indicators** | **TP** | | **AP** | | **CoM** | |
|---|---|---|---|---|---|---|
| | R2 | RMSE | R2 | RMSE | R2 | RMSE |
| | [-] | [m] | [-] | [m] | [-] | [m] |
| south | 0.74 | 43 | 0.84 | 71 | 0.03 | 36 |
| north | 0.86 | 55 | 0.97 | 55 | 0.19 | 38 |
| distance | 0.84 | 89 | 0.95 | 114 | 0.04 | 59 |

(the middle section), and the reduction of the cross-shore extent of the volumetric shape. Lifetime is here expressed as the reduction of both these indicators with respect to their initial value after construction of the Sand Engine.

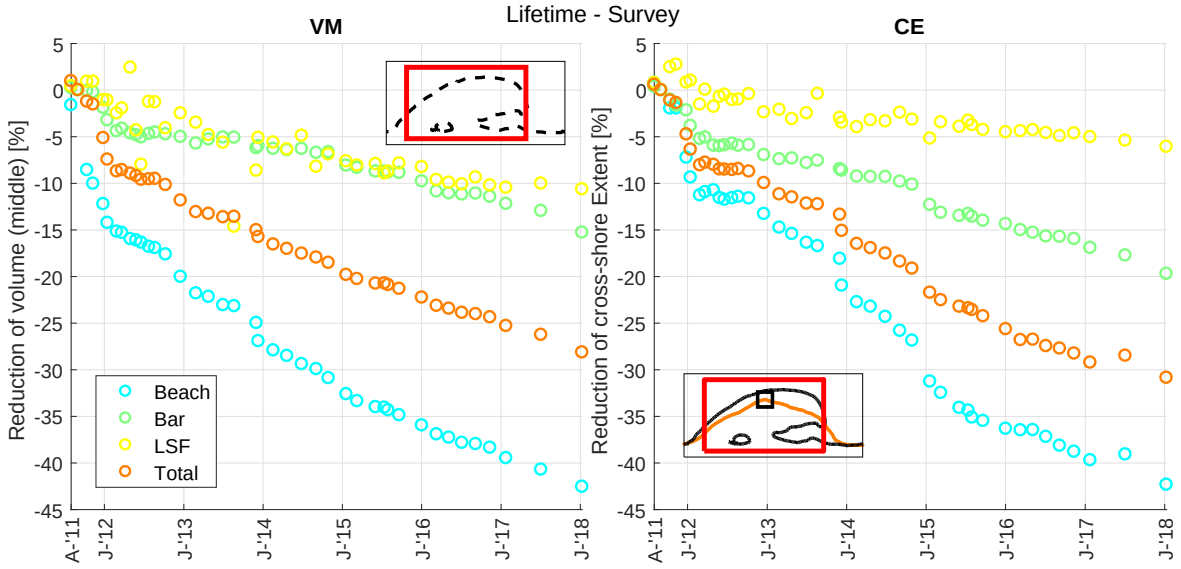


Figure 5.9: Lifetime of the Sand Engine for various depth regions a) Expressed in terms percentile of volume remaining in the middle after construction, and b) Expressed in terms of percentile reduction of the cross-shore extent of the volumetric shape.

Expressed in the eroded volume, the Beach region (-3/+3m + NAP) has eroded by 42% (3.3Mm$^3$) since the construction of the Sand Engine, while the volume of the Bar (-8/-3m + NAP) and LSF (-10/-8m + NAP) only decreased by 15% (0.8Mm$^3$) and 11% (0.2Mm$^3$) respectively (figure 5.9). Combined, this lead to the combined erosion of 28% of the initial volume (4.3Mm$^3$). Interestingly, the developments of the developments of the cross-shore extent is similar to the developments of the volume in the RoF. The reduction of the cross-shore extent (of the volumetric shape) is 43% (380m), 20% (140m), 7% (40), and 31% (240m) for the Beach, Bar, LSF, and Total region respectively. As shown in section 5.2.2, the curve-fits of the volume of the RoF described well the developments. This holds likewise for curve-fits of the cross-shore extent ($R^2$>0.95 and RMSNE < 20m)[4].

### 5.2.5. Summary of results

In this section, performance indicators were applied to the survey data available of the Sand Engine. It was verified whether the indicators are predictable, i.e. develop continuously. It was confirmed the volumetric performance indicators, geometric performance indicators, as well as lifetime indicators can be described well with square root curve-fits ($R^2$>0.95)[5].

The geometric performance was quantified by means of the Accretion Point, as well as by means of the CoM of the volumetric growth in the Regions of Contribution. The latter developed mildly less continuous.

[4]The curve-fit of the developments of the CE in the LSF performs poorer if expressed in the coefficient of determination ($R^2$>0.82), but expressed in the RMSE, the error of the curve-fit is lower than for the other fits (RMSE = 4m for the LSF vs RMSE = 7 - 20m for the Beach, Bar, and Total region).

[5]Performance of curve-fits for the volumetric growth, accretion points, and volume reduction of the middle. The Accretion Point on the south developed slightly less continuous, ($R^2$=0.84)

Interestingly, the Transition Point showed not to develop over time at all. Based on a visual comparison of the Pelnard-Considère solution, a migration of the Transition Points is expected. This results is further discussed in appendix I. The lifetime was quantified in terms of both the volume reduction, as well as the reduction of the cross-shore extent. Both showed to be able to serve as predictable performance indicators. Further, large differences in the developments over depth are observed. The velocity of feeding of the Beach region (-3/+3m +NAP) is a factor 3 (4) higher than the feeding of the Bar (-8/-3m + NAP) (LSF (-10/-8m + NAP)).

More specific to the case study of the Sand Engine, results showed that 4.3Mm$^3$ (28%) of the initial volume in the Region of the Feeder has eroded in 6.5 years. This is compensated for by volumetric growth in the adjacent coasts cumulating to 3.3Mm$^3$ (77% of the observed losses). An asymmetric growth of the adjacent coasts is observed, presumably caused by the dominant wave action from the south-west. A large difference in the volume reduction is observed over depth, with a reduction of 42% in the Beach region, versus a mere 10 - 15% in deeper regions.

## 5.3. The behaviour of the Sand Engine

In this section, the developments of the macro-scale behaviour of the Sand Engine are quantified. First, the indicators that quantitatively describe the behaviour are elaborated on. In the second section the behaviour of the Sand Engine is quantified using these indicators.

### 5.3.1. Behaviour indicators

From literature it was shown that the shape of the Sand Engine shows great similarities to a Gaussian bell shaped curve. In literature, the development was compared to the theory proposed by Pelnard-Considere (1956), who theorised a concentrated nourishment diffuses over time following a Gaussian distribution. The following quantifiable parameters and subsequent indicators are found from previous literature (De Schipper et al., 2016, Roest, 2017):

- The advective behaviour. Quantified with the centre of mass of the coastline and the alongshore movement of the most seaward cross-shore extent.
- The diffusive behaviour. Quantified with the theory by Pelnard-Considere (1956) with the cross-shore extent (y), using the relation $y \propto \frac{1}{\sigma}$, where $\sigma$ denotes the standard deviation of a Gaussian distribution.
- The asymmetrical behaviour. The shape of the Sand Engine was quantified by the skewness of the shoreline position.

Since a Gaussian bell shaped curve is a probability distribution, it is unsurprising these indicators in fact all describe a characteristic based on the method of moments. This method supports in proving convergence of a distribution, e.g. a Gaussian curve. The k$^{\text{th}}$ moment of a continuous function is:

$$m_k = \int (x-c)^k f(x)\,dx \tag{5.3}$$

In case $c = 0$, the raw moments are computed, while if $c = \bar{x}$, the central moments are computed, with $\bar{x}$ the mean value of the variable considered. Each order of the moment expresses a characteristic of a function. The surface area below a distribution function is equal to the zeroth order raw moment, which translates to a volume in the case of the surface area the variable considered is the volume integrated profile. Further, the advective behaviour is the first order raw moment (M1), diffusive behaviour the first order central moment (spreading, M2), and the asymmetrical behaviour the ratio of third and second central moments (the skewness, M3/M2). One popular indicator has not been quantified in previous research: the peakedness or flatness of the shape, the ratio of the fourth and second central order moment (kurtosis, M4/M2). It should be noted that the presence of asymmetry and peakedness means the distribution of a variable deviates from a Gaussian curve, since these characteristics are by definition absent in this type of a probability distribution (Diaconis, 1986).

### 5.3.2. Quantification of the behaviour

In this section four of the five described macro-scale behaviour indicators (M1 - M4) are quantified for the considered depth regions (section 5.1.2. The developments of the M0 (volumetric changes) are neglected here, since these were previously discussed.

The advective behaviour results in a linear movement of the CoM northward, up to a cumulative value of circa 1% of its initial width (120m in the first 6.5 years). This is observed over all depth regions, although the

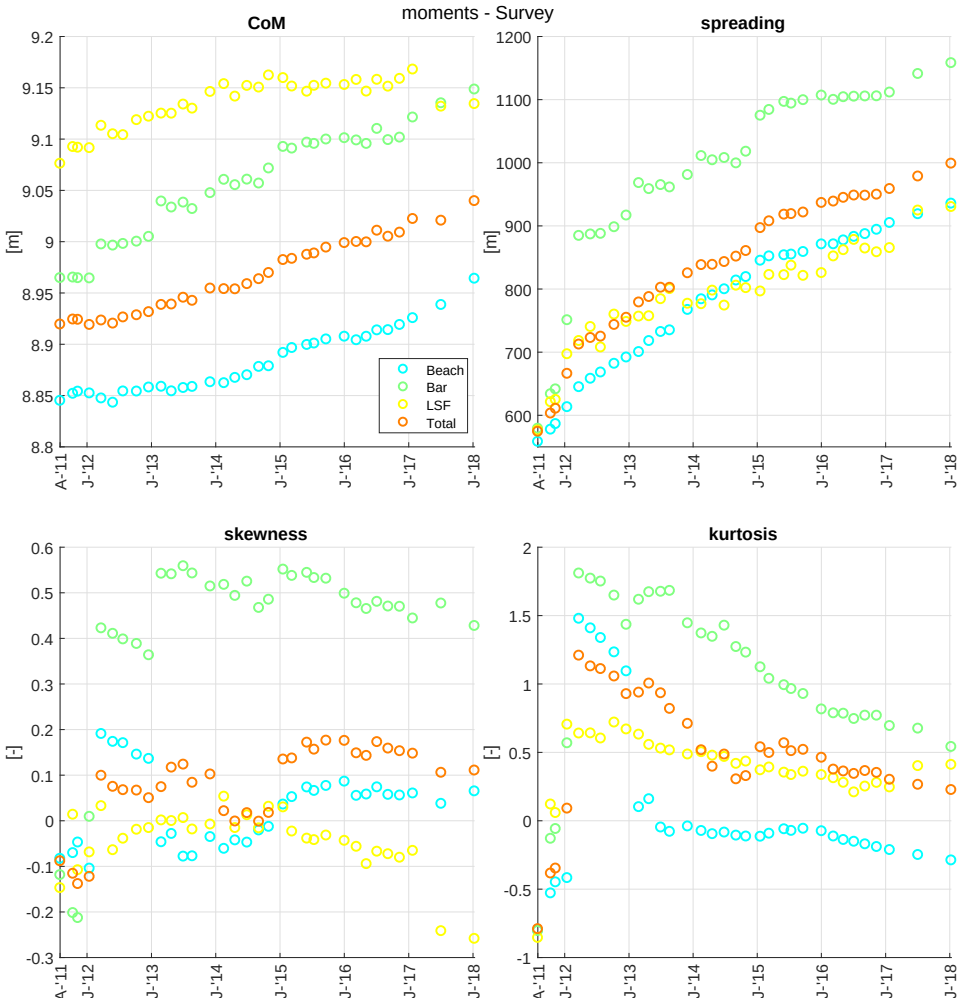


Figure 5.10: Behaviour indicators of depth regions of the Sand Engine

initial positions of the centres of mass differ per depth region 5.10. Second, the diffusive behaviour resulted in a spreading that has roughly doubled since the construction. The initial rapid development of the sub-tidal bars in the Regions of Contribution have resulted in a rapid spreading in this depth region. Trends in the asymmetric behaviour are far less clear. Neglecting the Bar region, the skewness is mild over all depth (<0.5), but not absent, nor is there a tendency where the shape migrates towards 0 skewness, which would agree with the shape of a Gaussian curve. On the contrary, the observed peakedness that initially increased due to a rapid feeding of the north, decays over time. In terms of the peakedness, the shape of the Sand Engine may be moving towards a Gaussian curve (which by definition has an excess kurtosis equal to zero), but this cannot be confirmed based on the current trends yet.

A curve-fit of a linear function describes the developments of the CoM of the Bar region (-8/-3m + NAP) and Beach (-3/+3m + NAP) well ($R^2$ = 0.9 and $R^2$ = 0.95). The curve-fit of a linear fit of the CoM in the LSF region (-10/-8m + NAP) describes the developments more poorly ($R^2$ =0.63), while a curve-fit of the movement of the CoM in the Total region (-10/+3m + NAP) performs well (($R^2$ = 0.98)). Square root curve-fits of the spreading show great results, with good performance of the Total and Beach region ($R^2$ = 0.99). Trends could not be used to describe the developments in the skewness of the shape ($R^2$ <0.3). The developments of the kurtosis could be described reasonably while an exponential fit that migrates towards 0 performs reasonable ($R^2$ = 0.8).

Roest (2017) suggested the migration of the centroid could be represented by the alongshore movement of the maximum cross-shore extent of depth contours. This approach, slightly adjusted since here volume densities are considered, is reapplied to the Total region (-10/+3m), and compared to the observed migration expressed in the M1. Results indicate the maximum cross-shore extent cannot be used to represent the migration of the centroid (see appendix D).

The capacity of a Gaussian curve to reflect the developments of the volumetric shape are quantified in terms of the coefficient of determination ($R^2$), and the Root Means Square Normalised Error, see figure 5.11. Particularly the $R^2$ shows the curve-fit performs well over time. A slight decrease of the performance in terms of the $R^2$ of the curve-fit can be identified over time. Whether this is due to the fact that the volumetric shape is diffusing (and thus flattening), or due to a larger growing deviation from a Gaussian is difficult to identify. The constant value of the RMSNE suggests the former is true. Results however, support the Sand Engine agrees with the concept of diffusion by a concentrated nourishment, in line with the findings by Pelnard-Considere (1956).

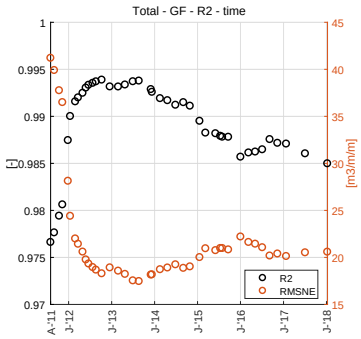


Figure 5.11: Performance of a curve-fit of a Gaussian over the volumetric shape. Note the different axes on the vertical.

### 5.3.3. Summary of results

Results have shown the behaviour indicators that quantify the volume (M0), the advection (M1/CoM), and the spreading (M2), develop continuously and therefore predictably, with good performances of curve fits ($R^2$). The curve-fit of a Gaussian confirms the Sand Engine develops following the diffusion concept as proposed by Pelnard-Considere (1956).

## 5.4. Dependence of performance on behaviour

Qualitatively, similarities between the developments of the performance indicators and the diffusive behaviour are readily established. Both the performance as well as the diffusive behaviour indicator showed a deceleration over time. The dependence of the performance indicators on the behaviour indicators is quantitatively verified in this section.

The development of the performance indicators since the construction over time is plotted against the change of the behaviour indicators. Here, the behaviour is quantified in terms of the spreading (M2). With the linear least square method a regression analysis the linear dependence of the performance indicators is quantified (Devore, 2011).

Plotting the volumetric performance indicators against the spreading, reveals a high dependence of the volumetric changes, with high coefficients of determinations ($R^2$>0.9, see figure 5.12). The curve fits quantify the effect of a meter of spreading of the Sand Engine. Every meter the M2 increases with 1m, the volume of the south grows by 2911m$^3$), and 5005m$^3$ on the north, while the middle loses 9882m$^3$. An asymmetry in the feeding is observed to the south and north.

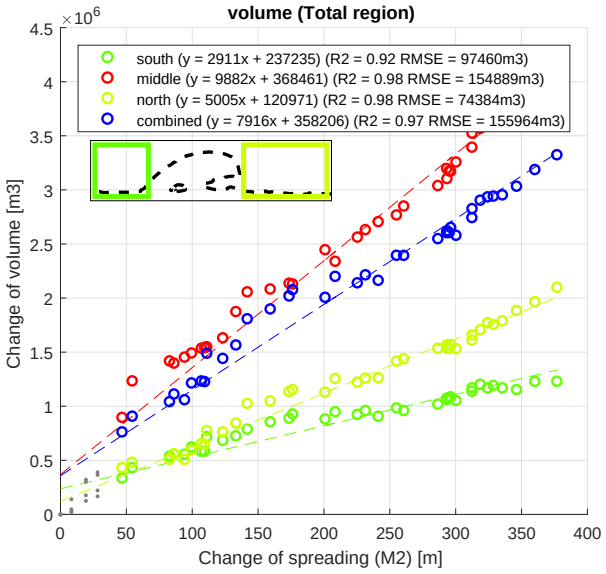


Figure 5.12: Dependence of volumetric performance indicators on spreading (M2). Legend includes the functions of the regression (with x the growth of the M2), and the performance of the curve-fits. Volumetric contributions in green. Combined contribution in blue. In red the volume reduction (absolute values) of the middle.

The geometric performance indicators showed great correlations with the spreading as well (figure 5.13a and figure 5.13b). The linear dependence of the movement of the centroids on the spreading is smaller than the dependence of the Accretion Points, making the latter a more representative performance indicator for the macro-scale behaviour. As could be observed for the volumetric contributions, an asymmetry in the growth can observed, with better performance on the north side. To assess the influence of the advective behaviour on the performance, the movements of the geometric indicators are normalised for the northward movement of the centroid of the overall Sand Engine (see figure 5.10a). Results show the difference between the movement of the Accretion Points north and south partially explained the advective behaviour (figure 5.13c). Normalisation does show to fully explain the difference between the movements of the centroids (figure 5.13d).

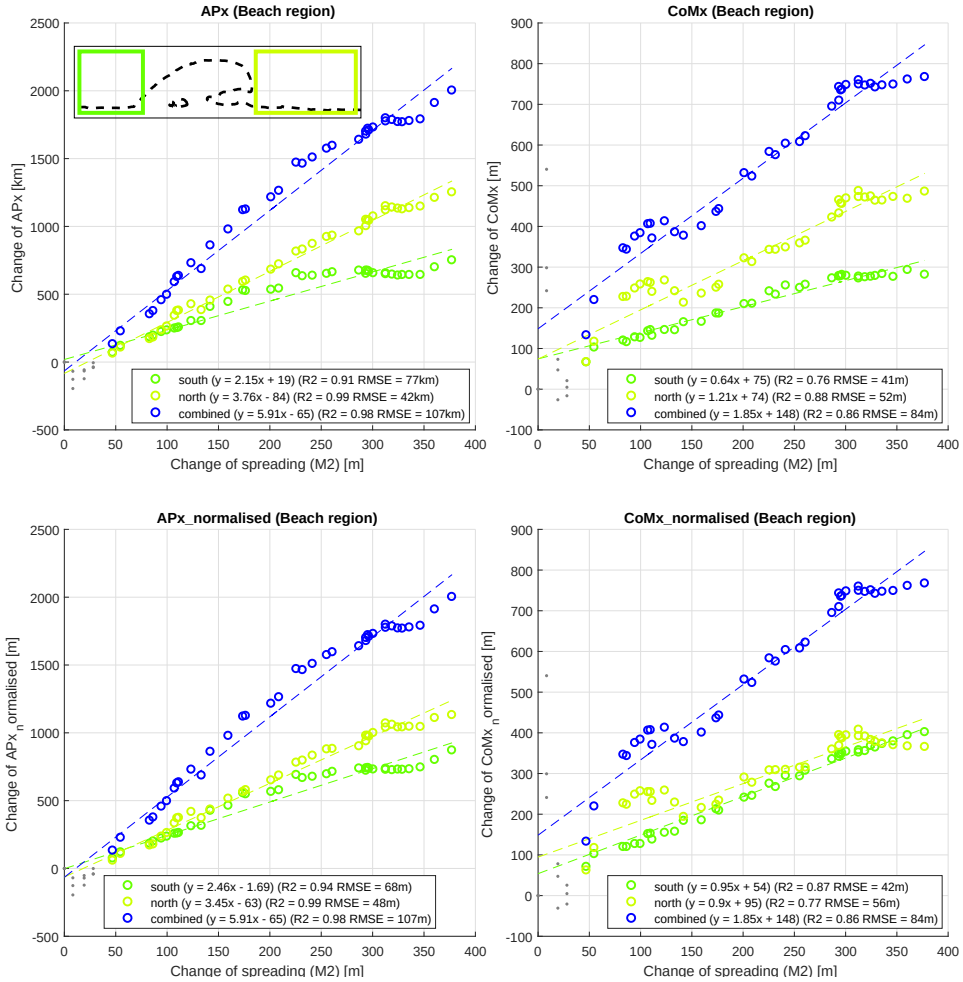


Figure 5.13: Dependence of geometric performance indicators on spreading (M2). The two top panel a and b depict the dependence of the observed movement of the Accretion Point and the centroids. The two bottom plots visualise the development of these indicators as well, but now normalised for the movement of the centroid of the overall Sand Engine, as quantified in figure 5.10a. The legend includes the functions of the regression (with x the growth of the M2), and the performance of the curve-fits. Geometric performance of the south and north in green. The distance between the indicators in blue.

One factor of great interest is the slope of the linear fit of the distance between the Accretion Points (*combined* in figure 5.13). This factor of 5.91 defines the increase of the Region of Influence as a function of the change of spreading (M2). The change of the Accretion Points can thus roughly be approximated by three times the spreading. In statistical terms, the M2 is equal to the standard deviation ($\sigma$), if a Gaussian curve is considered. In the case of a Gaussian curve at $3\sigma$ defines the band where , 99.7% of values lie within this band around the mean of a volume of the nourishment is located. The methodology of defining the Accretion Point thus agrees well with the point it is supposed to indicate: the region up until where accretion is observed.

The third quantifiable parameter of the performance and validation tool is the lifetime. Both, the volume reduction as well as the reduction of the cross-shore extent, show a high linear dependence on the spreading ($R^2 \approx 0.9$).

## 5.5. Conclusions

The performance and validation tool was applied to the Sand Engine. This to verify the development of the indicators is predictable. This was verified in two ways: 1) by assessing the performance of curve-fits through the developments of the performance indicators and 2) by verifying the performance indicators depend on the observed behaviour.

The performance volumetrically as well as geometrically is dominated by long-term trends. The developments of the performance indicators show a deceleration over time. Curve-fits can describe well the developments ($R^2 > 0.95$). From the verification, it is concluded the performance indicators develop predictable. The

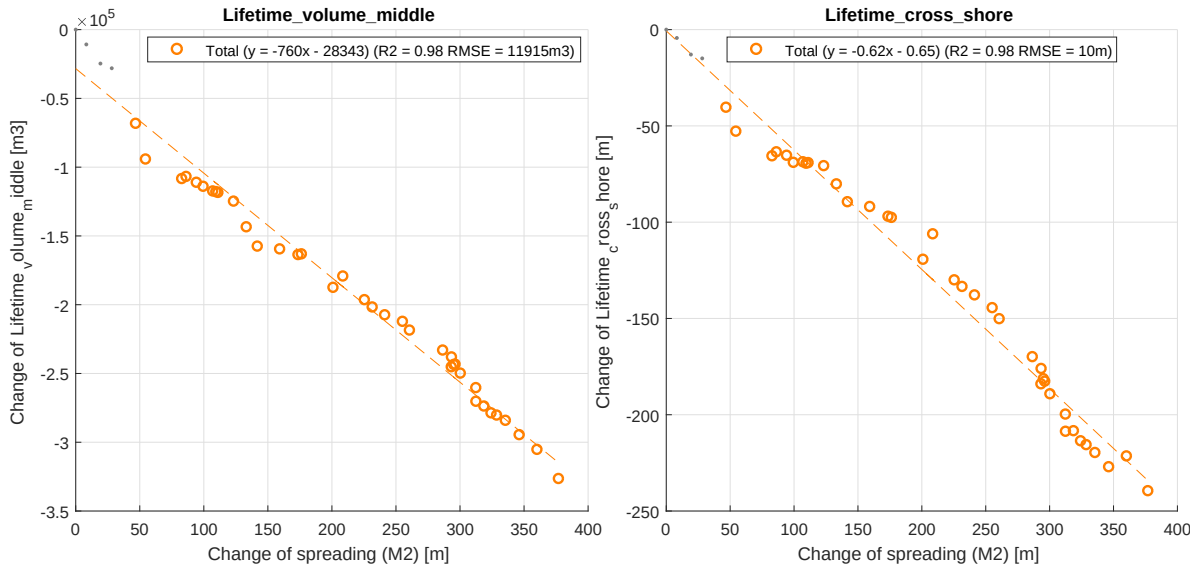


Figure 5.14: Dependence of Lifetime performance indicators on spreading (M2). The left panel depicts the dependence of the observed movement of volumetric reduction in the middle, the right panel the development of cross shore extent. The legend includes the functions of the regression (with x the growth of the M2), and the performance of the curve-fits. Developments in the Beach region in blue, Bar region in green, LSF region in yellow, and Total region in orange.

same observations were made for the behaviour indicators that quantify the advection and the diffusion ($R^2$ > 0.98). The dependence of the performance indicators on the behaviour indicators showed the indicators are behaviour-based, further proving the indicators can be predicted well.

More specific to the case study of the Sand Engine, 4.3$Mm^3$ (28%) of the initial volume has eroded in 6.5 years. This is compensated for by volumetric growth in the adjacent coasts cumulating to 3.3$Mm^3$ (77%) of the observed losses in the middle. An asymmetric growth of the adjacent coasts is observed, presumably caused by the dominant wave behaviour from the south-west. A large difference in the erosion-rate in the middle section is observed, with an erosion of 45% of the initial volume in the Beach region (-3/+3m), and a mere 10% in deeper regions.

In the Beach region (-3/+3m + NAP) volume reductions (43%) are larger than in lower regions (10 - 15%), three to four times faster. Further this, it is concluded no single depth region can be identified to represent the developments of the volumetric shape. However, a representative depth can be used to quantify the performance of the adjacent coasts, since volumetric contributions in the Regions of Contribution are more similar over depth. In the case of the Sand Engine, the Beach region could be used as a representative region. Whether this also holds for the shoreline is further elaborated on in the discussion (chapter 8).

The applicability of the indicators of the volumetric performance has been proven to be successful in previous research ((Arriaga et al., 2017), (De Schipper et al., 2016), (Luijendijk et al., 2017), (Roest, 2017)), as is confirmed here. The quantification of the geometric performance has been more troublesome in the past (Roest, 2017). Two new indicators were proposed to quantify the alongshore expansion: the Accretion Point and the centroids of the volumetric growth in the regions of contribution. The Accretion Point is easier to comprehend, while it could be argued that the centroids of the Regions of Contribution are better representatives of the widening. Since the Accretion Points showed to develop highly continuous, and since these were highly correlated with the behaviour indicators, it is concluded this indicator is the preferred alternative in representing the geometric performance.

# 6

# Model validation

In this chapter, models are validated for their capacity to describe the performance of the Sand Engine. The validation is executed to what extent analytical and numerical model approaches can be used to describe and predict the performance of a mega-feeder nourishment.

In the first section, several approaches of the analytical model adopted from the solution by Pelnard Considère are discussed, followed by a validation using performance and validation tool. One secondary objective of this thesis was to identify the dominant behavioural elements of a mega-feeder nourishment. the dominance of behavioural elements is quantified by means of the validation of model approaches with and without these elements. In the third section, three calibrated 2D numerical model approaches of Delft3D are validated as well. The validation also enables the assessment of the influence of acceleration technique, as well as the influence of a curved grid. The chapter is finalised with a review of the performance and validation tool.

## 6.1. Validation methods

The capacity of a model to reflect the performance of a mega-feeder nourishment is quantified with the proposed performance and validation tool, see chapter 4. Prior to this assessment, a more integral assessment is executed, by validation of the alongshore volume.

### 6.1.1. Validation of the alongshore volume

The alongshore volume is quantitatively compared by adjustment of an existing assessment methodology (see section 2.4.3) (Dean, 2002):

$$\epsilon_V = \frac{\sum_{xmin}^{xmax} |V_m(x,t) - V_o(x,t)|}{\sum_{xmin}^{xmax} V_o(x,t)} \tag{6.1}$$

Where $\epsilon_V$ denotes the total volumetric error as a fraction of the total observed volume along the considered alongshore coast (defined by xmin and xmax), $V_m$ denotes the computed alongshore volume of the model in an alongshore section and the subscript o the observed alongshore volume.

The second part of the validation of the alongshore volume comprises of a quantification of the model approaches resembling a Gaussian curve. In the performance and validation tool, indicators were introduced that quantify the performance of a mega-feeder nourishment. As it was shown that the development of the performance indicators of a mega-feeder nourishment develop proportional to the diffusion following a Gaussian curve, resemblance is a prerequisite for a model. If this condition is met, it is confirmed the behaviour is well represented by a model. If not, the performance indicators will develop differently than is to be expected. Predictions of these models will not lead to viable results. In order to validate this, a Gaussian curve is fitted onto the volumetric shape using a non-linear least square methodology, using the similar approach as De Schipper et al. (2016) and Roest (2017). The resemblance with a Gaussian curve is quantified by means of the $R^2$ and the RMSE, as described in 5.2.1.

### 6.1.2. Validation of the performance

The largest segment of the validation consists of the application of the performance and validation tool introduced in this thesis.

The capacity of the models to reflect the performance indicators is quantified by a number of frequently used statistical measures.

The validation comprises of a quantitative comparison of the performance indicators at each time step of a the bathymetric surveys. The errors used here include the Mean Absolute Error, and the (Root) Mean Squared Error, as introduced in section 5.2.1. Additionally, the Relative Mean Absolute Error, is a non dimensional measure that relates the mean absolute error to the observed cumulative change of a performance indicator:

$$RMAE = \frac{MAE(Y,X)}{MAE(X,x1)} \tag{6.2}$$

Where X and Y are sets of N of the measured, and modelled predictions respectively (e.g. X $x_1$,$x_2$,$x_3$,...,$x_N$) occurring at the same place and time.

## 6.2. Analytical model approaches

In chapter 5, it was concluded that the performance indicators of the adjacent coasts are linearly dependent on the behaviour indicator of the diffusivity. Secondly, previous research has shown the curve-fits of Gaussian curves perform excellently on depth contours of the Sand Engine ($R^2$ >0.9, (De Schipper et al., 2016, Roest, 2017)). These two results suggest the analytical model as proposed by Pelnard Considère can reflect the performance of a mega-feeder nourishment.

The analytical model cannot only serve as a model approach to describe and predict the performance of a mega-feeder nourishment, but it is used here as well to further increase the understanding of a mega-feeder nourishment. As described by (Diaconis, 1986), a major advantage of an analytical model, is that it results in a solution based upon a small number of parameters only. The dominance of the behaviour indicators is assessed here by the inclusion of the indicators in the analytical models. The influence is then quantified by means of the performance and validation tool.

In the first section, the application of the analytical model approaches are discussed. In the second section, the validation of the model approaches is elaborated on.

### 6.2.1. Application of analytical model approaches on the Sand Engine

The analytical model approaches are based upon the analytical solution proposed by Pelnard Considère as discussed in section 2.3.2, repeated here for clarity:

$$y(x,t) = \frac{Y}{\sqrt{4\pi G t}} e^{-\frac{(x-x')^2}{4Gt}} \tag{6.3}$$

With y the output, Y the (cross-shore) seaward extension of the nourishment, x is the location along the shoreline, and x' is the x-coordinate at the peak of the beach nourishment. G the diffusivity coefficient (where $2Gt = \sigma^2(t)$, with $\sigma$ the standard deviation). The output of the analytical model is the cross-shore distance from a reference line at a selected location x (with respect to the centroid) and time t since the construction. Since in this study the volumetric shape is considered rather than the shoreline position, the equation is rewritten to:

$$V(x,t) = \frac{VT}{\sqrt{4\pi G t}} e^{-\frac{(x-x')^2}{4Gt}} \tag{6.4}$$

*Non-calibrated model approaches*

Two deterministic approaches are applied. These approaches consist of the derivation of the diffusivity based upon bulk longshore sediment transport equations. Two alternatives are considered: 1) The classic **?** equation and the Kamphuis (1991) equation, see section 2.3.1 for a literature review.

When reviewing equation 6.4, it is observed the model assumes zero diffusivity at t=0. In reality however, the implemented mega-feeder nourishment does already have an initial spreading. To account for this difference, the model is adjusted, to match the initial diffusion with the observed diffusion:

$$V(x,t) = \frac{VT_{t=0}}{\sqrt{4\pi G(t+T_0)}} \exp\left[-\frac{(x-x'_{t=0}]^2}{4G(t+T_0)}\right] \tag{6.5}$$

The first deterministic approach is to infer the diffusivity coefficient from the CERC (1984) equation:

$$G = \frac{KH_b^{5/2}\sqrt{\frac{g}{\kappa}}}{8(s-1)(1-p)(h_c+B)} \cos 2\alpha_b \tag{6.6}$$

The second deterministic approach is to derive the diffusivity coefficient from the Kamphuis (1991) equation:

$$G = \frac{2K_2 H_b^2 T_p^{1.5} S^{0.75} D_{50}^{-.25}}{D} \frac{0.6}{\sin^{0.4} 2\alpha_b} \cos 2\alpha_b \tag{6.7}$$

The diffusivity coefficients that result from the equations based on the local conditions of the Sand Engine, as well as the observed diffusivity, derived from the M2, are shown in table 6.1. Results vary widely for the different approaches, with over-predictions by the CERC (1984) equation and the improved equation by Dean (2002), while the Kamphuis (1991) equation slightly under-predicts the diffusivity. The third columns depicts the square root of the diffusivity coefficients. These values are proportional to the movement of the M2 (spreading) over time, added here since the performance indicators were shown to be linearly dependent on the M2.

| Diffusivity | G [$m^2$/d] | $\sqrt{G}$ [m/$d^{\frac{1}{2}}$] |
|---|---|---|
| CERC | 2490 | 49.9 |
| Kamphuis | 93 | 9.6 |
| Observed | 170 | 13.0 |

Table 6.1: Diffusivity coefficients and square root of coefficients as per the different deterministic analytical model approaches, as well as the observed (mean) diffusivity.

From the literature review and the previous analyses, and assuming it is derived that the diffusivity coefficient, is equal to 0.9$km^2$/yr using the CERC equation, while using the Kamphuis equation, the value is equal to 0.034km2/yr, while the observed value for the diffusivity is 0.062$km^2$/yr (based on the curve-fit of the spreading (M2), from 5.10).

### *Calibrated model approaches*

Next to the deterministic approach, the diffusivity is derived from calibration of the data. Fits of the behaviour indicators, i.e. the migration of the centroid, the spreading, the skewness, and the kurtosis, are used to model the volumetric shape of the Sand Engine. These indicators were quantified in section 5.3.

One outlier in the analysis is the beta_fit. This fit is based on the four parameter beta probability function, that enables to incorporate developments in the skewness and kurtosis. For details on the probability functions, reference is made to respective literature (Kocherlakota et al., 1995, Steele, 1987). The aim of including this model approach in the analysis, is to assess the influence of skewness and kurtosis.

An overview of the differences between the analytical solutions is given in table 6.2. The model approaches with the most interesting results and differences are shown in this chapter, for the remaining outputs of the model approaches, reference is made to appendix E.

The resulting input from the approaches as described are depicted in figure 6.1. Figure 6.1c is visualises input for the model approaches, used to compute the development of the volumetric shape that serves as the input for the performance and validation tool. The spreading (M2), that quantifies the diffusive behaviour, is either computed with the diffusivity coefficients, or calibrated. The former values differ per approach, with over-predictions of the CERC approach, and under-predictions of the Kamphuis approach. The calibrated approaches are data-driven. This means that a curve-fit of a square-root function is used to describe the behaviour in terms of the diffusivity. All calibrated approaches therefore have an identical input in terms of the spreading. This explains why only the Plus-approach is visible; the other calibrated approaches lie behind the Plus approach. By definition the skewness and (excess) kurtosis are equal to zero in case of a Gaussian, as observed in the graphs.

| Alternative | PDF | volume | centroid | spreading | skewness | kurtosis |
|---|---|---|---|---|---|---|
| CERC | Gaussian | I | I | D | - | - |
| Kamphuis | Gaussian | I | I | D | - | - |
| Spreading_fit | Gaussian | I | I | C | - | - |
| Centroid_fit | Gaussian | I | C | C | - | - |
| Volume_fit | Gaussian | C | I | C | - | - |
| Plus_fit | Gaussian | C | C | C | - | - |
| Beta_fit | Pearson | C | C | C | C | C |

Table 6.2: Analytical model approaches. Non-calibrated approaches comprise of derivations of the diffusivity using the CERC and Kamphuis equations for bulk longshore sediment transport, while the approaches are based on curve-fits of the behaviour indicators. The 'D' denotes it is determined for that indicator over time. the 'C' it is calibrated, 'I' the initial value is assumed, and '-' the behaviour indicator is not included in the analytical solution.

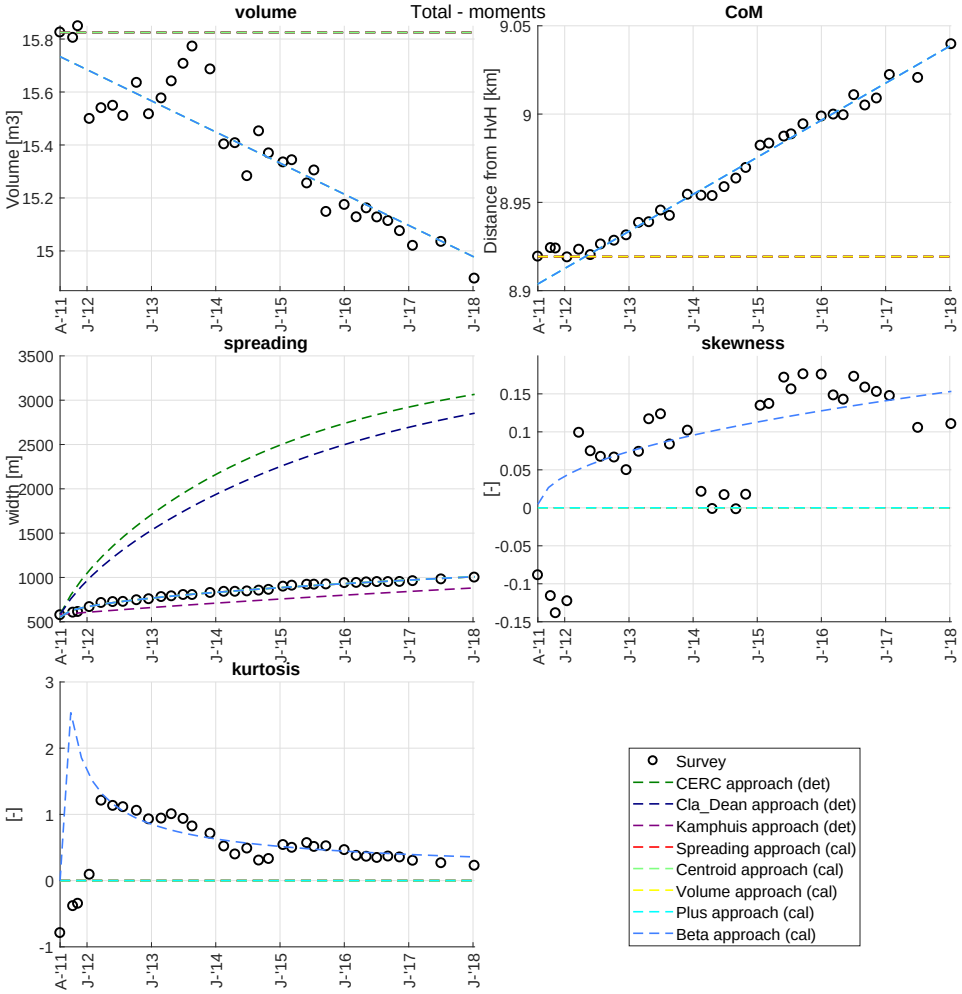


Figure 6.1: Input of analytical model approaches. The five panels depict the five behaviour indicators in accordance with the method of moments. Volume represents the M0, CoM the M1, spreading the M2, skewness the M3/M2, and kurtosis the M4/M2.

A few examples of the output of the analytical model in time are given in figure 6.2. Initially the volumetric shape of the output of the analytical model approaches deviates from the observed volumetric shape, but agreement increases rapidly. In terms of the CERC (1984) approach, the figure shows the consequence of the vast over-prediction of the spreading; the model has reached an almost constant distribution of the volume along the coast by 2018, whereas the observed distribution still shows a high concentration of volume around 9kms from HvH. On the other hand, the Kamphuis (1991) model approach shows reasonable agreement, as does the analytical model calibrated for the spreading.

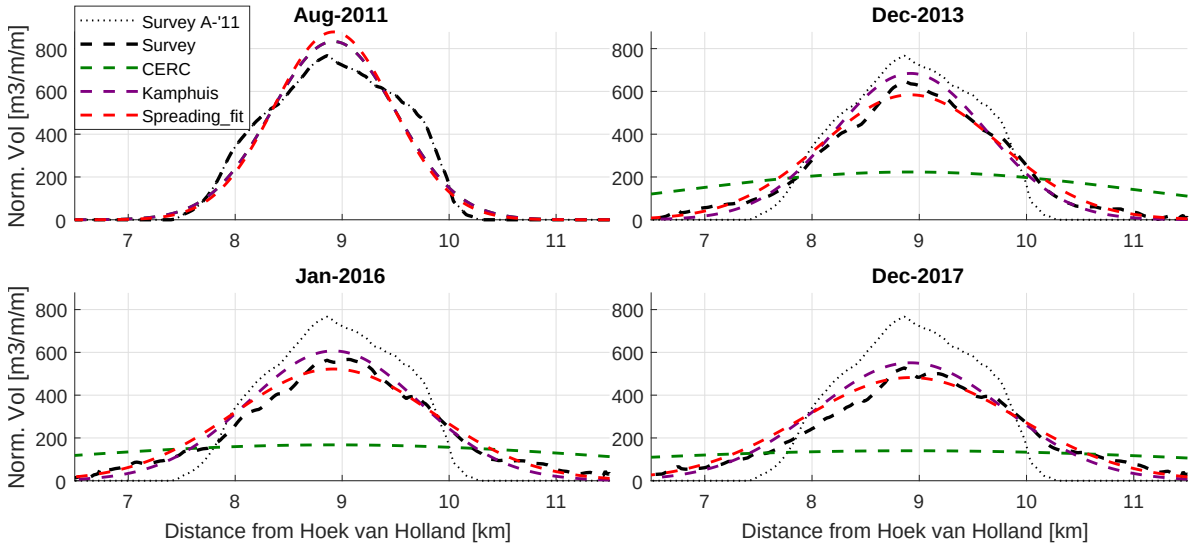


Figure 6.2: Volumetric shape observed versus analytical models (Total region [-10/+3m + NAP]). Panels include the modelled volumetric shape of two non-calibrated models: CERC (1984) and Kamphuis (1991), and the analytical model calibrated for the spreading.)

## 6.2.2. Validation of analytical model approaches

This section discusses the validation of the analytical model approaches. First the error of the alongshore volume is quantified, followed by the application of the performance and validation tool.

### Validation of the alongshore volume

The validation of the alongshore volume consists of a quantification of the mean gross error, and the resemblance of the model approaches with a Gaussian curve. Since the analytical model comprises of Gaussian curves, the latter is not quantified. The gross alongshore volumetric error is quantified per alongshore section (figure 6.3). After an initial rapid reduction of the error caused by the reshaping of the Sand Engine into Gaussian curve during the first eight months, the error of the calibrated analytical model approaches remains constant. The errors in the Regions of Contribution (the upper panels) are on average ~25% for the calibrated analytical model approaches, while the Kamphuis (1991) approach performs slightly poorer. The constant error of the calibrated analytical model approaches is explained by reviewing the results of figure 6.2. Structural errors are observed on the south and north, near the Transition Points and the Accretion Points. Near the Transition Points of the Sand Engine, the alongshore volumes are over predicted by all analytical models, while near the Accretion Points, the models under-predict the alongshore volume. Notoriously, the error of the Spreading approach is smaller in the north than the error of the Centroid approach. The Beta approach function performs slightly better overall, though only by a small margin.

### Validation of the performance

In this section the validation of the performance of a selected number of analytical model approaches is discussed. First the volumetric performance is reviewed, followed by the geometric performance, and the lifetime. For a full overview, reference is made to appendix E.

#### *The volumetric performance*

Table 6.3: Capacity of analytical model approaches to describe the volumetric performance, quantified by means of the Relative Mean Absolute Error.

| | **Non-calibrated** | | **Calibrated** | | |
|---|---|---|---|---|---|
| **Volumetric performance [%]** | CERC | Kamphuis | Spreading | Centroid | Beta |
| south | 151.5 | 39.7 | 23.9 | 6.8 | 13.5 |
| north | 181.5 | 47.7 | 9.5 | 26.7 | 10 |
| middle | 230.1 | 53.6 | 7.3 | 5.5 | 3.9 |

The volumetric performance is quantified here in terms of the volumetric changes of the south, middle, north, and the net developments of the regions combined, (figure 6.4). The CERC approach over-predicts the

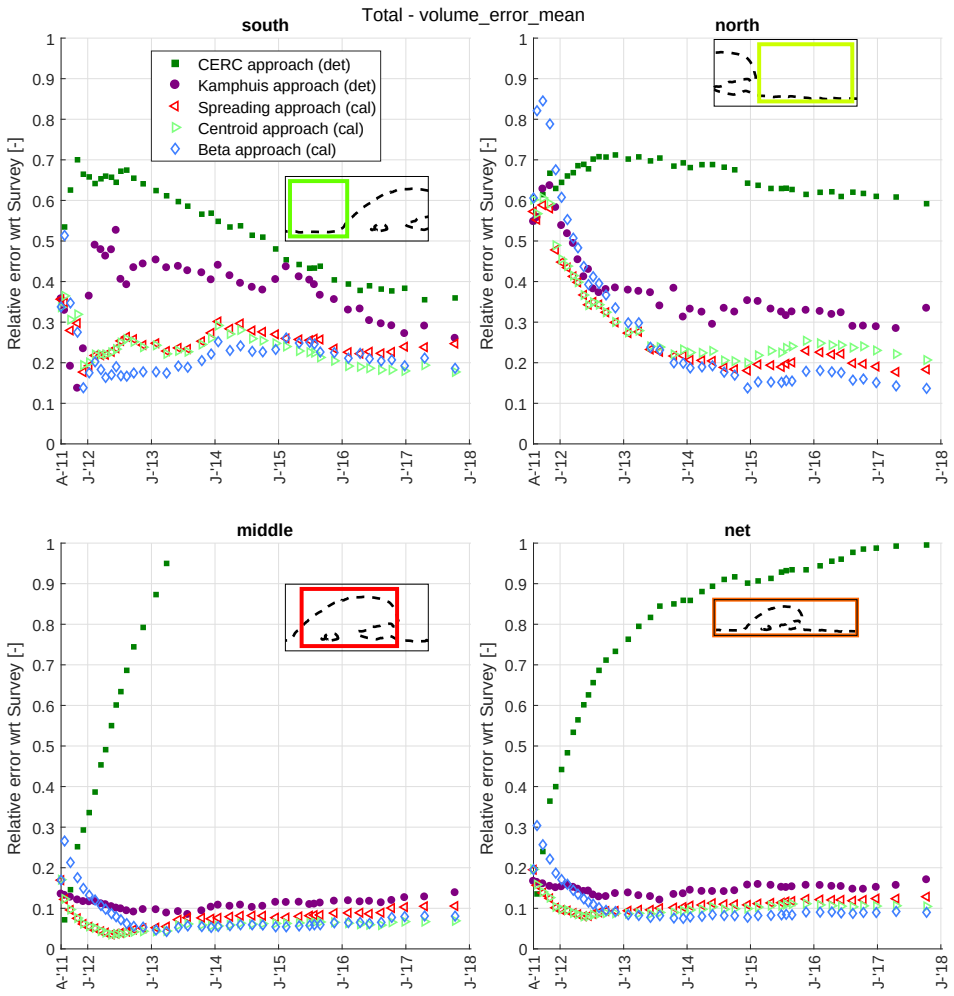


Figure 6.3: Alongshore relative mean gross volumetric error of numerical model approaches. Filled data points are non-calibrated approaches, triangles depict calibrated models.

volumetric changes that result in Mean Absolute Errors in the south, north, and middle of +152, +182, and -230 percent respectively (see table 6.3). More importantly, the decelerating trend observed in the surveys are is not resembled by the CERC (1984) model approach. The poor reflection is the result of the higher diffusivity (see figure 6.1). The predicted declines of the volumetric growth result from the fact that the model predicts the sediment will migrate from the RoF to beyond the defined outer edges of the Regions of Contributions. Application of the Kamphuis approach results in reasonable estimates of the volumetric performance, with Mean Absolute Errors of 40, 48, and 54 percent in the south, north, and middle respectively. Contrary to the CERC approach, the Kamphuis approach results in under-predictions of the volumetric growth on either sides. The Spreading fit approach, where the spreading is calibrated to the observed spreading, describes well the volumetric performance, with RMAE's of in the range of 24, 9.5, and 7.3 for the south, north, and middle. The Centroid fit, where both the spreading as well as the migration of the M1 are calibrated, mildly improves the reflection, while a the Beta approach does improve the description mildly.

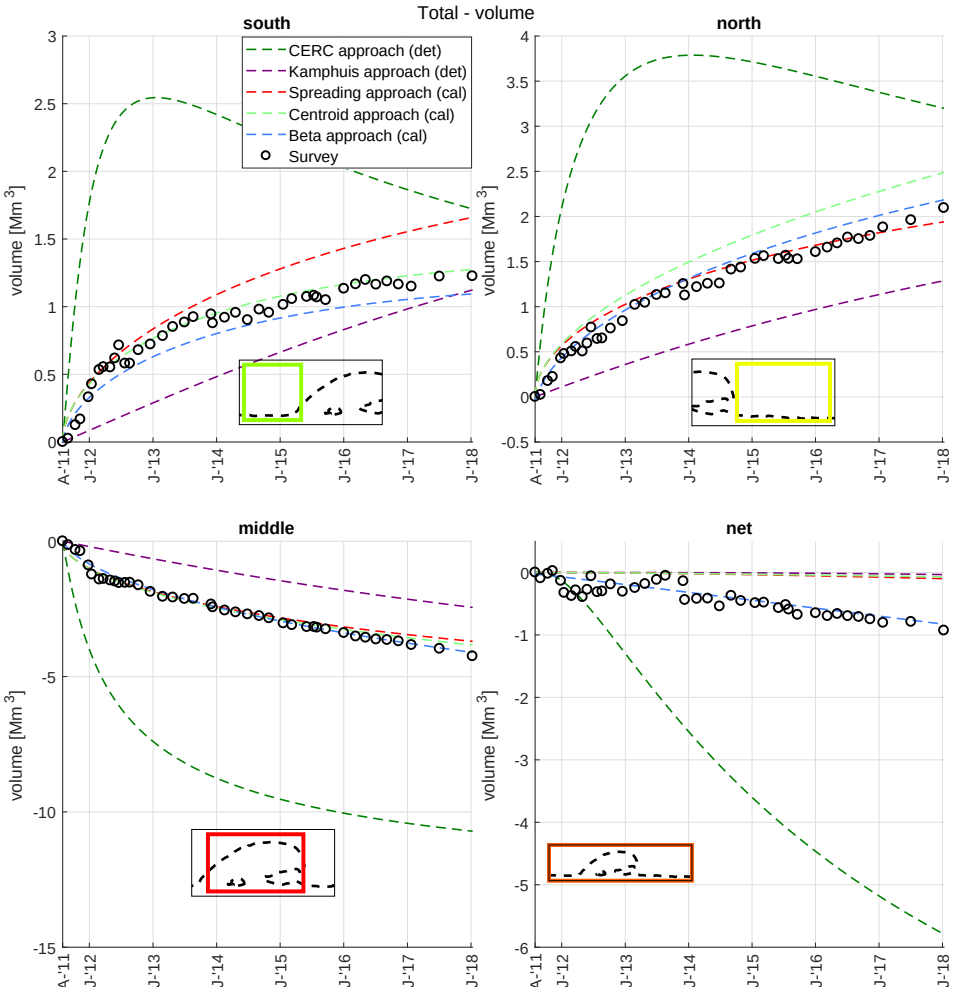


Figure 6.4: Volumetric performance by analytical model approaches. Observed versus model approaches. Note the different scales on the vertical axis per panel.

### *The geometric performance*

The geometric performance is validated based on the capacity a model reflects the Accretion Point. The Accretion Points, as defined as the alongshore location up until where accretion is observed, does not exist in the case of a Gaussian Curve, as by definition the curve never reaches a value of zero. To derive reflections of the Accretion Points nonetheless, the points were derived from the fixed ratio of $\tilde{3}$:1 between the Accretion Points and the spreading (M2) indicator that was identified in section 5.4).

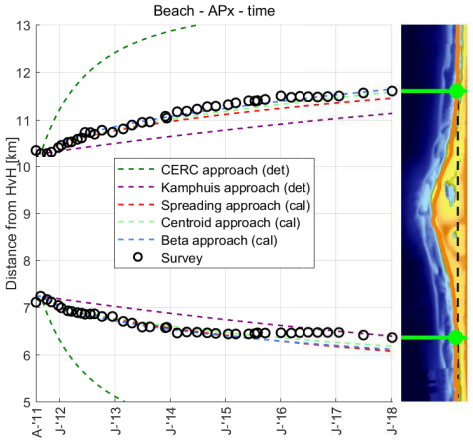


Figure 6.5: Accretion Points observed versus analytical model approaches

The application of this method leads to over-predictions of the migration of the Accretion Points by the CERC approach of over RMAE>200 percent (with Mean Absolute Errors of 1300m in the south, and 1800m in the north). The Kamphuis approach under-predicts the migrations, but describes the migration of the APs better. The RMAE is circa 50% for both sides, with translates to MAE of 240 and 400m on the south and north respectively.

Calibrated model approaches reflect the performance in terms of the Accretion Points well, with RMAE's all below 20%, equal to MAE<100m. Notoriously, the Beta approach describes the performance poorer than the Spreading and Centroid approach.

Table 6.4: Capacity of analytical model approaches to describe the geometric performance, quantified by means of the Relative Mean Absolute Error.

| | Non-calibrated | | Calibrated | | |
|---|---|---|---|---|---|
| **Geometric performance [%]** | CERC | Kamphuis | Spreading | Centroid | Beta |
| south | 229 | 42.0 | 13.5 | 11.0 | 13.1 |
| north | 242 | 54.3 | 19.1 | 14.0 | 11.4 |
| distance | 236 | 48.8 | 8.9 | 8.8 | 8.4 |

*The lifetime*

The third objective of a mega-feeder nourishment is related to the lifetime. The lifetime of the Sand Engine is represented by the percentile volumetric reduction of the middle section, as well as the reduction of the cross-shore extent. The CERC approach over-predicts the velocity of the volume reduction (Figure 6.6a), in line with findings of the other performance indicators. The Kamphuis approach under-predicts the reduction volumetrically, while the calibrated models approaches reflect the volume reduction well. No significant difference between the calibrated model is observed (RMAE = 5 - 7%) . Interestingly, the Lifetime cannot be described by any of the models using the percentile reduction of the maximum cross-shore extent. The model approaches show a more rapid reduction than observed. The good reflection of the Kamphuis (1991) approach is to be interpreted as a coincidence rather than a good description.

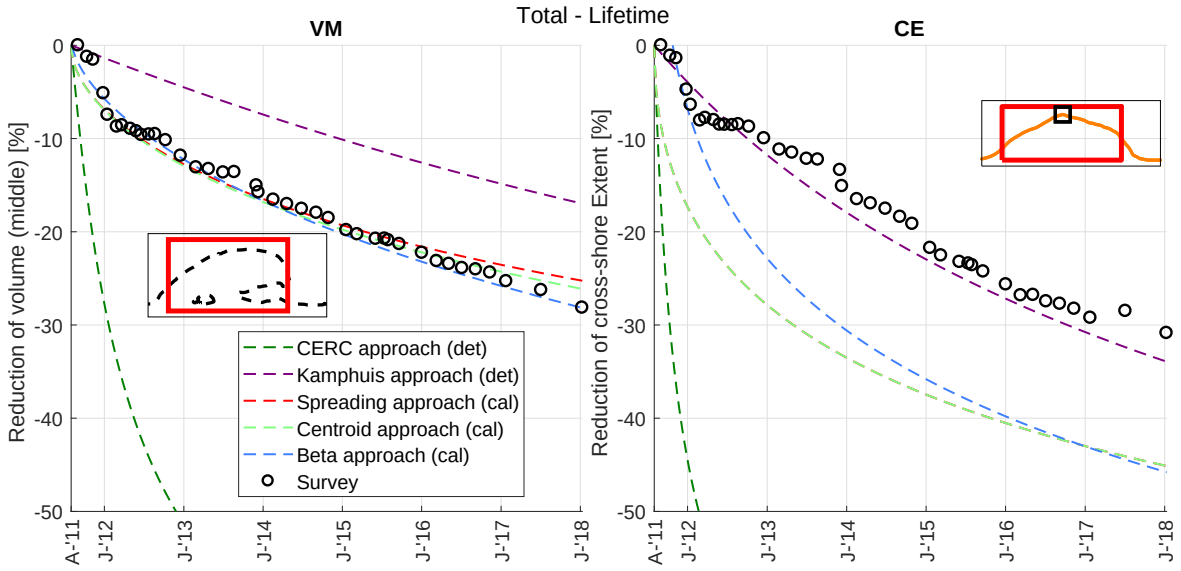


Figure 6.6: Lifetime indicators, observed versus analytical models. Left expressed in the volume reduction of the Region of the Feeder, right in the maximum cross-shore extent.

Table 6.5: Relative Mean Absolute Error of analytical model approaches to describe the lifetime indicators.

| | Non-calibrated | | Calibrated | | |
|---|---|---|---|---|---|
| **Lifetime [%]** | CERC | Kamphuis | Spreading | Centroid | Beta |
| Volume middle | 255 | 50.2 | 6.9 | 6.4 | 6.1 |
| Cross-shore extent | 319 | 12.0 | 96.0 | 96.0 | 73.2 |

### 6.2.3. Summary of results

The validation has shown description of performance indicators by an analytical model is a promising alternative to existing estimation methodologies. The validation consisted of two categories of model approaches: 1) non-calibrated approaches and 2) calibrated approaches. The former included the derivation of the diffusivity coefficient G based on the physical forcing conditions using bulk longshore sediment transport (LST) equations. The second type included the derivation of the input of the analytical model by curve-fitting of

behaviour indicators, such as the spreading (M2) and the centroid (M1).

The first LST approach, using the CERC (1984) equation, resulted in a vast over-prediction of the volumetric growth, alongshore expansion, and the lifetime. The $\sqrt{G}$[1], is a factor 4 too high, explaining these over-predictions. The second approach consisted of a derivation of the G from the Kamphuis (1991) LST equation. This approach resulted in reasonable reflections of the performance indicators (RMAE $\approx$ 50%), with mild under-predictions.

The second category of approaches consisted of using curve-fits behaviour indicator(s) as input for the analytical model. The Spreading approach, where the spreading (M2) was calibrated, resulted in great reflections of the gross alongshore volume and RMAE = 10%) and net volume reduction of the middle (RMAE = 7%). Approaches that included more behaviour indicators (e.g. the Centroid approach and the Beta approach) did not improve the reflections further. Reflections of the gross alongshore volumetric changes in the Regions of Contribution were good (RMAE $\approx$ 20 - 30%), as were the net volumetric changes (RMAE $\approx$ 10 - 30%). Interestingly, a significant improvement of the reflection of the volumetric growth was observed for the Beta approach, suggesting the asymmetry and kurtosis do play a role in the developments of the net volumetric changes. Reflection of the Accretion Points by the Spreading approach were great (RMAE = 10 - 20%), and mildly better for the Centroid approach (RMAE = 10 - 15%). , Inclusion of more behaviour indicators did not improve the reflections.

## 6.3. Numerical model approaches

In this section, the capacity of 2D numerical model approaches to reflect the performance of the Sand-Engine is discussed. With it, the influence of acceleration techniques, and the application of a rectangular nearshore grid is reviewed as well.

### 6.3.1. Overview of model approaches

Since the construction of the Sand Engine, a number of numerical model approaches have been developed, each with their own goals, e.g. predicting the future performance and behaviour, increasing the understanding of the Sand Engine, and/or to increase the performance of the numerical model approaches itself. In this thesis, three calibrated Delft 3D, 2D numerical models are reviewed for their capacity to reflect the performance of the Sand Engine. Reference is made to section 2.4 for a brief description of Delft3D and a selection of important model settings, and to section 3.7 for the background of the numerical model approaches. The model approaches considered are:

- The BruteForce model approach (Luijendijk et al., 2017). This most advanced and computationally extensive O (weeks) numerical model approach, enforces the physical forcing conditions onto the bathymetry as observed. A curved nearshore grid is applied to enable a movement of longshore sediment transport along the curved bathymetry of the Sand Engine.
- The MorMerge model approach by Luijendijk et al. (In preparation). For this model an acceleration technique is applied that reduces the computation time to O (days). The same curved nearshore grid is applied as was used for the Bruteforce model approach.
- The Stive model approach (Stive et al., 2013). Next to an acceleration technique, a nearshore rectangular grid is applied.

From a visual comparison of the observed and simulated bathymetries, it is concluded that the Stive approach has diverged from the observed developments (figure 6.7). The initial distinct hook shape can still be recognised in this simulation, which does not agree with the observed bathymetry. The MorMerge and Bruteforce approach visually agree better with the observed bathymetry in 2018.

[1] the performance indicators are linearly proportional to $\sqrt{Gt}$

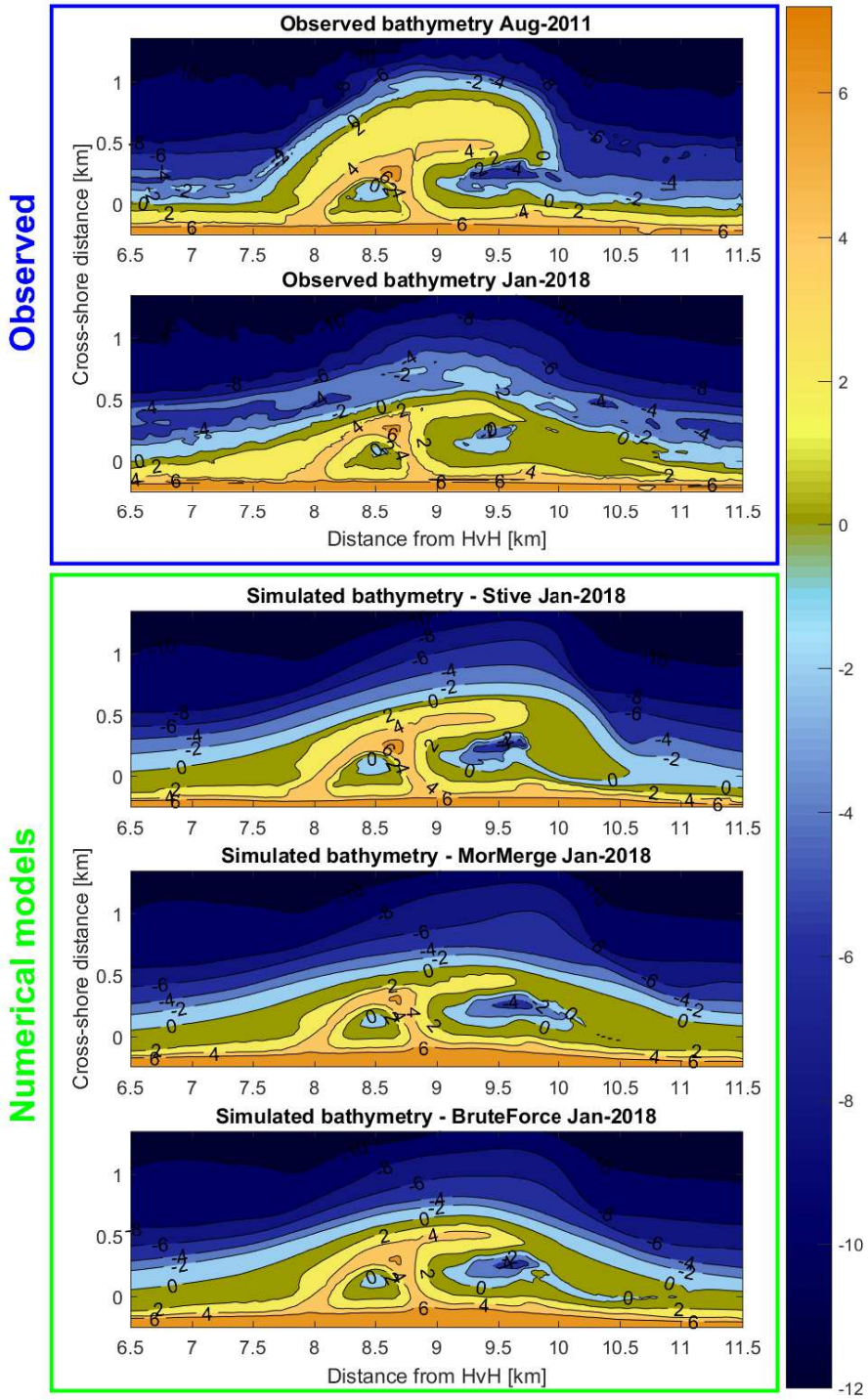


Figure 6.7: The two upper plots depict the initial and current (January 2018) bathymetry as surveyed. The three bottom plots depict the output of the simulations by the 2D numerical model approaches (Stive, MorMerge, and BruteForce)

From the simulated bathymetries of the numerical models, the volumetric shape was computed (figure 6.8). Interestingly, the Stive model approach shows a distinct northward feeding directly next to the initial location of the peninsula, instead of an overall spreading along the coast, as observed and simulated by the other two model approach. Further northward, the volumetric contribution is under-predicted. The MorMerge model seems to over-predict the erosion in the Region of the Feeder. Visually, the BruteForce model suggests to perform well.

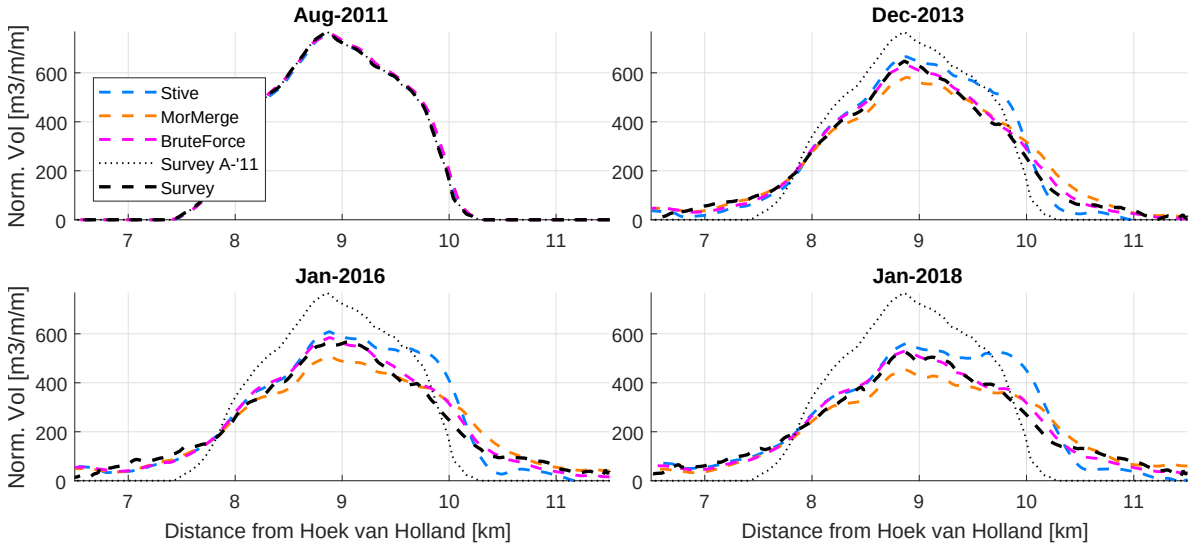


Figure 6.8: Volumetric shape, observed versus numerical models [Total region (-10/+3m + NAP)]. Dotted line depicts the initial volumetric shape as of August 2011 as a reference.

## 6.3.2. Validation of numerical model approaches

This section validates the capacity of numerical models to reflect the performance. Prior to application of the performance and validation tool, the alongshore volume is validated.

### Validation of the alongshore volume

The validation of the alongshore volume consists of a quantification of the mean gross volumetric error, and the assessment whether a model approach resembles a Gaussian curve.

The mean gross volumetric error of the BruteForce model is circa 30% in the south, 25% in the north, and a mere 5% in the middle section (figure 6.9). The MorMerge model performance mildly poorer for all sections. Most clearly, higher errors of the Stive model stand out, with error on the north approaching values in the same order of the observed net volumetric growth (In January 2015, the error is 90% of the observed net volumetric growth). Interestingly, the errors of the middle section show mild varieties in the error, while the errors in the Region of Contribution show a far larger variety in the errors. This suggests that assessment of the middle section is not representative for the performance of the Regions of primary interest: the adjacent coasts.

#### *Resemblance with Gaussian-curve*

Prior to the application of the performance and validation tool, it is required to assess the capacity to which the models develop (into) a Gaussian curve, as it was shown that the Sand Engine develops in accordance with the analytical model by Pelnard-Considere (1956).

The resemblance is validated by curve-fits of Gaussian curves on the volumetric shape of the numerical model approaches. Results show the Stive model approach deviates from a Gaussian curve, while the error of the model approaches with a curved nearshore grid show a performance equal to that observed for the Sand Engine (figure 6.10). Since the Stive model approach does not develop in accordance with a Gaussian curve, descriptions and predictions of the performance by the model approach will deviate from the observed developments.

### Validation of the performance

In this section the validation of the performance is discussed. First the volumetric performance is reviewed, followed by the geometric performance, and the lifetime. For a full overview of the quantifications of the reflections of the performances by the models, reference is made to appendix F. Despite the fact that it was shown the Stive model approach did not well resemble a Gaussian-curve was, its reflection on the performance is reviewed here to assess the influence of not meeting the conditions of a Gaussian curve.

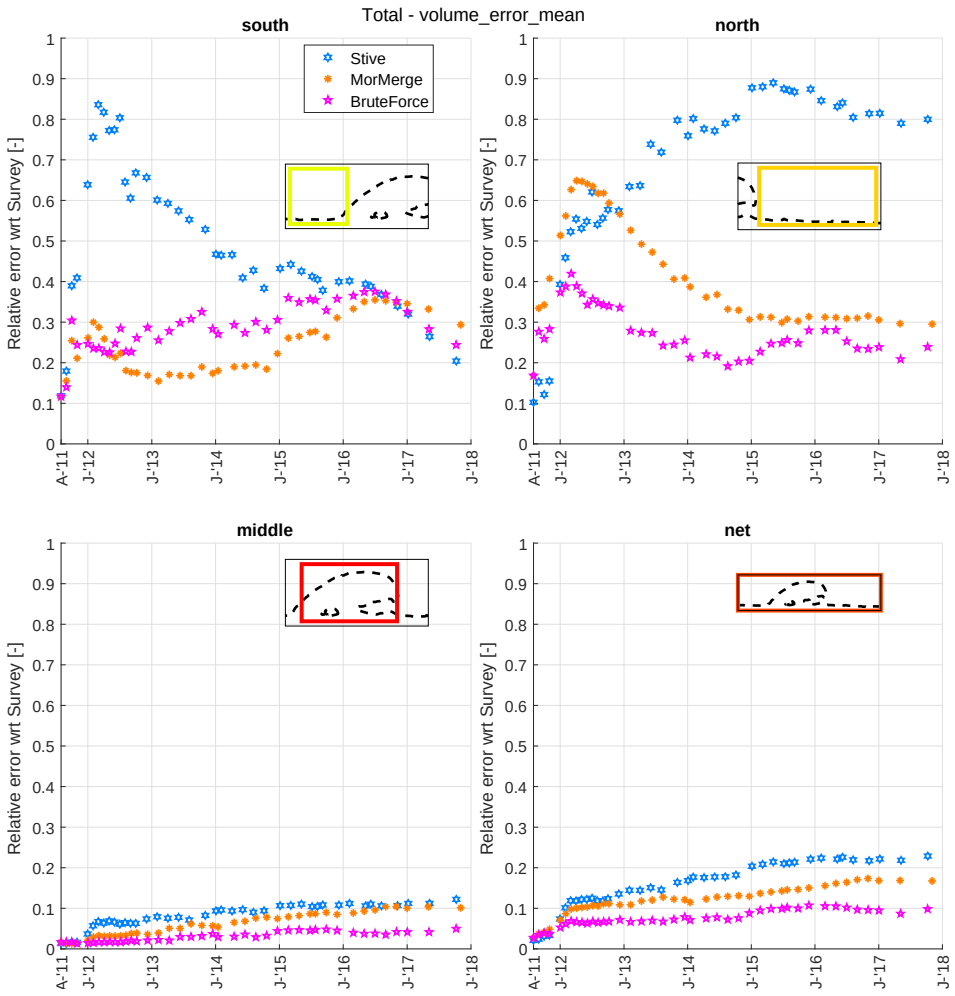


Figure 6.9: Alongshore relative mean gross volumetric error of numerical model approaches.

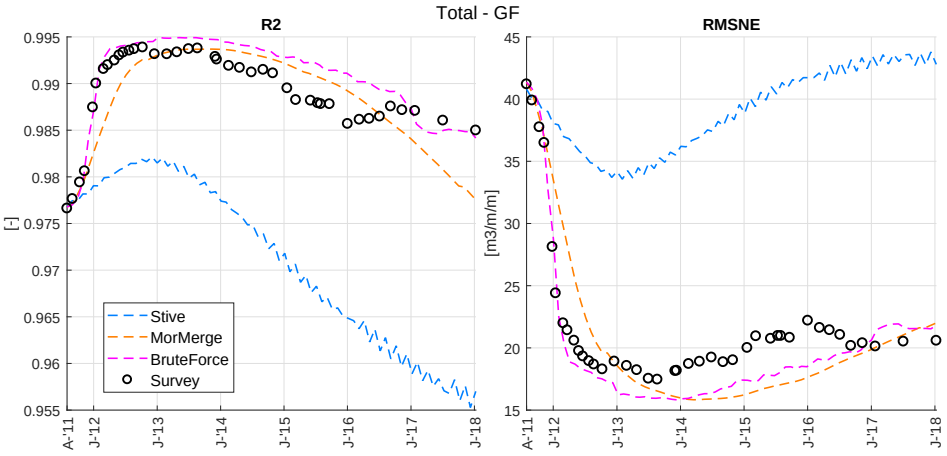


Figure 6.10: Quantification of the reflection of the numerical model approaches resembling a Gaussian curve. Left, the reflection quantified with the coefficient of determination ($R^2$, right with the Root Mean Square Normalised Error.)

### *Volumetric performance*

The volumetric performance is quantified by means of a validation of the net volumetric changes in the alongshore sections (south,middle,north,net) within the Total region (-10/+3m +NAP). The capacity of the model approaches to reflect the observed performance is quantitatively described with the Relative Mean Absolute

Error (see section 6.1.2 for an explanation).

The BruteForce model slightly underpredicts the volumetric growth on the south side (RMAE = 9.8%), while it performs well in the north and the middle with RMAE is 8.6% error and 9.8% respectively (figure 6.11). The reflection of the volumetric performance of the MorMerge model, is significantly poorer (south 10.3%, north 31.%, middle 21.9%). Expressed in MAE, the reflection of the volumetric performance on the south is similar to the reflection of the BruteForce model. However observation shows that the deviation of the numerical model develops differently from what is observed. More interestingly, its development agrees with the developments of the of the outcomes of the analytical CERC approach (figure 6.4). The Stive model approach reflects the volumetric performance poorly (south 24.5%, north 45.0%, and middle 50.9%). The volumetric changes of the separate sections do not develop the distinct decelerations that observed, which shows the influence of not meeting the requirement of the resemblance with a Gaussian curve.

Table 6.6: Relative Mean Absolute Error of numerical model approaches to describe the volumetric performance indicators.

| **Volumetric performance [%]** | **Stive** | **MorMerge** | **BruteForce** |
|---|---|---|---|
| South | 24.5 | 10.3 | 9.8 |
| North | 45.0 | 31.3 | 8.6 |
| Middle | 50.9 | 21.9 | 9.8 |
| Net | 120.7 | 53.6 | 35.4 |

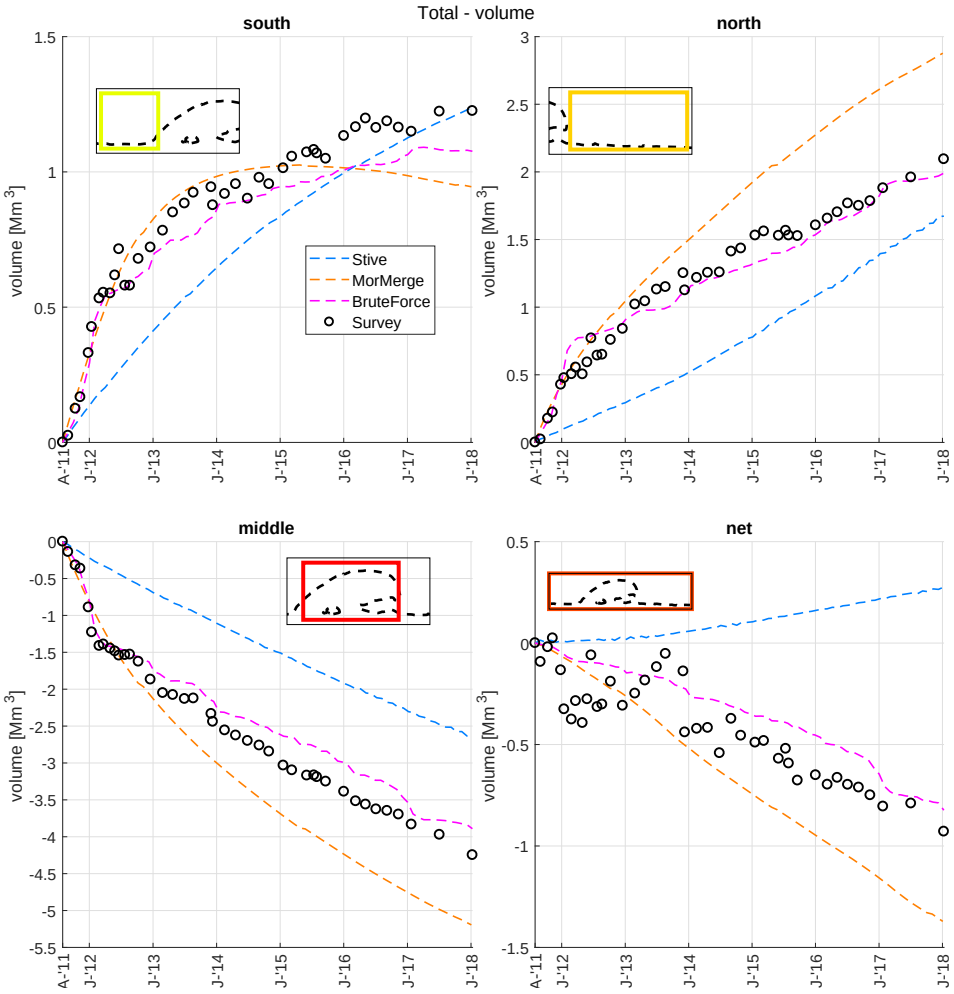


Figure 6.11: Volumetric performance observed vs numerical model approaches. Note the different scales on the vertical axis per plot.

### *Geometric performance*

The geometric performance is validated based on the capacity to which the model approaches can describe the developments of the Accretion Points in the Beach region (-3/+3m + NAP). Assessment of the centroids of the accreted volumes, as well as the Transition Points is included in appendix F.

None of the models reflect the Accretion Points well (figure 6.12a). Near the outer edges, the volumetric shape is not well reflected by any of the model approaches,resulting in deviations from the observed performance. This is more elaborately discussed in appendix I.

An alternative approach for reflecting the Accretion Points, is by means of the application of the fixed ratio between the movement of the Accretion Points and the spreading (M2), derived in section 5.4, which was found to be approximately 3:1. Application of this method leads to agreeable reflections of the Accretion Points, e.g. the RMAE's are in the order of 15 - 40 percent (table 6.7). The BruteForce approach is an effective method in improving the reflections, as is the application of the curved nearshore grid. Looking more closely to figure 6.12b, the alongshore extent is over-predicted by the MorMerge approach. The BruteForce approach is the preferred alternative for describing the developments of the AP, as for making predictions.

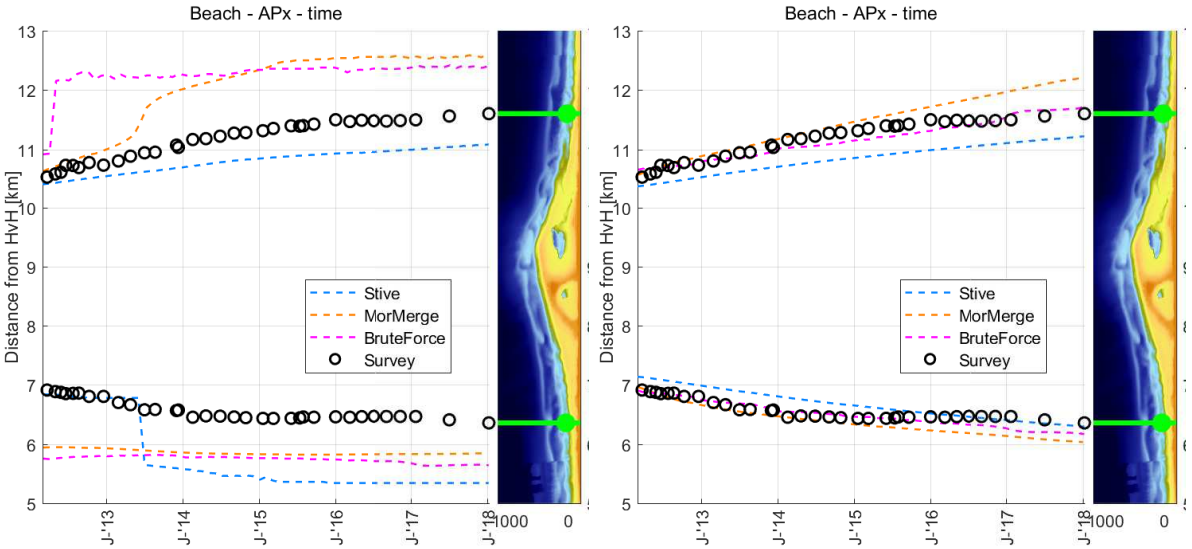


Figure 6.12: Reflection of Accretion Points by Numerical model approaches. Left panel the Accretion Points based on the definition of the location up until accretion is observed as a result of the feeding performance of the Sand Engine. On the Right panel, the Accretion Points computed via the identified ratio of the 3 AP: 1 M2.

Table 6.7: Relative Mean Absolute Error of numerical model approaches to describe the Accretion Points. AP normal quantifies the numbers of the errors if the AP is derived directly from the volumetric shape, see figure 6.12a, the AP from M2 numbers quantify the reflection based on the method visualised in figure 6.12b.

| **Geometric performance [%]** | | **Stive** | **MorMerge** | **BruteForce** |
|---|---|---|---|---|
| AP normal | south | 222 | 216 | 51 |
| | north | 64 | 124 | 182 |
| | distance | 49 | 157 | 207 |
| AP from M2 | south | 53 | 41 | 20 |
| | north | 61 | 31 | 18 |
| | distance | 56 | 34 | 15 |

### *Lifetime*

The third performance indicator for which the models are validated, is the capacity to which the approaches reflect the lifetime. In chapter 5, two indicators were proposed to quantify the lifetime: 1) the volume reduction of the Region of the Feeder, and 2) the reduction of the maximum cross-shore extent. Contrary to the poor representation of the maximum cross-shore extent by the analytical model approaches, the numerical model approach perform well for this indicator (figure 6.13). The model approaches also reflect the performance well in terms of the volume reduction.

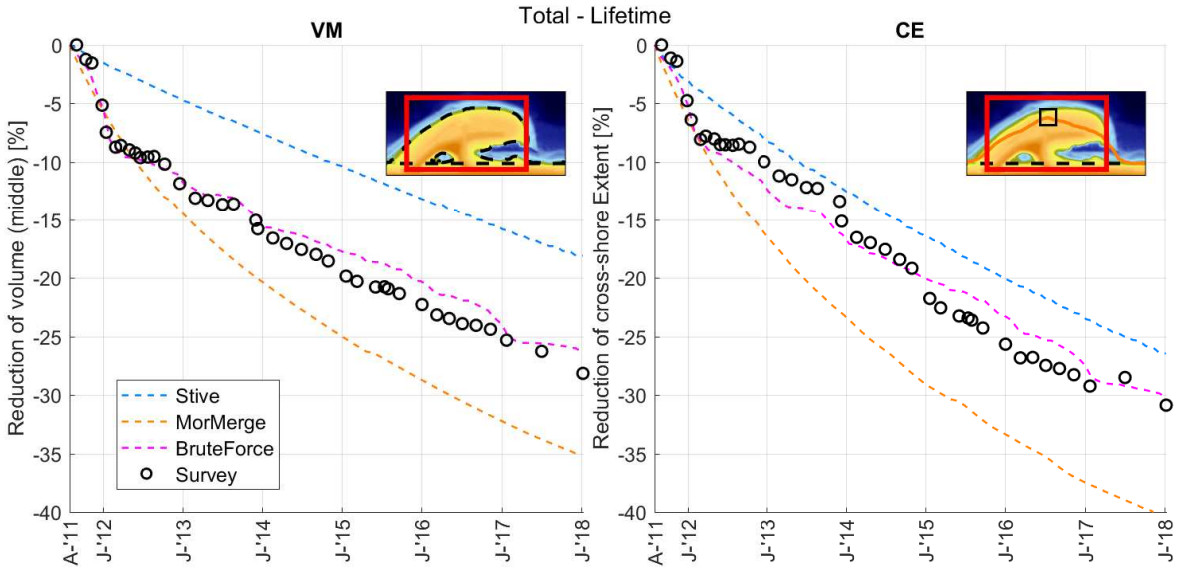


Figure 6.13: Lifetime indicators by Numerical model approaches. Left panel the volume reduction of the Region of the Feeder, right the reduction of the cross-shore extent.

Table 6.8: Relative Mean Absolute Error of numerical model approaches to describe the Lifetime indicators.

| **Lifetime [%]** | **Stive** | **MorMerge** | **BruteForce** |
|---|---|---|---|
| Volume Middle | 47.9 | 26.9 | 7.4 |
| Cross-shore extent | 21.3 | 39.1 | 9.3 |

### 6.3.3. Dependence of performance on behaviour indicators

In section 5.4, it was shown the performance indicators were linearly proportional to the advective and diffusive behaviour of the Sand Engine. In this section, the data from the numerical model approaches is used to verify this relation.

Quantification of the behaviour by means of the centroid (M1) and the spreading (M2), shows the behaviour indicators are linearly proportional to the performance indicators of a mega-feeder nourishment. In line with the observations from the performance indicators, the BruteForce model performs well in terms of reflecting both the CoM and the spreading (figure 6.14). It is remarked the centroid movement of the BruteForce model slightly non-linear, other than the distinct observed linear migration of the centroid. This may influence predictions of the model approach.

The MorMerge shows an acceleration of the CoM over time, and a spreading rate that exceeds that of the observations. Both indicators thus show more rapid developments than are observed. The accelerative migration of the centroid explains partially the observed decline of the volumetric growth on the south, as well as the higher volumetric growth on the north. The higher spreading rate also explains the over-predictions of the velocity of developments in the reflections of the performance indicators.

The Stive approach shows a milder migration of the centroid, as well as lower spreading. Interestingly, the observed errors of the Stive approach in reflecting the developments are not significantly poorer than the reflections by the MorMerge approach, which showed to reflect the performance than the Stive approach. This shows the importance of the prerequisite of the resemblance with a Gaussian curve (section 6.3.2). During the validation of the resemblance with a Gaussian curve, it was shown the Stive approach did not reshape into a Gaussian. As a result, the behaviour indicators reflected by the Stive approach, cannot by used to represent the behaviour in the same manner as for the data, and the MorMerge and BruteForce model approach.

### 6.3.4. Summary of results

Three calibrated 2D numerical model approaches were validated: 1) A computationally extensive O (weeks) BruteForce approach, where no acceleration techniques were applied, 2) A MorMerge approach that included acceleration techniques to reduce the computation time to O (days), and 3) a Stive approach where accelerating techniques were used and a simplified rectangular grid was applied. Validation consisted of two seg-

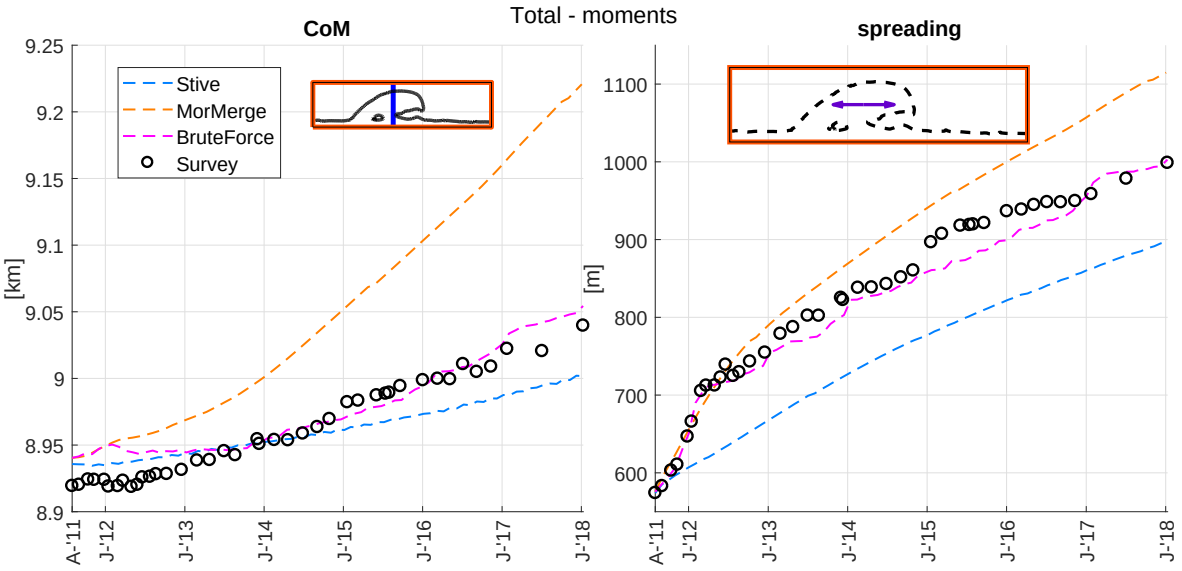


Figure 6.14: Advective and diffusive behaviour, observed vs numerical model approaches. Note the different vertical scales.

ments: 1) validation of the model developing following the shape of a Gaussian curve, and 2) validation of the capacity to reflect the performance.

The BruteForce model approach reflects well the developments following a Gaussian curve. Validation of the performance showed the approach reflects well the performance of a mega-feeder nourishment. The MorMerge approach showed to develop into a Gaussian shaped curve, but the velocity of developments of the performance indicators were over-predicted. Quantification of the behaviour indicators showed both the migration of the centroid, as well as a too high spreading caused these over-predictions. The Stive approach did not lead to a reshaping into a Gaussian curve. The performance indicators were not well described by the model, as a result of the deviation.

## 6.4. Review of performance and validation tool

In this study, the alongshore sectioning was based upon the Transition Points defining the Region of the Feeder, and two fixed points at the outer edges that define the Region of Influence. This alongshore sectioning determines to a high degree the outcome of for example the quantification of the volumetric performance. Theoretically, the regions considered could be chosen such, that description of model results agree well with the observed developments, although in fact the model does not describe well the performances. Since this decision is vital to an objective assessment, considerations are elaborated on in appendix I.

Two items are emphasised here. First, the discussion shows that application of a fixed middle section may in other cases than the Sand Engine, not be applicable. In case of milder azimuths, the Region of the Feeder is likely to widen over time. Second; if possible, Region of Influence, that defines the alongshore outer bounds of a mega-feeder nourishment, should be defined based upon the Accretion Points, to prevent subjectiveness in future studies.

Both the analytical model approaches as well as the numerical model approaches could not describe the Accretion Points directly. Analysis revealed that the Accretion Points could be described well by the linear dependence of the Accretion points on the spreading (M2), with a ratio of 3:1.

Analytical model cannot reflect the lifetime of a mega-feeder nourishment based on the reduction of the cross-shore extent. In section 5.2.4 it was observed that the percentile reduction of the maximum cross-shore extent showed similar developments as the reduction of the volume of the middle section. Validation of the analytical model approaches of these indicators resulted in a poor reflection of the cross-shore extent. Because of this limited applicability, the volume reduction is the preferred indicator for quantification of performance and validation of models.

In this study a large number of indicators have been introduced. The indicators give a quantification of a specific entity of a model. One pitfall of the indicators is to lose the link with reality, and consider the

indicators as a truth. Synthesis and interpretation of the application of the performance and validation tool is therefore highly important. Quantification of individual indicators may suggest a good reflection of a specific type of performance, while a model does not describe well other indicators. This particularly holds for the reflection of the volumetric performance of the middle section, an indicator often used to assess how well a model describes the observations. Results have shown that although the middle may be described well, reflection of the performance in the Regions of Contributions is not guaranteed.

A second point of consideration, entails the validation of model performance over time. In this chapter, validation of models was executed based on indicators that develop over time. It is advised to validate the model approaches as such, to prevent wrong interpretations. One example of this is the coincidental excellent agreement of the Stive model approach for the volumetric growth in the south (figure 6.11). Development over time indicates a more linear development over time. Future predictions of the model approach will most likely over-predict the performance.

## 6.5. Conclusions

A number of models were validated using the performance and validation tool. From the validation, it is concluded that the analytical model approach can be used as a first description method to quantitatively estimate the performance of a mega-feeder nourishment. If the LST equation by Kamphuis (1991) is used to derive the diffusivity coefficient, it can serve as a method to predict the performance during circa the first 25% of the lifetime of a mega-feeder nourishment. Current results suggest it under-predicts the diffusivity, but that is considered positive, as it will therefore result in conservative estimates.

On the longer-term, after e.g. the first five years, monitoring of the Accretion Points can be used to calibrate the diffusivity. Preferably, the migration of the centroid is also known. Calibration for this behaviour indicator showed to further improve the description of the performance. Calibration of the volumetric net losses of the Sand Engine only mildly improved the description of the performance. The poorer predictability of the skewness and kurtosis results in poorer performance of the Beta approach. It is not recommended to apply these behavioural elements unless trends can reflect the developments well, or the understanding of these elements has increased.

For a more comprehensive prediction, a calibrated bruteforce 2D numerical model with a curved nearshore grid is advised. The results of the validation have shown that in the case of the Sand Engine, that entails a concentrated nourishment with sharp angles with the original shoreline, application of a curved nearshore grid is a necessity to simulate the reshaping into a Gaussian curve. Further, results have shown that the MorMerge approach, which included several acceleration techniques to reduce the computation time, over-predicted the development of the performance. Quantification of the behaviour indicators showed that the MorMerge approach over-predicted both the velocity of the spreading as well as the centroid.

# 7

# Prediction of the performance of the Sand Engine

## 7.1. A prediction of the performance of the Sand Engine

In this section estimates of the future performance and macro-scale behaviour are described based on the previous results, recapitulated here briefly.

- First, In section 5.2, the applicability of indicators was reviewed via application to Sand Engine. This lead to the conclusion that for most of the indicators great ($R^2 \approx$ 0.9- - 0.95) trends were identified, showing the indicators can be used for predictive purposes.
- Second, the capacity to which analytical can reflect the performance with the indicators was analysed in section 6.2. It was concluded that analytical model approaches could well reflect the performance, if calibration for the diffusivity. The best reflections were observed for a model approach where the net volume of the Sand Engine (M0), the centroid (M1) and the spreading were calibrated. This approach proved as a valuable method to predict the future performance of a mega-feeder nourishment.
- Third, three 2D numerical model approaches were validated in section 6.3. It was concluded that 2D numerical model can reflect the performance to satisfaction, with the requirement that the model is calibrated, a curved nearshore grid is applied, and the physical forcing conditions are imposed as observed, i.e. if no acceleration techniques are applied.

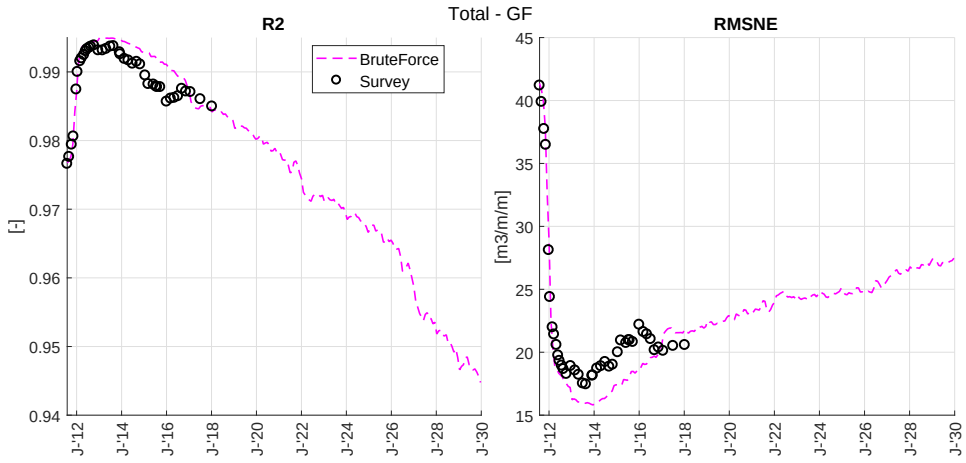


Figure 7.1: Prediction of resemblance of a Gaussian curve by BruteForce numerical model

Whether the shape of the Sand Engine will remain in that of a Gaussian-curve, is reviewed in figure 7.1. The deviations are expected to increase over time, though not to values as were observed by the Stive et al. (2013), here used as a benchmark to state whether the Gaussian-curve assumption is no longer met.

For the predictions, the BruteForce model was calibrated on the first five years after construction of the Sand Engine. The observed forcing conditions were iterated every five years. Further, the Region of Influence was extended to 5 - 14 km (from 6.4 - 12.8km) to accommodate for the expected alongshore expansion of the Sand Engine in the future. As a result, the reflections of the performance differ from the results of the validation in the previous chapter.

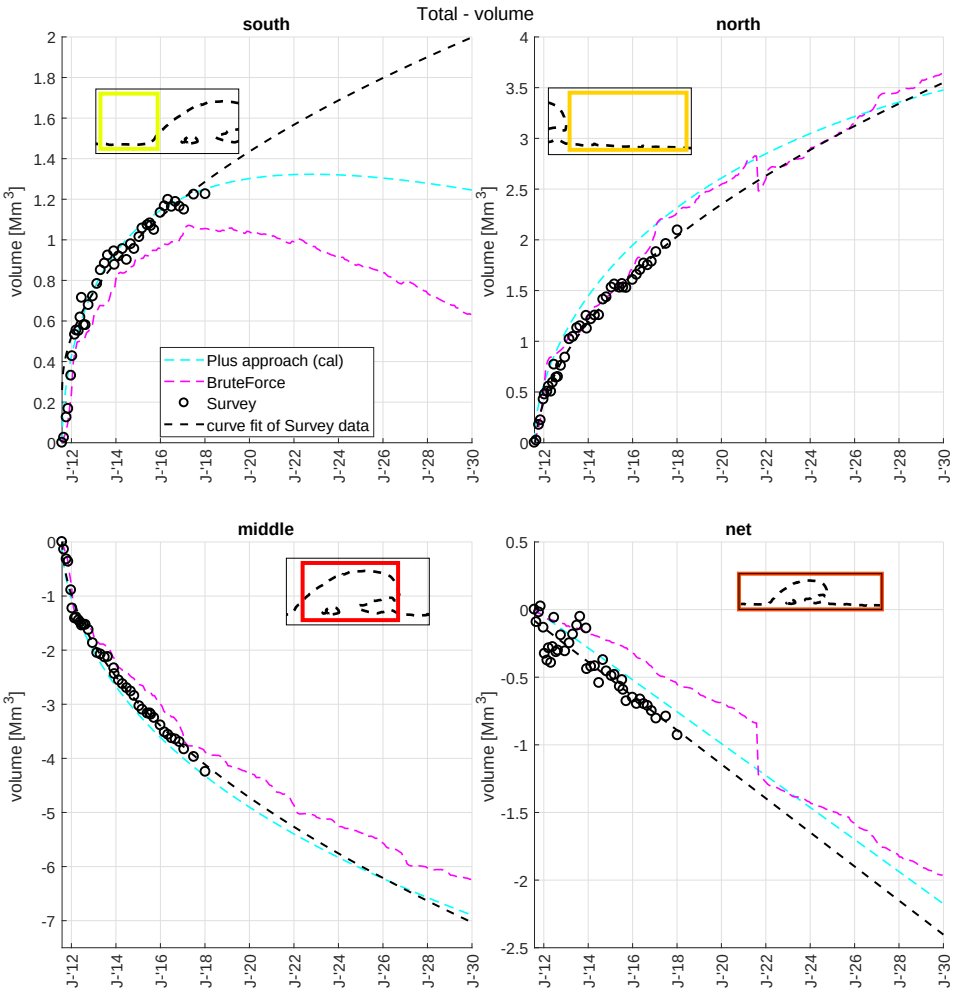


Figure 7.2: Predictions of volumetric changes.

In terms of the volumetric performance (figure 7.2), the estimation methods predict similar results of the middle, north and net region. By 2030 the Sand Engine is predicted to reach its half-life, with a predicted erosion of the middle near 50% (7 - 8Mm $^3$) in the Total region (-10/+3m + NAP). The north will continue to grow as well to circa 3.5 - 4 Mm$^3$ (50% of the eroded volume). The Sand Engine of all regions combined (net) will continue to erode mildly cumulating to roughly 15% of the eroded volume (2 - 2.75Mm$^3$).

Predictions of the volumetric growth on the south show a larger variety. The analytical Plus approach predicts a full stagnation of the growth, while the BruteForce approach predicts a retreat of the volumetric growth[1]. Predicted volumetric growth by the model approaches is between 0.6 - 1.2Mm$^3$ (10-20% of the eroded volume). On the other hand, extrapolation of a curve-fit of the observed growth suggests a a continuation of the feeding on the south side, up to 2Mm$^3$ in 2030 (25%). Predictions of the analytical and numerical model approach are more likely. It is expected the relative influence of the linear migration of the centroid of the Sand Engine will increase over time. This development of relative importance cannot be described, hence the curve-fit is said here not to be a reliable method for predictive purposes.

The alongshore extent is expected to continue to widen over time (figure 7.4). The model approaches

[1] It must be noted that this volumetric growth here is computed for a larger area. The volumetric growth per m alongshore will decrease even more, assuming a southward spreading

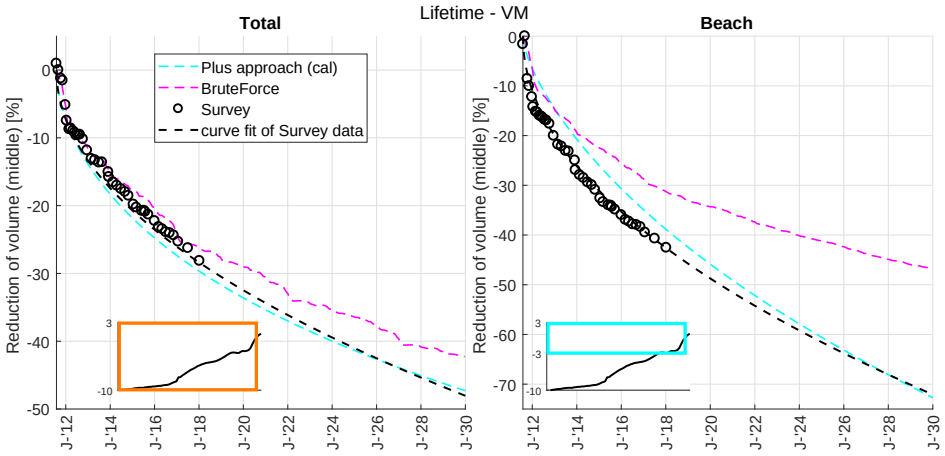


Figure 7.3: Predicted lifetime of SE (based on the volume reduction of the Region of the Feeder)

and curve-fit show small differences in their predictions. The total width in the Beach region (-3/+3m) is expected to surpass a width of 6km between 2020 and 2022, while a width of 7km is not to be expected before 2030, according to the analytical model. All estimations reveal the Transition Points will remain at their initial position: the region where a net erosion is observed since its construction will not widen over time.

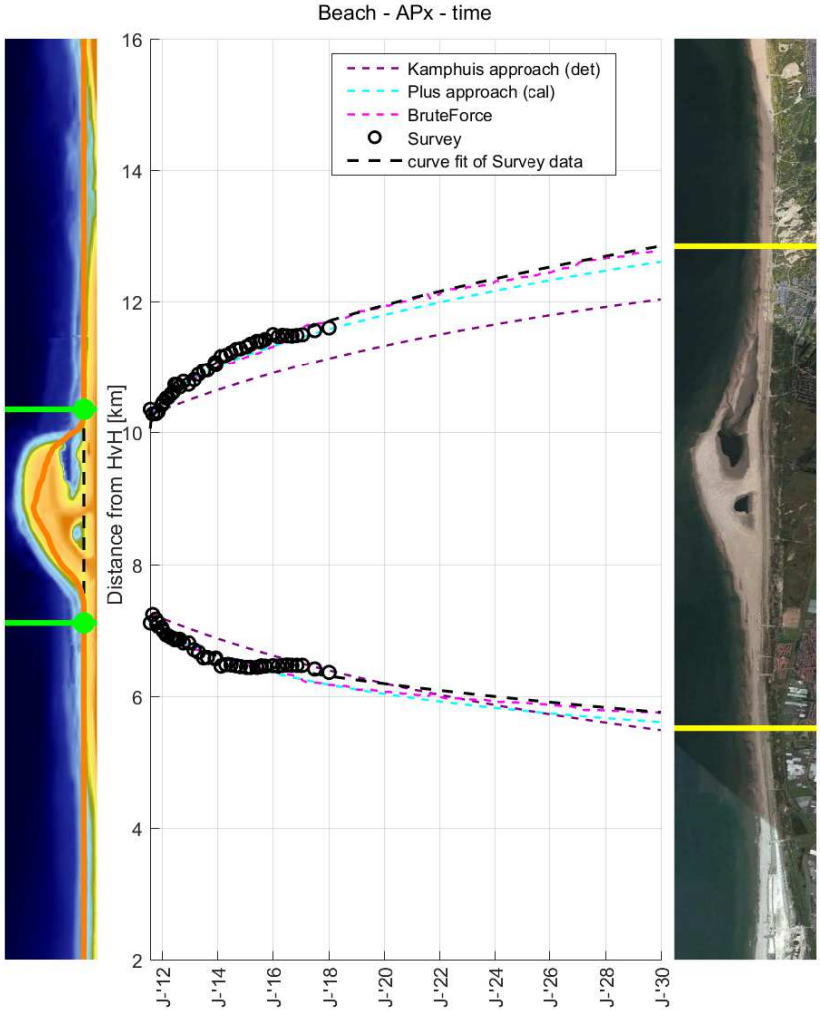


Figure 7.4: Predictions of the Alongshore expansion, expressed in the Accretion Points

In terms of the lifetime, expressed in the volume reduction, shows the Sand Engine is expected to almost

reach its half life by 2030, whereas this is already expected in 2021 in the Beach-region. It is remarked that the 2D numerical model cannot reflect the more rapid developments of the Beach region.

The deeper regions, i.e. the Bar region (-8/-3m + NAP) and the LSF (-10/-8m + NAP) reach their half life only after approximately 40 years (± 2050). The volume reduction of the Beach region thus occurs circa four times faster than in the lower regions. This must be taken into account in future designs of mega-feeder nourishments.

## 7.2. A prediction of the volumetric contribution at Kijkduin

The current assessment method of the Dutch coast (TCL < BCL), see section 2.2.4, is a one dimensional requirement which matches with the current nourishments strategy (repairing the coastline locally via beach and foreshore nourishments). The assessment does not include a potential future alongshore feeding by a mega-feeder nourishment. In this section, an extension to the benchmarking methodology is proposed.

One alternative solution to the current limitation of the Dutch policy would be to extent the policy rule by inclusion of a parameter that accounts for alongshore feeding, e.g.

$$TCL(x,t) = MCL(x)_{t=0} + e(x,t) + MFN(x,t) \tag{7.1}$$

Where x is the location along the beach the nourishment is to protect, e the erosion rate computed from the past ten years of shoreline development - as was done for the 1D approach - and MFN represents the expected contribution of a mega-feeder nourishment to an alongshore coordinate x at time t.

In section 6.2, it was shown that the average gross error of the alongshore volume of analytical model approaches, was in the order of 25% of the observed volume. These solutions may thus proof a valuable asset in objectively estimating the volume of the alongshore coast near mega-feeder nourishments. The proposed equation can therefore be solved by application of the analytical model.

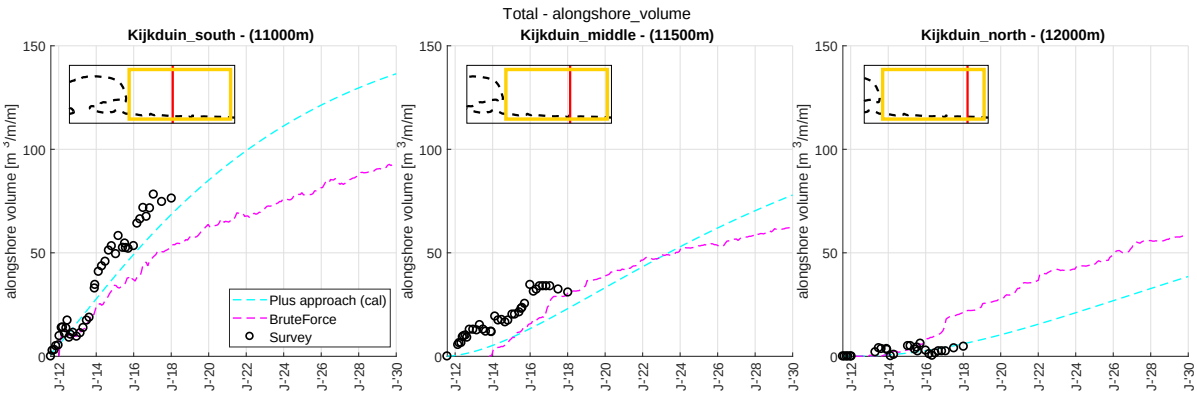


Figure 7.5: Example of application of the proposed extension of the Dutch policy rule

The application is exemplified in figure 7.5 for the Case Study of Kijkduin. This area is of interest, since current estimates based on the MCL suggest the area needs to be nourished to sustain the shoreline. Based on analyses by experts it was argued the Sand Engine will start to feed this region soon, therefore removing the need of additional nourishments (Hoogwaterbeschermingsprogramma, 2016). In general, the Plus model approach shows reasonable results, with deviations of the predicted shoreline in the order of 2.5 - 10m (expressed in the normalised volumes). The results confirm the qualitative statement of the experts, that the Sand Engine will feed sediment in the future along the case of Kijkduin.

## 7.3. Conclusions

The strategic objective of the Sand Engine was to increase the coastal safety of the Delfland coastal cell. The objectives of the Sand Engine were interpreted as to increase the coastal safety (Dunes, MCL, and Coastal Foundation)) between Hoek van Holland and Scheveningen, over a period of 20/50 years, see section 3.3. In this research, the feeding performance of the Sand Engine influenced by Marine processes were assessed. With respect to this area, which includes the MCL and the upper part of the Coastal Foundation, it is concluded that the Sand Engine will provide a higher coastal safety between the area Hoek van Holland and Scheveningen. Though, it is also concluded that it is unlikely that it will meet the requirement of feeding

the entire Westland Coast in the next 10 to 50 years. The current trends quantifying the Region of Influence, suggest a widening of up to 2030 of 7km, while the should increase up to 17.2km in the next decades. Based on the current study, it is expected the alongshore sections that lie out of the Region of Influence (<6km and >13km with respect to HvH), will not be influenced by the Sand Engine within the next decade. Within the Region of Influence, the Sand Engine will contribute volumetrically. Whether this is sufficient, can further be quantified using the analytical model provided in this thesis.

Further, application of the model approaches to extent the current Dutch policy rule for assessing the need for additional nourishments, has proven a to work well. From the previous chapter it was already shown that the mean error in describing the volumetric error by the model approaches in the south and north is circa 25% (see section 6.2.2 and section 6.3.2). Given its high simplicity, the calibrated analytical model approach provides an estimation method that can be applied by policymakers with relative ease.

# 8

# Discussion

In this chapter, first application of the performance and validation tool to the output of the Delft3D Tonnon (2008) is used to compare the predicted and observed performance of the Sand Engine. Second, the applicability of the Momentary Coastline, and the shoreline as a representative depth region c.q. contour is reviewed. Third, the development of the diffusivity coefficient at the Sand Engine is to discussed.

## 8.1. Comparison of predicted performance and observed performance

In the previous chapter, the quantification of the Sand Engine was based upon the performance and validation tool. The tool is used here to review the expected developments of the Sand Engine, by application on the original study of the EIA in 2010. Secondly, an estimation of the performance of the Sand Engine is given based upon the analytical models and the BruteForce model, which were shown to perform excellently.

The developments of the Sand Engine was originally predicted during the Environmental Impact Assessment using a non-calibrated 2D numerical model with a rectangular grid, highly similar to the Stive et al. (2013) approach assessed in chapter 6), see figure 8.1.

Application of the performance and validation tool onto the output of the Tonnon (2010) model approach reveals it has under-predicted the volumetric growth by a factor 2 in the first five years, and under-predicted the geometric performance as well. Based on the spreading, the Region of Influence was would have been 4300m in July 2016, whereas the observed width in August 2016 was 5000m, i.e. the difference in widening of the alongshore expansion was under predicted by 50%.

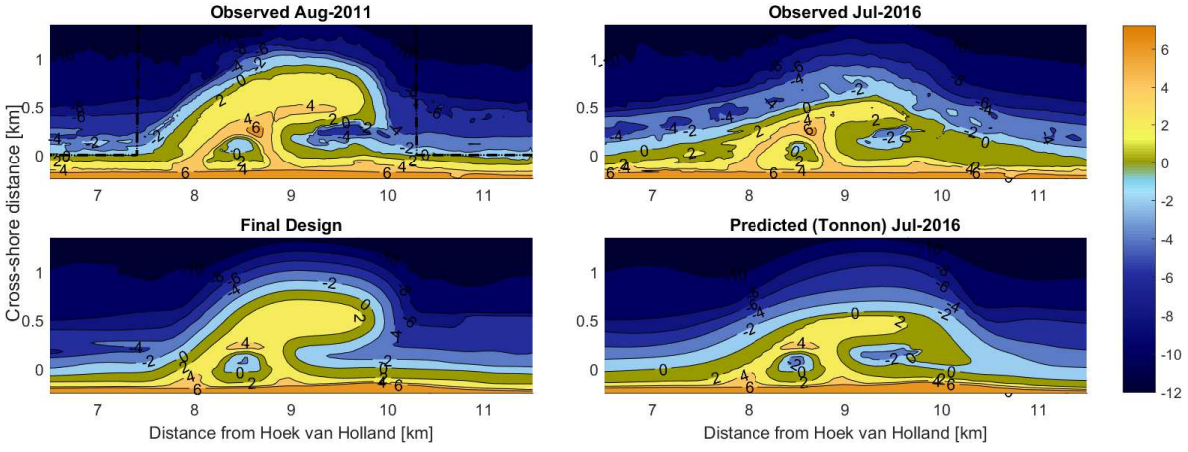


Figure 8.1: Visualisation of the bathymetry, observed (top panels) versus predicted (bottom panels) by the Tonnon (2010) approach. Colours represent the height of the bathymetry, further indicated with the contours with respect to NAP (≈Mean Sea Level).

The difference in the bathymetry results in an interesting difference with the Stive model. The difference in the nourished volumes and the final design on macro-scale, are the milder slope on the south side, and the

lower volumes that were nourished on the in the middle section. These lower volumes resulted in a milder azimuth. As a consequence, the direction of the sediment that is fed to the adjacent coasts, moves along a milder angle than in the calibrated model. As a result, the model can develop better into a Gaussian curve than the rectilinear calibrated model, see figure 8.2.

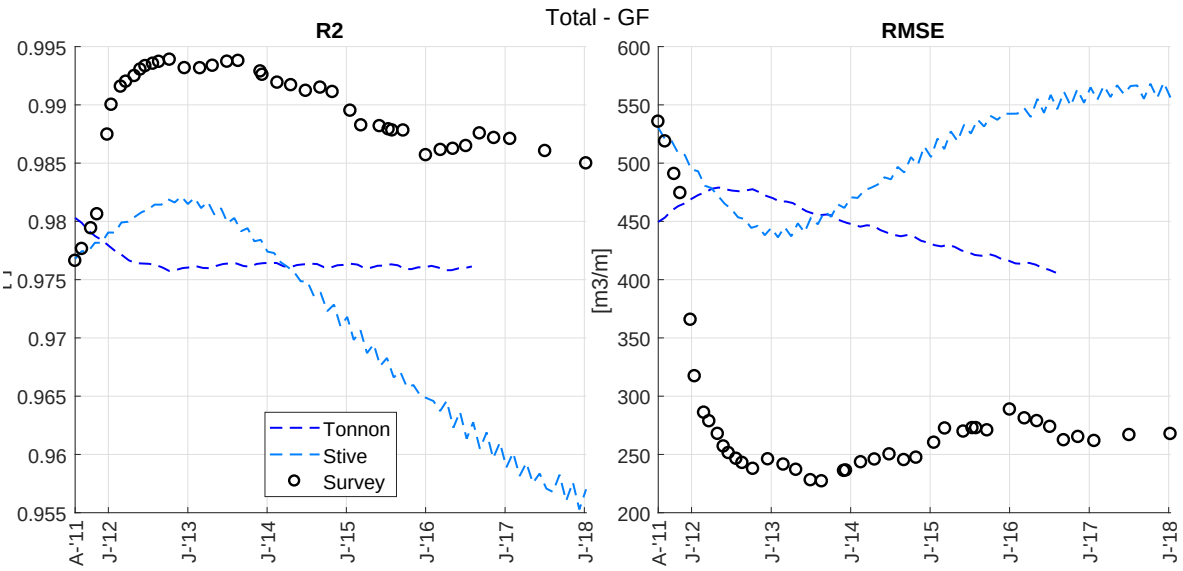


Figure 8.2: Comparison of the resemblance of a Gaussian curve, Tonnon (2010) versus Stive et al. (2013) approach.

## 8.2. The applicability of the Momentary Coast Line and shoreline

The Dutch policy applies a representative depth region, the Momentary Coast Line (-4.4/+3m + NAP), to assess the coastal safety, see section 1.1. Globally, the shoreline is the most popular method for assessment of the coastal safety, or the health of the beach. These two frequently used measures are reviewed here for their representativeness of the developments, by comparing them by the results obtained in this thesis. For brevity, only the results of the volumetric developments are shown here to support the conclusions. Reference is made to appendix H for the results of the other indicators.

The volumetric performance of the MCL, which in the case of the Sand Engine consists of the Beach region and parts of the sub-tidal bars present in the case of the Sand Engine, develops differently in the south (figure 8.3). This is due to the initial rapid development of the bars, and has shown a stagnation since then, deviating from the developments in the Total region. On the north, the performance is well represented by the MCL, short an initial bias of circa 20%. The shoreline shows large fluctuations of the volumetric growth on the south side, with no clear trends over time. On the north, the shoreline shows a more steady development since 2016, after a larger bias during the first years. In the middle section, both the MCL and the shoreline show clear trends, but over-predict the erosion rate of the Total region, circa 40% by the MCL, and 60% by the shoreline.

Both the MCL as well as the shoreline thus show deviations of the observed volumetric performance. The differences in development of the MCL are blurred by the sub-tidal bar behaviour in the south, as well as the different velocities of the erosion in the middle section. The shoreline shows large fluctuations, which obscures any trend in the south and leads to a bias on the north during the first four years.

In terms of the geometric performance, the MCL tends to under-predict the expansion, while the shoreline has, in terms of the Accretion Point, not widened since mid 2015. The MCL can be used as a representative depth region to derive the Transition Points, while derivations of the TPs from the shoreline would lead to small deviations (<100m).

To represent the volumetric performance, an alternative depth region was already proposed in paragraph 5.2. The Beach region was shown to reasonably represent the performance in the Regions of Contribution. From this it is concluded that during the derivation of a representative depth region as for example the Momentary Coast Line, the (expected) presence of sub-tidal bars should be taken into account.

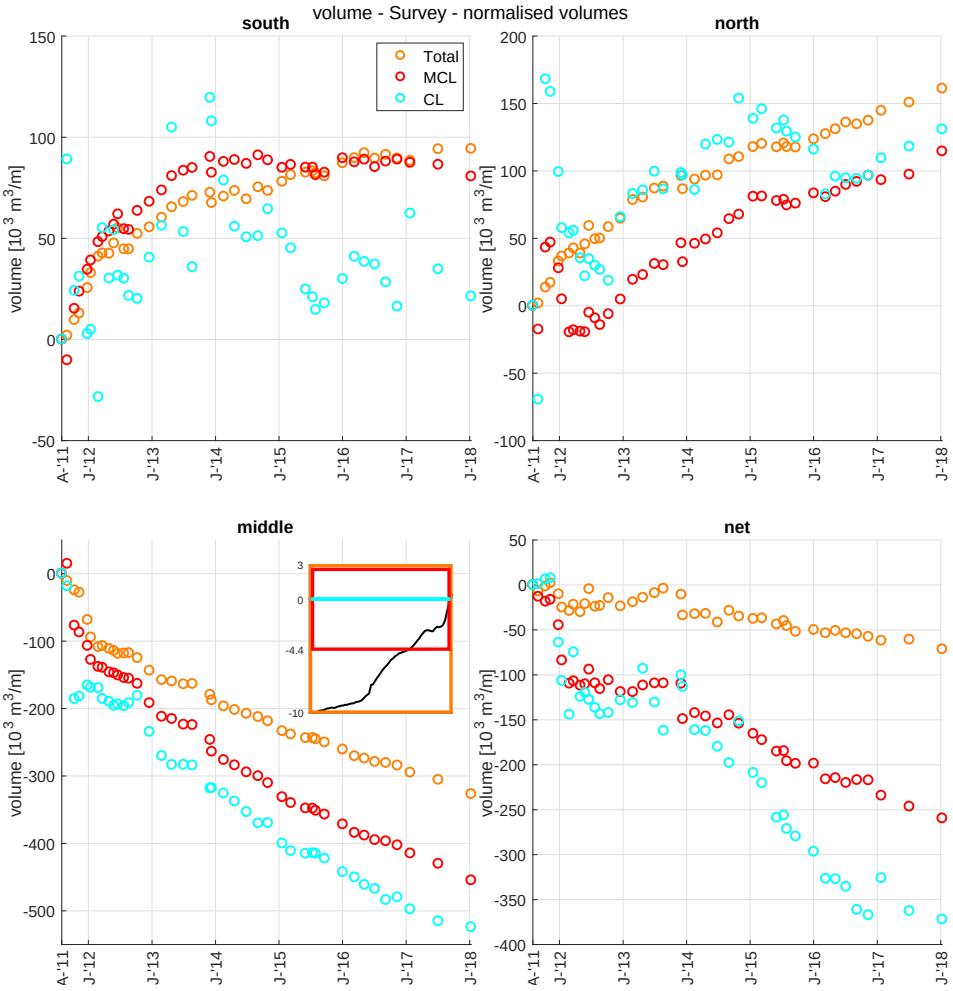


Figure 8.3: Comparison of volumetric performance: Total region (-10/+3m + NAP) vs MCL (-4.4/+3m + NAP) vs Shoreline (CL) (0m + NAP).

## 8.3. On the diffusive behaviour of a mega-feeder nourishment

Based on the capacity of different approaches of the analytical models, the dominant behaviour of a mega-feeder nourishment has been identified. Firsts, the diffusivity is discussed, followed by the advection.

An analytical model to describe a mega-feeder nourishment has been applied successfully, see 6.2.2. The results have shown that using the longshore sediment transport equation by CERC to derive the diffusivity coefficient G, leads to an over-prediction of the feeding performance. The analytical (one-line) model is repeated here for convenience:

$$y(x,t) = \frac{Y}{\sqrt{4\pi G t}} \exp\left[-\frac{(x-x(t)')^2}{4Gt}\right] \tag{8.1}$$

The model was extended with an inclusion of a migration of the centroid (x(t)'). The diffusivity coefficient derived from the CERC equation is:

$$G = \frac{K H_b^{5/2} \sqrt{\frac{g}{\kappa}}}{8(s-1)(1-p)(h_c+B)} \cos 2\alpha_b \tag{8.2}$$

Based on this CERC (1984) approach, the value of the diffusivity was shown to be G = 0.9km$^2$/yr, while using the Kamphuis (1991) approach, G = 0.03$^2$/yr. Using the CERC approach leads to a large over-prediction compared to the observed value, equal to 0.05km$^2$/yr as of January 2018 (figure 8.5a).

Arriaga et al. (2017) computed the diffusivity of the Sand Engine based on the classical diffusivity equation:

$$G_{cla} = 2\mu \frac{H_b}{h_c} cos(\alpha_b) \tag{8.3}$$

With calibration of the $\mu$, a value that controls the magnitude of the alongshore sediment transport, a value of 0.16km$^2$/yr was found. For the active depth $h_c$, a value of 8m was assumed, 50% lower than the value assumed in this thesis (12m). The computed value by Arriaga et al. (2017) agrees better with the observe diffusivity G„ as a result of the calibration of coefficient $\mu$.

Arriaga et al. (2017) derived the observed diffusivity of the Sand Engine based upon the relation $y \propto \sigma$ and found a somewhat higher constant value of 0.069km$^2$/yr, after an initially faster diffusion 8.4. Deriving the diffusivity from the cross-shore extent y is discouraged. The reduction of the cross-shore extent is highly dependent on the depth region or contour considered. The preferred alternative is derivation of the diffusivity coefficient G from the 'spreading (M2), which was shown to be less dependent on the depth region, see section 5.3.

According to the analytical solution by Pelnard-Considere (1956), the diffusivity coefficient is a constant variable. Whether this holds in the case of the Sand Engine is reviewed here using the CERC equation for longshore sediment transport. Additionally, the influence of two variables is analysed. First, the influence of the coarsening of the sediment, as observed by Huisman et al. (2016), depicted on the left plot. Second, the influence of the wave power is assessed [1].

Rather than a constant value, the diffusivity decreases over time (figure 8.5). Huisman et al. (2016), showed a clear coarsening of the sediment of 90$\mu$m to 150 $\mu$m. The coarsening of the sediment results in a lowering of the transport coefficient (see equation 8.2). Assuming an average increase of 120$\mu$m, the coarsening has resulted in a reduction of the transport coefficient K from 1.3 to 0.9 as of January 2018 (based on figure 2.7). Simplifying this to a linear development over time, the influence of this reduction of the coefficient has been removed from the coefficient simply by eliminating the influence from the observed diffusivity $G_{obs}$ $G_K = G_{obs}/K(t)$. Results are however inconclusive. Indeed, a large section of the decrease is explained by the coarsening, though a mild decrease is still observed.

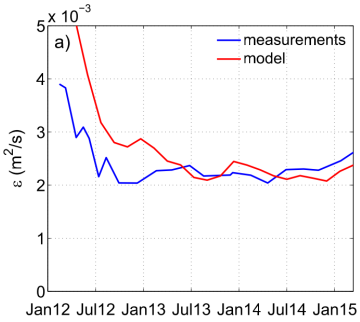


Figure 8.4: Diffusivity coefficient, observed versus modelled (Q2D morfo model)

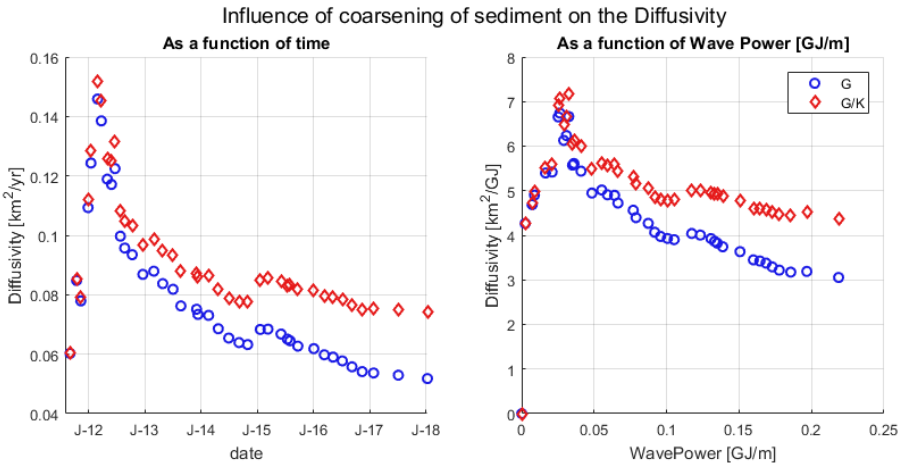


Figure 8.5: Assessment of the diffusivity coefficient over time (a) and Wave Power (b) (note the different units). In blue the observed diffusivity expressed in $G_{obs}$, while in red, the diffusivity coefficient normalised for the coarsening is shown.

The diffusivity shows a more gradual behaviour, if plotted against the Wave Power. Apparently, the initially rapid diffusion is partially explained by the high storms in the winter of 2011. Though, the diffusivity coefficient still shows a peak, presumably as a result of flattening of the cross-shore profiles. What's more, the diffusivity shows a more continuous decrease of the diffusivity over time, also if the coarsening is taken into account.

[1] The cumulative wave power is computed here as $P_{cum} = \sum 1/16 \rho g H_s^2 c_g$

Results deviate from the analytical solution by Pelnard-Considere (1956); the diffusivity coefficient does decrease over time, even if the coarsening of the sediment is taken into account. Explanations for this deviations may perhaps be found in one of the many assumptions based on which the diffusivity coefficient is derived, as a part of these assumptions are not met in the case of the Sand Engine.

In section 2.3.3, the assumptions and limitation of an analytical solution were discussed. Whether the assumption of an equilibrium beach profile is met, is an interesting debate. Results have shown the accretive regions more or less accretes similarly in the active region. On the other hand, in the middle section a clear deviation is observed. Whether the deviations in the middle section can be neglected, requires additional fundamental analyses of the origin of the assumption in future research.

A second assumption that may explain the decreasing diffusivity, is the assumption of a limited azimuth of the nourishment. At the Sand Engine, the shoreline angle near the outer edges of the nourishment do not agree with the assumptions of a small shoreline change (Elko and Wang, 2007, From Grevens et al., 2003). From this, it is concluded that the applied linearisation on which the diffusivity equation was based, is formally not applicable in the case of the Sand Engine, or concentrated/mega-feeder nourishments.

Neglecting the linearisation is violated, two other assumptions were that the amplitude of the longshore sediment transport was independent of x and t, i.e. no gradient in the alongshore sediment transport is present (shown to be valid in case the Sand Engine (Van Rijn, 1995)), and a constant incident wave angle (possibly violated). If these are not constants, the diffusivity equation is to be extended with:

$$G\frac{\delta^2 y}{\delta x^2} + \frac{d\epsilon}{dx}\frac{\delta y}{\delta x} = \alpha_0 \frac{d\epsilon}{dx} + \frac{\delta y}{\delta t} + G\frac{d\alpha_0}{dx} \tag{8.4}$$

Solutions of this equation would unfortunately turn out rather complicated, therewith losing the elegance of the application methodology. Resuming the above, multiple assumptions are not met in the case of the Sand Engine. Though, application of the solution still resulted in agreeable results. A more fundamental analysis of the assumptions is recommended in the future to increase the understanding on the influence of the violations of these assumptions on the expected behaviour, and possible derivation of the diffusivity coefficient.

# 9

# Conclusion

The concept of a mega-feeder nourishment has recently been applied as a new alternative to respond to the expected accelerated sea-level rise. Engineers and policymakers are interested in quantifications of (predictions of) the performance of a mega-feeder nourishment, to support in decision making. Secondly, model approaches to describe and predict the developments of a mega-feeder nourishment, have not been validated specifically to describe the feeding performance. The research question of this thesis is hence: *"How to describe and predict mega-feeder nourishment performance with behaviour based coastal indicators?"*

The study is split up into three segments that support in answering the research question. First, a performance and validation tool is developed, that comprises of indicators that quantitatively represent the objectives. Second, the performance and validation tool is verified by means of application to the unique case study of a mega-feeder nourishment, the Sand Engine. Third the performance and validation tool is used to validate analytical and numerical model approaches. Finally, models that were shown to reflect well the performance, were used to predict the future performance of the Sand Engine.

A performance and validation tool was introduced that quantifies performance of a mega-feeder nourishment in feeding adjacent coasts. If bathymetric data is assessed, the data is reduced to volume densities of the active regions (-10/+3m + NAP). Second, the nourishment is split up into sections (figure 9.1). The Region of Influence, the alongshore section where a contribution of sediment can be observed due to the feeding mechanism of the nourishment. The Regions of Contribution are the sections where accretion of sediment can be observed, while the Region of the Feeder is defined by the region where the sediment fed to adjacent coasts, originates from. The sectioning is based upon the observed developments of the alongshore volumes. The Region of the Feeder is defined based upon Transition Points. These points mark the alongshore location where a net accretion turns to erosion left of the middle section, and vice versa on the right. By means of doing so, the sum of the net volumetric changes per sections are well represented.

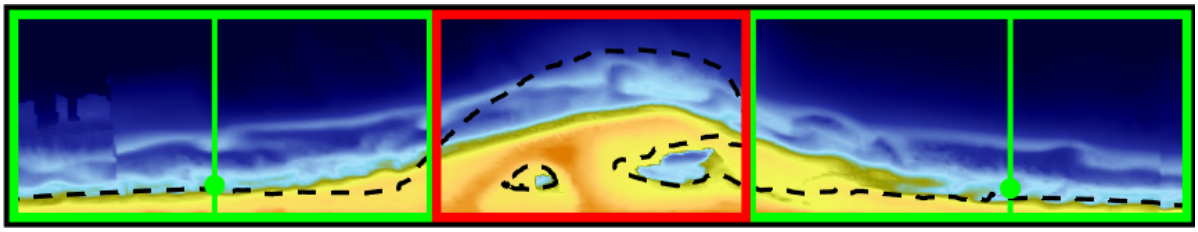

Figure 9.1: The proposed performance tool. The black box on the edges denotes the Region of Influence, the green boxes depict the Regions of Contributions, and the red box shows the Region of the Feeder. The green circles indicate the Accretion Points.

In the next step, the performance is quantified by a set of indicators. The performance indicators represent the objectives of a mega-feeder nourishment. The objective of a mega-feeder nourishment is here defined as to contribute sediment (volume) along adjacent coasts (region) for a specified duration (lifetime). The elements between brackets are quantified by indicators. First, the *volumetric* growth is measured by the net changes in the Regions of Contribution. Second, the Accretion Points mark the *region* where accretion is observed due to the feeding mechanism. Third, the age or *lifetime* is quantified by the reduction of the volume in the Region of the feeder.

The performance and validation tool was verified by application to the Sand Engine, a unique case study. This Sand Engine, constructed during the spring of 2011, has a nourishment volume of 21.5Mm$^3$, initially spanned a width of 2.4km and extended 1km into the sea. The performance tool was successfully applied to the case study. Application showed that the volumetric growth, Accretion Points, and the volume reduction could all well be described by square root fits ($R^2$ >0.9). This suggests the developments of the performance are predictable. To verify further the predictability, the relation with the behaviour was reviewed. The behaviour is defined as the change of the planform shape as a result of forcing conditions, e.g. wind, waves, and tide. The behaviour was quantified by means of the second order central moment (M2) that represents the diffusivity, as well as by the first order raw moment M1, that represents the advection. Both indicators showed to develop highly continuous with a decelerating and linearly development respectively ($R^2$ = 0.98). The performance indicators where shown to be linearly proportional to the behaviour indicators, which showed the indicators can be related to the physical forcing conditions.

The quantification of the performance showed that 4.3Mm$^3$ had eroded from the Region of the Feeder. Volumetrically, the performance showed that the majority of this eroded sediment is compensated for by accretions along the adjacent coasts, with 2.1Mm$^3$ (48% of the eroded volume) to the north, and 1.2Mm$^3$ (28% of the eroded volume) to the south. In terms of the geometric performance, the distance between the Accretion Points, i.e. the Region of Influence, has widened from 3km to 5.25km (+60%) during the first six and a half years. Thirdly, the age of the Sand Engine was quantified with the volume reduction, which so far reduced by 28% in the active depth. The cross-shore profile was split up into homogeneous depths. This revealed that the foreshore of the beach (-3/+3m + NAP), already reduced by 43% volumetrically, while the volume reduction in the shoreface (-10/-3m +NAP) was circa four times lower, i.e. a mere 10 - 15%. Contrary to these differences over depth in the Region of the Feeder, such distinct differences were not observed in the Regions of Contribution, suggesting a net offshore migration of sediment from the Beach region to lower regions.

An analytical model approach adopted from the Pelnard-Considere (1956) solution was validated, as well as three types of numerical model (Delft3D) approaches using the performance and validation tool. The first analytical model approach comprised of a non-calibrated method. Derivation of the spreading from the bulk longshore sediment transport equation by Kamphuis (1991), showed a reasonable method to predict the performance during the first years (e.g. first 25% of the lifetime). Current results suggest it under-predicts the diffusivity, but that is considered positive, as it will therefore result in conservative estimates. For longer-term predictions (50 - 100% of the lifetime), bathymetric monitoring is required to calibrate the the developments in terms of advection and diffusion. A calibrated bruteforce 2D numerical model with a curved nearshore grid is recommended for descriptions and predictions of smaller scale developments, e.g. the approach channel, spit development. Application of a curved nearshore grid is a necessity to simulate the reshaping into a Gaussian curve. Further, results have shown that application of acceleration techniques, over-predicted the development of the performance, from which it is concluded this approach can currently not be used to predict the macro-scale performance of a mega-feeder nourishment.

Predictions of the volumetric performance indicate the Sand Engine will continue to contribute sediment to the north (right) of the Sand Engine, up to 4Mm$^3$ by 2030. On the other hand, it is expected the volumetric contribution to the south will stagnate. The alongshore expansion will increase to approximately 7km. From this it is concluded it will not provide coastal protection to the entire section between Hoek van Holland and Scheveningen (17.2km wide). By 2030, the Sand Engine will approximately have reached its half-life, indicating the lifetime is significantly longer than the design lifetime of 20 years. Next to predictions of the performance, the analytical model may find application directly for policymakers. Currently, the assessment of the Momentary Coastline does not incorporate alongshore feeding. To account for this mechanism, the alongshore volumetric contribution can be estimated using the calibrated analytical model approach. Given its simplicity, the calibrated analytical model approach provides an estimation method that can be applied by policymakers with relative ease.

# 10

# Recommendations

Three types of recommendations are given: research, design, and the Dutch policy for coastal safety.

Three recommendations are given in the context of future research. First, in the discussion (section 8.3), the development of the diffusivity coefficient was elaborated on. Results showed that the reduction of the coefficient over time could partially be explained by the coarsening of the sediment. In the discussion possible explanations were discussed. It is recommended to elaborate on the derivation of the diffusivity coefficient, to improve predictions of the diffusive behaviour of a mega-feeder nourishment and therewith the performance of predictions by non-calibrated analytical models. Secondly, it was concluded that in the long term, it is expected that advection also has an influence on the performance of a mega-feeder nourishment. It is therefore recommended to develop relations between the physical forcing conditions and the identified advection. A second recommendation is given with respect to the analytical model approaches. In this thesis the analytical modelling approach has proven to describe well the performance of a mega-feeder nourishment deterministically. This model can quite easily be extended to a probabilistic model, by deriving upper and lower estimates of the diffusivity coefficient. Such an extension will support policy makers further in decision making of future nourishments near mega-feeder nourishments. The third recommendation is related to the 2D numerical modelling. The 2D numerical model that applied a bruteforce technique showed to describe well the performance of a mega-feeder nourishment. Though, the computational effort of the bruteforce technique O (weeks), makes it a less attractive alternative. Because of this computation time, the mormerge approach has been a popular alternative. However this study showed the approach lead to over-predictions of the performance. It is recommended to use the observed diffusion and advection as a means to calibrate the model to improve the descriptions and predictions of model result.

In terms of future design of a mega-feeder nourishment, the following is advised. Although contradicting the entire concept of a *mega*-feeder nourishment, results suggest it may be more desirable to nourish the coast with a higher number of smaller feeder nourishments. The sediment that was nourished near the shoreline has fed nearly half of its sediment to adjacent coasts in just six and half years, whereas the sediment placed below the surf zone, has only lost 10%, four times fewer. This sediment could perhaps be better placed in higher regions. Indeed, this is a compromise, but may serve as an interesting alternative still to existing beach nourishments.

Two recommendations are given with respect to the Dutch policy of coastal safety. First, in case of a mega-feeder nourishment, the application of analytical models can serve as an elegant and simplistic method to objectively assess whether nourishments along a coast near a mega-feeder nourishment are required. Currently, this is done based upon expert judgement of the developments of the MCL. Such a tool can be of great value to objectively assess whether nourishments need to be planned near a mega-feeder nourishment. A second recommendation is given towards the use of the Momentary Coastline as a representative depth to assess the need for nourishment. When deriving the boundaries of the MCL, it is recommended to take into account the presence of sub-tidal bars. In the case of the Sand Engine, it has been shown that the observed developments in the MCL are not fully representative, and under estimate contributions. This is even more so in case the shoreline is used, therefore more strongly discouraged.

# Bibliography


Arriaga, J., Rutten, J., Ribas, F., Falqués, A., and Ruessink, G. (2017). Modeling the long-term diffusion and feeding capability of a mega-nourishment. *Coast. Eng.*, 121:1–13.

Ashton, A., Murray, A. B., and Arnault, O. (2001). Formation of coastline features by large-scale instabilities induced by high-angle waves. *Nature*, 414(6861):296–300.

Bars, D. L., Drijfhout, S., and Vries, H. D. (2017). A high-end sea level rise probabilistic projection including rapid Antarctic ice sheet mass loss. *Environ. Res. Lett.*

Booij, N., Ris, R. C., and Holthuijsen, L. H. (1999). A third-generation wave model for coastal regions: 1. Model description and validation. *J. Geophys. Res. Ocean.*, 104(C4):7649–7666.

Bruun, P. (1954). *Coast Erosion and the Develop ment of Beach Profile.* U.S. Beach Erosion Board, Washington.

Bruun, P., Dette, H. H., Fuehrboeter, A., and Raudviki, A. (1996). Interdependence of Beach fill volumes and Repetition intervals. *J. Waterw. Port, Coastal, Ocean Eng.*, 122:103–104.

CERC (1984). Shore protection manual. 3 volumes(4th ed., 2 Vol).

Cooke, B. C., Jones, A. R., Goodwin, I. D., and Bishop, M. J. (2012). Nourishment practices on Australian sandy beaches: A review. *J. Environ. Manage.*, 113:319–327.

Dasgupta, S., Laplante, B., Meisner, C., Wheeler, D., and Yan, J. (2009). The impact of sea level rise on developing countries: A comparative analysis. *Clim. Change*, 93(3-4):379–388.

De Ronde, J. G. (2008). Toekomstige langjarige suppletiebehoefte. Technical report, Deltares.

De Schipper, M. A., De Vries, S., Ruessink, G., De Zeeuw, R. C., Rutten, J., Van Gelder-Maas, C., and Stive, M. J. (2016). Initial spreading of a mega feeder nourishment: Observations of the Sand Engine pilot project. *Coast. Eng.*, 111:23–38.

De Weerdt, B. (2015). *Effectiveness of the Sand Engine.* PhD thesis, Delft University of Technology.

Dean, B. R. G. and Yoo, C.-h. (1993). Beach-Nourishment Performance Predictions. 118(6):567–586.

Dean, R. (1992). Beach Nourishment: Design Principles. Technical report.

Dean, R. G. (2002). *Beach nourishment: theory and practice.* World Scientific Press, Florida, vol 18 edition.

Deltares (2014). Delft3D-FLOW, User Manual. Technical report.

Deltares and IMARES (2011). Uitvoeringsprogramma Monitoring en Evaluatie pilot Zandmotor. page 154.

Devore, J. (2011). Probability and Statistics for Engineering and the Sciences. *Brooks/Cole*, page 776.

Diaconis, P. (1986). Application of the method of moments in probability and statistics. Technical report, Stanford University, Stanford.

Elko, N. A. and Wang, P. (2007). Immediate profile and planform evolution of a beach nourishment project with hurricane influences. *Coast. Eng.*, 54(1):49–66.

Falqués, A. and Calvete, D. (2005). Large-scale dynamics of sandy coastlines: Diffusivity and instability. *J. Geophys. Res. C Ocean.*, 110(C03007):1–15.

Grunnet, N. M., Ruessink, B. G., and Walstra, D. J. R. (2005). The influence of tides, wind and waves on the redistribution of nourished sediment at Terschelling, The Netherlands. *Coast. Eng.*, 52(7):617–631.

Hallermeier, R. J. (1978). Uses for a Calculated Linit Depth to Beach Erosion. *Proc. 16th Int. Conf. Coast. Eng.*, pages 1493–1512.

Hallermeier, R. J. (1981). Terminal settling velocity of commonly occurring sand grains. *Sedimentology*, 28(6):859–865.

Hamm, L., Capobianco, M., Dette, H. H., Lechuga, A., Spanhoff, R., and Stive, M. J. (2002). A summary of European experience with shore nourishment. *Coast. Eng.*, 47(2):237–264.

Hanson, H., Brampton, A., Capobianco, M., Dette, H. H., Hamm, L., Laustrup, C., Lechuga, A., and Spanhoff, R. (2002). Beach nourishment projects, practices, and objectives - A European overview. *Coast. Eng.*, 47(2):81–111.

Hanson, H. and Kraus, N. C. (1987). Analytical solutions of the one-line model of shoreline change. Technical report, United States Army Corps of Engineers.

Hendriks, A. (2011). *The Impact of re-surfacing groins on hydrodynamics and sediment transport at the delfland coast.* thesis, Delft University of Technology.

Hillen, R. and Roelse, P. (1995). Dynamic preservation of the coastline in the Netherlands. *J. Coast. Conserv.*, 1:17–28.

Hillen, R., Ruig, D. J., Roelse, P., and Hallie, F. (1991). De basiskustlijn, een technisch/ morfologische uitwerking. Technical report, Rijkswaterstaat, Den Haag.

Hinton, C. and Nicholls, R. J. (1998). Spatial and Temporal Behaviour of Depth of Closure Along the Holland Coast. *26th Int. Conf. Coast. Eng.*, pages 2913–2925.

Hoogwaterbeschermingsprogramma (2016). Onderbouwing actualisatie suppletieprogramma 2016-2019. Technical report, Rijkswaterstaat.

Horikawa, K. (1988). *Nearshore dynamics and coastal processes: theory, measurement, and predictive models.* University of Tokyo Press.

Huang, J., Jackson, D. W. T., and Cooper, J. A. G. (2002). Morphological Monitoring of a High Energy Beach System Using GPS and Total Station Techniques , Runkerry , Co . Antrim , Northern Ireland. *J. Coast. Res.*, (36):390–398.

Huisman, B. J., de Schipper, M. A., and Ruessink, B. G. (2016). Sediment sorting at the Sand Motor at storm and annual time scales. *Mar. Geol.*, 381:209–226.

Hurst, M. D., Rood, D. H., Ellis, M. A., Anderson, R. S., and Dornbusch, U. (2016). Recent acceleration in coastal cliff retreat rates on the south coast of Great Britain. *Proc. Natl. Acad. Sci.*, 113(47):13336–13341.

Janssen, G. M., Kleef, H., Mulder, S., and Tydeman, P. (2008). Pilot assessment of depth related distribution of macrofauna in surf zone along Dutch coast and its implications for coastal management. *Mar. Ecol.*, 29(SUPPL. 1):186–194.

Kabat, P., Fresco, L. O., Stive, M. J. F., Veerman, C. P., Van Alphen, J. S. L. J., Parmet, B. W. A. H., Hazeleger, W., and Katsman, C. A. (2009). Dutch coasts in transition. *Nat. Geosci.*, 2(7):450–452.

Kamphuis, J. W. (1991). Alongshore Sediment Transport Rate. *J. Waterw. Port, Coastal, Ocean Eng.*, 117(6):624–640.

Kocherlakota, S., Johnson, N. L., Kotz, S., and Balakrishnan, N. (1995). Continuous Univariate Distributions.Vol. 1. *Biometrics*, 51(4):1582–1583.

Komar, P. (1998). *Beach Processes and Sedimenattion.* Prentice Hall.

Komar, P. D. and J., M. R. (1983). Handbook of coastal processes and erosion. Technical report.

Larson, M., Hanson, H., and Kraus, N. C. (1997). Analytical Solutions of One-Line Model for Shoreline Change near Coastal Structures. *J. Waterw. Port, Coastal, Ocean Eng.*, 123:180–191.

Latteux, B. (1995). Techniques for long-term morphological simulation under tidal action. *Mar. Geol.*, 126(1-4):129–141.

Leatherman, S. P., Zhang, K., and Douglas, B. C. (2000). Sea level rise shown to drive coastal erosion. *Eos (Washington. DC).*, 81(6):55–57.

Lesser, G. R., Roelvink, J. A., Van Kester, J. A., and Stelling, G. S. (2004). Development and validation of a three-dimensional morphological model. *Coast. Eng.*, 51(8-9):883–915.

Luijendijk, A. P., De Schipper, M. A., and Ranasinghe, R. (In preparation). Upscaling techniques for decadal predictions of sandy interventions.

Luijendijk, A. P., Ranasinghe, R., de Schipper, M. A., Huisman, B. A., Swinkels, C. M., Walstra, D. J., and Stive, M. J. (2017). The initial morphological response of the Sand Engine: A process-based modelling study. *Coast. Eng.*, 119:1–14.

Margheritini, L., Firgaard, P. B., and Wahl, N. A. (2007). A Holistic Evaluation of a Typical Coast Nourishment on the Danish West Coast. In *ICCCM'07 Proc. 2nd Int. Conf. Coast. Conserv. Manag. Atl. Mediterr.*, Hammamet - Tunisia.

Mol, A. C. S. (2007). Schematisation of boundary conditions for morphological simulations. Technical report, WL Delft Hydraulics.

Mulder, J. P., Hommes, S., and Horstman, E. M. (2011). Implementation of coastal erosion management in the Netherlands. *Ocean Coast. Manag.*, 54(12):888–897.

Parry, M., Canziani, O., Palutikof, J., Van der Linden, P., and Hanson, C. (2007). Climate Change 2007: impacts, adaptation and vulnerability: contribution of Working Group II to the fourth assessment report of the Intergovernmental Panel. Technical report, IPCC, Cambridge, UK.

Pelnard-Considere, R. (1956). Essai de theorie de l'evolution des formes de rivage en plages de sable et de galets. *Les Energies la Mer Compte Rendu Des Quatr. Journees L'hydraulique, Paris 13, 14 15 Juin 1956; Quest. III, Rapp. 1, 74-1-10*, pages 289–298.

Peterson, C. H., Bishop, M. J., Johnson, G. A., D'Anna, L. M., and Manning, L. M. (2006). Exploiting beach filling as an unaffordable experiment: Benthic intertidal impacts propagating upwards to shorebirds. *J. Exp. Mar. Bio. Ecol.*, 338(2):205–221.

Pilkey, O. H. and Cooper, J. A. G. (2014). *The last beach.* Duke University Press Books.

Projectteam Zandmotor (2010). Projectnota/MER Aanleg en zandwinning Zandmotor Delflandse kust. Technical report.

Rijkswaterstaat (1990). A new coastal defence policy for the Netherlands.

Roelse, P. (1996). *Evaluatie van zandsuppleties aan de Nederlandse kust 1975-1994, een morfologische beschouwing.* Number RIKZ-96.028.

Roelse, P. (2002). Water en zand in balans. Technical report, Rijksinstituut voor Kust en Zee.

Roelvink, J. A. (2006). Coastal morphodynamic evolution techniques. *Coast. Eng.*, 53(2-3):277–287.

Roest, L. W. M. (2017). *The influence of the Sand Engine on the sediment transports and budgets of the Delfland coast.* Thesis, Delft University of Technology.

Roest, L. W. M., De Vries, S., De Schipper, M. A., and Aarninkhof, S. (Submitted) .The influence of a mega feeder nourishment on a coastal cell: Five years of Sand Engine morphodynamics. *Coast. Eng.*

Ruessink, B. G. and Jeuken, M. C. J. L. (2002). Dunefoot dynamics along the Dutch coast. *Earth Surf. Process. Landforms*, 27(10):1043–1056.

Silva, R., Martínez, M. L., Hesp, P. A., Catalan, P., Osorio, A. F., Martell, R., Fossati, M., Miot da Silva, G., Mariño-Tapia, I., Pereira, P., Cienguegos, R., Klein, A., and Govaere, G. (2014). Present and Future Challenges of Coastal Erosion in Latin America. *J. Coast. Res.*, 71:1–16.

Speybroeck, J., Bonte, D., Courtens, W., Gheskiere, T., Grootaert, P., Maelfait, J. P., Mathys, M., Provoost, S., Sabbe, K., Stienen, E. W., Van Lancker, V., Vincx, M., and Degraer, S. (2006). Beach nourishment: An ecologically sound coastal defence alternative? A review. *Aquat. Conserv. Mar. Freshw. Ecosyst.*, 16(4):419–435.

Steele, J. M. (1987). Non-Uniform Random Variate Generation (Luc Devroye). *SIAM Rev.*, 29(4):675–676.

Stive, M. J., De Schipper, M. A., Luijendijk, A. P., Aarninkhof, S. S., Van Gelder-Maas, C., Van Thiel de Vries, J. S., De Vries, S., Henriquez, M., Marx, S., and Ranasinghe, R. (2013). A New Alternative to Saving Our Beaches from Sea-Level Rise: The Sand Engine.

Sutherland, J., Peet, A. H., and Soulsby, R. L. (2004). Evaluating the performance of morphological models. *Coast. Eng.*, 51(8-9):917–939.

Swann, W. H. (1969). A survey of non-linear optimization techniques. *FEBS Lett.*, 2:S39—-S55.

Tonnon, P. (2008). Bijdrage startnotitie MER. Technical report.

Tonnon, P. K. (2010). Morfologische berekening geoptimaliseerd ontwerp zandmotor.

Tonnon, P. K., Huisman, B. J., Stam, G. N., and van Rijn, L. C. (2018). Numerical modelling of erosion rates, life span and maintenance volumes of mega nourishments. *Coast. Eng.*, 131:51–69.

Tonnon, P. K. and Nederhoff, K. (2016). Monitoring en Evaluatie Pilot Zandmotor, eindevaluatie onderdeel morfologie. Technical report, Deltares.

U. S. Army Corps Of Engineers (2002). Coastal Engineering Manual. Technical Report August 2001.

van Den Berg, N., Falqués, A., and Ribas, F. (2012). Modeling large scale shoreline sand waves under oblique wave incidence. *J. Geophys. Res. Earth Surf.*, 117(3):1–18.

Van Duin, M. J., Wiersma, N. R., Walstra, D. J., van Rijn, L. C., and Stive, M. J. (2004). Nourishing the shoreface: Observations and hindcasting of the Egmond case, The Netherlands. *Coast. Eng.*, 51(8-9):813–837.

Van Koningsveld, M. and Mulder, J. P. M. (2004). Sustainable Coastal Policy Developments in The Netherlands. A Systematic Approach Revealed. *J. Coast. Res.*, 202:375–385.

Van Rijn, L. (1995). Sand budget and coastline changes of the central coast of Holland between Den Helder and Hoek van Holland period 1964-2040.

Van Rijn, L. C., Walstra, D. R., and Van Ormondt, M. (2007). Unified View of Sediment Transport by Currents and Waves. IV: Application of Morphodynamic Model. *J. Hydraul. Eng.*, 133(7):776–793.

Wijnberg, K. M. (2002). Environmental controls on decadalmorphologic behaviour of the Holland coast. *Mar. Geol.*, 189:227–247.

Wijnberg, K. M. and Terwindt, J. H. (1995). Extracting decadal morphological behaviour from high-resolution, long-term bathymetric surveys along the Holland coast using eigenfunction analysis. *Mar. Geol.*, 126(1-4):301–330.

Zanten, S. C. V. (2015). *Towards engineering the ecosystem services of a.* thesis, Delft University of Technology, Delft.

# A

# Westland coast

## A.1. Historical developments

For centuries, the Dutch have fought to protect its "Neder land" (old Dutch for low land) from the sea. The southern part of the Holland coast, the Westland coast, has eroded predominantly due to high waves and strong currents, see Figure A.1.From the 1500s numerous attempts were made to counter the erosion. This started off by means of planting dune vegetation, and the construction of wooden and stone structures. Around the 1600s, a sand dike was built near Ter Heide, which was washed away and rebuilt multiple times, each time shifting landwards after its destruction. Between 1500 and 1800 the retreat of the coastline in these areas was in the order of 3 to 5 m/year Van Rijn (1995), accumulating to a retreat of circa 1500m.

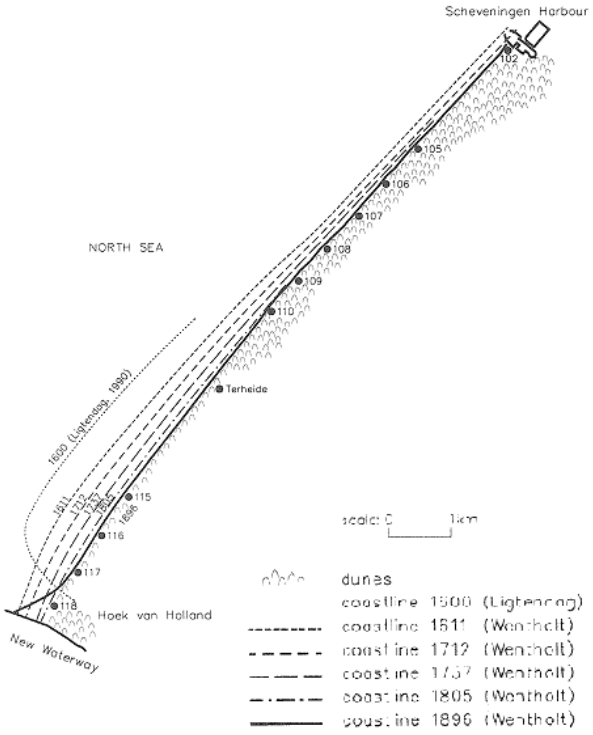


Figure A.1: Development of the coastline along the Westland (1600 - 1900) Van Rijn (1995)

During a storm flood in 1791, the sand dike suffered an irreparable damage. It was then decided to defend the Westland coastline more actively by building and extending groins offshore, up until a length of circa 350 m (Van Rijn, 1995). Also, to ensure a safe approach for larger vessels, long rubble-mound breakwaters normal to the shore near Hoek van Holland and IJmuiden were built around 1870. Over the years the number of groins increased at the Westland coast, to 68 by 1930 (Hendriks, 2011). These breakwaters caused sedimentation of the fluvial sediment in the vicinity of the entrance of the Rotterdam, explaining the accretion near the south edge of the Westland coast. The strategy showed to be effective: it considerably reduced the retreat of the coastline to approximately 0.5 - 1 m/year.

After hundreds of years of fighting the sea, a major political shift took place in the 1970s, when it was decided to counter the structural erosion by means of sand nourishments instead of groins (Hanson et al., 2002). After the shift from groins to nourishment in the 1970s, structural erosion became less and less acceptable. Eventually, in 1990, this lead to the acceptance of the Dynamic Preservation Act (DPA) by the Dutch government, which stated the coastline position was to be maintained at its position of 1990, see section 2.2.4.

## A.2. Overview of previous nourishments

Table A.2 includes the cumulative nourishments, to support in understanding the developments of the Westland Coasts. Two large nourishments stand out: One at the Van Diexhoorn Driehoek on the south, with almost 19Mm$^3$, and the Sand Engine in the 'Midden' section (see figure A.3 for the alongshore locations). Figure A.4 visualises the cumulative nourishment volumes along the Westland coast.

| Deelgebieden | 1970-1975 | 1975-1990 | 1990-2007 | 2007-2012 | 2012-2016 | Totaal |
|---|---|---|---|---|---|---|
| Scheveningen Zuid | 0 | 0 | 0 | 925.000 | 0 | 925.000 |
| Kijkduin | 0 | 0 | 22.860 | 3.820.000 (200.000) | 0 | 3.892.860 |
| ZM Noord | 0 | 96.000 | 757.338 | 1.830.000 (200.000) | 0 | 2.733.338 |
| ZM Midden | 0 | 896.000 | 3.764.191 | 18.500.000 (16.500.000) | 0 | 23.660.191 |
| ZM Zuid | 0 | 576.000 | 2.673.910 | 1.400.000 | 0 | 4.649.910 |
| Ter Heijde | 0 | 960.000 | 2.485.038 | 4.280.655 (1.700.000) | 0 | 8.025.693 |
| 's Gravenzande | 0 | 640.000 | 676.549 | 2.251.049 | 600.000 | 4.167.597 |
| van Dixhoorndriehoek | 18.940.000 | 2.702.000 | 2.917.189 | 5.065.697 | 900.000 | 30.524.886 |
| **Totaal deelperiode** | **18.940.000** | **5.870.000** | **13.297.075** | **38.072.402** | **1.500.000** | **78.579.476** |
| *Totaal per jaar* | *3.788.000* | *391.333* | *782.181* | *7.614.480* | *375.000* | *1.708.249* |

Figure A.2: Overview of cumulative nourishment volumes [m$^3$] per area between 1970 and 2007. (from Tonnon and Nederhoff (2016)

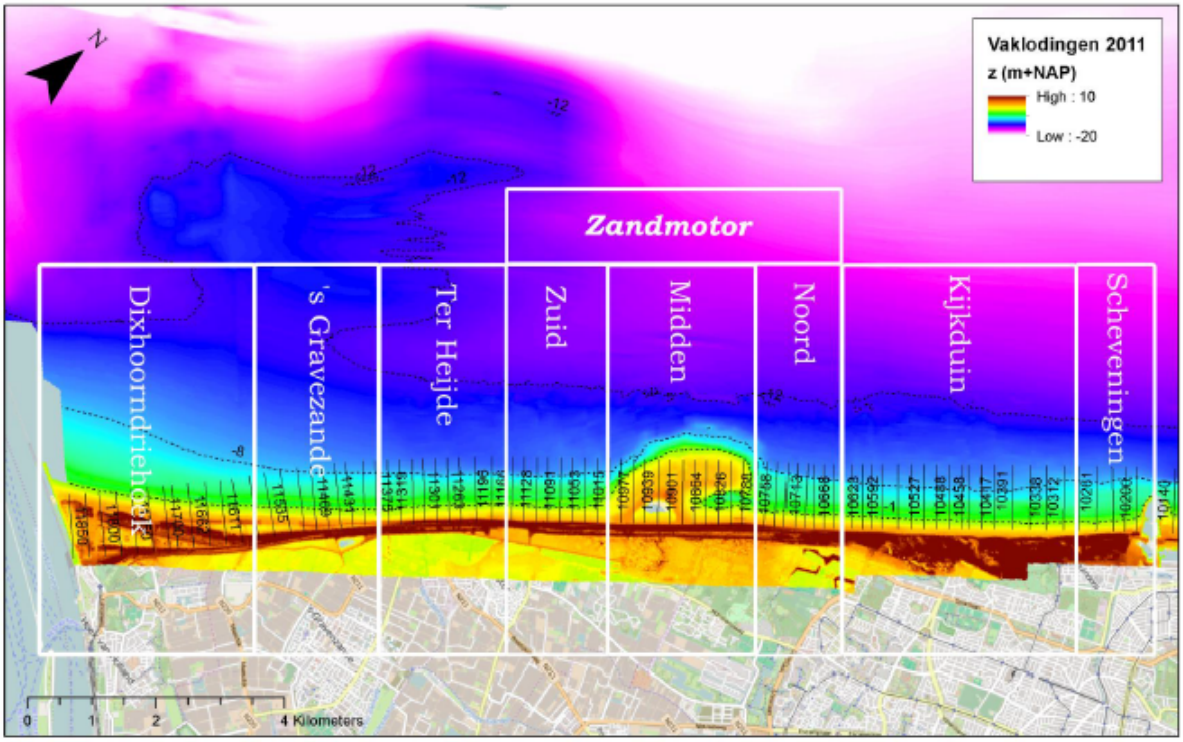


Figure A.3: Sectioning by Deltares Tonnon and Nederhoff (2016))

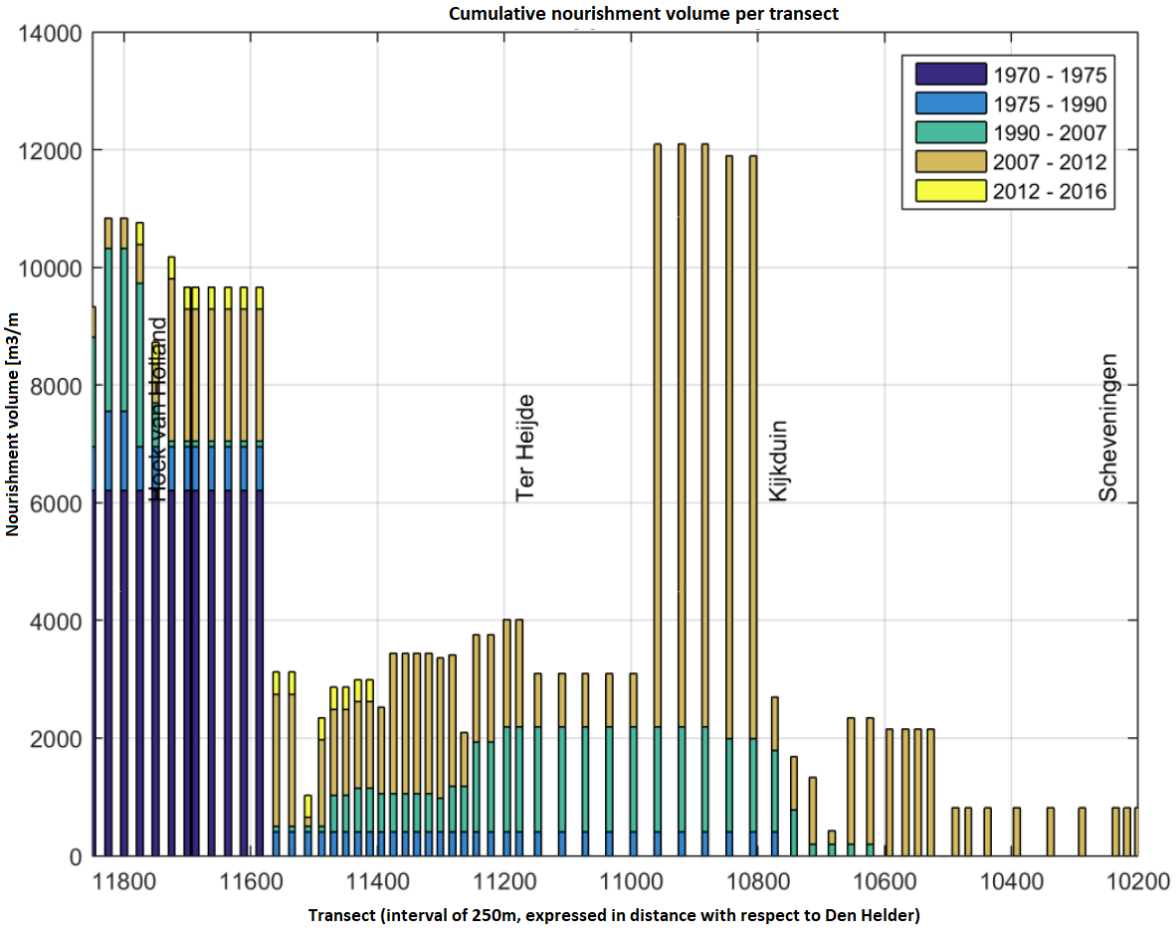


Figure A.4: Overview of cumulative nourishment volumes per transect (cross-shore profile of the coast each 250m). Horizontal axis expresses the distance with respect to Den Helder, see figure 3.1, adjusted from Tonnon and Nederhoff (2016)

# B

# Representative wave climates of numerical models

Tables below show the representative wave climates used as input for three 2D numerical model approaches; the Tonnon (2010) approach, the Stive et al. (2013) approach, and the Luijendijk et al. (In preparation) (MorMerge) approach. Bruteforce not included here, as this approach imposed the wave climate as observed.

Table B.1: Representative Wave climate of Tonnon Model

| Condition | Hs | Ts | $\theta$ | $V_{wind}$ | $\theta_{wind}$ | set up | weight factor |
|---|---|---|---|---|---|---|---|
| unit | [m] | [s] | [$^\circ N$] | [m/s] | [m/s] | [m] | [-] |
| wc29 | 1.48 | 5.34 | 232 | 9.97 | 231 | 0.04 | 0.1224 |
| wc31 | 2.46 | 6.34 | 232 | 13.37 | 227 | 0.12 | 0.0685 |
| wc40 | 1.97 | 5.99 | 246 | 11.09 | 210 | 0.2 | 0.0118 |
| wc49 | 1.48 | 5.45 | 261 | 8.24 | 197 | 0.16 | 0.0006 |
| wc61 | 2.47 | 6.53 | 277 | 11.44 | 175 | 0.42 | 0.046 |
| wc62 | 2.97 | 7 | 277 | 13.3 | 171 | 0.59 | 0.0109 |
| wc90 | 1.97 | 6.59 | 322 | 8.65 | 126 | 0.22 | 0.1206 |
| wc92 | 2.96 | 7.71 | 322 | 11.93 | 127 | 0.53 | 0.0036 |
| wc99 | 1.47 | 6.07 | 337 | 5.69 | 107 | 0.02 | 0.0652 |
| wc108 | 0.96 | 5.63 | 352 | 3.62 | 73 | -0.08 | 0.0823 |

Table B.2: Representative Wave climate of Stive Model

| Condition | Hs | Ts | $\theta$ | $V_{wind}$ | $\theta_{wind}$ | set up | weight factor |
|---|---|---|---|---|---|---|---|
| unit | [m] | [s] | [$^\circ N$] | [m/s] | [m/s] | [m] | [-] |
| wc29 | 1.48 | 5.34 | 232 | 9.97 | 232 | 0.04 | 0.1224 |
| wc31 | 2.46 | 6.34 | 232 | 13.37 | 232 | 0.12 | 0.0685 |
| wc40 | 1.97 | 5.99 | 246 | 11.09 | 246 | 0.2 | 0.0118 |
| wc49 | 1.48 | 5.45 | 261 | 8.24 | 261 | 0.16 | 0.0006 |
| wc61 | 2.47 | 6.53 | 277 | 11.44 | 277 | 0.42 | 0.046 |
| wc62 | 2.97 | 7 | 277 | 13.3 | 277 | 0.59 | 0.0109 |
| wc90 | 1.97 | 6.59 | 322 | 8.65 | 322 | 0.22 | 0.1206 |
| wc92 | 2.96 | 7.71 | 322 | 11.93 | 322 | 0.53 | 0.0036 |
| wc99 | 1.47 | 6.07 | 337 | 5.69 | 337 | 0.02 | 0.0652 |
| wc108 | 0.96 | 5.63 | 352 | 3.62 | 352 | -0.08 | 0.0823 |

Table B.3: Representative Wave climate of MorMerge Model. Differs from the Stive approach input by exclusion of wc49, which showed to have negligible influence on simulation.

| Condition | Hs | Ts | $\theta$ | $V_{wind}$ | $\theta_{wind}$ | set up | weight factor |
|---|---|---|---|---|---|---|---|
| unit | [m] | [s] | [$^{\circ}N$] | [m/s] | [m/s] | [m] | [-] |
| wc29 | 1.48 | 5.34 | 232 | 9.97 | 232 | 0.04 | 0.1224 |
| wc31 | 2.46 | 6.34 | 232 | 13.37 | 232 | 0.12 | 0.0685 |
| wc40 | 1.97 | 5.99 | 246 | 11.09 | 246 | 0.2 | 0.0118 |
| wc61 | 2.47 | 6.53 | 277 | 11.44 | 277 | 0.42 | 0.046 |
| wc62 | 2.97 | 7 | 277 | 13.3 | 277 | 0.59 | 0.0109 |
| wc90 | 1.97 | 6.59 | 322 | 8.65 | 322 | 0.22 | 0.1206 |
| wc92 | 2.96 | 7.71 | 322 | 11.93 | 322 | 0.53 | 0.0036 |
| wc99 | 1.47 | 6.07 | 337 | 5.69 | 337 | 0.02 | 0.0652 |
| wc108 | 0.96 | 5.63 | 352 | 3.62 | 352 | -0.08 | 0.0823 |

# C

# Data pre-processing

This section visualises the step by step that make up the pre-processing of the data. First the point cloud data is loaded, freely available[1], see figure C.1. Secondly, the data is translated to transects, as done by Roest (2017) (figure C.2). In the third step, the data is translated to a rectangular grid of 20x20m, see figure C.3. Then the grid is rotated to an orthogonal axis, see figure C.4. In the last step, a Survey updating technique is applied, where data from the Zandmotore, NeMo and JarKus surveys are combined, see figure C.5.

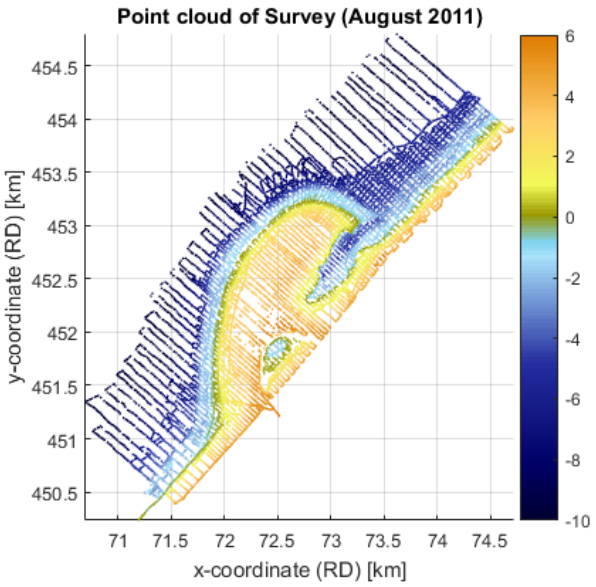


Figure C.1: Point cloud of the retrieved data from the Zandmotor program (https://data.4tu.nl/repository/collection:zandmotor)

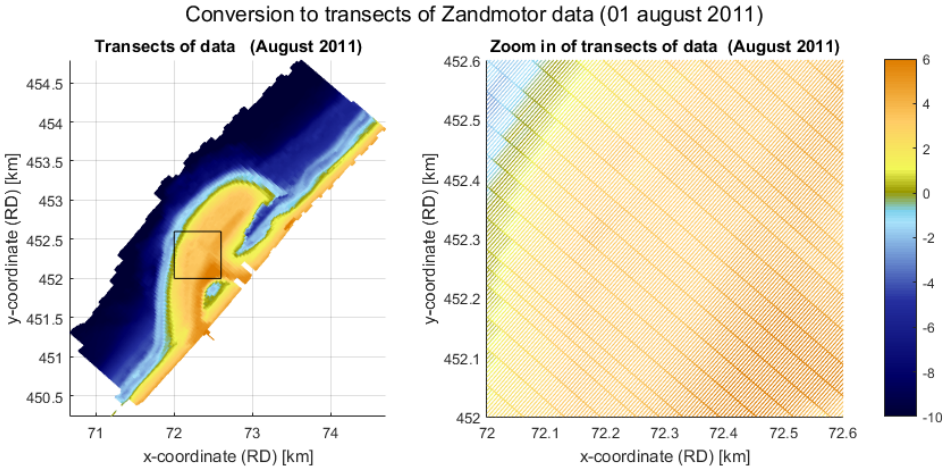


Figure C.2: Conversion from point cloud to transects by Roest (2017)

[1] https://data.4tu.nl/repository/collection:zandmotor

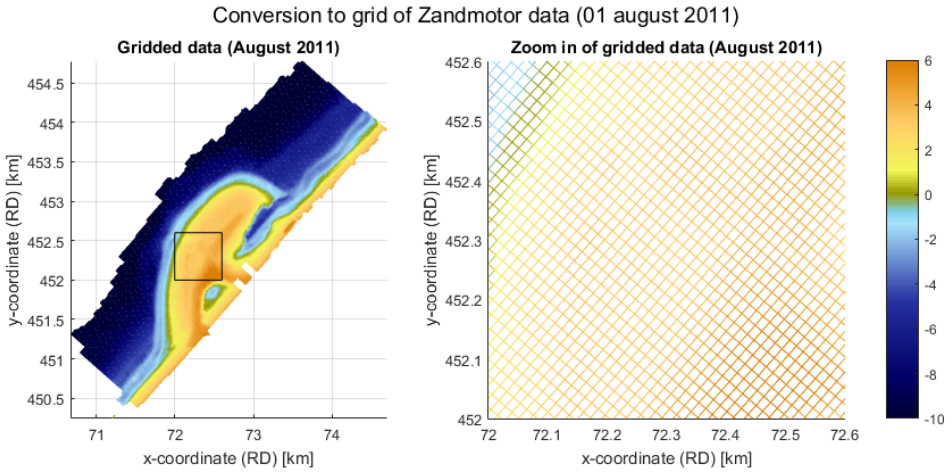


Figure C.3: Conversion from transects to grid (20x20m))

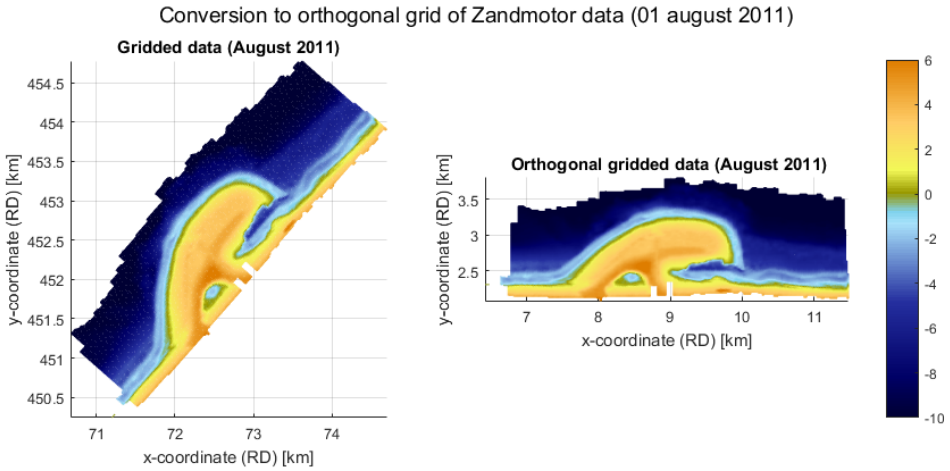


Figure C.4: Conversion from Rijksdriehoeken coordinate system to orthogonal grid)

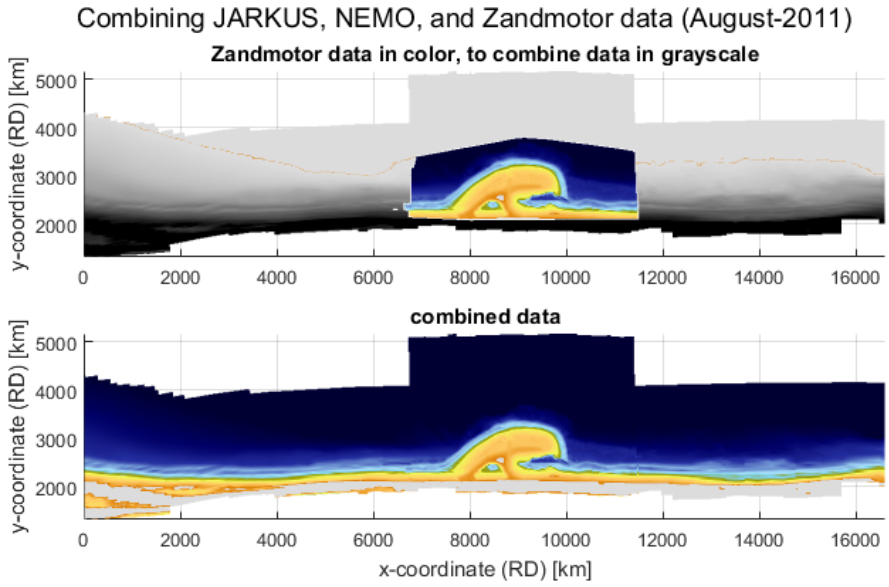


Figure C.5: Combining of JarKus, NeMo, and Zandmotor data. Upper panel shows the Zandmotor Data (coloured) and JarKus and NeMo on the background in grey. Bottom Panel shows the merging of the data.

# D

# Additional results of quantification of the Sand Engine

## D.1. Representation of the cross-shore extent

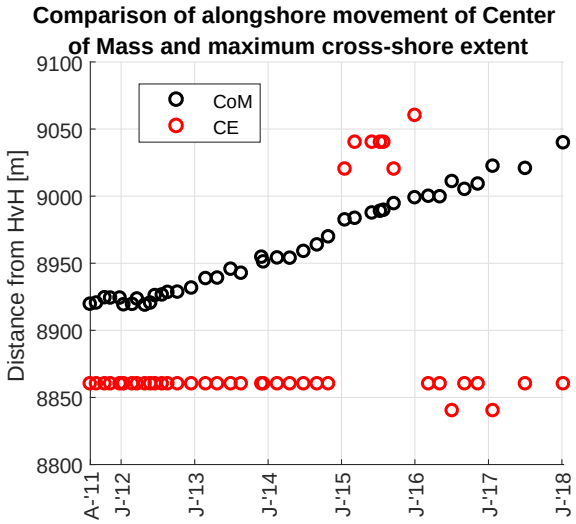


Figure D.1: Alongshore movement of centroid (CoM )versus maximum cross-shore extent (CE).

In figure D.1, the migration of the centroid (M1) is compared to the migration of the maximum cross-shore extent. Results show the latter cannot represent the alongshore migration in the case volume densities are considered. Therefore, it is discouraged to use this indicator as a measure to quantify the alongshore migration of the sediment.

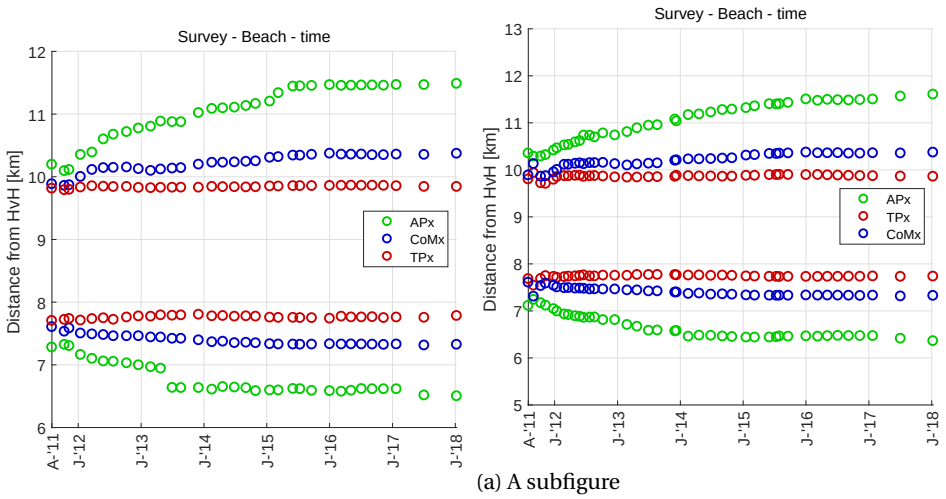


(a) A subfigure

Figure D.3: Assessment of the use of a moving average on the volumetric shape. Left plot Geometric indicators withouth, and right plot with application of a moving average.

## D.2. Erosion of the Regions of Influence

In section 5.2.2, it was shown that within the Region of Influence (between 6.4 and 12.8km from HvH), a mild net erosion of sediment could be observed. To verify whether this loss is attributed offshore or alongshore, the net volumetric change of the Westland coast is computed as well (see D.2). Results show the Westland section as a whole does not erode over time, whereas the Region of Influence does erode. Apparently, the mild erosions observed in thee RoI are thus found in the other sections of the Westland coasts. Sediment likely to have transported this larger distance is likely to be fines. The results confirms the sediment does not migrate offshore, i.e. sediment is not lost.

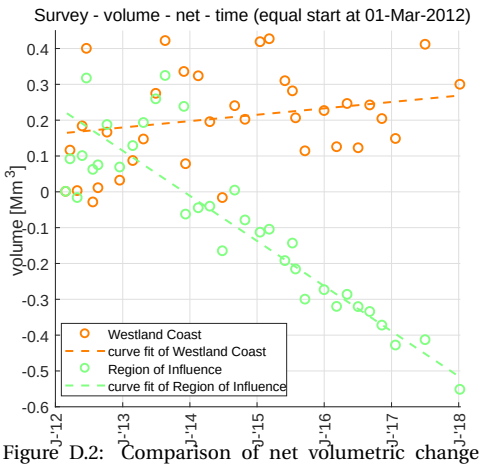


Figure D.2: Comparison of net volumetric change within the Region of Influence versus the Westland Coast. Cumulative differences as of March 2012.

## D.3. The influence of application of the moving average

Figure D.3 depicts the influence of the use of the moving average. The influence is mild. The 'jumps', observed when no moving average is applied, are spread out over time with the application of the moving average.

## D.4. The relation of the macro-scale behaviour to WavePower

Section 5.2.2 showed excellent performance of square root curve-fits of the volumetric performance of each of the sections separately. Additionally, a seasonality was observed in the feeding behaviour. The Pelnard Considère equation suggests the diffusive behaviour of a concentrated nourishment is dominated by the wave power of breaking waves ($\sigma^2 = 2Gt \sim WP \sim H_b^{2.5}$). With it, is assumed there is a constant attack of waves throughout the entire year, while in reality, The observed wave power shows great variations per season. More specifically, storms are suggested to have a large influence on the shape of the Sand Engine Luijendijk et al. (2017).

The spreading of the Sand Engine appeared mildly more gradual if related to the wave power instead of time (D.4). The initially rapid spreading, as well as the observed jump after the storm of January 2015, depicts the influence. Though, the performance is only mildly improved. Apparently, the long term diffusive behaviour dominates the spreading of a mega-feeder nourishment.

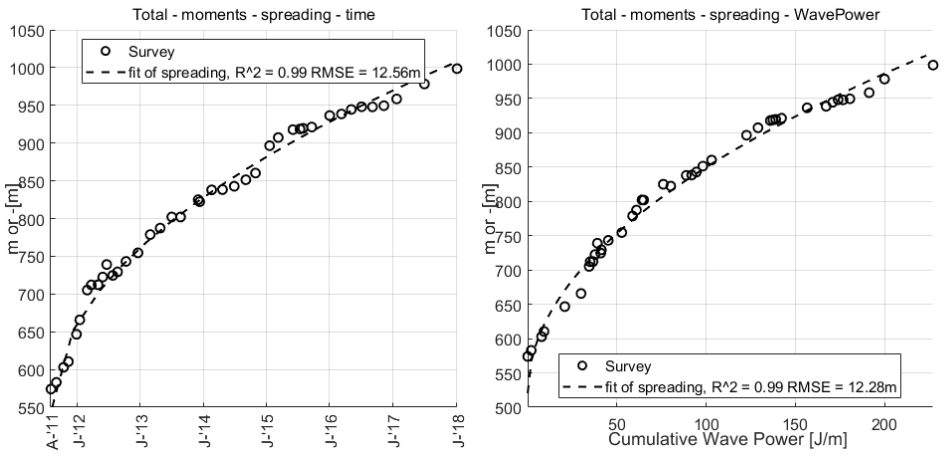


(a) A subfigure (b) A subfigure

Figure D.4: A figure with two subfigures

| **APx** | corrcoef | R2 | RMSE |
|---|---|---|---|
| | [-] | [-] | [m] |
| south | 0.95 | 0.84 | 71.31 |
| north | 0.99 | 0.97 | 55.36 |
| distance | 0.98 | 0.95 | 114.07 |

Table D.3: Survey - Beach - APx

## D.5. Performance of curve-fits

The tables below quantify the capacity of curve-fits to describe the developments of the performance indicators. Quantification in terms of the correlation coefficient $\rho$, coefficient of determination $R^2$, and the Root Mean Square Error.

| **volume** | corrcoef | R2 | RMSE | RMSNE |
|---|---|---|---|---|
| | [-] | [-] | [Mm3] | [Mm3/m] |
| south | 0.97 | 0.95 | 45724.89 | 8522.56 |
| north | 0.99 | 0.99 | 59631.60 | 4671.14 |
| middle | 0.99 | 0.99 | 68379.06 | 9439.09 |
| net | 0.90 | 0.91 | 47137.08 | 8232.77 |

Table D.1: Survey - Total - volume

| **moments** | corrcoef | R2 | RMSE |
|---|---|---|---|
| | [-] | [-] | [m] |
| volume | 0.90 | 0.80 | 104074.75 |
| CoM | 0.99 | 0.98 | 5.03 |
| spreading | 0.99 | 0.99 | 12.56 |
| skewness | 0.74 | 0.25 | 0.05 |
| kurtosis | - | 0.87 | 0.12 |

Table D.2: Survey - Total - moments

| **TPx** | corrcoef | R2 | RMSE |
|---|---|---|---|
| | [-] | [-] | [m] |
| south | 0.18 | 0.03 | 36.24 |
| north | 0.43 | 0.19 | 38.33 |
| distance | 0.19 | 0.04 | 58.58 |

Table D.4: Survey - Beach - TPx

| **CoMx** | corrcoef | R2 | RMSE |
|---|---|---|---|
| | [-] | [-] | [m] |
| south | 0.86 | 0.74 | 42.73 |
| north | 0.93 | 0.86 | 54.86 |
| distance | 0.92 | 0.84 | 89.49 |

Table D.5: Survey - Beach - CoMx

# E

# Additional results of analytical model

## E.1. Validation of the geometric performance

In chapter 6, the validation of the geometric performance , was limited to the assessment of the Accretion Points. Two other indicators that also represent the performance geometrically, are the centroids of the accreted volumes and the Transition Points. Results of the validation of these indicators are discussed here.

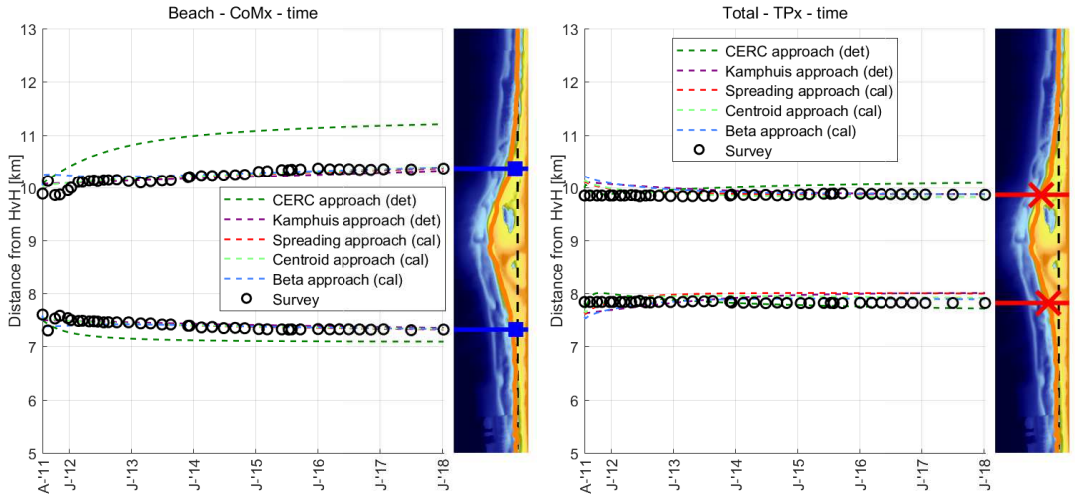


Reflections by the CERC approach of the centroid movement of the Regions of Contribution lead to high RMAEs (250 - 500%). The Kamphuis model approach reflects the performance in terms of the centroids better (RMAE ≈ 30 -40%). Interestingly, the RMAE of the calibrated model approaches are not better than those for the Kamphuis approach. Part of the reason the RMAE's are higher than for the APs, is a result of the fact that the change of the centroids is lower, so therefore the RMAE tends to increase. MAEs are in the order of 30 - 40m, a factor 2 smaller than the MAE of the APs. The Transition Points are in general well described by the analytical model approaches, with MEA of circa 100m.

## E.2. Additional graphs of results of analytical model approaches

The figures below visualise the capacity of the calibrated Volume (spreading and volume fitted) and Plus (spreading, centroid, and volume fitted) to reflect the performance indicators.

## E.3. Quantification of reflection of performance indicators by analytical models

The tables below show the quantified reflection of the performance indicators by the analytical model approaches. In each of the tables, the reflection is quantified in terms of the Mean Absolute Error, the Relative

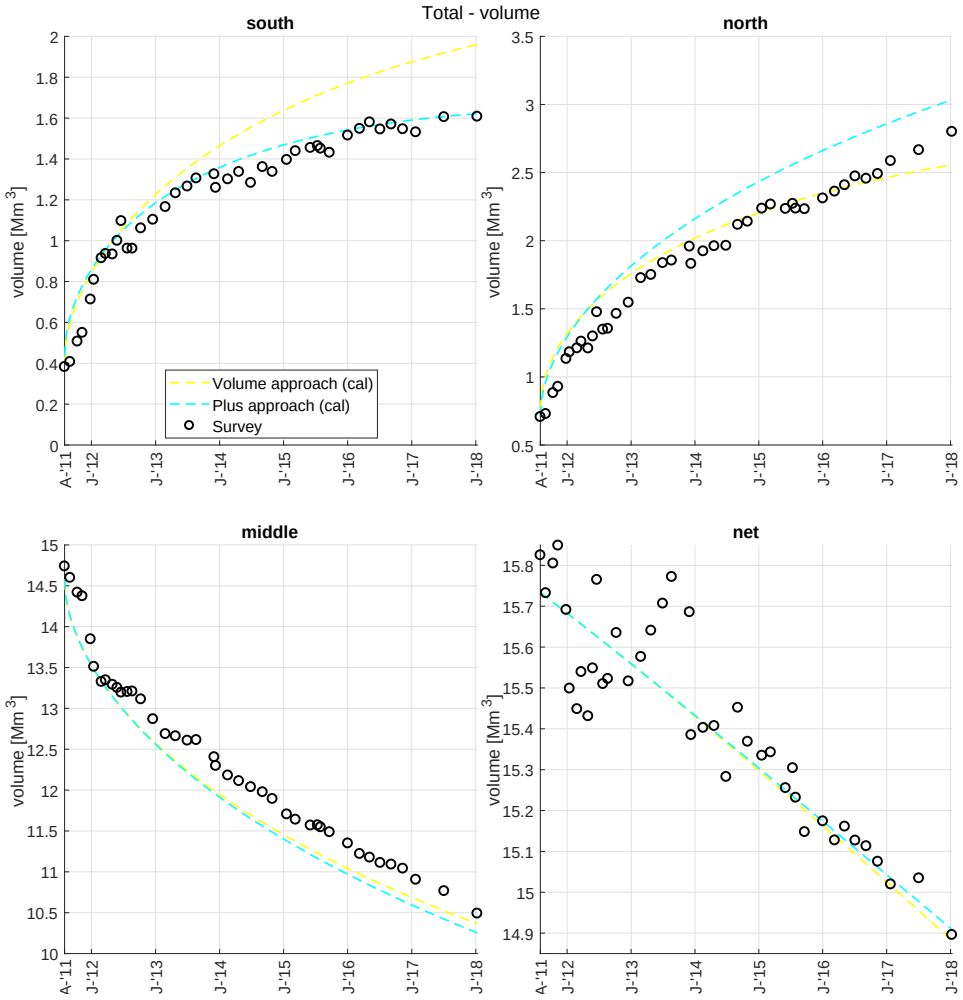


Figure E.2: Capacity of analytical model approaches (Volume and Plus fit) to reflect the volumetric changes of the Sand Engine.

Mean Absolute Errors, the Normalised Mean Absolute Error, and the Root Mean Squared Normalised Error or the Root Mean Squared Error.

| **CERC** | MAE | RMAE | NMAE | RMSNE |
|---|---|---|---|---|
| **volume** | [Mm3] | [%] | [Mm3/m] | [Mm3/m] |
| south | 1238435.12 | 151.50 | 95264.24 | 101479.62 |
| north | 2030156.59 | 181.50 | 156165.89 | 162775.47 |
| middle | 5379505.32 | 230.10 | 413808.10 | 434212.47 |
| net | 2129494.86 | 528.10 | 163807.30 | 206265.63 |

Table E.1: CERC - Total - volume

| **Kamphuis** | MAE | RMAE | NMAE | RMSNE |
|---|---|---|---|---|
| **volume** | [Mm3] | [%] | [Mm3/m] | [Mm3/m] |
| south | 324160.90 | 39.70 | 24935.45 | 26952.18 |
| north | 534055.47 | 47.70 | 41081.19 | 43927.02 |
| middle | 1253475.24 | 53.60 | 96421.17 | 102052.43 |
| net | 396528.36 | 98.30 | 30502.18 | 35627.25 |

Table E.2: Kamphuis - Total - volume

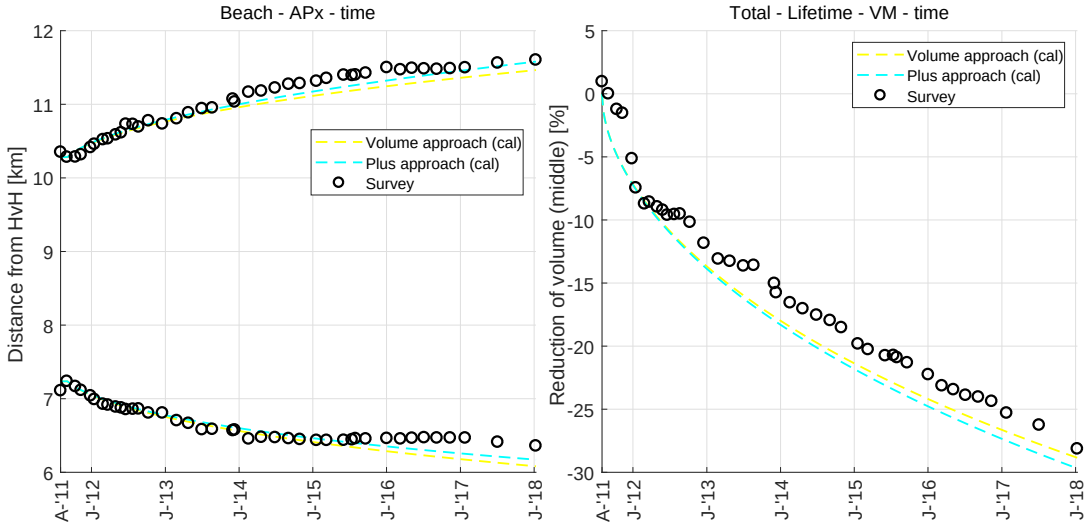


Figure E.3: a) Capacity of analytical model approaches (Volume and Plus fit) to reflect the alongshore expansion of the Sand Engine b) the reduction of the volume of the middle section.

| **Centroid-fit** | MAE | RMAE | NMAE | RMSNE |
|---|---|---|---|---|
| **volume** | [Mm3] | [%] | [Mm3/m] | [Mm3/m] |
| south | 55501.70 | 6.80 | 4269.36 | 5471.25 |
| north | 298428.09 | 26.70 | 22956.01 | 24437.50 |
| middle | 128609.44 | 5.50 | 9893.03 | 13161.67 |
| net | 381103.11 | 94.50 | 29315.62 | 34176.04 |

Table E.4: Centroid-fit - Total - volume

| **Spreading-fit** | MAE | RMAE | NMAE | RMSNE |
|---|---|---|---|---|
| **volume** | [Mm3] | [%] | [Mm3/m] | [Mm3/m] |
| south | 195262.40 | 23.90 | 15020.18 | 17732.11 |
| north | 106048.21 | 9.50 | 8157.55 | 10004.97 |
| middle | 170399.02 | 7.30 | 13107.62 | 16572.43 |
| net | 375198.61 | 93.00 | 28861.43 | 33538.49 |

Table E.3: Spreading-fit - Total - volume

| **Volume-fit** | MAE | RMAE | NMAE | RMSNE |
|---|---|---|---|---|
| **volume** | [Mm3] | [%] | [Mm3/m] | [Mm3/m] |
| south | 157649.18 | 19.30 | 12126.86 | 14115.65 |
| north | 104040.81 | 9.30 | 8003.14 | 10116.10 |
| middle | 143695.99 | 6.10 | 11053.54 | 13266.46 |
| net | 101458.81 | 25.20 | 7804.52 | 9849.54 |

Table E.5: Volume-fit - Total - volume

| **Plus-fit** | MAE | RMAE | NMAE | RMSNE |
|---|---|---|---|---|
| **volume** | [Mm3] | [%] | [Mm3/m] | [Mm3/m] |
| south | 44655.41 | 5.50 | 3435.03 | 4798.73 |
| north | 240537.37 | 21.50 | 18502.87 | 19399.81 |
| middle | 191499.89 | 8.20 | 14730.76 | 16496.45 |
| net | 106587.76 | 26.40 | 8199.06 | 10071.29 |

Table E.6: Plus-fit - Total - volume

| **Beta-fit** | MAE | RMAE | NMAE | RMSNE |
|---|---|---|---|---|
| **volume** | [Mm3] | [%] | [Mm3/m] | [Mm3/m] |
| south | 110072.15 | 13.50 | 8467.09 | 9130.03 |
| north | 111354.73 | 10.00 | 8565.75 | 9937.24 |
| middle | 91828.01 | 3.90 | 7063.69 | 10334.93 |
| net | 98498.12 | 24.40 | 7576.78 | 9405.09 |

Table E.7: Beta-fit - Total - volume

| **CERC** | MAE | RMAE | NMAE | RMSNE |
|---|---|---|---|---|
| **moments** | [m/-] | [%] | [m/-/m] | [m/-/m] |
| CoM | 233.79 | 587.30 | 233.79 | 272.24 |
| spreading | 629.51 | 272.40 | 629.51 | 658.98 |
| skewness | 0.10 | 63.00 | 0.10 | 0.12 |
| kurtosis | 1.30 | 119.50 | 1.30 | 1.36 |

Table E.8: CERC - Total - moments

| **Kamphuis** | MAE | RMAE | NMAE | RMSNE |
|---|---|---|---|---|
| **moments** | [m/-] | [%] | [m/-/m] | [m/-/m] |
| CoM | 39.32 | 98.80 | 39.32 | 52.13 |
| spreading | 103.04 | 44.60 | 103.04 | 109.84 |
| skewness | 0.09 | 55.90 | 0.09 | 0.10 |
| kurtosis | 0.66 | 60.20 | 0.66 | 0.73 |

Table E.9: Kamphuis - Total - moments

| **Spreading-fit** | MAE | RMAE | NMAE | RMSNE |
|---|---|---|---|---|
| **moments** | [m/-] | [%] | [m/-/m] | [m/-/m] |
| CoM | 35.62 | 89.50 | 35.62 | 47.08 |
| spreading | 12.12 | 5.20 | 12.12 | 14.87 |
| skewness | 0.07 | 45.20 | 0.07 | 0.08 |
| kurtosis | 0.70 | 64.40 | 0.70 | 0.77 |

Table E.10: Spreading-fit - Total - moments

| **Centroid-fit** | MAE | RMAE | NMAE | RMSNE |
|---|---|---|---|---|
| **moments** | [m/-] | [%] | [m/-/m] | [m/-/m] |
| CoM | 6.82 | 17.10 | 6.82 | 8.60 |
| spreading | 11.31 | 4.90 | 11.31 | 14.15 |
| skewness | 0.08 | 47.90 | 0.08 | 0.09 |
| kurtosis | 0.69 | 63.70 | 0.69 | 0.76 |

Table E.11: Centroid-fit - Total - moments

| **Volume-fit** | MAE | RMAE | NMAE | RMSNE |
|---|---|---|---|---|
| **moments** | [m/-] | [%] | [m/-/m] | [m/-/m] |
| CoM | 35.62 | 89.50 | 35.62 | 47.08 |
| spreading | 12.12 | 5.20 | 12.12 | 14.87 |
| skewness | 0.07 | 45.20 | 0.07 | 0.08 |
| kurtosis | 0.70 | 64.40 | 0.70 | 0.77 |

Table E.12: Volume-fit - Total - moments

| **Plus-fit** | MAE | RMAE | NMAE | RMSNE |
|---|---|---|---|---|
| **moments** | [m/-] | [%] | [m/-/m] | [m/-/m] |
| CoM | 6.82 | 17.10 | 6.82 | 8.60 |
| spreading | 11.31 | 4.90 | 11.31 | 14.15 |
| skewness | 0.08 | 47.90 | 0.08 | 0.09 |
| kurtosis | 0.69 | 63.70 | 0.69 | 0.76 |

Table E.13: Plus-fit - Total - moments

| **Beta-fit** | MAE | RMAE | NMAE | RMSNE |
|---|---|---|---|---|
| **moments** | [m/-] | [%] | [m/-/m] | [m/-/m] |
| CoM | 7.05 | 17.70 | 7.05 | 8.35 |
| spreading | 13.05 | 5.60 | 13.05 | 15.78 |
| skewness | 0.08 | 52.10 | 0.08 | 0.11 |
| kurtosis | 0.46 | 42.60 | 0.46 | 0.64 |

Table E.14: Beta-fit - Total - moments

| **CERC** | MAE | RMAE | RMSE |
|---|---|---|---|
| **APx** | [m] | [%] | [m] |
| south | 1317.79 | 229.10 | 1367.05 |
| north | 1778.44 | 242.30 | 1870.53 |
| distance | 3096.23 | 236.50 | 3235.72 |

Table E.15: CERC - Beach - APx

| **Kamphuis** | MAE | RMAE | RMSE |
|---|---|---|---|
| **APx** | [m] | [%] | [m] |
| south | 241.45 | 42.00 | 262.50 |
| north | 398.45 | 54.30 | 446.77 |
| distance | 638.29 | 48.80 | 691.66 |

Table E.16: Kamphuis - Beach - APx

| **Spreading-fit** | MAE | RMAE | RMSE |
|---|---|---|---|
| **APx** | [m] | [%] | [m] |
| south | 77.71 | 13.50 | 110.13 |
| north | 140.31 | 19.10 | 160.91 |
| distance | 116.42 | 8.90 | 141.44 |

Table E.17: Spreading-fit - Beach - APx

| **Centroid-fit** | MAE | RMAE | RMSE |
|---|---|---|---|
| **APx** | [m] | [%] | [m] |
| south | 63.27 | 11.00 | 80.96 |
| north | 102.56 | 14.00 | 115.95 |
| distance | 115.73 | 8.80 | 139.64 |

Table E.18: Centroid-fit - Beach - APx

| **Volume-fit** | MAE | RMAE | RMSE |
|---|---|---|---|
| **APx** | [m] | [%] | [m] |
| south | 77.71 | 13.50 | 110.13 |
| north | 140.31 | 19.10 | 160.91 |
| distance | 116.42 | 8.90 | 141.44 |

Table E.19: Volume-fit - Beach - APx

| **Plus-fit** | MAE | RMAE | RMSE |
|---|---|---|---|
| **APx** | [m] | [%] | [m] |
| south | 63.27 | 11.00 | 80.96 |
| north | 102.56 | 14.00 | 115.95 |
| distance | 115.73 | 8.80 | 139.64 |

Table E.20: Plus-fit - Beach - APx

| **Beta-fit** | MAE | RMAE | RMSE |
|---|---|---|---|
| **APx** | [m] | [%] | [m] |
| south | 75.61 | 13.10 | 99.23 |
| north | 83.75 | 11.40 | 93.41 |
| distance | 109.44 | 8.40 | 126.23 |

Table E.21: Beta-fit - Beach - APx

| **CERC** | MAE | RMAE | RMSE |
|---|---|---|---|
| **TPx** | [m] | [%] | [m] |
| south | 68.82 | 626.00 | 81.73 |
| north | 135.09 | 1024.20 | 147.09 |
| distance | 166.14 | 695.50 | 189.62 |

Table E.22: CERC - Total - TPx

| **Kamphuis** | MAE | RMAE | RMSE |
|---|---|---|---|
| **TPx** | [m] | [%] | [m] |
| south | 126.76 | 1153.10 | 139.05 |
| north | 102.00 | 773.40 | 132.45 |
| distance | 194.37 | 813.70 | 227.01 |

Table E.23: Kamphuis - Total - TPx

| **Spreading-fit** | MAE | RMAE | RMSE |
|---|---|---|---|
| **TPx** | [m] | [%] | [m] |
| south | 142.93 | 1300.20 | 152.48 |
| north | 54.56 | 413.70 | 81.09 |
| distance | 148.75 | 622.70 | 171.20 |

Table E.24: Spreading-fit - Total - TPx

| **Centroid-fit** | MAE | RMAE | RMSE |
|---|---|---|---|
| **TPx** | [m] | [%] | [m] |
| south | 100.96 | 918.40 | 105.47 |
| north | 68.21 | 517.10 | 89.11 |
| distance | 133.70 | 559.70 | 156.38 |

Table E.25: Centroid-fit - Total - TPx

| **Volume-fit** | MAE | RMAE | RMSE |
|---|---|---|---|
| **TPx** | [m] | [%] | [m] |
| south | 120.79 | 1098.80 | 128.73 |
| north | 65.90 | 499.60 | 86.98 |
| distance | 118.50 | 496.10 | 144.71 |

Table E.26: Volume-fit - Total - TPx

| **Plus-fit** | MAE | RMAE | RMSE |
|---|---|---|---|
| **TPx** | [m] | [%] | [m] |
| south | 81.26 | 739.20 | 85.85 |
| north | 61.26 | 464.40 | 88.44 |
| distance | 105.31 | 440.80 | 133.43 |

Table E.27: Plus-fit - Total - TPx

| **Beta-fit** | MAE | RMAE | RMSE |
|---|---|---|---|
| **TPx** | [m] | [%] | [m] |
| south | 82.76 | 752.90 | 100.80 |
| north | 98.34 | 745.60 | 139.76 |
| distance | 157.17 | 657.90 | 221.95 |

Table E.28: Beta-fit - Total - TPx

| **CERC** | MAE | RMAE | RMSE |
|---|---|---|---|
| **CoMx** | [m] | [%] | [m] |
| south | 243.42 | 253.20 | 247.01 |
| north | 658.41 | 511.90 | 687.12 |
| distance | 900.33 | 486.70 | 926.57 |

Table E.29: CERC - Beach - CoMx

| **Kamphuis** | MAE | RMAE | RMSE |
|---|---|---|---|
| **CoMx** | [m] | [%] | [m] |
| south | 45.86 | 47.70 | 58.37 |
| north | 67.68 | 52.60 | 85.64 |
| distance | 109.69 | 59.30 | 136.10 |

Table E.30: Kamphuis - Beach - CoMx

| **Spreading-fit** | MAE | RMAE | RMSE |
|---|---|---|---|
| **CoMx** | [m] | [%] | [m] |
| south | 27.60 | 28.70 | 43.68 |
| north | 44.81 | 34.80 | 66.85 |
| distance | 67.97 | 36.70 | 99.65 |

Table E.31: Spreading-fit - Beach - CoMx

| **Centroid-fit** | MAE | RMAE | RMSE |
|---|---|---|---|
| **CoMx** | [m] | [%] | [m] |
| south | 31.19 | 32.40 | 46.14 |
| north | 43.17 | 33.60 | 65.57 |
| distance | 66.59 | 36.00 | 98.81 |

Table E.32: Centroid-fit - Beach - CoMx

| **Volume-fit** | MAE | RMAE | RMSE |
|---|---|---|---|
| **CoMx** | [m] | [%] | [m] |
| south | 27.60 | 28.70 | 43.68 |
| north | 44.81 | 34.80 | 66.85 |
| distance | 67.97 | 36.70 | 99.65 |

Table E.33: Volume-fit - Beach - CoMx

| **Plus-fit** | MAE | RMAE | RMSE |
|---|---|---|---|
| **CoMx** | [m] | [%] | [m] |
| south | 31.19 | 32.40 | 46.14 |
| north | 43.17 | 33.60 | 65.57 |
| distance | 66.59 | 36.00 | 98.81 |

Table E.34: Plus-fit - Beach - CoMx

| **Beta-fit** | MAE | RMAE | RMSE |
|---|---|---|---|
| **CoMx** | [m] | [%] | [m] |
| south | 46.65 | 48.50 | 60.74 |
| north | 82.06 | 63.80 | 122.08 |
| distance | 115.51 | 62.40 | 174.79 |

Table E.35: Beta-fit - Beach - CoMx

| **CERC** | MAE | RMAE | NMAE | RMSNE |
|---|---|---|---|---|
| **Lifetime** | [] | [%] | [/m] | [/m] |
| VM | 38.52 | 255.00 | 38.52 | 40.34 |
| CE | 50.21 | 319.10 | 50.21 | 51.51 |

Table E.36: CERC - Total - Lifetime

| **Kamphuis** | MAE | RMAE | NMAE | RMSNE |
|---|---|---|---|---|
| **Lifetime** | [] | [%] | [/m] | [/m] |
| VM | 7.59 | 50.20 | 7.59 | 8.07 |
| CE | 1.89 | 12.00 | 1.89 | 2.10 |

Table E.37: Kamphuis - Total - Lifetime

| **Spreading-fit** | MAE | RMAE | NMAE | RMSNE |
|---|---|---|---|---|
| **Lifetime** | [] | [%] | [/m] | [/m] |
| VM | 1.04 | 6.90 | 1.04 | 1.38 |
| CE | 15.11 | 96.00 | 15.11 | 15.46 |

Table E.38: Spreading-fit - Total - Lifetime

| **Centroid-fit** | MAE | RMAE | NMAE | RMSNE |
|---|---|---|---|---|
| **Lifetime** | [] | [%] | [/m] | [/m] |
| VM | 0.97 | 6.40 | 0.97 | 1.32 |
| CE | 15.11 | 96.00 | 15.11 | 15.46 |

Table E.39: Centroid-fit - Total - Lifetime

| **Volume-fit** | MAE | RMAE | NMAE | RMSNE |
|---|---|---|---|---|
| **Lifetime** | [] | [%] | [/m] | [/m] |
| VM | 1.84 | 12.20 | 1.84 | 2.01 |
| CE | 16.31 | 103.70 | 16.31 | 16.71 |

Table E.40: Volume-fit - Total - Lifetime

| **Plus-fit** | MAE | RMAE | NMAE | RMSNE |
|---|---|---|---|---|
| **Lifetime** | [] | [%] | [/m] | [/m] |
| VM | 2.18 | 14.40 | 2.18 | 2.33 |
| CE | 16.31 | 103.70 | 16.31 | 16.71 |

Table E.41: Plus-fit - Total - Lifetime

| **Beta-fit** | MAE | RMAE | NMAE | RMSNE |
|---|---|---|---|---|
| **Lifetime** | [] | [%] | [/m] | [/m] |
| VM | 0.92 | 6.10 | 0.92 | 1.07 |
| CE | 11.52 | 73.20 | 11.52 | 12.55 |

Table E.42: Beta-fit - Total - Lifetime

# F

# Additional results of validation numerical model approaches

## F.1. Validation of the geometric performance

In chapter 6, the validation of the geometric performance was limited to the assessment of the Accretion Points. Two other indicators that also represent the performance geometrically, are the centroids of the accreted volumes and the Transition Points. Results of the validation of these indicators are discussed here.

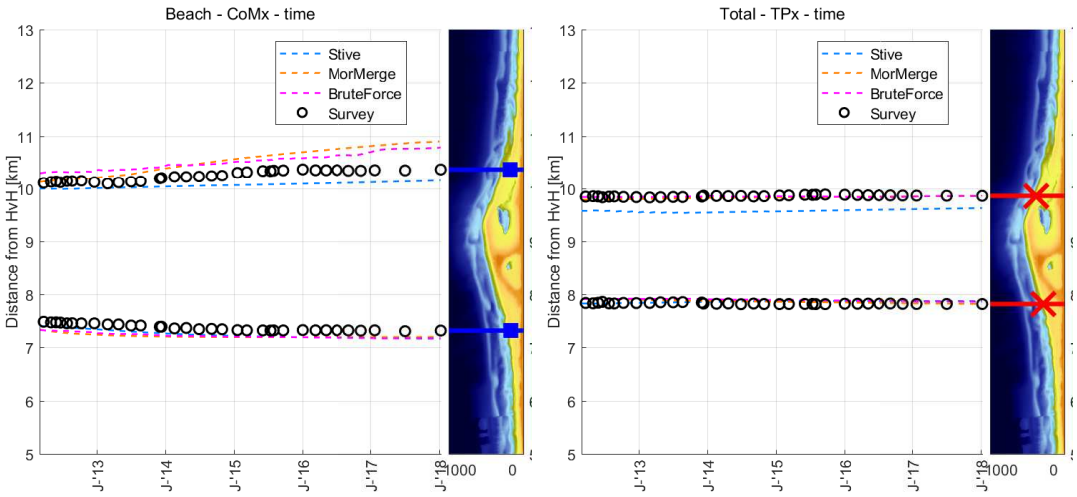


The model approaches reflect the performance poorly in terms of the movement of the centroids (RMAE ≈ 30 - 80, MAE ≈ 60 - 200m). The capacity is mildly improved by exclusion of acceleration techniques and application of a curved nearshore grid, but errors remain high. Transition Points however, are well described by all the models (MAE<70m), although the Stive approach diverges on the north, with an error of nearly 300m on average.

## F.2. Quantification of performance of analytical models

Tables in which the capacity of the numerical model approaches is quantified in the Mean Absolute Error, the Relative Mean Absolute Error, the Normalised Mean Absolute Error, the Root Mean Square Error. For the reflection of the volumetric performance, also the Root Mean Square Normalised Error is included.

| **Tonnon** | MAE | RMAE | NMAE | RMSNE |
|---|---|---|---|---|
| **volume** | [Mm3] | [%] | [Mm3/m] | [Mm3/m] |
| south | 492046.66 | 60.20 | 37849.74 | 40263.41 |
| north | 944054.55 | 84.40 | 72619.58 | 80751.99 |
| middle | 1626743.12 | 69.60 | 125134.09 | 136764.54 |
| net | 209532.89 | 52.00 | 16117.91 | 18760.04 |

Table F.1: Tonnon - Total - volume

| **Stive** | MAE | RMAE | NMAE | RMSNE |
|---|---|---|---|---|
| **volume** | [Mm3] | [%] | [Mm3/m] | [Mm3/m] |
| south | 200081.26 | 24.50 | 15390.87 | 17860.08 |
| north | 503654.87 | 45.00 | 38742.68 | 41307.74 |
| middle | 1189221.33 | 50.90 | 91478.56 | 96503.47 |
| net | 486792.09 | 120.70 | 37445.55 | 44798.34 |

Table F.2: Stive - Total - volume

| **MorMerge** | MAE | RMAE | NMAE | RMSNE |
|---|---|---|---|---|
| **volume** | [Mm3] | [%] | [Mm3/m] | [Mm3/m] |
| south | 84205.34 | 10.30 | 6477.33 | 8305.32 |
| north | 349932.57 | 31.30 | 26917.89 | 33497.03 |
| middle | 512101.88 | 21.90 | 39392.45 | 46614.70 |
| net | 216231.83 | 53.60 | 16633.22 | 19352.28 |

Table F.3: MorMerge - Total - volume

| **BruteForce** | MAE | RMAE | NMAE | RMSNE |
|---|---|---|---|---|
| **volume** | [Mm3] | [%] | [Mm3/m] | [Mm3/m] |
| south | 79845.24 | 9.80 | 6141.94 | 7285.75 |
| north | 96453.26 | 8.60 | 7419.48 | 9219.40 |
| middle | 230020.08 | 9.80 | 17693.85 | 20897.76 |
| net | 142698.26 | 35.40 | 10976.79 | 12517.94 |

Table F.4: BruteForce - Total - volume

| **Tonnon** | MAE | RMAE | RMSE |
|---|---|---|---|
| **moments** | [m/-] | [%] | [m/-] |
| CoM | 51.68 | 129.80 | 56.61 |
| spreading | 133.37 | 57.70 | 141.94 |
| skewness | 0.41 | 251.30 | 0.44 |
| kurtosis | 0.51 | 46.90 | 0.68 |

Table F.5: Tonnon - Total - moments

| **Stive** | MAE | RMAE | RMSE |
|---|---|---|---|
| **moments** | [m/-] | [%] | [m/-] |
| CoM | 15.56 | 39.10 | 17.94 |
| spreading | 88.48 | 38.30 | 93.73 |
| skewness | 0.47 | 286.60 | 0.51 |
| kurtosis | 0.42 | 38.40 | 0.59 |

Table F.6: Stive - Total - moments

| **MorMerge** | MAE | RMAE | RMSE |
|---|---|---|---|
| **moments** | [m/-] | [%] | [m/-] |
| CoM | 67.10 | 168.60 | 79.98 |
| spreading | 44.42 | 19.20 | 54.12 |
| skewness | 0.19 | 119.80 | 0.25 |
| kurtosis | 0.44 | 40.40 | 0.60 |

Table F.7: MorMerge - Total - moments

| **BruteForce** | MAE | RMAE | RMSE |
|---|---|---|---|
| **moments** | [m/-] | [%] | [m/-] |
| CoM | 12.27 | 30.80 | 14.89 |
| spreading | 17.51 | 7.60 | 21.78 |
| skewness | 0.22 | 137.50 | 0.25 |
| kurtosis | 0.34 | 31.10 | 0.50 |

Table F.8: BruteForce - Total - moments

| **Tonnon** | MAE | RMAE | RMSE |
|---|---|---|---|
| **APx** | [m] | [%] | [m] |
| south | 379.85 | 66.00 | 438.39 |
| north | 520.93 | 71.00 | 579.52 |
| distance | 249.02 | 19.00 | 284.02 |

Table F.9: Tonnon - Beach - APx

| **Stive** | MAE | RMAE | RMSE |
|---|---|---|---|
| **APx** | [m] | [%] | [m] |
| south | 636.99 | 110.70 | 803.00 |
| north | 334.91 | 45.60 | 380.14 |
| distance | 393.17 | 30.00 | 455.07 |

Table F.10: Stive - Beach - APx

| **MorMerge** | MAE | RMAE | RMSE |
|---|---|---|---|
| **APx** | [m] | [%] | [m] |
| south | 779.36 | 135.50 | 804.12 |
| north | 650.60 | 88.70 | 782.56 |
| distance | 1429.95 | 109.20 | 1455.44 |

Table F.11: MorMerge - Beach - APx

| **BruteForce** | MAE | RMAE | RMSE |
|---|---|---|---|
| **APx** | [m] | [%] | [m] |
| south | 900.78 | 156.60 | 931.09 |
| north | 949.65 | 129.40 | 1049.48 |
| distance | 1850.43 | 141.40 | 1893.03 |

Table F.12: BruteForce - Beach - APx

| **Tonnon** | MAE | RMAE | RMSE |
|---|---|---|---|
| **APx** | [m] | [%] | [m] |
| south | 244.38 | 42.50 | 262.59 |
| north | 405.50 | 55.30 | 455.91 |
| distance | 649.02 | 49.60 | 699.55 |

Table F.13: Tonnon - Beach - APx-From-M2

| **Stive** | MAE | RMAE | RMSE |
|---|---|---|---|
| **APx** | [m] | [%] | [m] |
| south | 163.47 | 28.40 | 187.00 |
| north | 315.99 | 43.10 | 350.27 |
| distance | 465.17 | 35.50 | 500.86 |

Table F.14: Stive - Beach - APx-From-M2

| **MorMerge** | MAE | RMAE | RMSE |
|---|---|---|---|
| **APx** | [m] | [%] | [m] |
| south | 122.82 | 21.40 | 159.95 |
| north | 164.14 | 22.40 | 221.33 |
| distance | 280.06 | 21.40 | 377.72 |

Table F.15: MorMerge - Beach - APx-From-M2

| **BruteForce** | MAE | RMAE | RMSE |
|---|---|---|---|
| **APx** | [m] | [%] | [m] |
| south | 63.87 | 11.10 | 87.30 |
| north | 97.51 | 13.30 | 113.35 |
| distance | 129.79 | 9.90 | 157.91 |

Table F.16: BruteForce - Beach - APx-From-M2

| **Tonnon** | MAE | RMAE | RMSE |
|---|---|---|---|
| **TPx** | [m] | [%] | [m] |
| south | 277.56 | 2525.00 | 278.36 |
| north | 178.69 | 1354.80 | 180.62 |
| distance | 456.26 | 1910.00 | 458.62 |

Table F.17: Tonnon - Total - TPx

| **Stive** | MAE | RMAE | RMSE |
|---|---|---|---|
| **TPx** | [m] | [%] | [m] |
| south | 29.23 | 265.90 | 36.51 |
| north | 281.25 | 2132.40 | 281.88 |
| distance | 303.91 | 1272.20 | 306.24 |

Table F.18: Stive - Total - TPx

| **MorMerge** | MAE | RMAE | RMSE |
|---|---|---|---|
| **TPx** | [m] | [%] | [m] |
| south | 49.92 | 454.10 | 56.83 |
| north | 38.80 | 294.20 | 42.27 |
| distance | 88.71 | 371.40 | 98.37 |

Table F.19: MorMerge - Total - TPx

| **BruteForce** | MAE | RMAE | RMSE |
|---|---|---|---|
| **TPx** | [m] | [%] | [m] |
| south | 69.71 | 634.20 | 70.75 |
| north | 14.83 | 112.40 | 19.01 |
| distance | 82.87 | 346.90 | 84.35 |

Table F.20: BruteForce - Total - TPx

| **Tonnon** | MAE | RMAE | RMSE |
|---|---|---|---|
| **CoMx** | [m] | [%] | [m] |
| south | 284.51 | 296.00 | 288.44 |
| north | 320.34 | 249.10 | 329.01 |
| distance | 604.84 | 327.00 | 609.39 |

Table F.21: Tonnon - Beach - CoMx

| **Stive** | MAE | RMAE | RMSE |
|---|---|---|---|
| **CoMx** | [m] | [%] | [m] |
| south | 114.37 | 119.00 | 119.07 |
| north | 171.67 | 133.50 | 185.02 |
| distance | 90.62 | 49.00 | 115.35 |

Table F.22: Stive - Beach - CoMx

| **MorMerge** | MAE | RMAE | RMSE |
|---|---|---|---|
| **CoMx** | [m] | [%] | [m] |
| south | 152.69 | 158.80 | 157.15 |
| north | 214.44 | 166.70 | 259.18 |
| distance | 365.98 | 197.90 | 390.25 |

Table F.23: MorMerge - Beach - CoMx

| **BruteForce** | MAE | RMAE | RMSE |
|---|---|---|---|
| **CoMx** | [m] | [%] | [m] |
| south | 141.33 | 147.00 | 145.17 |
| north | 221.65 | 172.30 | 232.10 |
| distance | 361.83 | 195.60 | 372.76 |

Table F.24: BruteForce - Beach - CoMx

| **Tonnon** | MAE | RMAE | RMSE |
|---|---|---|---|
| **Lifetime** | [] | [%] | [] |
| VM | 8.69 | 57.50 | 9.54 |
| CE | 4.83 | 30.70 | 5.42 |

Table F.25: Tonnon - Total - Lifetime

| **Stive** | MAE | RMAE | RMSE |
|---|---|---|---|
| **Lifetime** | [] | [%] | [] |
| VM | 7.23 | 47.90 | 7.67 |
| CE | 3.34 | 21.30 | 3.75 |

Table F.26: Stive - Total - Lifetime

| **MorMerge** | MAE | RMAE | RMSE |
|---|---|---|---|
| **Lifetime** | [] | [%] | [] |
| VM | 4.07 | 26.90 | 4.69 |
| CE | 6.16 | 39.10 | 6.83 |

Table F.27: MorMerge - Total - Lifetime

| **BruteForce** | MAE | RMAE | RMSE |
|---|---|---|---|
| **Lifetime** | [] | [%] | [] |
| VM | 1.12 | 7.40 | 1.30 |
| CE | 1.46 | 9.30 | 1.63 |

Table F.28: BruteForce - Total - Lifetime

# G

# Comparison of the predicted versus the observed performance

In this appendix the results of the application of the performance and validation tool are given. The results show the Tonnon approach under-predicted the feeding performance in terms of volumetric growth of the Regions of Contribution, alongshore expansion, and the lifetime.

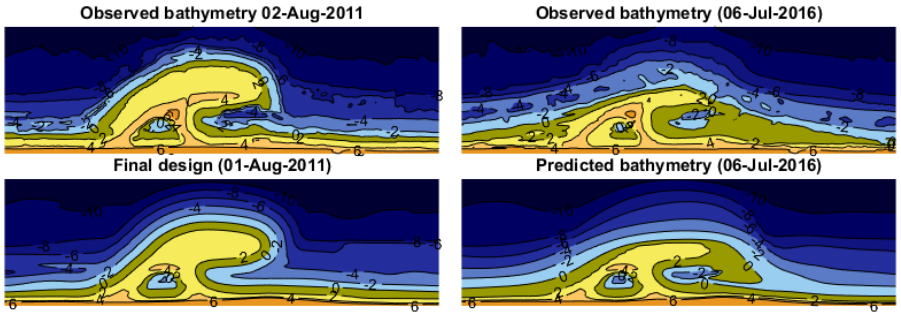


Figure G.1: Comparison of the observed versus the predicted (by Tonnon (2010)) initial bathymetry and the bathymetry as of July 2016.

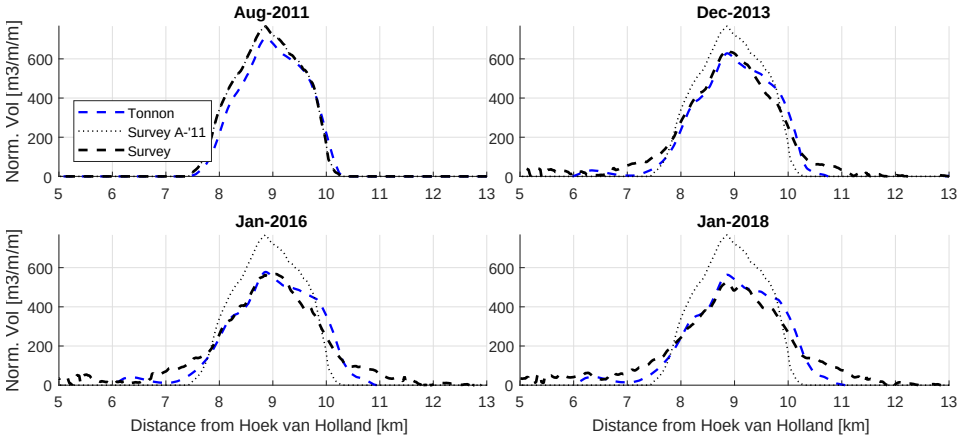


Figure G.2: Normalised volumes of the Sand Engine. Survey data versus Tonnon (2010) approach.

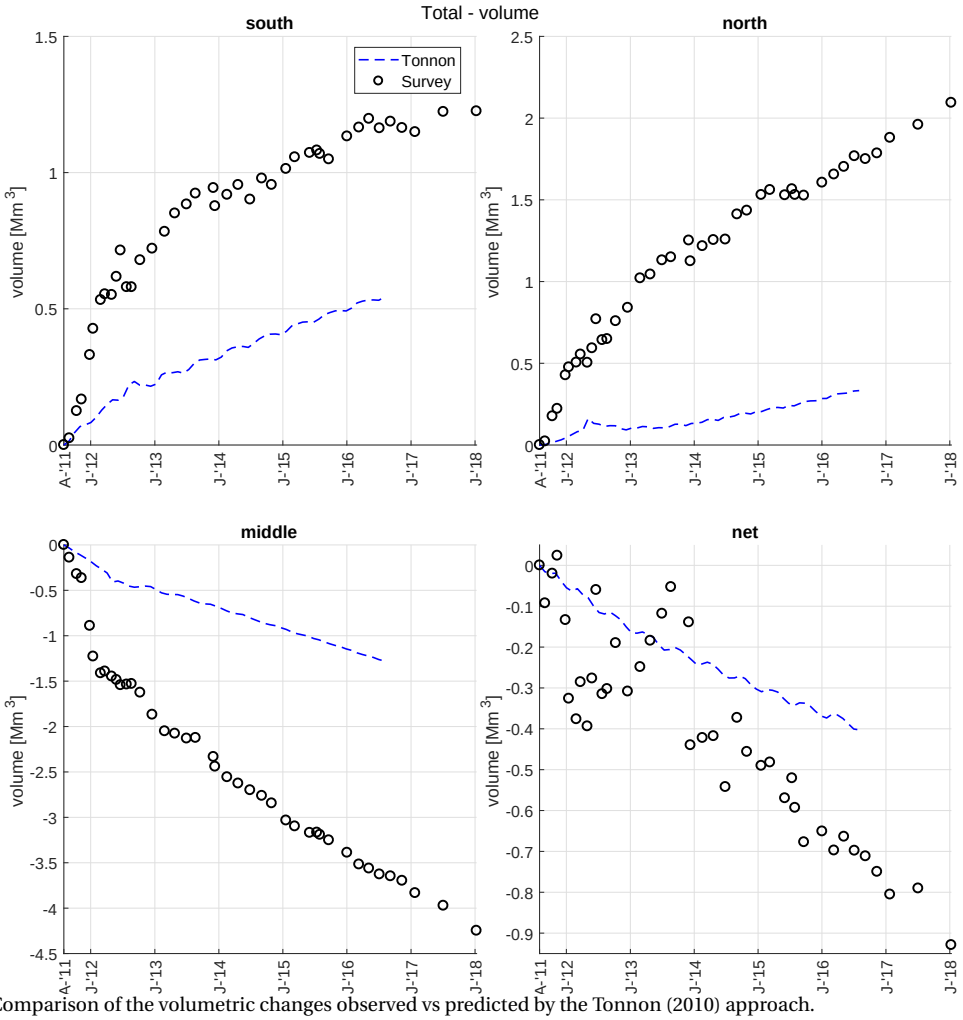


Figure G.3: Comparison of the volumetric changes observed vs predicted by the Tonnon (2010) approach.

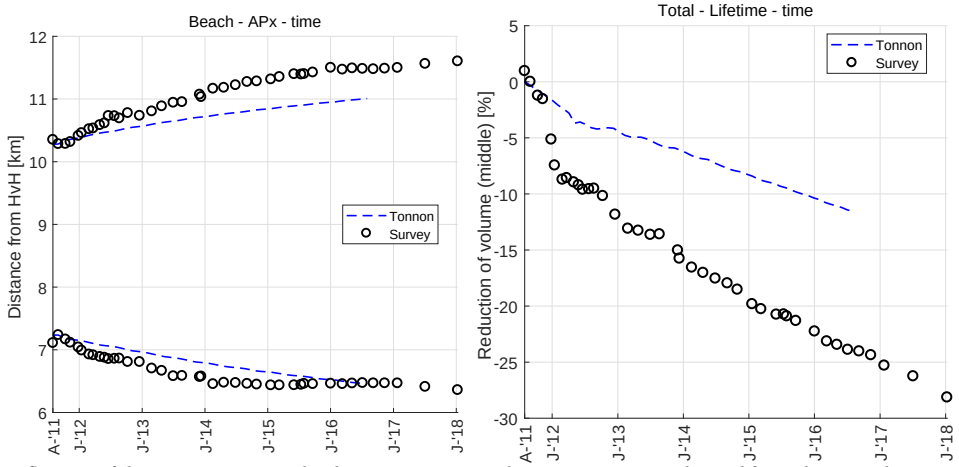


Figure G.4: a) Reflection of the Accretion Points by the Tonnon approach. Accretion Points derived from the spreading (M2). b) Lifetime as reflected by approach, expressed in the percentile volume reduction of the pensinsula since the construction.

# H

# Applicability Momentary coastline and shore line

This appendix includes the quantification of the geometric performance indicators of the Accretion Points and the Transition Points, as well as the behaviour indicators, i.e. the centroid (M1) and the spreading (M2). The results show the MCL (-4.4/+3m + NAP) reflects the developments of the Beach region (-3/+3m + NAP) well in terms of the geometric performance indicators. An initial difference is observed in terms of the centroid. Further, the MCL has shown a mild stagnation of the spreading, not observed in the Beach region.

The developments of the shoreline suggest a retreat of the alongshore expansion since 2015, which is a concrete different reflection than observed in the Beach region. The developments in the shoreline are far less stable in terms of the centroid, while the spreading shows a full stagnation in the shoreline as of 2015. Therefore, the shoreline is stated not to correctly represent the developments in case of the Sand Engine.

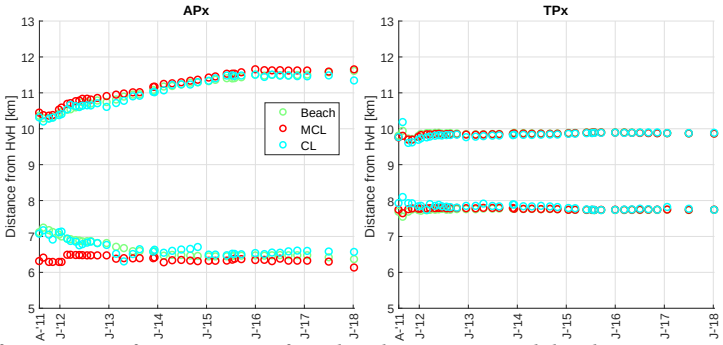


Figure H.1: Comparison of geometric performance (APx) of Beach and MCL region, and shoreline (CL)

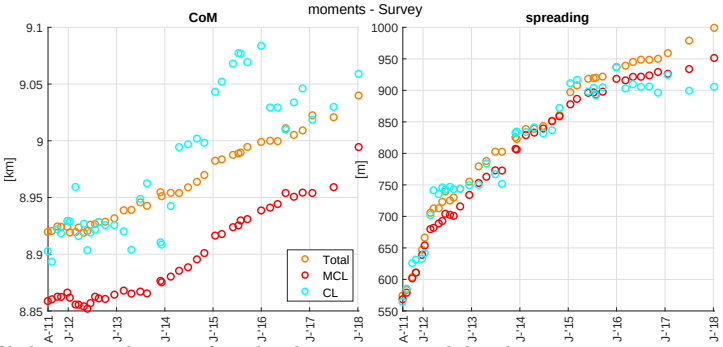


Figure H.2: Comparison of behaviour indicators of Total and MCL region, and shoreline (CL)

# A discussion on the alongshore sectioning

Alongshore sections must be defined to enable quantification of the feeding performance of a mega-feeder nourishment. The sensitivity of the applied sections for the results is discussed in this appendix.

This appendix goes into this topic more elaborately. First previously applied alongshore sections are reviewed briefly. Second, an interesting finding observed during the quantification of the Transition Points of the analytical model approaches (section 6.2.2) are discussed here more elaborately. In the third section, the influence of the sectioning on the numerical models is discussed.

## I.1. Comparison of applied alongshore sectionings

The following figures show the applied sectioning in previous research. De Schipper et al. (2016) derived the sectioning from the initial shape at the shoreline. Roest (2017) used a similar approach. Arriaga et al. (2017) used an interesting alternative approach where the erosions of the left and north were split up, although the lack of a full coverage prevents a full assessment of developments.

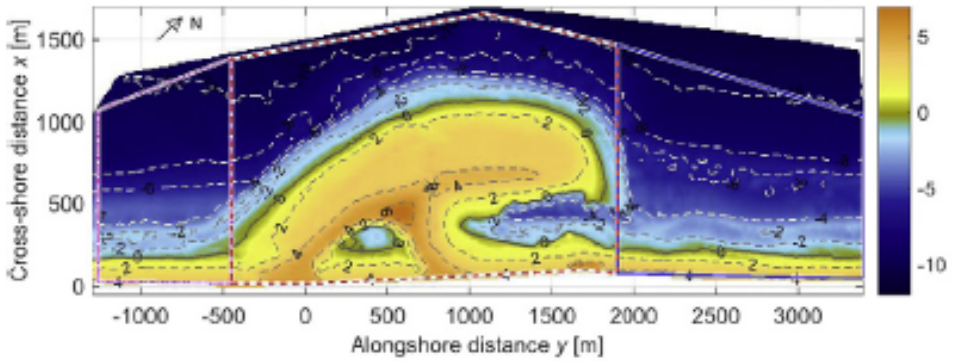


Figure I.1: Applied sectioning by De Schipper et al. (2016)

Comparing the previously applied sections, shows the derivation of sections based on the initial shoreline causes a mild bias. The section of the peninsula wider than applied in this thesis. From a feeding performance perspective this may be an attractive option. Though it must be kept in mind that part of the accretion also occurs in this middle peninsula, most dominantly on the south side the difference is circa 300m. This puts perspective on the observed results of earlier research. It explains less clear trends found in volumetric feeding performance than identified based on results of this thesis.

Secondly, the outer bounds were previously derived from limitations in the Zandmotor surveys rather than the observed accretions, resulting in a too small Region of Contribution. This may also explain differences between the current results and previous research. What the influence of the applied sectioning can be, is further discussed in the next section.

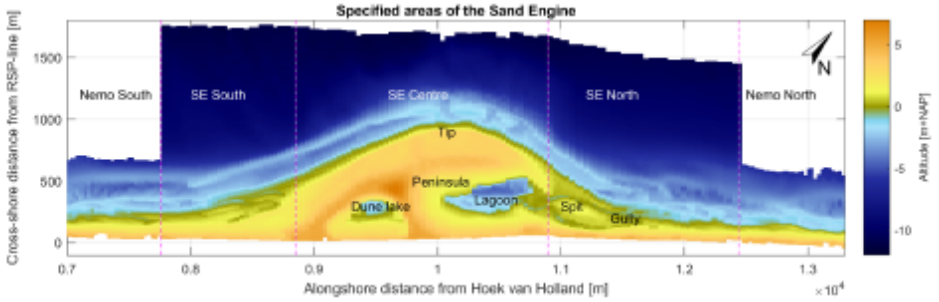


Figure I.2: Applied sectioning by Roest (2017)

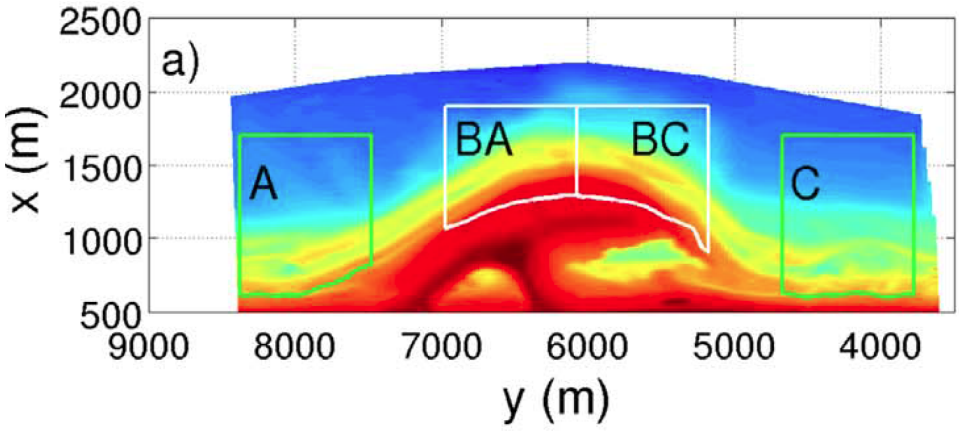


Figure I.3: Sectioning by Arriaga Arriaga et al. (2017))

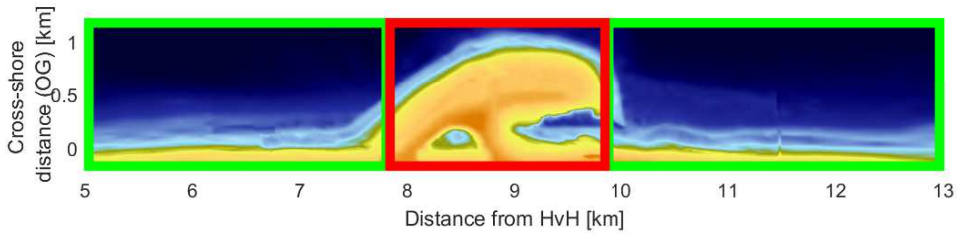


Figure I.4: Sectioning applied in this thesis

## I.2. Influence of sectioning on the reflection of indicators by the numerical model approaches

In this thesis, the outer bounds were defined based on an analysis of the alongshore volumetric growth, see section 5.1.3. The outer bounds were set equal for both the analysis of the survey data, as well as for the model approaches to enable a homogeneous comparison.

However, if model approaches deviate in developments of the volumetric shape, application of these sections may lead to results that deviate from 'actual' feeding performance simulated by models. To assess the influence of the applied sectioning, a larger alongshore regions is observed here for the numerical model approaches. The Region of Influence is adjusted such that the sections have an equal width (extending 5km south and northward from the initial centroid at x = 9000m, instead of 6400m - 12800m).

It reveals the 'actual' spreading of the Bruteforce model is slightly higher, while the centroid migrates more moderately. The volumetric feeding performance is approximately equal. The influence of the sectioning on the MorMerge model is negligible. The larger sectioning does significantly influences the output of the Stive approach. The volumetric feeding performance is approximately equal to the south and north according to the model approach; which deviates from the observed developments. The centroid of the SE in fact migrated southward, while the 'actual' spreading of the model surpasses that of the observations in January 2018. This

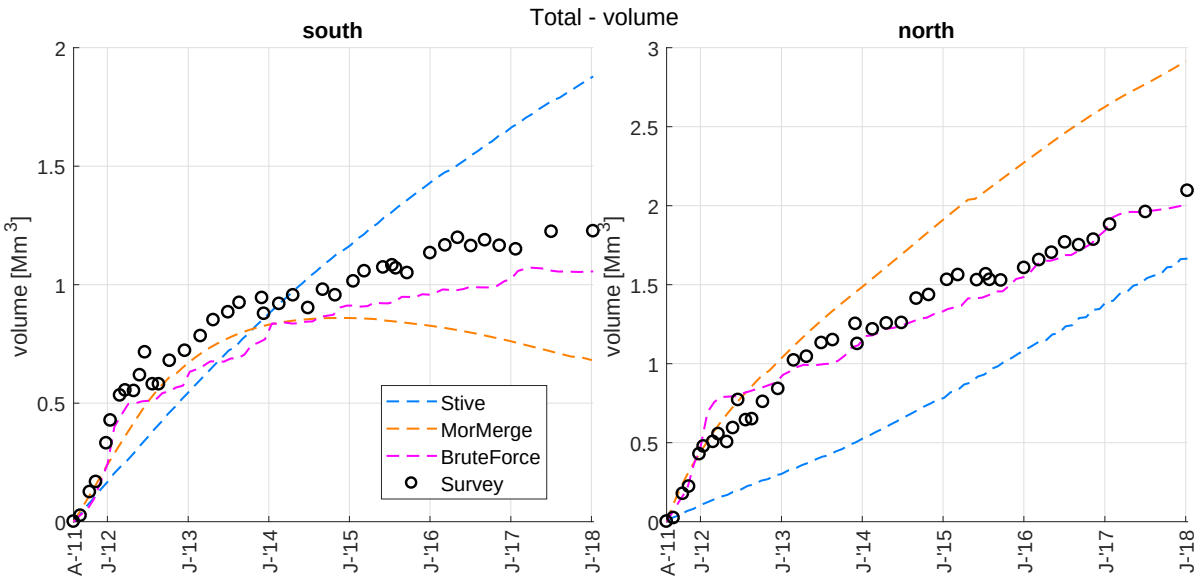


Figure I.5: Volumes observed (original sectioning) vs models (widened sectioning)

differs from the results based on the smaller sections, since there the centroid migrated northward and the spreading was smaller than observed from the Survey data. Remarkably, its curvature is approximately equal, it is the rate that is higher.

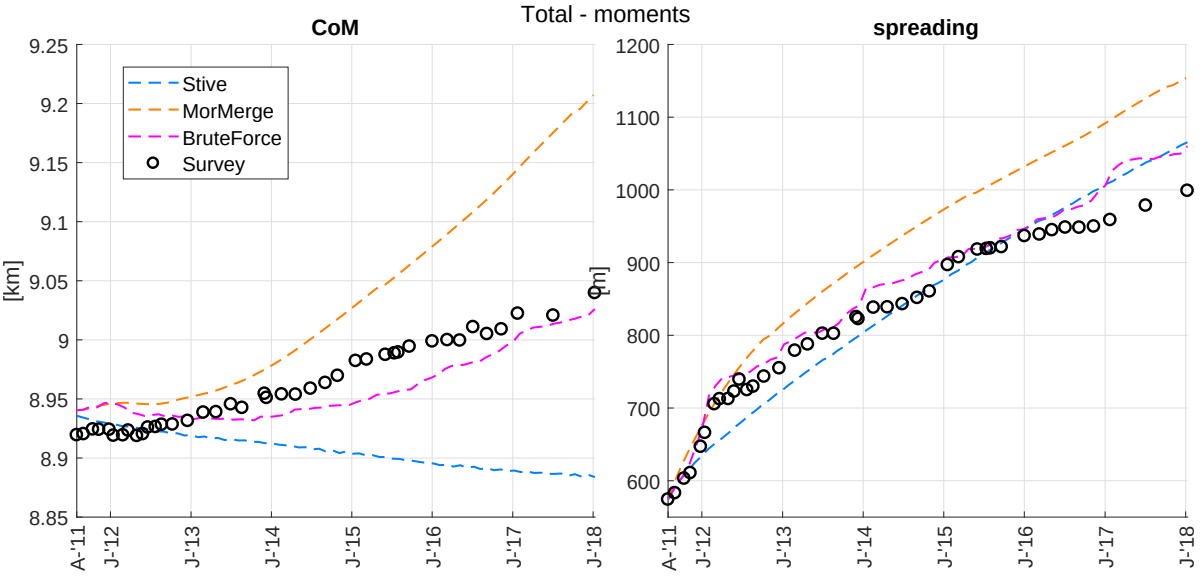


Figure I.6: Moments observed (original sectioning) vs models (widened sectioning)

The analysis shows the importance of carefully selecting the alongshore sections prior to any analysis, whilst keeping in mind that incorrect selection may lead to biased results. It is therefore perhaps even a method sensitive to wishful thinking. This wishful thinking could be eliminated if the Accretion Point could be used to define the Regions of Influence. This requires further improvement of the indicator. One suggestion may be the definition of the Region of Influence based on a fixed ratio of the spreading, e.g. a factor 4.

## I.3. Derivation of the Transition Points from the analytical model approaches

The Transition Point is defined by the alongshore location where the erosion of the middle section turns to accretion, with respect to the initial bathymetry. In chapter 5 it was shown that the in the case of the

Sand Engine, the Transition Points have not migrated over time in the first six and a half years. Therefore, defining sections that do not develop over time can be applied successfully in the case of the Sand Engine. This partially confirms the previously applied alongshore sections agree with the methodology introduced here to derive the alongshore sections. Though, the application of fixed sections should be applied with care. Reflection of the Transition Points by the analytical model approaches is used to exemplify the need for caution.

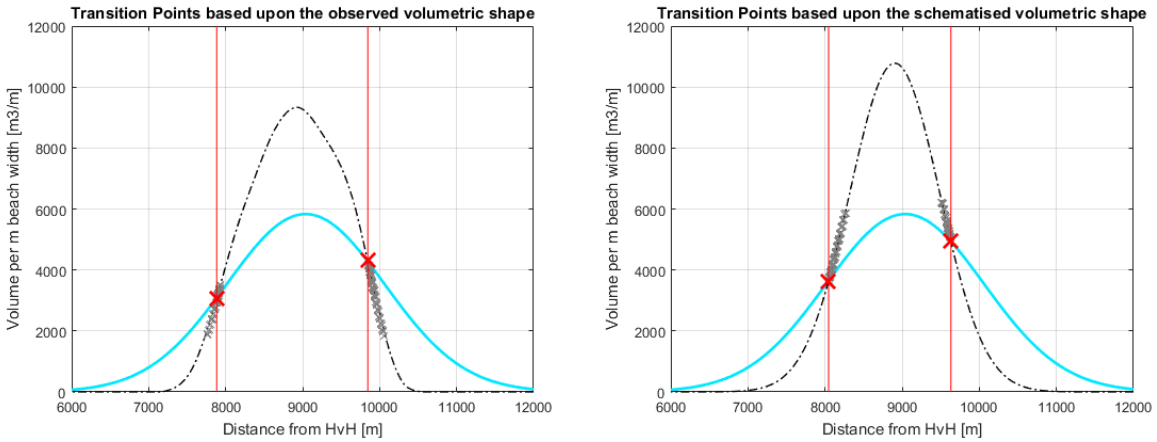


Figure I.7: Influence of the initial bathymetry on Transition Point indicator. In black the volumetric shape used to define the Transition Point, whereas the blue line depicts the reproduction of the volumetric shape of the Plus approach. Red crosses mark the Transition Point (as of August 2016), grey crosses are the previous locations of the TPs. a) Transition Point based upon initial volumetric shape as schematised by Gaussian curve (Plus) b) Transition Point based upon initial volumetric shape as observed.

In the case of the Sand Engine, the location of the Transition Points along the shoreline are roughly constant (figure I.7a). The initially high angles of the volumetric shape near the Transition Point with the original shoreline cause this constance. If the initial volumetric shape was schematised by a Gaussian curve (figure I.7), see figure I.7b, the Transition Points would migrate causing a widening of the Region of the Feeder. This shows the development of the Transition Point is not influenced by the physical conditions, but by the distinct initial bathymetry instead. In the scenarios that the azimuth is milder, as in the schematised example of the left plot, a fixed sectioning will lead to a bias in the results. In this scenario, the Region of the Feeder will widen over time. As a result, application of a fixed sectioning would under-value the observed erosion, while accretions would be under-valued.

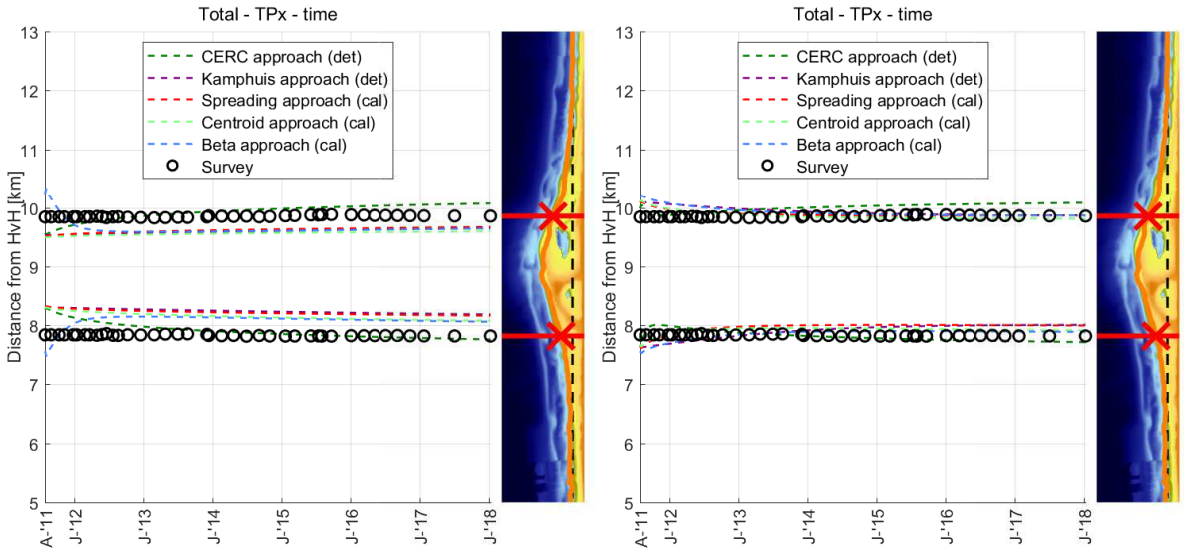


Figure I.8: Reproductions of the Transition Points by the analytical models. a) the Transition Points are derived from the Gaussian-curve at the initial time-step, b) the Transition Point of the analytical models are derived with the initial bathymetry of the Sand Engine.

# I.4. Derivation of the Accretion Points from the numerical model approaches

In section 6.3.2, the reflection of the numerical model approaches of the Accretion Points was discussed. It was shown the models could not reflect the points well. In this section, the volumetric shape is visualised to support the results obtained.

The difficulty in deriving the Accretion Point based on the numerical model is that not by definition a location is present where no accretion is observed, e.g. in the case of the Stive approach on the south (middle panel), or the MorMerge and BruteForce approach on the north (bottom panel). In those cases, a local minimum is interpreted as the location that represents the Accretion Point. Further, one can observe Sand Wave like shapes, best observable on the south. These cause an additional migration of the Accretion Points that do not reflect the observed developments.

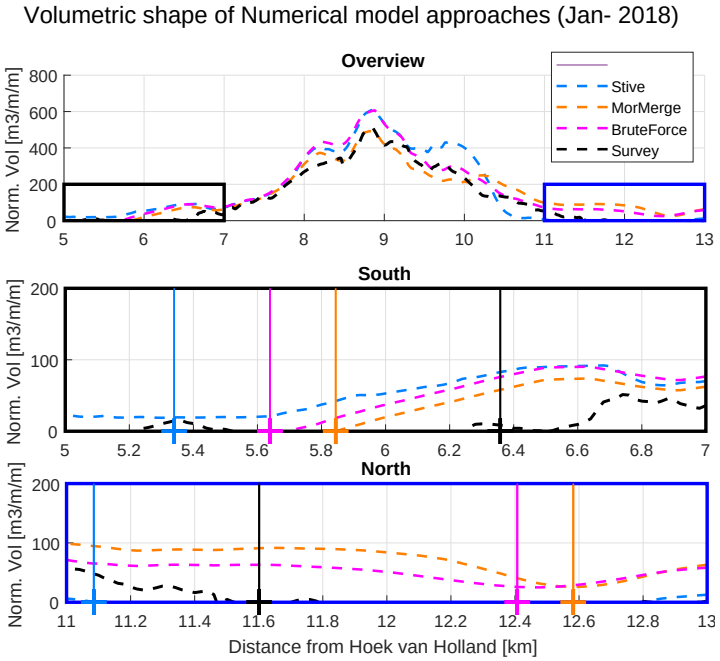


Figure I.9: Visualisation of derivation of Accretion Points by numerical model approaches.